2009

Analysis and Design of Innovative Composite Storm Shelter Against Wind Hazards

Tonga T. Nguyen

ANALYSIS AND DESIGN OF INNOVATIVE COMPOSITE STORM SHELTER AGAINST WIND HAZARDS

by

TONGA T. NGUYEN

NASIM UDDIN, COMMITTEE CHAIR
JASON T. KIRBY
LIANXIANG DU

A THESIS

Submitted to the graduate faculty of the University of Alabama at Birmingham,
in partial fulfillment of the requirements for the degree of
Master of Science in Civil Engineering

BIRMINGHAM, ALABAMA

2009

2009ANALYSIS AND DESIGN OF INNOVATIVE COMPOSITE STORM SHELTER AGAINST WIND HAZARDS

TONGA T. NGUYEN

CIVIL, CONSTRUCTION AND ENVIRONMENTAL ENGINEERING

ABSTRACT

Every year extreme windstorms such as tornadoes and hurricanes have imposed disastrous consequences to the United States community, economy and population. Having a community shelter can protect civilians from these dangerous events. This study focused on providing detailed design guidance in addition to demonstrating the design and analysis of a safe, on-ground, stand-alone community shelter to resist extreme wind forces. The storm shelter must be able to resist 300 mile per hour wind gusts and flying debris impacts of such storms. The primary objective was to develop an innovative and cost-effective Fiber Reinforced Polymer (FRP) panelized construction system. The technique allows the shelter to be sub-divided into basic elements that can be pre-fabricated and shipped to the construction site, where they can be assembled into the finished structure. The design must meet the requirements recommended by the Federal Emergency Management Agency (FEMA) with life safety as the primary consideration.

The design wind pressures for the community shelter were calculated per the American Society of Civil Engineering (ASCE) 7-05 code provision and modeled in the Computational Fluid Dynamic (CFD) software named HYBRID3D. Comparison was made between the ASCE 7-05 and CFD wind pressures to validate the accuracy of the ASCE 7-05 design methodology.

Two different FRP materials were proposed for the design and analysis of the FRP panels. The design of FRP panels was based on the performance and minimum wind

load design criteria of the ASCE 7-05. The finite element analysis (FEA) software package called ANSYS 11.0 was used to carry out the design of the FRP panels under the wind pressure loading. In addition, the FEA was conducted on the bolted joint connections of the shelter. Further analysis was carried out on the bolted joint connections per the Load Resistance Factor Design (LRFD) code to determine if the bolts had sufficient strength to resist the applied external loadings.

Keywords: Extreme Wind, FRP, ASCE 7-05, FEA, Connection, Community Shelter

DEDICATION

This thesis is dedicated to my grandparents, parents, and sister.

ACKNOWLEDGEMENTS

Ideas and recommendations come from many teachers and students from UAB. Any suggestions whether for a whole new chapter or a simple word change, is considered and activated whenever possible. It is hoped that this thesis will bring forth comments and requests.

First, thanks go to Dr. Nasim Uddin for the all the time, support and effort during the development of the research. Second, thanks also go to the committee members, Dr. Du and Dr. Kirby, for their time input and support. Last, thanks go to Dr. Koumullil ahd Dr. Ito for generating mesh of the CFD model in the initial stage.

I also would like to thank Ian Hosch for his knowledge of modeling, support, advice, and patience from the start to finish of the project. Without him, the project would be difficult and would not be able to finish early as expected.

To all the students and friends whose names have not been mentioned, your friendship, help and support are also acknowledged.

Most importantly, I would like to thank my family for their love and support, and have always loved me unconditionally. I would have never achieved this goal without them.

TABLE OF CONTENTS

Page

Page

Page

LIST OF TABLES

Table *Page*

Table *Page*

LIST OF FIGURES

Figure *Page*

Figure *Page*

Chapter 4

Figure *Page*

Figure *Page*

Figure *Page*

LIST OF ABBREVIATIONS

ASCE	American Society of Civil Engineers
C&C	Components and Cladding
CFD	Computational Fluid Dynamic
CSIP	Composite Structural Insulated Panel
EPS	Expanded Polystyrene
FEA	Finite Element Analysis
FEM	Finite Element Method
FEMA	Federal Emergency Management Agency
FRP	Fiber Reinforced Polymer
LSS	Layer Stacking Sequence
LRFD	Load and Resistance Factor Design
MWFRS	Main Wind Force Resisting System
OSB	Oriented Strand Board
PMC	Polymer Matrix Composite
PP	Polypropylene
SIP	Structural Insulated Panel

CHAPTER 1

INTRODUCTION

1.1—Purpose

Tornadoes and hurricanes are destructive forces of nature that produce high wind forces and can destroy nearly anything in their paths. They can have sustained wind speeds up to 250 mph or greater that often affect the structural integrity of structures [1]. They can have structures collapse in minutes or possibly seconds. Therefore, developing a safe shelter during these events can reduce the effects of injury and death. People who cannot find a safe shelter, or for any particular reasons that they cannot go to a safe shelter, often fall victim to these windstorms. For example, Hurricane Katrina in 2005 destroyed thousands of houses; property damages were up to $81.2 billion dollars in insured losses; the storm also caused 1,800 deaths that made it the largest-natural disaster in the U.S history [1], [2].

Because of the harmful effects from previous hurricanes and tornadoes, structural designers are now more aware of the structural performance and are concern with issues such as developing design wind pressures in accordance to building codes safe or not. Some have questioned whether the structural damages from the past-wind events were due to weakness in building codes, inadequate maintenance and insufficient attention to the details of connections, or insufficiency in the construction process [1], [2]. All these concerns have made designers skeptical about designing structures to withstand extreme-

wind forces in accordance to building codes. As with many storm events not discussed in this section, the events from Hurricane Katrina represent only a small percentage of the intense and destructive potential of extreme-wind forces. The extreme-wind storms from tornadoes and hurricanes will continue to cause death, injury, and property damage and continue to illustrate the need for shelters and safe rooms capable of protecting human lives.

Even though there has been considerable research on developing building materials for resisting-wind loads resulted from tornadoes and hurricanes; many people still cannot avoid the threats of tornado- and hurricane-windstorms. Unfortunately, the threats of tornado- and hurricane-windstorms have caused people property, structural damage, injury and death. Because of the devastating effects that people have received from the windstorms, many people do not want to discuss the issue of engineering failures. However, despite the prevalence of this problem, an understanding of building designs for extreme-wind events have to be addressed for future successes of structures.

When a severe-weather event such as a tornado or hurricane threatens, it is necessary for people to have a safe place to go and sufficient time to get there. Seeking shelter inside one's home is considered not a safe shelter, unless the house was designed to withstand the forces of the extreme winds and the impact of windborne missiles. According to the Federal Emergency Management Agency (FEMA) [1], [3], most houses are not strong enough to withstand high tornado or hurricane winds, and ultimately, they are not strong enough to protect occupants within the houses. The reason is that most houses are built in accordance to the minimum requirements of the local building codes in their areas, and the tornados and hurricanes have wind speeds that are much stronger

than the wind speeds of the local building codes are based; therefore, most houses often fail, and put people at great risks.

Therefore, the question arises when one decides that his/her house is no longer a safe place to be in when a severe weather threaten, where he/she should go to find protection. The best answer for that is for him/her to find a safe community shelter nearby his/her house. *This thesis provides specific guidance on how to analyze and design an effective community shelter (40 ft x 12 1/2 ft x 7 ½ ft) to be able to resist 300 mph wind-induced forces that can save lives when severe weather threatens away from home.*

The main purpose of this research was to provide detailed guidance that would help engineers in analyzing and designing a safe, on-ground, stamd-alone community shelter that offers occupant protection during the tornado- and hurricane- wind events. Two reasons for designing on-ground community shelters instead of in-ground community shelters are: (1) to provide easy access to the public, including for those people who are in wheelchairs, (2) to provide protection from flood events. Because of these reasons, the design of an on-ground community shelter is proposed in this research instead of the design of an underground community shelter. The recommended floor area per person is five square foot [1]. The occupancy of the proposed shelter is 100 people.

It is important to know that the community shelter proposed in this research is considered as a stand-alone shelter. The community shelter is developed for use in new houses. Modifying an existing house, walls and foundations to put in new shelter foundations, walls, and so on, to accomdate the shelter is more difficult. As a result, the design of shelter proposed in this thesis is not practical adding inside existing houses;

instead the shelter is designed and built as an entirely separate structure or in freestanding addition to the basement/house. Regardless of where the shelter is built, an appropriate shelter location to protect occupant safety from high wind, debris impact and flood events should be (1) outside of 50-year or 100-year flood plain, and (2) a location where people can have sufficient time to get there. The designer can check with the community service section of the local phone book or the local emergency management to know about storm surge evacuation information and determine if the constructed shelter is in the flood plain area. In cases where some people can not get to a community shelter within a reasononable time frame recommended by the local management agencies, it is recommended that they should consider retrofitting a portion of their housses to use as a shelter. When the shelter is not occupied, it can be used for other purposes such as storage room, day-care facility, and so on.

It is aslo important to know that detailed guidance on how to design for an extremely high capacity shelter such as a stadium was beyond the scope of this research. For this reason, the design of an extremely large capacity shelter is not included in this research. Nevertheless, the concepts in this research might help one in gathering information for developing the design wind pressures and selecting the building materials for their strength and durability that can withstand the forces of extreme winds and the impact of wind borne missiles. In addition, the intent of the shelter was not to provide protection for a long time, but rather a short-term, high wind event that lasts no more than 36 hours [1], [3]. The factors that go into developing the design wind pressures for the shelter are discussed in this research. The cost and benefit for constructing a community shelter are discussed in Chapter 2 of this thesis.

The goal of this research was to present an alternative of building materials and methods that can improve the performance of the community shelter in hazard-prone areas during and after high-wind events. Two alternative composite materials have been investigated for this research, due to the corrosive nature of steel and concrete, and disintegration of wood in the water. FRP composites have been used in many Civil Engineering applications due to their lightweight, high strength, non-conductive and non-corrosive properties [4]. In addition to their high durability, and their relatively large strength to weight ratio, FRP composites are great candidates to withstand the corrosive and imposing environment for which they would embody. Moreover, forms of FRP composites, such as sandwich composite panels, are known for their good, insulating properties to provide for walls and roof panels, which make them also very attractive for reducing energy costs. For these reasons, FRP composites were proposed as the building materials for this research. In addition, the panelized-construction technique proposed in this research is supposed to offer faster-construction time and ease of assembly, which ultimately reduces the overall cost of the structure. The proposed panelized-construction technique is a new method of construction that is allowed the prefabricated elements to be put together at the construction site into the finish structure.

The objectives of this research were to design and analyze the FRP materials and the connections of the community shelter through finite element analysis (FEA) software package ANSYS 11.0. It has the capability of structural, thermal, magnetic, electric and fluid analysis [5]. The FEA is used to determine the stresses in the FRP panels as well as the stresses in the connections most critical for protecting the uninterrupted operation of the shelter in hurricane and tornado prone areas. The 300 mph wind speeds used for

analyzing the FRP materials and the connections for the shelter is based on the wind speeds that are rarely exceeded in the United States [1], [3]. Therefore, the shelter built based on this research is expected to oppose the forces imposed on it by the extreme winds without failing. The wind forces may cause fractures or other signs of stress in the materials or connections used in the shelter, and they may cause materials or connections to yield. However, the intent of the design was not to produce the shelter that will always remain completely undamaged, but rather the shelter will protect its occupants to survive an extreme windstorm with little or no injury.

1.2—Problem Definition

The research focused on designing a safe, on-ground community shelter that used FRP as the building materials to be able to resist the 300 mph wind speeds resulted from tornadoes and hurricanes. The shelter was created through the innovative, panelized-construction system using glass fiber reinforced polymer panels. The research proposed two composite models. The first model proposed for this research was made up of two fiberglass face sheets impregnated with polypropylene (Glass/PP) and a layer of expanded polystyrene (EPS) foam core. The top and bottom Glass/PP layers were adhered to the inner EPS foam core layer to form the structural insulated panels (SIPs) or commonly called the sandwich composite panels. The second model proposed for this research was consisted of several glass fibers and several wire-meshed glass fibers reinforced with polyester polymer. Each layer of the composite was considered as a thin laminate. Several thin laminates were put together and assembled into the layer stacking sequence (LSS) to produce a thin laminated composite. The main reinforcement of the

proposed laminated composite was the wire-meshed glass fibers, which were twisted and wrapped within the laminate. From this point on forward of this thesis, this model will be called as the wire-meshed model.

The design and analysis of the FRP panels were based on the performance and the minimum wind load design criteria of the ASCE 7-05 methodology. The design wind loads were determined in accordance to the ASCE 7-05 design methodology, which were then compared to the wind loads obtained from the Computational Fluid Dynamic (CFD) code called HYBRID3D. Connection designs were based on the Load and Resistance Factor Design (LRFD) methodology. Both the design and analysis of the FRP panels and connections were carried out through FEA in order to see the local stress flow, overall load path between the panels and the stress concentration developed around the bolt holes even when the holes are occupied by the bolts. The FEA was used as a tool to solve and mimic real practical problems, which would otherwise take time and effort to solve by hand. For the most part, ANSYS 11.0 was used throughout this research.

1.3—Study Objectives

The overall objectives of the research were (1) to determine whether the proposed composite panels would be suitable for resisting 300 mph wind speeds, (2) to determine whether the proposed composite panels could hold the stress induced from the connections, and (3) to determine if the bolt connections could transfer the wind load through the Main Wind Force Resistance (MWFRS) effectively. To determine these two objectives, the following tasks were performed:

1. Determine the appropriate design wind pressures in accordance to the ASCE 7-05 code.
2. Model the wind flow and the geometry of the shelter in the CFD software to determine the wind pressures for the shelter.
3. Compare the wind pressures obtained from the ASCE 7-05 design code and CFD analysis.
4. Develop, analyze, and design FRP panels that used the following construction materials:

   (a) E-glass and Polypropylene (PP) face-sheets with EPS foam core (sandwich composite model),

   (b) E-glass and Polyester laminates with wire-meshed glass fiber and polyester laminates (wire-meshed model).
5. Design and analyze the bolted joint connections for the two models under 300 mph wind-induced pressure loading.

1.4—Work Plan

In order to achieve the tasks mentioned above, the following outline is followed in this research:

- Chapter 2 describes the literature review of topics including tornadoes and hurricanes, FRP, and FEA. They can be divided into separate sections as follows:
    1. Background of tornadoes and hurricanes.

2. Characteristics of tornadoes and hurricanes, which describe the building effects, caused by tornado and hurricane winds.
3. Objectives of designing community shelters, which describe the primary objective was to protect the occupants within the shelters from tornado and hurricane winds.
4. This section discusses risk assessment concepts, which include determining design wind speeds from wind speed map, tornado and hurricane histories, singl and annual event deaths, evaluating existing areas to be used as a shelter, and shelter costs.
5. Overview, application, and design limitation of FRP.

- Chapter 3 describes the FRP materials used for the shelter. This chapter provides the materials properties and physical properties of the sandwich composite model and the wire-meshed model
- Chapter 4 discusses the determination of the design wind loads for the shelter in accordance to the ASCE 7-05 design and then compares the wind loads to the CFD HYBRID3D's wind loads. It discusses the design criteria of wind load for the shelter, which details shelter size, location, wind directionality, and occupancy factor. It also details the best approach to use for design.
- Chapter 5 presents the experimental testing and the FEA carried out on a Glass/PP and EPS panel of the first model. This was done to study the flexural behavior and validate the design of the FRP panel under the flexural loading before more FEA analysis was carried out on the FRP panels of the second model (wire-meshed model). The Glass/PP and EPS panel was carried out on

a reduced scale beam under a three-point bending test. The experimental results of the FRP beam were then compared to the FEA results for the design validation. Validation of the FEA results was useful for further analysis of the full-scale FRP panels. If the FEA results from the first model were similar to the experimental results under the flexural testing, then the FEA of the wire-meshed model can be assumed to act as the experiment under loading and this means that no experiment will be carried out on the wire-meshed model. In addition, the FEA could be used as a tool to conduct further analysis on the full-scale FRP panels under the wind pressure loading. This is where Chapter 6 comes in to present the analysis and design of the full-scaled FRP panels.

- Chapter 6 discusses the design and analysis of the full-scaled FRP panels of the two models under the wind pressure loading. The FEA modeling parameters for determine the stresses of the FRP panels resulted from the 300 mph wind induced forces of tornadoes and hurricanes are presented. The parameters include geometry, element type, material properties, meshing, loading and boundary conditions.
- Chapter 7 discusses the design and analysis of the bolted joint connections that are responsible for holding the shelter together. Two separate connection designs are presented for the two models.
- Chapter 8 presents the summary and conclusions of the study.

CHAPTER 2

LITERATURE REVIEW

2.1—Background of Tornadoes and Hurricanes

Section 2.1.1 and 2.1.2 provide background information about tornadoes and hurricanes, respectively. Section 2.1.3 provides information about post-disaster assessments, research activities, and wind shelter design development carried out by the Federal Emergency Management Agency (FEMA) and other organizations.

2.1.1—Background of Tornadoes

Tornadoes typically occur in the spring and summer time, but they can occur anytime and anywhere in the United States. "Tornadoes are among the most destructive forces of nature that frequently put people at risks," says FEMA [1], [2]. People who live in the paths of tornadoes are at serious risks because the most aggressive tornadoes are capable of great destruction with wind speed of 250 mph near ground level [1], [2]. The consequences of living in the paths of violent tornadoes are damage of structures, loss of property, injury and death. These high-wind forces must be accounted for in the shelter design to create the strongest and safest structures. According to FEMA [1], [2], more than 1,270 tornadoes occurred in the United States since 1997; 5,506 deaths and 93, 287 injuries had occurred since 1950 to 2006; the amount of personal and property damages was up to one billions of dollars.

The reported damages have damage paths over 50 miles long and over 1 mile wide [1], [2]. The amount of destruction a tornado causes to buildings, after a tornado has passed is often rated by the Fujita Scale as seen in Table 2.1 [1], [2].

Table 2.1. Fujita Scale

F-Scale Number	Intensity Phrase	Wind Speed (mph)	Type of Damage Done
F0	Gale	40-72	Some damage to chimneys.
F1	Moderate	73-112	Snaps off small trees, damage signboards, peels surface of roofs. Mobile homes pushed over, moving cars pushed off the road, large trees snapped, or up rooted.
F2	Significant	113-157	Considerable damage, roofs torn off frame, mobile homes demolished, cars pushed over, large trees snapped, or up rooted.
F3	Severe	158-206	Roofs and some walls are torn from structures, trains over turned, most trees in the forest are up rooted
F4	Devastating	207-260	Well-constructed houses leveled, structures with weak foundations, blown off some distance, cars thrown a long distance
F5	Incredible	261-318	Strong frames houses lifted off of foundations, and carried off, car sized missiles fly further than 100 meters, tree debarked, steel reinforced concrete structures badly damaged

2.1.2—Background of Hurricanes

Hurricanes and other tropical storms such as typhoons are also among the most destructive forces of natures that can produce strong winds and flood damages. A hurricane wind with great velocity can cause violent seas and drive ocean water inland while spawning tornadoes and producing rains and floods that can affect the strength of structures. According to FEMA [1], [2], [3], the average number of hurricanes that make landfall to the United States every three years is approximately five hurricanes. Two of the five storms are considered major hurricanes with Category 3 or greater based on the Saffir-Simpson Scale, which is shown in Table 2.2 [1], [2]. From 1900 to 2006,

hurricanes caused 17,832 deaths, substantial number of injuries, and extensive personal and property losses.

Buildings that are along the hurricane paths are most vulnerable to damage. Hurricane winds can last up to several days; therefore, buildings along the hurricane paths not only experience high winds, but also flood damage. In recent years, multiple hurricanes have caused extensive damage to the coastal areas in the southern Atlantic and Gulf coast regions of the United States. Hurricane Andrew, for example, caused severe-wind damage and made landfall in southeastern Florida on August 24, 1992 [1], [2]. It caused 15 deaths and ¼ million people homeless. Based on the Saffir-Simpson Scale, Hurricane Andrew was a Category 4 hurricane with wind speeds ranging from 131 mph to 155 mph. Hurricane Andrew is considered a significant hurricane because it had caused extensive damage to all building types and had serious effects on the people and the communities. The storm made landfall and caused unprecedented, economic devastation. The amount of damage was up to $21 billion dollars in insured losses. The storm also caused 15 deaths and left almost one-quarter million people homeless [1], [2].

The greatest catastrophe in the nation's history caused by a hurricane was Hurricane Katrina. It made the first landfall in August 25, 2005, on the southeast coast of Florida as a Category 1. It gained strength to a Category 5 as it crossed Florida into the Gulf of Mexico. It then weakened to a Category 3 hurricane when it crossed into southeast Louisiana and Mississippi. Hurricane Katrina was different from Hurricane Andrew that Hurricane Katrina caused the greatest damage due to storm surge flooding, whereas Hurricane Andrew caused extensive damage due to high wind. The amount of damage caused by Hurricane Katrina was up to $81.2 billion dollars in insured losses.

The storm also caused 1,800 deaths that made it the largest-natural disaster in the U.S history [1], [2].

Table 2.2. Saffir-Simpson Hurricane Scale

Strength	Sustained Wind Speed (mph)*	Sustained Wind Speed (mph)**	Typical Damage
Category 1	74-95	89-116	Minimal: no real damage is done to structures on permanent foundations.
Category 2	96-110	117-134	Moderate: some trees are toppled; some roof coverings are damaged; major damage is done to manufactured homes.
Category 3	111-130	135-159	Extensive Damage: large trees are toppled, some roofs are damaged, some manufactured homes are destroyed, and some structural damage is done to small homes and utility buildings.
Category 4	131-155	160-189	Extreme Damage: extensive damage is done to roofs, windows, and doors; roof systems on small buildings completely fail; some curtain walls fail.
Category 5	>155	>189	Catastrophic Damage: roof damage is considerable and widespread; window and door damage is severe; there are extensive glass failures; some buildings fail completely.

*1minute sustained over open water; ** 3 second wind gusts over open water

2.1.3—Post-Disaster Assessments, Research, and Design Development

Following tornado and hurricane disasters, FEMA [1], [2], [3] sent out field investigators to "inspect building damage impacted by storm, assess the performance of the buildings evaluate design and construction practices, and evaluate building code requirements and enforcement in order to make any recommendations for improving building performance in future storm events."

During assessments conducted after many extreme-wind events, field investigators have found that most buildings in the affected areas failed because of inadequate of design and construction, application of inappropriate design criteria and standards, and building components [1], [2]. They have found that most critical facility such as the fire stations, police stations, community shelter, hospital, and assisted daycare facilities were quite old and were constructed well before the introduction of modern codes and standards. Since these buildings were not designed up to codes and standards, where the design wind speeds are much greater than the ones the buildings were originally designed for, these building were most vulnerable to damage. As a result, when tornado winds or hurricane winds hit the buildings with greater wind forces than the building's design wind forces, these building suffered damage. In addition, these buildings failed because (1) most building components such as roofs, windows, or doors had deteriorated due to inadequate maintenance, (2) the impact of the flying debris (referred to as windborne debris missiles) caused by the extreme-wind forces. They found that the wind speeds were high enough that caused the missiles to be thrown at a building with enough force to penetrate the windows, roof, or walls.

Since the building science issues associated with poor building performances from the impact of high wind events were summarized by FEMA, many research institutes have been focused on wind subjects to improve building performances. Since the early 1970s [2], there have been studies conducted to determine design parameters for shelters intended to provide protection from extreme-wind events. Studies conducted to provide protection from tornadoes and hurricanes have been involved with construction materials such as steel, concrete, wood, and FRP to resist windborne debris impact. The

building members of interest from past studies included roof, walls, windows and doors. FEMA had developed design guidance and construction plans specific for providing shelter from extreme-wind events [1], [2], [3]. Most of the results of research, guidance and recommendations from FEMA are obtained from many research institutions that have provided FEMA with various important findings. Table 2.3 shows a listing of safe room and shelter publications and guidance documents that have been produced by FEMA over the past 32 years [1].

Table 2.3. Past FEMA Safe Room and Shelter Publications and Guidance [1]

Date	Publication
April 1976	FEMA TR-83B, *Tornado Protection: Selecting and Designing Safe Areas in Buildings*
September 1980	FEMA TR-83A, *Interim Guidelines for Building Occupant Protection From Tornadoes and Extreme Winds*
September 1998	FEMA 320, *Taking Shelter from the Storm (First Edition)*
May 1999	FEMA *National Performance Criteria for Tornado Shelters*
August 1999	FEMA 320, *Taking Shelter From the Storm (Second Edition)*
July 2000	FEMA 361, *Design and Construction Guidance for Community Shelters*
October 2001	FEMA 388, Safe Room and Shelter Resource – CD
November 2003	FEMA 431, *Tornado Protection- Selecting Refuge Areas in Buildings*
March 2007	*2007 Florida Tornado Outbreak- Tornado Recovery Advisories*
September 2007	*Greensburg, KS Tornado- Tornado Recovery Advisories*
August 2008	FEMA 361, *Design and Construction Guidance for Community Shelters,(Second Edition)*

2.2—Characteristics of Extreme Winds

This section provides information about characteristics of extreme winds and their effects on buildings. Section 2.2.1 provides information about the general wind effects on buildings. Section 2.2.2 provides information about the effects of extreme winds. Section

2.2.3 described the building failure modes. Section 2.2.4 provides information about the cyclic loading of tornadoes and hurricanes. Section 2.2.5 discusses the windborne debris impact resulted from tornadoes and hurricanes. Section 2.2.6 describes forces generated by the design wind speed.

2.2.1—General Wind Effects on Buildings

Both positive and negative pressures occur simultaneously when wind interacts with a building as shown in Figure 2.1. Figure 2.1 shows the typical-wind pressure around a rectangular building, where the pressure is positive on the windward wall. The leeward wall, sidewalls and roof all have negative pressure. Positive pressure means that pressure is acting toward the surface of a structure, and negative pressure means that suction is acting on the surface of a structure. Wind forces on various parts and components of the buildings depend on both the external and the internal pressures. For this reason, buildings must be designed with sufficient strength to resist the wind-induced pressures (positive and negative pressures) to prevent building failure. If they are not designed and constructed to withstand the wind forces, then they are more likely to fail. Properly design to transfer the load through the structural system to the foundation into the ground is a crucial consideration to prevent any building failures.

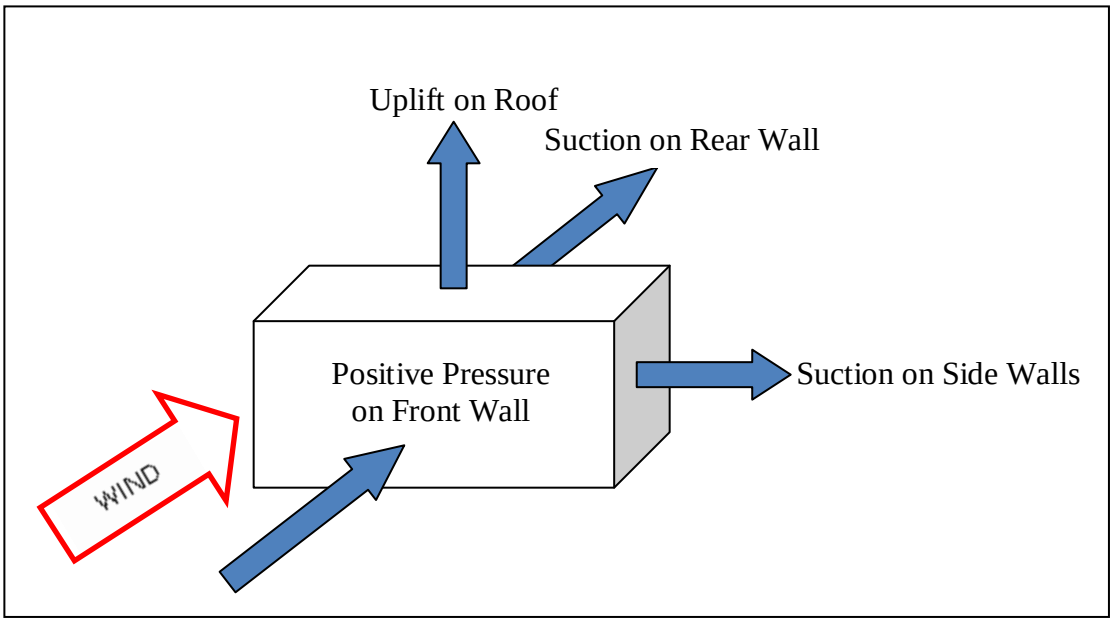

Figure 2.1. Illustration of Wind-Induced Pressure on a Building.

2.2.2—Effects of Extreme Winds and Tornado Forces

Windstorms can cause several damages to a building. It is important to know that extreme-wind speeds are not constant when they strike a building. They rapidly increase and decrease because of the changes in wind directions. For example, a blocked, neighboring building that is in the path of the wind causes the wind to change direction and increases wind load on buildings nearby. The effects of fluctuating-wind speeds and changes in wind direction increase wind loads on the buildings nearby. As a result, the building nearby may fail, depending on the design strength of the building components. Building components include building connections, doors, and roof.

A door or window left open during a storm can influence the magnitude of internal pressure. The internal pressure of the building increases when the building is changed from “enclosed” to “partially enclosed” building [6], [7]. The variation of the

internal pressure of a building with an opening condition is illustrated in Figure 2.2 and Figure 2.3.

It can be seen from Figure 2.2 that a single opening exists on the windward side of the building, and no openings exist elsewhere. When the building is pressurized, the internal pressure pushes up on the roof. The push from below the roof and suction on top the roof creates an increase upward wind pressure (uplift) on the roof. The side and rear walls also experience from the push of internal pressure. The forces due to internal pressure are in the same directions as those due to the external pressure for the roof and the three suction walls. The combination of the outward push and the suction on the exterior side of these walls cause large-wind loads on the roof and the suction walls. As a result, the rapid, build-up internal pressure can blow the building apart.

Contrarily, when the building is depressurized as shown in Figure 2.3, (where the only opening is on a suction cladding such as the leeward wall, sidewalls, or roof), the magnitude of the uplift pressure exerted on top of the roof decreases while the internal pressure pulls the roof down. In addition, the decreased internal pressure also pulls on the windward wall, which increases the wind load on the windward and reduces wind loads on the suction sides as seen in Figure 2.3. In such cases, the increase in wind load may cause a structural system to fail. Therefore, it is critical to have the walls, roof, and connections between the building components design for the largest-possible combination of external and internal pressures in order to protect a building from windstorms. In addition, a building should be designed as an enclosed building with no large or dominant openings to minimize the internal pressurization from a wind event.

The variation of internal pressure with building openings as described in the previous paragraphs has profound implications. For instance, if during a high wind, a person opens windward door, or leeward door, or window of a house that allows the wind to enter the building, he or she greatly increases the chance that the roof will be lifted off due to increased internal pressure. The loss of the roof may in turn cause wall failure and destruction of the entire house. Likewise, once a windward door or window is forced open by high winds, or broken by windborne debris, the house may be endangered in the same manner.

In order to overcome the internal pressure issues, the ASCE 7-05 wind design procedure [6] accounts for the influence of internal pressure on the wall and roof loads. It provides positive and negative internal pressure coefficients for used in the load calculations. As described in the ASCE 7-5 code, partially enclosed buildings are buildings that are designed to accommodate full pressurization; enclosed buildings are buildings that intend to experience little internal pressurization; buildings that do not experience internal pressurization are referred to as opened buildings.

Not only are the strength and stability major concerns when extreme winds strike, flying debris impact from these windstorms can cause damage to a building. When wind speeds are high enough, they can throw missiles with enough force to infiltrate the windows, walls, or roofs of a building. Extensive testing by the Texas Tech University [3] and other wind engineering research facilities has shown that walls, ceilings, and doors commonly used in the house construction cannot withstand the impact of missiles carried by extreme winds. For example, according to the research done by the Texas Tech University [3] and Uddin [8], an object such as a 2 x 4 wood stud weighing 15 lbs can

have a horizontal speed of 100 mph, when carried by 250 mph wind. This horizontal speed travels with enough speed to penetrate most common building materials used in houses today. Even a reinforced masonry wall will be penetrated unless it has been designed and constructed to resist debris impact during these events, as seen in Figure 2.4.

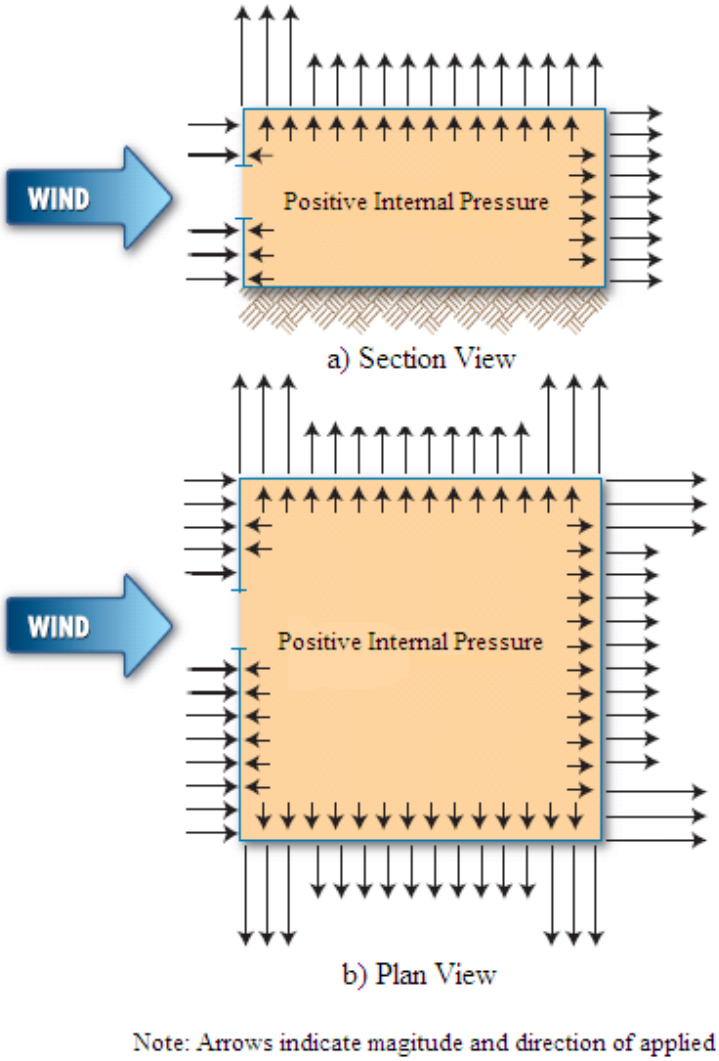

Figure 2.2. Schematic of Internal Pressure Condition when the Dominant Opening is in the Windward Wall [1].

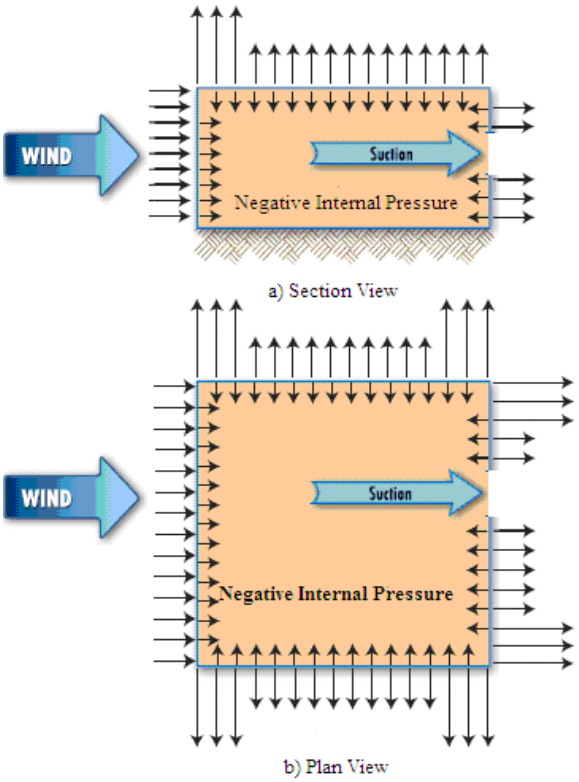

Figure 2.3. Schematic of Internal Condition when the Dominant Opening is in the Leeward Wall [1].

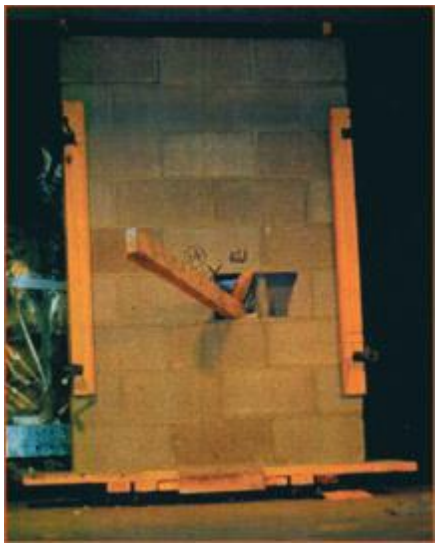

Figure 2.4. 2 x 4 Wood Stud Launched at 100 mph Pierces Un-reinforced Masonry Wall [3].

2.2.3—Building Failure Modes- Elements, Connections, and Materials

The wind forces act on a building as both inward-acting and outward-acting forces (see Section 2.2.2). The direction and magnitude of forces are controlled by the direction of the wind, location of the building, height, shape of the building, and other conditions based on the terrain surrounding the building [7]. Winds move around a building may cause a structure to experience translation (sliding), overturning, racking, or material failure, if the winds are higher than the design wind loads (Figure 2.5).

When there is a gap in wall continuity, the building is exposed to vulnerability that causes it to fail by one or a combination of the four failure modes. A sliding failure occurs when wind forces move around a building that causes the building to slide laterally and off its foundation. An overturning failure occurs when a combination of the lateral and vertical wind forces cause the entire building to rotate about one its side. A racking failure occurs when the building remains connected to the foundation system while the building's structural system fails laterally. Lastly, a material failure occurs when the materials of the building are struck by high-wind events or windborne debris impacts. Component failures may be either full-system failures or individual element failures.

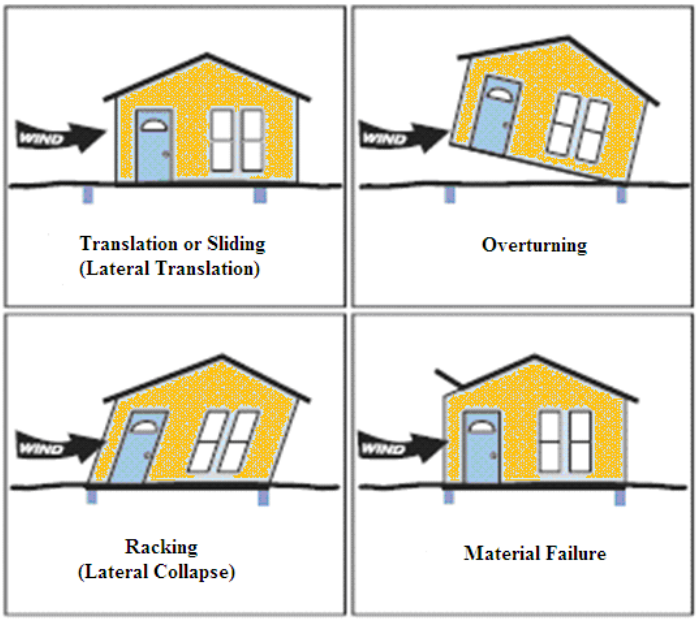

Figure 2.5. Building Failure Modes Due to Wind Moving Around a Building [1].

To prevent a building failing as a whole, it is recommended by FEMA 361 [1] and ASCE 7-05 [6] that a building should have a continuous load path to prevent any disrupted operations in the shelter. A continuous load path means that the loads must be transferred from the Components and Claddings (C&C) to the Main Wind Force Resistance System (MWFRS), where in turn they must be transferred through the foundation into the ground. The MWFRS acts as the main structural system of the building that works to transfer wind loads to the ground. The MWFRS consists of diaphragms, roof systems, frames, cross bracing, and load bearing walls. C&C elements include wall, roof members (e.g., joints, purlins, and studs), windows, doors, fasteners, siding, to name a few. C&C elements receive wind loads directly and then transfer the loads to other components or the MWFRS. The continuous load path can be achieved by creating continuous sheeting from one floor to the next and connecting sheeting to the

foundation where joist must be intact. The building must have continuous load path to limit the effects of local collapse, and to prevent or minimize progressive collapse after the loss of one or two primary structural members, such as a column.

2.2.4—Cyclic Loading

The nature of tornado and hurricane winds is unpredictable and destructive. Both tornado and hurricane winds have unsteady wind patterns within their circular wind field [1], [6], [7]. These effects cause cyclic loading on buildings. Cyclic loading is particularly important when either a structure or component is flexible or when the fastening system receives repetitive loading. Tornado winds typically affect a site in a very short time, while hurricane winds affect a site for a very long time. Wind experts believe that cyclic periods in tornadoes are short and less frequent than those cyclic periods in hurricanes. Therefore, cyclic loading is not recommended in design of tornado shelters, but hurricane shelters are recommended to include cyclic loading in design [1].

2.2.5—Windborne Debris – Missile

Besides determining the appropriate wind pressures for a shelter, windborne debris impact is another issue that needs to be considered in design. Tornado and hurricanes produce a large amount of debris that becomes airborne. If wind speeds are significant enough, flying objects can be thrown at a building with enough force to penetrate windows, walls, or roof that may kill or injure occupants inside the building [1], [7].

2.2.6—Forces Generated by the Design Wind Speed

The design wind speed for a community shelter should be determined from a wind speed map of a design standard. The reason is that most wind-speed maps in use today reflect a specific MRI that was adopted as a risk factor for that design standard [1], [7]. The design wind speed is used to predict forces on both the MWFRS and C&C.

The effects of wind on a building in accordance to ASCE 7-05 [6] and Liu [7] can be summarized as follows:

- Inward-acting pressures act on the windward walls are considered positive pressures.
- Outward-acting pressures act on the leeward walls, and sidewalls are considered negative pressures.
- Airflow separates from building surfaces at sharp edges and at points where the building geometry changes.
- Windows, doors, and other openings are subjected to wind pressures and the impact of windborne debris. If the wind pressures or windborne debris causes any windows or doors, for example, to fail, then the entire building becomes subjected to higher wind pressures as compares to the building remained fully enclosed.
- Negative pressures and localized suction at ridge, eaves, edges, and the corners of the roofs and walls might affect the loads on C&C because these pressures are caused by turbulence and flow separation.

The design wind load for a community shelter depends on many factors. The magnitude of the design wind loads is a function of the following primary factors:

- *Exposure*. The characteristics of the terrain surrounding the building influence the wind loading. Some of the characteristics include the general roughness of the surrounding terrain, including open, built-up, and forested areas. Beside coefficients for internal and external pressures, ASCE 7-05 also incorporates the exposure condition for determining the design wind speed. It defines three exposure categories: B, C, and D. Exposure B is the roughest terrain, and exposure D is the smoothest terrain. Exposure B includes urban, suburban, and wooded area. Exposure C includes flat open terrain with scattered obstructions and is adjacent to water surface in hurricane-prone regions. Unlike Exposure C, Exposure D includes areas adjacent to water surface outside hurricane-prone regions. One point to note with the exposure condition is that the smoother the terrain, the higher the wind pressure, and the rougher the terrain, the lower the wind pressure. Therefore, a shelter located in Exposure C would receive higher wind loads than those located in Exposure B, even at the same basic wind speed.
- *Basic wind speed*. ASCE 7-05 provides the basic wind speed map for determine the design wind loads. The basic wind load for design depends on what region and location of the shelter. It is important to note that the basic wind speed is measured at 33 ft above grade in Exposure C (flat open terrain). If a building is located in Exposure D, or B, rather than C, then an adjustment must be accounted for in the design wind load. An adjustment for the actual exposure is made in the ASCE 7-05 calculation procedure.

- *Topography*. Land surface elevations such as escarpments or isolated hills can create a speedup effect of wind. Therefore, a building located near the flat land has lower wind pressures than a building located near a ridge. ASCE 7-05 also accounts for this matter.
- *Building height.* As height of a building above ground increases, wind speed increases. The higher the building, the greater the wind pressures. ASCE 7-05 provides procedure to account for building height.
- *Building shape*. The configuration of the building also influences wind loads. Building shape affects the value of pressure coefficients, and, therefore, the loads applied to various building surface. For example, the steeper the slope of the roof, the lower the uplift loads. The uplift loads on a low-slope roof are larger than the uplift load on a gable or hip roof. Therefore, roof shape plays a significant role in roof performance, both structurally and with respect to the magnitude of the wind loads.
- *Internal pressure* (building pressurization/depressurization). An opening during a storm can greatly influence the magnitude of internal pressure. See Section 2.2.2 above for more detail.

2.3—Protection Objectives

The main objective of designing the shelter is to protect the occupants inside the shelter. This section describes issues relating to the protection objectives. However, the guidelines presented as follows will help one in knowing what to do before, during, and after a tornado.

Tornado winds occur rapidly and frequently, while hurricane winds do not. That is why this section will dissuss risk assessments for tornado winds, not for protection against flooding. When a tornado is coming, one only has a short amount of time to make life-or-death decisions. Therefore, advance planning and quick response are the keys to survive the threats of a tornado. These are a few guides [9] that help one preparing for a tornado:

Before a tonado,

- Conduct tornado drills each tornado season.
- Designate an area, for example a home, to be used as a shelter, and practice having everyone in the family go there in response to a tornado threat.
- Make sure everyone know the difference between a “tornado watch” and a “tornado warning.”
- Contact the local emergency management or listen to the forecast for more information on tornadoes.
- Have disaster supplies on hand.
- Develop an emergency communication plan to make sure everyone in the family can get back together.
- Pay attention to tornado watches and warnings. A tornado watch is issued by the National Weather Service when tonardoes are possible in areas. A tornado warning is issued when a tornado has been sighted or indicated by weather radar.

During a tornado,

If at home:

- Immediately go to one's designated storm shelter. If he/she doesn't have a storm shelter, it is recommended that he/she should go to the lowest level of the house such as the basement.
- If there is no basement, he/she should go to an inner hallway or a smaller inner room without windows, such as a bathroom or close. According to FEMA [1], small room usually survives a tornado.
- Stay away from windows and doors. They are the critical components of buildings that often fail.
- Stay away from corners because they tend to attract debris.
- Get under a piece of furniture to cover head.
- Use arms to protect head and neck.
- If in a mobile home, get out and find shelter elsewhere.

If at work or school:

- Go to the designated storm shelter.
- If there is no storm shelter available, go to the basement or to an inside hallway at the lowest level.
- Avoid places with wide-span roofs such as auditoriums, cafeterias, large hallways, and so on.
- Get under a piece of furniture to cover head.
- Use arms to protect head and neck.

If outdoors:

- If possible, get inside a building.
- If shelter is not available or there is no time to get indoors, lie in a ditch or low-lying areas or crouch near a strong building. Be aware of the potential of flooding.
- Use arms to protect head and neck.

If in a car:

- Never try to out drive a tornado in a car or truck. Tornadoes can change directions quickly and can lift up a car or truck and toss it through the air.
- Get out the car immediately and take shelter in a nearby building.
- If there is no time to get indoors, lie in a ditch or low-lying areas or crouch near a strong building. Be aware of the potential of flooding.

After a tornado,

- Help injured or trapped persons.
- Give first aid when appropriate. Don't try to move seriously injured unless they are in immediate danger or further injury.
- Call for help.
- Turn on radio or television to get the latest emergency information.
- Stay out of damaged buildings. Return home only when authorities say it is safe.
- Leave buildings if there are gas and chemical fumes.
- Take pictures of building and property damages for insurance purposes.

- Inspect utilities in a damaged home for gas leaks, electrical system damage, sewage and water lines damage.

2.3.1—Occupant Safety

This research presents guidance to design a community shelter that would protect occupants during high wind-events. The primary objective of this research was the safety of the occupants within the shelters. It was intended to minimize the probability of death or injury during a high wind-event by providing protection to its occupants.

2.3.2—Occupant Risk Levels and Life Safety

It is important to know that not all parts of the United States have the same equal risk of death or injury from tornadoes and hurricanes. The design wind speeds for shelters can be obtained from the wind speed map shown in Figure 2.6. It is important to know that design wind speeds from the wind speed map are based on the combination of tornado and hurricane wind threats. Therefore, designing shelters for a particular region of the United States based on the wind speed map will meet the design criteria of building codes, which is to protect occupants inside the shelters. This paper was intended to guide one through the process of identifying the risk of severe winds in a particular region and mitigating that risk.

2.3.3—Design Limitations

Design codes, which are actually laws or ordinances, specify minimum design loads, design stresses, construction types, material quality, and other factors. They vary

considerably from city to city, a fact that causes some confusion among architects and engineers.

No matter how many specifications are written, it is impossible for building codes to cover every possible design situation. As a result, no matter which building code or specification is or is not being used, the ultimate responsibility for the design of a safe structure lies with the structural designer. Perhaps the most important and most difficult task faced by the structural designer is the accurate estimation of the loads that may applied to a structure during its life. Nevertheless, the estimation of these forces can by no means be classified as an exact science. The magnitudes of wind loads vary with geographical locations, heights above ground, types of terrain surrounding the buildings, including other nearby structure, and other factors. No loads that may reasonably be expected to occur may be overlooked. After loads are estimated, the next problem is to determine the worst possible combinations of the loads that might occur at one time.

The accurate calculation of the most severe wind pressures that need to be considered for the design of buildings is quite an involved problem. Obviously the intent of this research was that the loading used for design be the one that caused the largest stresses. In addition, the intent of the research was not to override or replace current codes and standards for designing a safe community shelter against high wind events, but rather to provide important guidance and design of the shelter, where none has been available before.

2.4—Risk Assessment Concepts

The decision to design and construct a shelter can be based on a single factor or a collection of factors. The potential for loss of life or injury is usually the main single factor, while a collection of factors includes the type of hazard event, probability of event occurrence, severity of the event, possible single and total annual event deaths, shelter costs, and results benefits and costs of the shelter project. This section describes the risk assessment concepts.

2.4.1—Design Wind Speed Map for Risk Assessment and Shelter Design

To mitigate the risk of high wind events such as tornadoes and hurricanes, FEMA 361 [1] has produced a map of extreme wind speeds that is consistent with the wind speed map of the ASCE 7-05 [6]. Figure 2.6 shows the design-wind speed map based on combined tornado and hurricane threats that reflect different wind speeds within different geographic regions of the United States. The United States has been divided into four zones that geographically reflect the number and intensity of extreme windstorms. Each zone of the map has its risks, meaning that not every part of the United States has equal risks. Zone 4 on the map has experienced the strongest tornado activity, whereas, Zone 3 has experienced significant tornado activity and includes areas that are susceptible to hurricanes [1], [6]. For example, Alabama falls within Zone 4 region of the wind speed map; therefore, a community shelter would be designed for the extreme wind speed of at least 250 mph to resist extreme wind events.

The design professionals can use the wind speeds shown on the map to design a shelter that provides protection for a specific geographic region within the United States.

The shelter design in this research was based on extreme wind speeds and the primary consideration was the life safety. FEMA 361 [1] recommends design wind speeds for shelters that range from 130 to 250 mph for tornado hazards and from 160 to 255 mph for hurricane threads, depending upon the locations. Therefore, a design wind speed of 250 mph is considered a reasonable maximum design wind speed for the entire country. However, according to the Fujita Scale (Table 2.1) that rates past tornado intensity, F5 tornadoes have wind speeds between 261 and 318 mph. Because of this factor, the chosen wind speed for the research was taken as 300 mph as the average wind speed of Fujita Scale F5.

The tornado and hurricane design wind speeds for shelter design are unified to one averaging time of 3 seconds [1], [6], [7]. The wind speeds stated on the map are 3-second gusts, Exposure C, and correspond to an elevation of 33 ft above grade [1]. The resulting 3-second gusts are consistent with the reference wind speeds used in the ASCE 7-05 [6]. Ultimately, they can be used in conjunction with the ASCE 7-05 to determine the design wind loads for community shelters as will be discussed in Chapter 4.

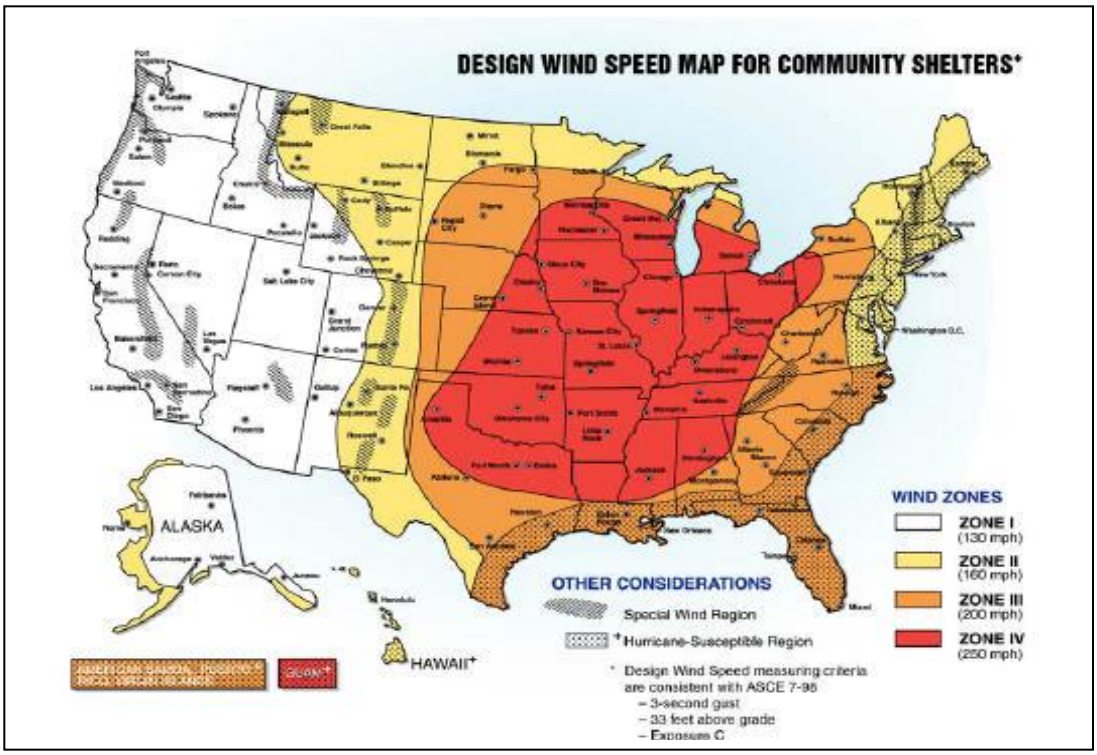

Figure 2.6. FEMA 361 Design Wind Speed Map for Community Shelters [1].

2.4.2—Tornado and Hurricane Histories

An important factor in the decision-making process of whether to design and construct a community shelter for protection against high wind events is the history of occurrence of tornado and hurricane in a given area. Figure 2.7 presents the recorded historical data of F3, F4, and F5 tornado occurrence per 1,000 square miles in the United States [1]. As one can see, the probability of occurrence is depended upon the location. As shown in Figure 2.7, only a few areas of the county frequently experience tornado, and the west experiences very little tornadoes. The design wind speed map from FEMA 361 [1] was developed from the history of hurricanes from 1900 to 1999. The historical data indicated that there were 79 Category 3, 4, and 5 hurricanes struck the southeast and gulf coast states during that time [1].

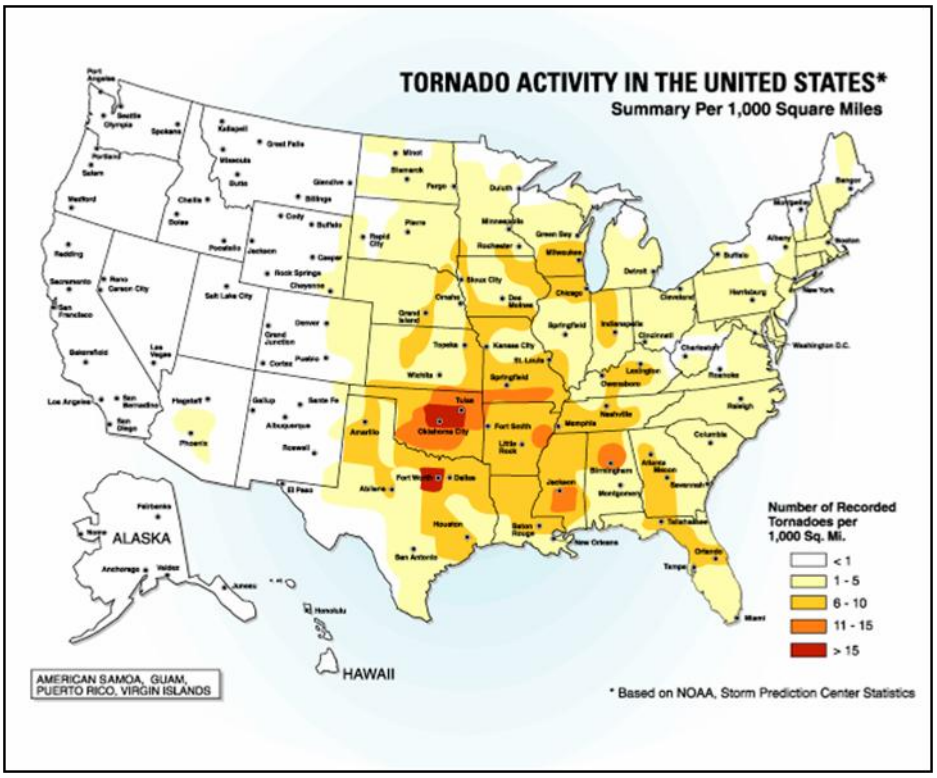

Figure 2.7. Tornado Occurrence in the United States Based on Historical Data [1].

2.4.3—Single and Annual Event Deaths

Another important factor in decision-making process to design and construct a community shelter to protect occupants from high wind events is the number of deaths linked with an event. Annualized data on event deaths contributes to decision-making process to construct or not construct a shelter at a given site. FEMA 361 [1] states: "regardless of the probability of a high-wind event occurring at a given site, a certain number of deaths are a good enough reason to construct a shelter."

2.4.4—Evaluating Existing Areas to be Used as a Shelter

Before one decides to build a shelter, evaluating shelter areas in an existing building helps one to determine if an entire building or a section of the building can be used as a potential shelter area. In addition, it helps to recognize possible ways to make existing areas safer, and it helps to determine whether it is needed to design for a stand-alone shelter. A preliminary evaluation may be done by a design professional.

2.4.5—Shelter Costs

Another important factor that must be considered in the decision-making process of constructing a shelter is the costs of shelter. Costs for the design, construction, and maintenance of community shelters will depend on location and construction type. Many of the shelter costs are associated with entire building dimensions, shelter area, shelter-construction type, location, mitigation construction costs, mitigation maintenance costs, mitigation useful life, and mitigation effectiveness against injury and mortality for various wind speeds. Developing benefit and cost models will help one in determining whether the shelter should be designed and constructed.

2.5—Fiber Reinforced Polymer (FRP) Composites

This section describes the overview, applications, characteristics and design considerations of FRP composites.

2.5.1—Overview of Composite Materials

For many years, civil engineers have been in search for alternative materials to steel, concrete and wood to combat the high cost of repair and maintenance of structures damaged by corrosion, disintegration, and heavy use [4]. For example, cost estimates for maintenance of bridge decks composed of steel-reinforced concrete are up to $90 billion dollars per year [4]. This represents only a small portion of all the bridge infrastructures not included all the housing infrastructures that have problems with corrosion. The problem of maintaining structures corrosion free is the high cost of maintenance over the years, which makes steel not so desirable for construction. Another problem that is associated with the housing industry is the usage of wood, which often disintegrates when associated with water.

Incremental thinking and engineering refinements have led to better visions and are beginning to emerge on the composite materials in a significant way. Since 1940s, composite materials have gained popularity in the engineering field for their high structural performance [4]. FRP is relatively a new class of composite material manufactured from fibers and resins. FRP composites have proven efficient and economical for the development and repair of new and deteriorating structures in civil engineering. In addition, they are currently being designed and implemented in various fields, including aerospace, naval vessels, transport vehicles, infrastructure, sports and marine for their load bearing capability, design flexibility, high strength at low weight, and ease of making of complicated shapes [10].

The key components of composites are reinforcing agents and matrix. FRP (or commonly called Polymer Matrix Composites (PMC)) is normally organized into a

laminated structure such that each lamina (or flat layer) contains an arrangement of unidirectional fibers implanted within a thin layer of light polymer matrix material. A great deal of research has been focused on the different fiber types, fiber-to-matrix volume fraction, architecture, and orientation. The common fiber reinforcement occupies 30% - 70% of the matrix volume in the composites [11].

Fiberglass, aramid, and carbon are the most common types of fibers used in advanced composites for structural applications. The fibers act as the reinforcement and provide the strength and stiffness. The fibers are available in different forms such as continuous, chopped, woven, non-woven, stitched, braided, multi-axial, and combinations of these. There are two types of matrices known as thermoset and thermoplastic. Their roles are to bind and keep the fibers from damage, and transfer the stresses between the fibers. Common thermoset matrices are polyester, epoxy or nylon. A common thermoplastic matrix is polypropylene (PP). Other substances, such as fillers, can be used to improve process-ability and dimensional stability [11].

The mechanical properties of a composite are a combination of the properties of the constituent polymer and fibers. The properties of composites depend on many variables such as fiber types, orientations, architecture, fiber volume fraction, the interface between the fiber and the matrix, and the presence of porosity, cracks and defects [4], [12], [13]. The fiber architecture refers to the braiding, knitting, or weaving configuration of the fibers. A composite can be made from different fiber types and directions. For this reason, composites are considered anisotropic materials and their strengths vary with the fiber directions. Their stress-strain curve is linearly elastic up to the point of failure by rupture (Figure 2.8). Composites have many excellent structural

qualities including high strength, material toughness, and fatigue endurance, lightweight, high resistance to elevated temperature, abrasion, corrosion, and chemical attack.

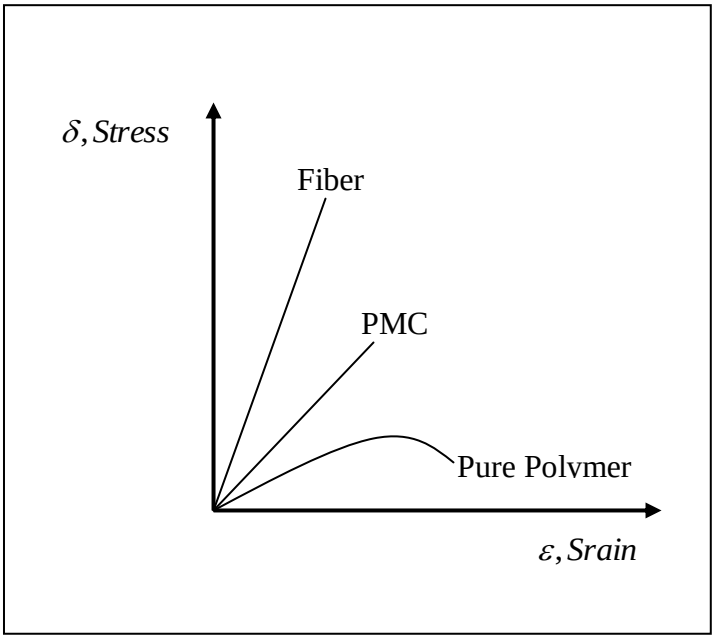

Figure 2.8. Schematic of Composite Strength, Which is based on the Modulus of Polymer and Fiber.

The advantages of using composites in structural members include the ease of manufacturing, fabrication, handling, erection, and short delivery time [4], [13]. Due to the composite natures for high performance and extended service life, they can be formulated and designed to tailor and meet any desired specifications. If durability can be proven to last 75 years, composites can be economically justified using life cycle cost method.

Some of disadvantages in the use of composites, for example, in bridges, are high first cost, creep, and shrinkage. The composites have a potential for environmental degradation, for example, alkalis' attack and ultraviolet radiation exposure. In addition,

there is a lack of design specifications, joining and/or fastening system technology, guidelines, standards, testing methods and methodologies to develop composites. Because of the use of thin sections, there are concerns in local and global buckling [4].

2.5.2—Sandwich Composites

Another composite beside the laminated composite is a sandwich composite. Sandwich composite designs have been established as structurally efficient members that provide an excellent combination of high stiffness and strength. They are typically comprised of two identical, thin faceplates and a thick, relatively weak, core. The faceplates are bonded to the core using strong adhesives to achieve load transfer between the components. The faceplates are used to carry all, or almost all, of the bending and in-plane normal load. Conversely, the core is assumed to carry the entire transverse load [10].

The core of a sandwich structure, in general, falls into four types: (a) foam or solid core, (b) honey foam core, (c) web core, and (d) truss core (Figure 2.9). Different core types can be used depending upon the application. A foam core sandwich (Figure 2.9a) is a sandwich composite filled with foam core in the middle of the two faceplates. A honey foam core sandwich (Figure 2.9b) and a web core sandwich (Figure 2.9c) are composite sandwiches where the cores of the composites are in the form of honeycomb and have some interstitial spaces in them. A truss core sandwich (Figure 2.9d) is a sandwich structure that has the core arranged in truss-type series. Each core provides its own advantages and can be used depending upon the application.

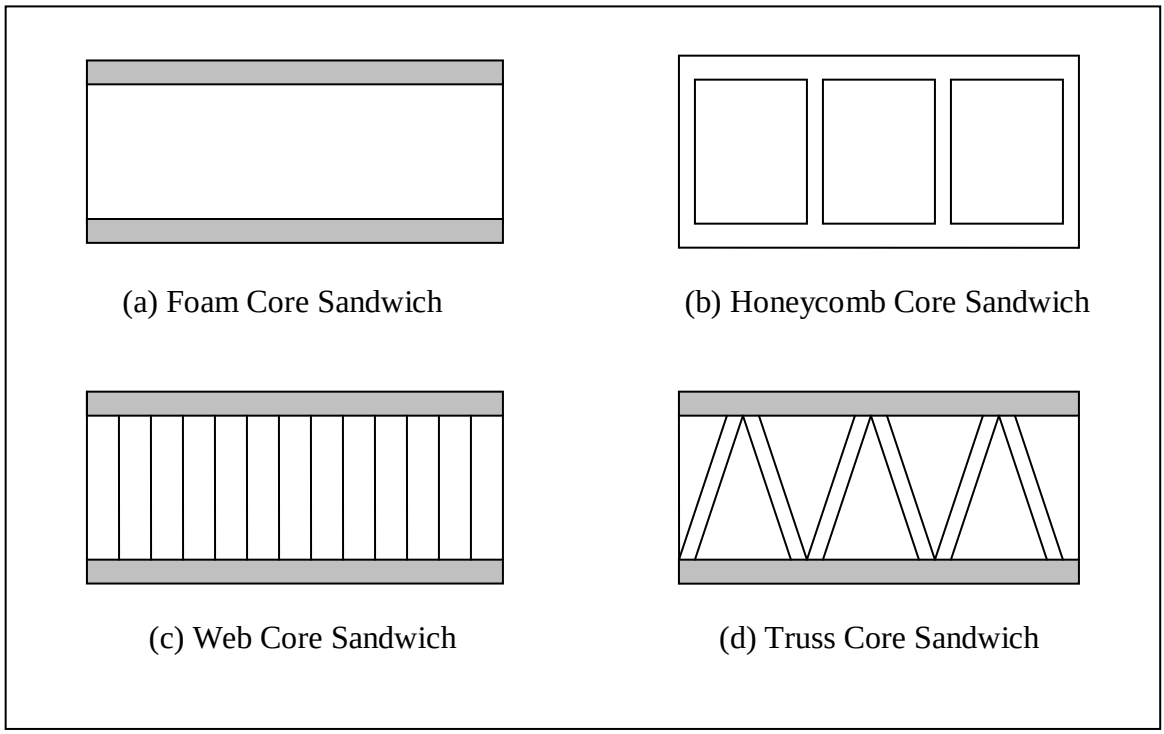

Figure 2.9. Different Types of Foam Core of Sandwich Structures.

2.5.3—Glass Fibers

Glass fibers were chosen as the reinforcement for both models proposed in this research because they offer high performance to cost ratio [14]. They possess high strength and stiffness, which are suitable for even primary structural applications, such as indoor elements in housing, and temporary outdoor applications like low-cost housing for defense and rehabilitation.

2.5.4—Polypropylene (PP) and Polyester Polymers

Before deciding to build an FRP panel, it is important to understand the roles and general behaviors of the polymer for thermoset and thermoplastic composites in certain applications where the plastic material must give structural support. The difference

between thermoset and thermoplastic polymers is the type of crosslinking or crystallinity bond in their structures [15]. Crosslinking is an important structural factor that contributes to high elastic properties. Crosslinking is made from the chemical reactions between the materials' molecular chains during the curing process in which permanent bonds are achieved between the molecular chains.

Many polymers can be obtained in a range of crystallinity, which allows the designer a wide choice of material property. Crystallinity is a basic property of plastics that should be considered in the selection of a polymer for any application [15]. Crystalline describes the regularity of the entanglement of polymer chains. In many polymers, however, the entanglement can be very regular with large regions of the chains packaging together to form closely repeating structural patterns, as illustrated in Figure 2.10. When this happens, these regularly packed regions are called crystals and the polymer is said to be crystalline. The region that is without shape is called the amorphous region.

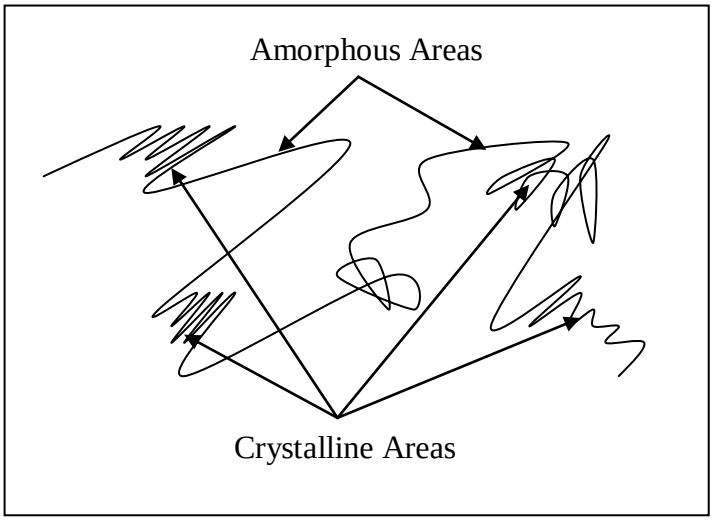

Figure 2.10. Crystalline and Amorphous Regions in a Polymer Structure.

The areas of crystallinity are composed of repeated chains that are held together by crystal bonds or commonly called as secondary bonds. These bonds are responsible for the physical properties of polymers. Higher degree of crystallinity results in higher tensile strength and higher density because of the high resistance to movement in the crystalline regions and the need to overcome the intermolecular forces [15]. Furthermore, higher degree of crystallinity results in lower impact energy [15]. Meaning, crystalline regions of a polymer are not as effective in absorbing and dissipating energy as the amorphous regions because the atoms in crystalline regions are not free to move or rotate.

Thermoset polymer such as polyester is a material that cures or hardens into a desired shape through the application of thermal [15]. Thermoset material will not remelt or regain processibility if it had been cured before. The advantages of thermoset polyester include high mechanical properties, chemical resistance, thermal stability, and overall durability.

Opposite of thermoset is thermoplastic. When the polymer is heated, the material becomes soft and turns to fluid at high heat [15]. After it is cooled into a desired shape, the material can be reheated again. The crystallinity of PP structure is about 60-70% [15], which means a lot of heat energy must be added to allow vibrations, rotations and other localized movement. It also means that about 30-40% of the amorphous regions are suitable for impact energy, which is an excellent property for considering in shelter design. Since crystallinity requires a lot of heat energy to break the secondary bonds that hold the structure, it dissolves in specific solvents at very high temperature, meaning it has very sharp melting point. For example, PP dissolves in specific solvents at temperature higher than 100^{o}C. For this reason, thermoplastic polymer is a poor thermal

conductor as compared to metal. Thermal conductivity is a measure of the ability of a material to conduct thermal energy. This lack of thermal conductance allows composites to be used extensively as insulated walls and roof panels. Overall, thermoplastic PP offers advantages in terms of high toughness, superior impact property, easy of reshaping and recycling, and low-cost raw material.

2.5.5—Expanded Polystyrene (EPS) Foam Core

In a sandwich composite structure, the core plays significant roles not only in taking almost all the shear stresses, but also in absorbing impact energy. EPS has been widely used in the housing industry because it possesses the physical and mechanical properties for most insulation specifications [16]. EPS insulation is easily fabricated to meet specific and dimensional requirements. Furthermore, EPS is extremely lightweight, which makes it easy to be shipped, stored, handled, and installed on the job site.

2.5.6—Material Costs

This section compares the cost of the traditional oriented strand board (OSB) SIPs to the cost of CSIPs. The traditional OSB SIPs are consisted of sheet metal or OSB (wood board) and foam core. The OSB represents the facesheets within the SIPs. CSIPs are composite structural insulated panels, which typically consist of fibers impregnated with thermoplastic or thermoset resin and foam core. The fibers impregnated with thermoplastic or thermoset resin represent the facesheets of the CSIPs. CSIPs are generally stronger, stiffer than the OSB SIPs because of strong fibers and thermplastic/thermoset relationships described in the previous sections. Table 2.4

presents the cost of the traditional OSB SIPs and CSIPs. Even though the OSB SIPs are cheaper than the CSIPs, the OSB SIPs do not have good structural properties as the CSIPs. The structural properties of CSIPs include excellent load bearing capabilities, high tensile strength, excellent impact resistance and exceptional insulation.

Table 2.4. Material Cost Comparison of Traditional OSB SIPs and CSIPs

Materials	OSB SIPs ($/ft^2)	CSIPs ($/ft^2)
Facesheets	0.32	3.4
EPS Foam Core	2.07	2.07
Adhesive	0.26	15.70 (film)
		0.12 (spray)
Total	4	24.57 (film)
		8.99 (spray)

Note: The cost of OSB was obtained from [17], cost of composite facesheets for CSIPs from [18], cost of EPS foam from [19], cost of spray adhesive from [20], cost of film adhesive from [21], and total cost of traditional SIPs from [22].

CHAPTER 3

PROPOSED TWO DIFFERENT TYPES OF FRP COMPOSITES

3.1—Material Choice

To make sure that the candidate materials representing the shelter panels offer high structural performance and functional benefits, two types of composites were proposed for the analysis. The first one proposed for the shelter panels featured the CSIPs, whereas, the second one proposed for the shelter panels featured the composite laminated characteristics. The reason for using two different types of composites for the shelter was to give one the options to choose based on the structural performance to cost ratio, superior environmental resistance, high modulus, and strength of each type of composite.

The first model proposed for the analysis was made up of E-glass/PP facesheets and EPS foam core. CSIP was analyzed and modeled as the sandwich composite panel. The second model proposed for the analysis was made up of several layers of E-glass fibers impregnated with polyester resin. Table 3.1 summaries the materials used for the panels of the shelter. From this point on forward of this thesis, the first and second models will be called for short as the sandwich composite model and wire-meshed model, respectively.

Table 3.1. Composite Materials Used for the Shelter

Model 1	Model 2
E-Glass/PP Facesheets and EPS Core (Sandwich Composite Model)	E-Glass/Polyester Laminates with E-Glass Wire-Meshed/Polyester Laminates (Wire-Meshed Model)

3.1.1—Model 1: E-Glass/PP Face Sheets and EPS Foam Core

The first model representing the shelter focused on using a sandwich composite made up of the E-glass/PP face sheets and the EPS foam core. The reason for using CSIP was that CSIP is suitable for external wall panels and floor panels of a structure [13]. In addition, it provides excellent insulation properties, load bearing capabilities, and windborne missiles resistance [13]. Table 3.2 shows the properties of the E-glass/PP face sheets and the EPS core for the sandwich composite panels. Figure 3.1 shows a representation of the CSIP used for the first model in this thesis.

Table 3.2. Properties of E-Glass/PP and EPS Foam Core of Sandwich Composite Model [13]

(a) Properties of E-Glass/PP Face Sheets

Properties	E-Glass/PP Face Sheets	
Fiber Reinforcement	70%, Bi-Directional Fibers	
Tensile Strength	317 MPa	46,000 psi
Tensile Modulus	15,169 MPa	2,200,000 psi
Flexural Strength	414 MPa	60,000 psi
Flexural Modulus	13,790 MPa	2,000,000 psi
Poisson’s Ratio	0.22	0.22
Face Sheet Thickness	0.00304 m	0.12 in
Material Designation	Orthotropic	

(b) Properties of EPS Foam Core

Properties	EPS Foam Core	
Density	1.6 E 7 mg/m^3	1 pcf
Young's Modulus	1.2-1.5 MPa	180-220 psi
Flexural Modulus	0.1-0.2 MPa	25-30 psi
Shear Modulus	1.9-2.2 MPa	280-320 psi
Shear Strength	0.1-0.15 MPa	18-22 psi
Poisson's Ratio	0.25	0.25
Core Thickness	0.1397 m	5.5 in
Material Designation	Isotropic	

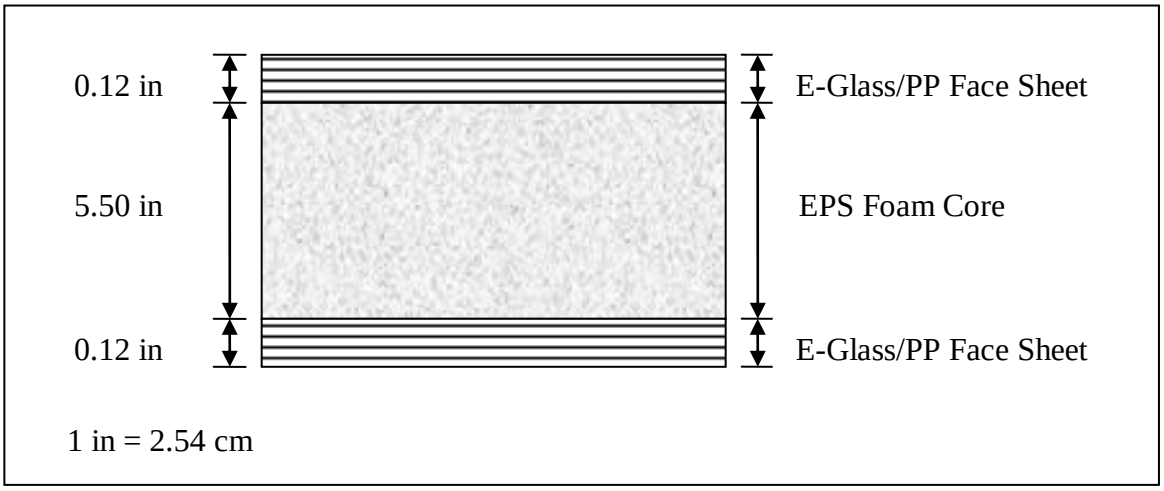

Figure 3.1. Illustration of CSIP of Sandwich Composite Model.

3.1.2—Model 2: E-Glass/Polyester and E-Glass Wire-Meshed/Polyester Laminates

The second model representing the shelter was considered a laminated composite, which was made up of the E-glass fibers impregnated with the Polyester polymer. This model was consisted of two types of E-glass fiber reinforcements. The first type of reinforcement, named Backup Laminate in this thesis, was made up of 25% to 30% glass

content by weight, randomly chopped fibers impregnated with Isophthalic Polyester Resin. The second type of reinforcement, named Wire Laminate in this thesis, consisted of 81% by weight of unidirectional glass fibers impregnated with Isophthalic Polyester Resin. The percent of fiber to volume ratio was 35%. The reason for using these reinforcements was that they offer high bending modulus and impact resistance, which are the properties required to resist extreme wind events. These types of reinforcements within the face sheets can be used to resist high wind events by themselves without combining a foam core as in the first model.

Like its name, the Backup Laminate was used to increase the thickness of the face sheets and offer some stress resistance. The major reinforcement for the analysis was the Wire Laminate, where several E-glass fibers were twisted around each other to give a cord diameter of 0.035 in. (0.0889 cm), as shown in Figure 3.2 [23]. This type of fiber arrangement provides very high tensile load and shear stress, which can be seen in Table 3.3. Table 3.3 shows the properties of E-glass/Polyester laminates and E-glass wire-meshed/Polyester laminates used for the wire-meshed model. Figure 3.3 represents the material orientations of the fibers, which can be read concurrently with Table 3.3. Table 3.4 shows the thickness of each layer corresponding to the layer's name and layer-fiber direction. Figure 3.4 shows the material section of the panel. The second model will be called as the wire-meshed model for simplicity.

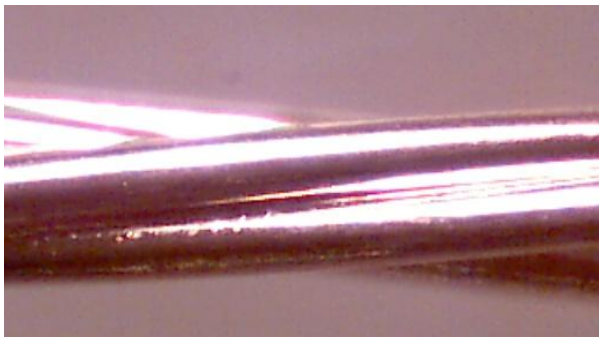

Figure 3.2. Illustration of Several E-Glass Fibers Twisted around Each Other to Give a Cord Diameter of 0.035 inch Within Wire Laminate.

Table 3.3. Properties of Wire-Meshed Model [23]

(a) Backup Laminate Properties

Properties	Backup Laminate	
Fiber Reinforcement	25 % – 30 % Randomly Chopped Fibers	
Material Designation	Isotropic	
Tensile Strength	0.08274 GPa	12,000 psi
Flexural Strength	0.1379 GPa	20,000 psi
Flexural Modulus	6.205 GPa	900,000 psi
Compressive Strength	0.1172 GPa	17,000 psi
Young's Modulus	6.2 GPa	899,234 psi
Density	1500 kg/m^3	0.05419 lb/in^3
Poisson's Ratio	0.33	0.33
Laminate Thickness (Varies)	0.003175 m or 0.0004064 m	0.125 in or 0.016 in

(b) Wire Laminate Properties

Material		Wire Laminate	
Fiber Volume		35 % Unidirectional Fibers	
Young's Modulus	E_x	74.8 GPa	10,848,823 psi
	E_y	7.80 GPa	1,131,294 psi
	E_z	7.80 GPa	1,131,294 psi
Poisson's Ratio	ν_{xy}	0.35	0.35
	ν_{yz}	0.30	0.30
	ν_{xz}	0.35	0.35
Shear Modulus	G_{xy}	4.1 GPa	594,657 psi
	G_{yz}	2.9 GPa	420,609 psi
	G_{xz}	4.1 GPa	594,657 psi
Tensile Strength	*LW*	1,133 MPa	164,211 psi
	CW	1,133 MPa	164,211 psi
Density		3,433 kg/m^3	0.1248 lb/in^3
Laminate Thickness		0.0012192 m	0.048 in
Material Designation		Orthotropic	

LW = Lengthwise
CW = Crosswise

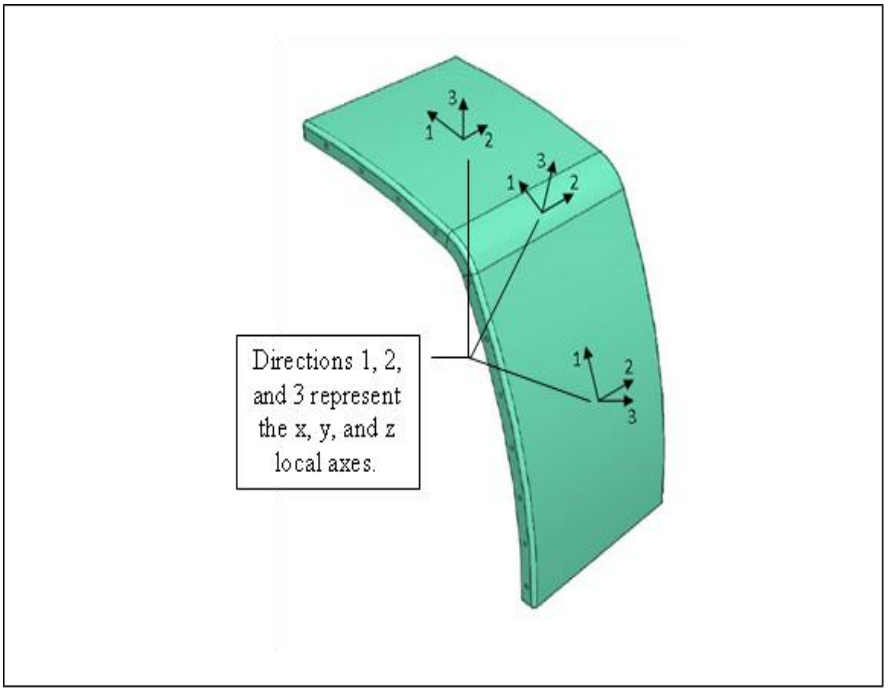

Figure 3.3. Material Orientations of Wire-Meshed Panel.

Table 3.4. Material Layers of Wire-Meshed Model

Layer	Name	Local Fiber Orientation	Thickness (m)	Thickness (in)
1	Gel Coat	0º	0.000508	0.020
2	Backup Laminate,	0º	0.003175	0.125
3	Wire Laminate	0º	0.0012192	0.048
4	Wire Laminate	90º	0.0012192	0.048
5	Wire Laminate	90º	0.0012192	0.048
6	Wire Laminate	90º	0.0012192	0.048
7	Backup Laminate	0º	0.0004064	0.016
8	Wire Laminate	0º	0.0012192	0.048
9	Wire Laminate	0º	0.0012192	0.048
10	Wire Laminate	0º	0.0012192	0.048
11	Wire Laminate	90º	0.0012192	0.048
12	Backup Laminate	0º	0.003175	0.125
13	Gel Coat	0º	0.020	0.020
		Total Thickness	0.017526	0.690

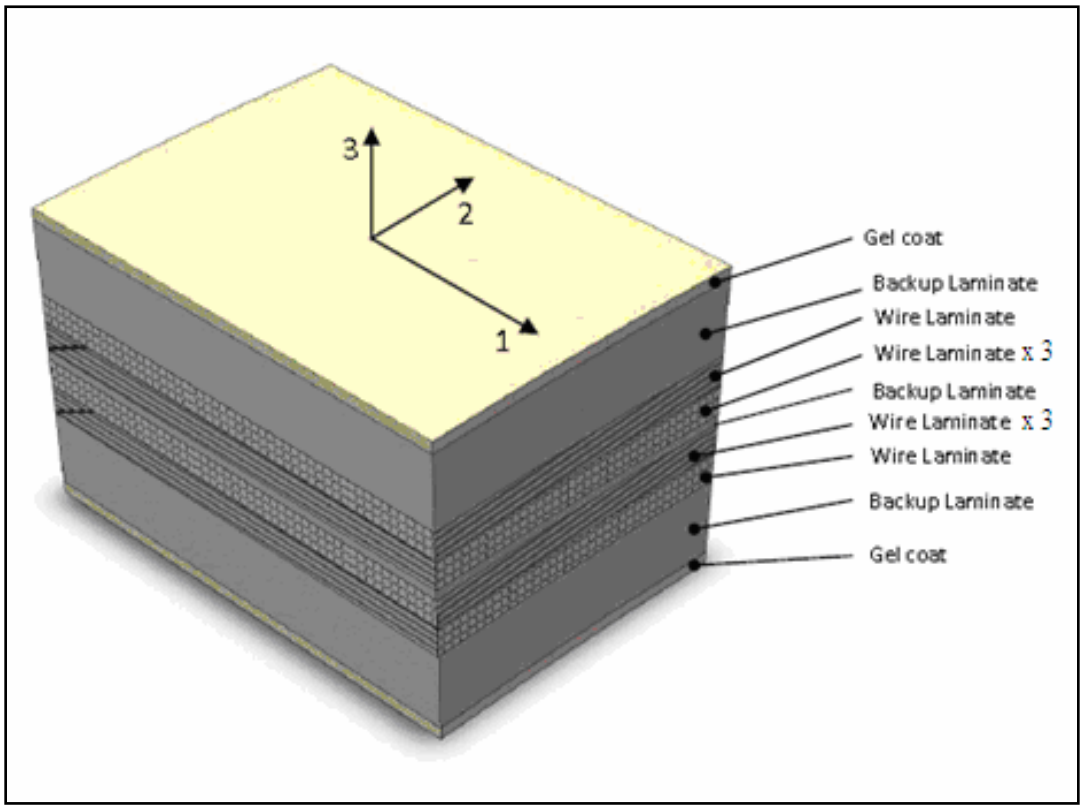

Figure 3.4. Material Section of Wire-Meshed Model.

CHAPTER 4

DETERMINATION OF DESIGN WIND PRESSURES FOR THE SHELTER

This chapter discusses the design wind parameters for the studied shelter. Two design methodologies (ASCE 7-05 and CFD) for determining the wind pressures are presented.

4.1—Proposed Shelter Size

Guidance given by FEMA 361 [1] for community shelters may be applied for shelters of all sizes and heights although that would lead to overly conservative designs for properly vented small shelters. According to FEMA 361 [1], storm shelters are defined small if the interior volume is less than 500 ft^3 (14.16 m^3), whereas shelters are considered large if the interior volume is greater than 1000 ft^3 (28.32 m^3). For these types of shelter, the recommended amount of floor area per person is about five square feet. As shelter sizes increase, wind loads become more prominent in design and that in large shelters wind loads usually control design of the main structure.

Wind pressure calculations for a vented shelter with dimensions of 40 ft x 12 ½ ft x 7 ½ ft (12.20 m x 3.81 m x 2.29 m) and with interior volume greater than 1000 ft^3 (28.32 m^3) are presented in this research (Figure 4.1a). Figures 4.1b shows the lines and the equations that made up the shape of the shelter. It is important to know that the shape of the shelter was chosen to account for the aerodynamic forces on the shelter. Round or

smooth surfaces often reduce the uplift load on the roof, whereas sharp corners increase the uplift load on the roof. For this reason, the shelter had a rounded shape where the geometry changes in height.

Each panel was 4 ft (1.22 m) wide along the length of the shelter. The length of the shelter curve for each panel was 12 ft (3.66 m); and the height of each panel was and 7½ ft (2.29 m). There were four flanges per panel: one top flange, one bottom flange, and two side flanges (Figure 4.1c and Figure 4.1d). The width of the flanges varied depending on the materials used in each model. The flange width of the sandwich composite model was 9 in. (0.23 m) as presented in Figure 4.1c. The flange width of the wire-meshed model was 6 in. (0.15 m) as presented in Figure 4.1d. Along the length of the shelter, there were 10 panels on each side, and 20 panels on both sides. The panels were connected to each other through the bolted joint connections.

For the purposes of the wind pressure calculation and the application of wind pressures on different surface areas of the FEA models, each panel of the shelter was split into three different sections in order to represent how the wind acts on the shelter. However, in reality, the shelter is consisted of continuous panels.

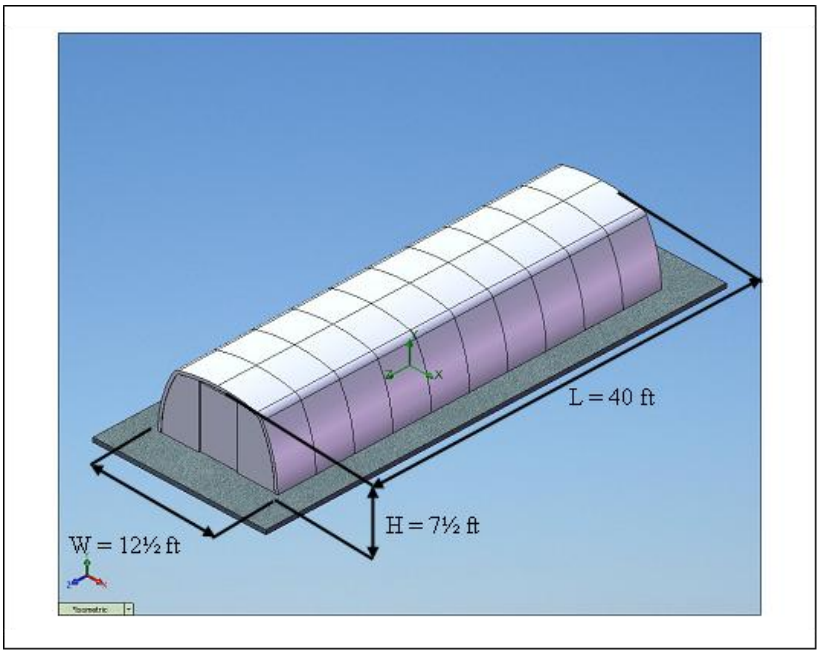

(a) Studied Shelter Dimensions

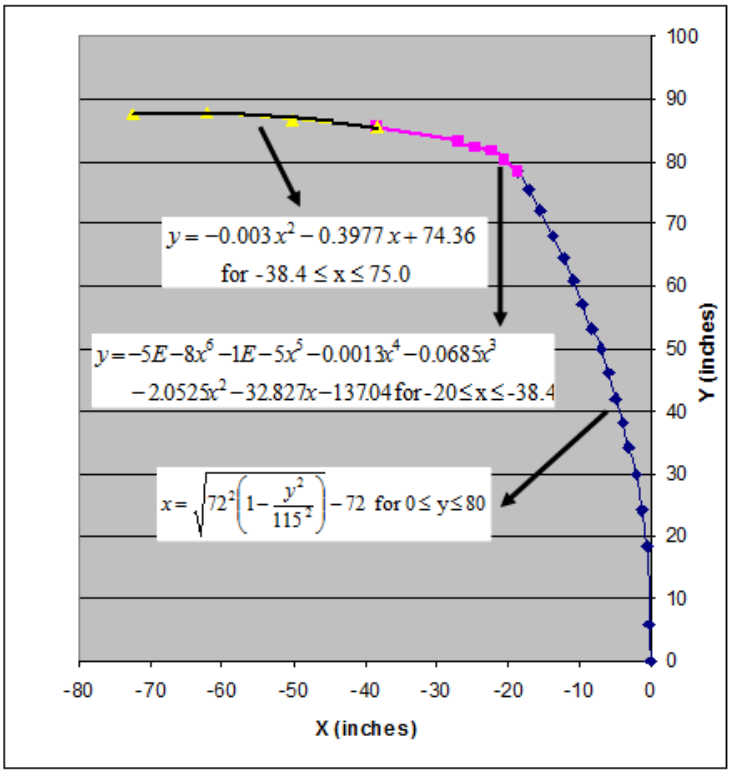

(b) Lines and Equations that Made Up the Shape of Shelter
Length of Shelter Curve =12 ft (3.66 m)

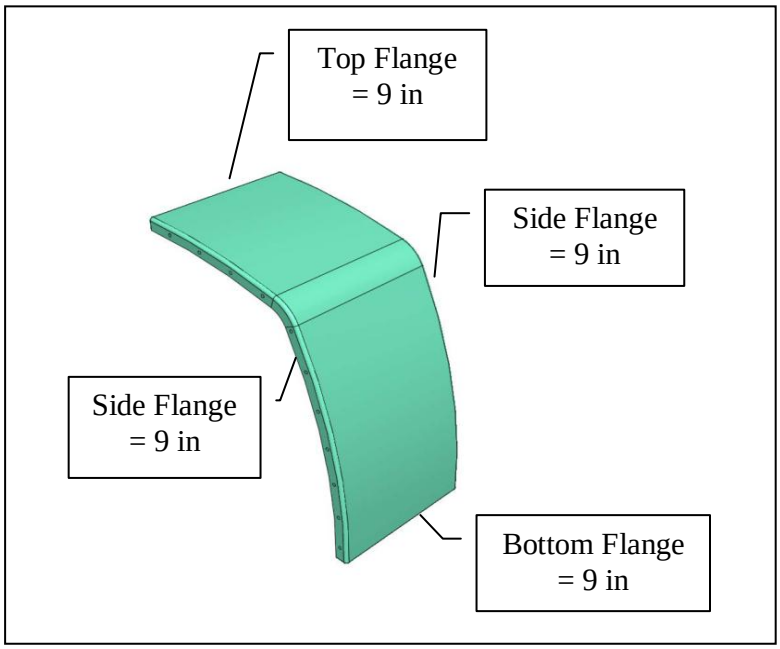

(c) Flange Width Dimensions of Sandwich Composite Panel

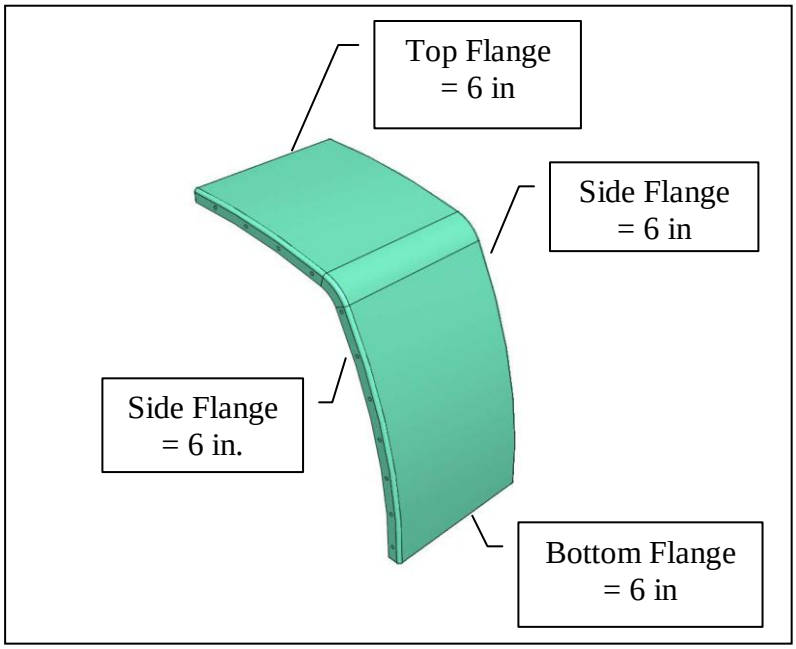

(d) Flange Width Dimensions of Wire-Meshed Panel

Figure 4.1. Dimensions of Shelter.

4.2—Consideration of Shelter Location

In designing for the shelter wind pressures, the shelter surroundings had to be taken into consideration in order to design for the strongest and safest shelter. Choosing an appropriate location for a shelter depends on topography and exposure. Topographical features such as mountains, valleys, hills, cliffs, and so on, can cause drastic change of local wind speed and direction. Buildings that locate on or near these features often have strong, complex effects. It is, therefore, recommended by the FEMA 361 [1] that shelters not be located on the upper part of a steep hill or an escarpment. In addition, shelters should not be located in a storm surge area or other areas subject to flooding. Storm surge refers to the rise in the ocean water that results from the effects of wind pushing the water onto land and the drop in the atmospheric pressures associated with hurricane storms. Furthermore, the shelter should be designed with the worst exposure to the wind since most vegetation and buildings are most often destroyed, making the terrain equivalent to flat, open terrain.

4.3—Determination of Shelter Wind Loads and Directions

Design wind speeds for large site-built shelters may be taken from the zone map presented in Figure 2.6. Two methods of determining the shelter wind loads and directions are discussed below. The first method followed the ASCE 7-05 code provision and the second method was done in Computational Fluid Dynamic (CFD) software called HYBRID3D.

ASCE 7-05 is a standard code that is widely used in most current building designs for determining design wind loads or pressures. It is a straightforward design process for

small wind loads; however, it is quite complex for determining structures with high-wind loads such as tornado and hurricane events. As discussed in Chapter 2, in high-wind events, wind loads or pressures may cause different effects on different response components of a structure, and may have significantly different values for structures with similar, geometric profile and associated wind load characteristics. Predicting the wind-load behaviors is impossible, therefore, ASCE 7-05 accounts for different risk factors in the design process to account for the uncertainty of wind characteristics.

CFD, on the other hand, is a method that involves defining a concise mathematical model that represents the motion of wind. The motion of wind can be modeled with laminar characteristics, or turbulence characteristics, or a combination of laminar and turbulence characteristics. This method provides greater accuracy in predicting wind loads; however, it is quite complex. It requires skills and knowledge to be able to develop a model that represents the real scenario of wind characteristics and interaction with a building.

4.4—ASCE 7-05 Wind Pressure Design Approach

The analytical procedure in the ASCE 7-05 [6] has two steps for determining the wind pressures of Main Wind Force Resistance System (MWFRS) and Components and Claddings (C&C). The first step considers the properties of the wind flow and the second accounts for the properties of the structure and its dynamic response to the longitudinal and transverse wind turbulence. The velocity pressure can be calculated from Equation 4.1, which is taken into account of the properties of wind flow. Equation 4.1 represents the velocity pressure at elevation z [6]:

$$q_z = 0.00256 K_z K_{zt} K_d V^2 I \left(lb / ft^2 \right) \quad (4.1)$$

where

q_z = *velocity pressure (psf) calculated at height z above ground*

K_z = *velocity pressure exposure coefficient at height z above ground*

K_{zt} = *topographic factor*

K_d = *directionality factor*

V = *design wind speed (mph)* (from Figure 2.6)

I = i*mportance factor*

Once the *velocity pressure* q_z is determined, the pressures on MWFRS or C&C of the shelter can be obtained. It is determined from the following equation of the ASCE 7-05 [6]:

$$p = qGC_p - q_i (GC_{pi)})(lb / ft^2) \quad (4.2)$$

where

p = *pressure (psf)*

q = q_z *for windward walls calculated at height z above ground*

q= q_h *for roof surfaces and all other walls*

G = *gust effect factor*

C_p = *external pressure coefficients*

q_i = q_h = *velocity pressure calculated at mean roof height*

GC_{pi} = *internal pressure coefficients*

Wind pressure calculations for the shelter were first done per ASCE 7-05 [6] code provision with shelter dimensions of 40 ft x 12 ½ ft and 7 ½ ft. Wind loads depend on many factors such as wind speed, topography, building geometry, height, exposure and enclosure. Therefore, appropriate choices of variables and coefficients were made to establish the wind loads. For the studied shelter, these choices were as follows:

- ASCE 7-05, Method 2- Analytical Procedure was used
- Wind speeds used were 3 second gusts with wind speed of 300 mph specified in Figure 2.6
- *Exposure Category* = C
- *Importance Factor* = 1.00
- The shelter was assumed not protected by other parts of the building
- *Velocity Exposure Coefficient,* K_z =0.85, used value for the correct height of the shelter above ground
- *Topographic Factor,* K_{zt} = 1.00, assuming that shelter was located on a flat ground, not on an escarpment, or on the upper half of a hill
- *Directionality Facto,* K_d = 0.85
- *Gust Effect Factor, G* = 0.85
- *External Pressure Coefficient,* C_p, for MWFRS was used for buildings of all heights
- *External Pressure Coefficient,* (GC_{pi})*, for C&C* was used for buildings with *mean roof height h* less than 60 ft

- *Internal Pressure Coefficient,* $GC_{pi} = \pm 0.55$ was used because the shelter was assumed as partially enclosed building with no venting assumed.

The reasoning behind these choices is presented below:

Topography, Exposure, and Directionality

The effects of topography on tornado wind fields are not known. It is recommended that the shelter should not be located on the upper part of a steep hill or an escarpment. The shelter for this research was assumed to be on a flat, open terrain; therefore, the *Topographic Factor,* K_{zt}, was equal to 1.00 [6]. However, if a shelter was located on top of a steep hill or an escarpment, then a higher value of K_{zt} must be used.

In severe tornadoes and hurricanes, ordinary vegetation and buildings in wooded areas are flattened and destroyed, exposing shelters to winds coming from open terrain. In addition, variation of wind speed with height above ground in tornado storms was not well established. Therefore, *Exposure C* was assumed, which reflected that the surrounding space is open.

The *Wind Directionality Factor,* K_d, for the MWFRS and C&C in ASCE 7-05 [6], is taken as 0.85 because winds of tornadoes and hurricanes are complex and their wind directions may change considerably. A building may be affected from more than one direction; therefore, K_d for the shelter was set as 0.85.

Importance Factor:

It is important to understand the notion of probability of occurrence of design wind speeds during the service life of buildings. The general expression for probability P that a design wind speed will be exceeded at least once during the exposed period of *n* years is given by [6]:

$$P = 1 - \left(1 - P_a\right)^{\bar{n}} \tag{4.3}$$

where

P_a = annual probability of being exceeded (reciprocal of the mean recurrence interval)

n = exposure period in years

Considering a building in Dallas designed for a 50-year service life. A return period of 50 years corresponds to a probability of occurrence of 1/50 = 0.02 = 2 %. The probability of exceeding the design wind speed at least once during the 50-year lifetime of the building is

$$P = 1 - (1-0.02)^{50} = 1 - 0.36 = 0.64 = 64\ \%$$

The probability that wind speeds of a given magnitude will be exceeded increases with a longer exposure period of the building and the mean recurrence interval used in the design. Therefore, the *Importance Factor*, *I* in the ASCE 7-05 [6] documents reflects the probability that the structure will experience winds higher than the design wind speed during the service life of a structure. Mean recurrence intervals of 50 years are generally used in building design and are considered standard in the ASCE 7-05 documents [7]. A 50-year mean recurrence interval is reflected in the values shown on the design wind speed maps of ASCE 7-05 documents. Wind speeds shown in Figure 2.6 have already

considered low probability of occurrence (high mean recurrence interval) of these wind speeds. For this reason, the *Importance Factor* for the shelter should not be adjusted above 1.00.

Venting and Internal Pressure Coefficient

A large shelter with interior volume of 1,000 ft^3 (28.32 m^3) or more would require a venting area based on its volume to relieve internal pressure caused by atmospheric pressure change (APC) [7]. Provision for providing sufficient venting to relieve APC without creating a problem with the wind blowing through the shelter is a very complex matter. When a tornado passes over a building, "the atmospheric pressure in the center of the tornado vortex is lower than the ambient atmospheric pressure; the outside pressure is lower than the ambient pressure inside the building" as stated by FEMA 361 [1]. This atmospheric pressure change in a tornado may cause all surfaces of the building to experience outward acting pressures. If there is sufficient venting in the building that allows air to flow through the openings, then the APC-induced forces will not be a problem and that the atmospheric pressures inside and outside the building can be equalized. However, it should be noted that openings in the building can create another problem in the building envelop because these openings can also allow the wind to enter the building and cause the internal pressures and wind-induced aerodynamic external pressures to increase.

According to the ASCE 7-05 [6] and FEMA 361 [1], the *Internal Pressure Coefficient, GC_{pi},* may be taken as ± 0.18 (for fully enclosed building) when venting area of 1 square foot per 1,000 ft^3 of interior safe room volume is provided to account for

APC. An *Internal Pressure Coefficient, GC_{pi},* equals to ± 0.55 may be used to accommodate for internal pressure caused by APC [1], [6]. This was seen as an alternative to designing appropriate ventilation for the shelter. For this reason, the *Internal Pressure Coefficient, GC_{pi},* was taken as ± 0.55 for the shelter. No venting to relieve atmospheric pressure change was assumed in designing this shelter although code-compliant ventilation for habitable spaces is required.

Load Cases on Shelter

In order to design the wind pressures for the shelter, analyses were made to ascertain their ability to carry the design wind loads associated with 300 mph wind speed. Wind pressure on a given surface of the shelter depends on whether the wind is blowing normal to the short wall (lengthwise) or the long wall (crosswise) of the shelter. These two cases of wind directions were considered in the analysis and consistent with ASCE 7-05 [6]. The first case considered the wind blowing normal to the long wall of the shelter, whereas the second case considered the wind blowing normal to the short wall of the shelter. Figure 4.2 shows the two cases where the wind directions were assumed.

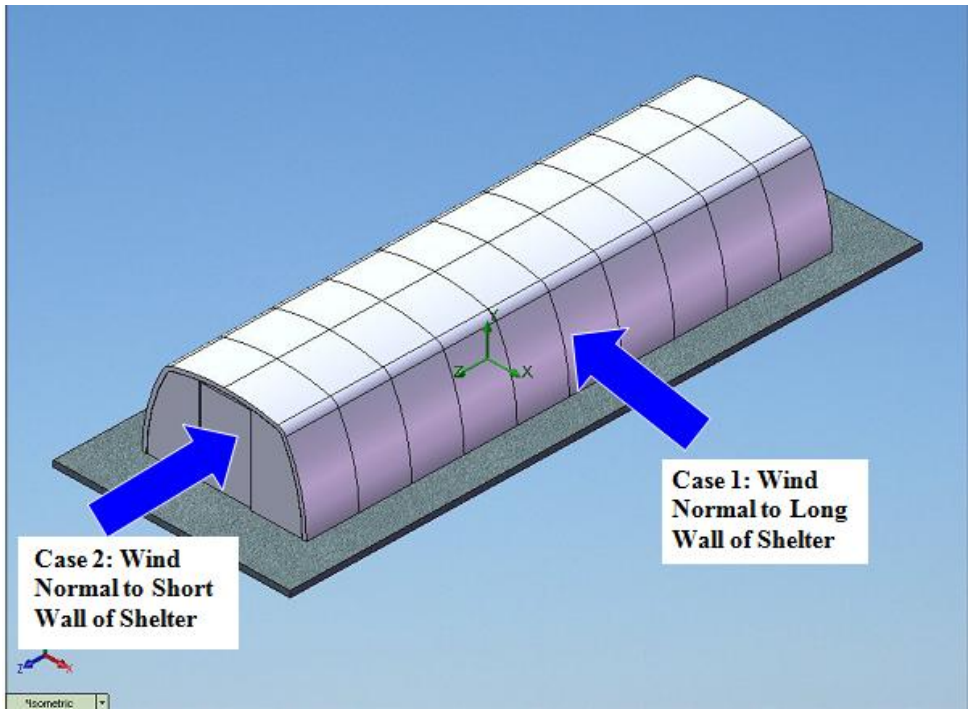

Figure 4.2. Two Load Cases of Wind Applied on Shelter.

Loads on Shelter

Wind pressures on a given surface depend on whether the wind is blowing on the long wall or the short wall of the shelter. This is expressed by the *Wall Pressure Coefficient*, C_p, for the MWFRS, which is a function of the ratio L/B. The critical case for resisting building shear and overturning occurs when the windward and leeward walls are of breadth (*B*) greater than (*L*). Building, *L*, in ft, is measured parallel to the wind direction, whereas, building, *B*, in ft, is measured normal to wind direction. Though the calculation shown in this research considered the two wind directions described above, the wind direction perpendicular to the wall of greatest breadth is expected to control the design.

4.4.1—Loads on MWFRS

Equations 4.1 and 4.2 were used to determine the wind pressures for the MWFRS of the shelter. Section 4.4.1.1 provides the wind pressures on the surfaces of the shelter assuming the wind blew normal to the long wall of the shelter. Section 4.4.1.2 provides the wind pressures on the surfaces of the shelter assuming the wind blew normal to the short wall of the shelter. The appendix section provides the calculations of the wind pressures for these two load cases.

4.4.1.1—First Case: Wind Normal to Long Wall of Shelter for MWFRS

The first wind load case assumed the wind flowing normal to the long wall (normal to ridge) of the shelter in order to be consistent with the ASCE 7-05 code provision. Design parameters and considerations were discussed in the previous sections. Internal pressures may act inward or outward; and they are combined with external pressures on shelter roofs and walls. Total horizontal shear is not affected by internal pressure. Table 4.1 and Figure 4.3 represent the wind pressures for the shelter where the wind blew perpendicular to the long wall of the 40 ft long shelter. It can be seen from Table 4.1 that the P*ositive Internal Pressure Coefficient, $+GC_{pi}$,* contributed to higher wind pressures than when used the N*egative Internal Pressure Coefficient, $-GC_{pi}$.* Hence, the higher wind pressures controlled the design. Figure 4.3 only represents the wind pressures on the MWFRS with positive internal pressure since this produced the maximum forces for instability conditions, i.e., maximum roof uplift and overturning moment. These pressures are used only for MWFRS, not C&C.

Table 4.1. MWFRS Wind Pressures on Shelter for when Wind Normal to Long Wall of Shelter, $\theta \leq 10^{o}$

Wind Pressure for MWFRS Normal to Long Wall					
Surface	Z (ft)	q_z (psf)	C_p	Design Pressure (psf)	
				($+GC_{pi}$)	($-GC_{pi}$)
Windward Wall	0-7.5	166.25	0.8	+21.61	+204.48
Leeward Wall	All	166.25	-0.5	-162.09	+20.78
Side Wall	All	166.25	-0.7	-190.35	-7.48
Roof (Horizontal Distance from Windward Edge)	0 to h/2	166.25	-0.956	-226.53	-43.66
	h/2 to 2h	166.25	-0.872	-214.66	-31.79
	h to 2h	166.25	-0.528	-166.05	+16.82

Note: (+) sign indicates the wind pressure acting toward the surface
(-) sign indicates the wind pressure acting away from the surface
1 in = 0.0254 m; 1ft = 0.3048 m; 1 ft^2 = 0.0290 m^2

4.4.1.2—Second Case: Wind Normal to Short Wall of Shelter for MWFRS

The design parameters and considerations for the second case remained the same as in the first case. The only difference was in the wind direction, where the wind was assumed blowing normal to the short wall of the shelter. Table 4.2 and Figure 4.4 represent the applied wind pressures on the surfaces of the shelter.

Table 4.2. MWFRS Wind Pressures on Shelter for Wind Normal to Short Wall of Shelter, $\theta \leq 10^{o}$

Wind Pressure for MWFRS Normal to Short Wall					
Surface	Z (ft)	q_z (psf)	C_p	Design Pressure (psf)	
				($+GC_{pi}$)	($-GC_{pi}$)
Windward Wall	0-7.5	166.25	0.8	21.64	204.75
Leeward Wall	All	166.25	-0.24	-125.51	57.60
Side Wall	All	166.25	-0.7	-190.60	-7.49
Roof (Horizontal Distance from Windward Edge)	0 to h/2	166.25	-0.9	-218.90	35.79
	h/2 to h	166.25	-0.9	-218.90	-35.79
	h to 2h	166.25	-0.5	-162.30	20.81
	> 2h	166.25	-0.3	-134.0	49.11

Note: (+) sign indicates the wind pressure acting toward the surface
(-) sign indicates the wind pressure acting away from the surface
1 in = 0.0254 m; 1ft = 0.3048 m; 1 ft^2 = 0.0290 m^2

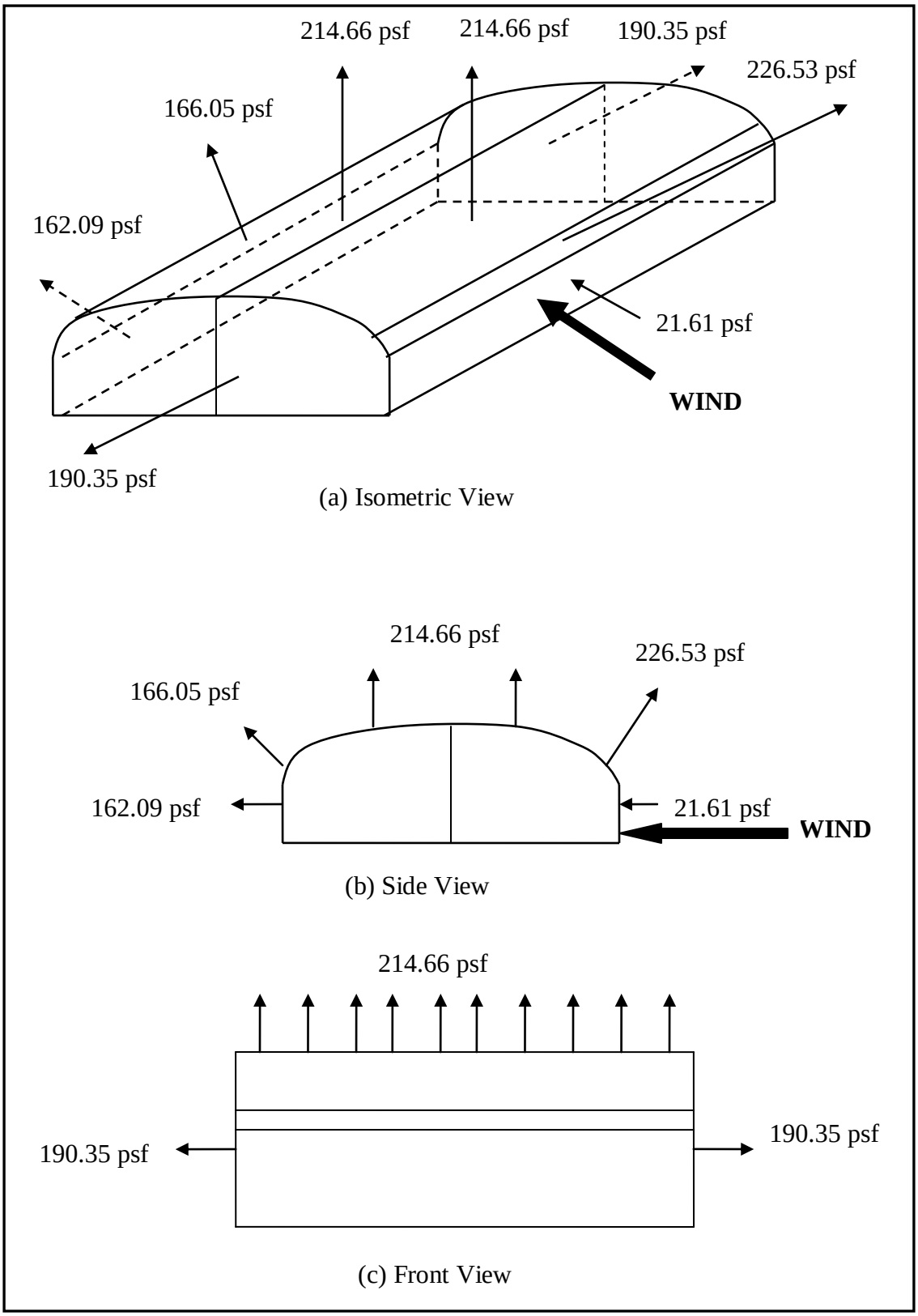

Figure 4.3. Critical MWFRS Pressures for Wind Normal to Long Wall of Shelter and Positive Internal Pressure. (Note: Arrows Indicate Pressures on Surface Areas.)

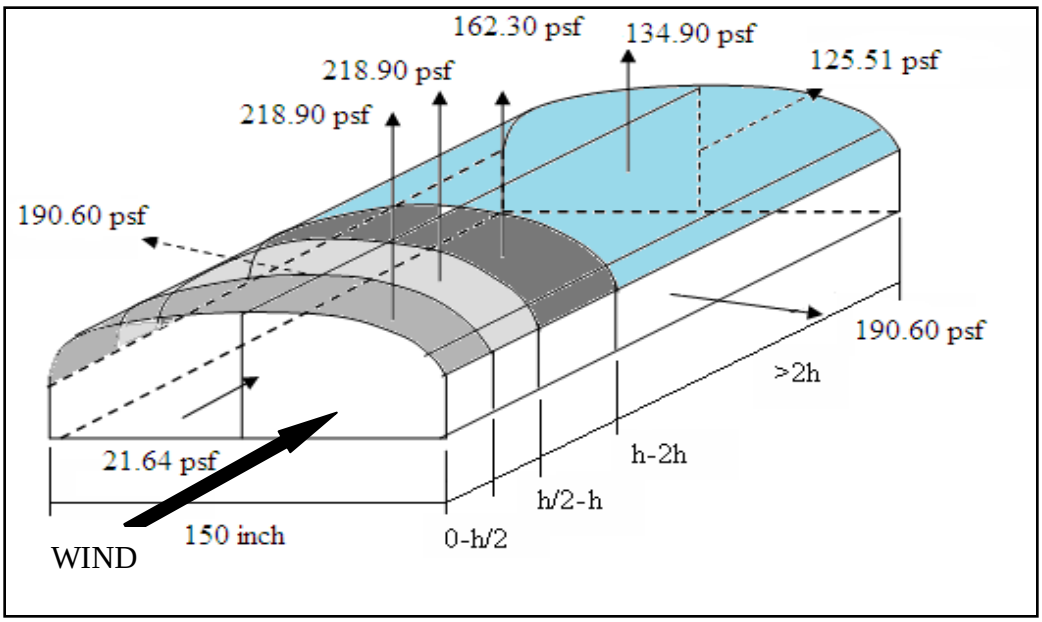

(a) Isometric View

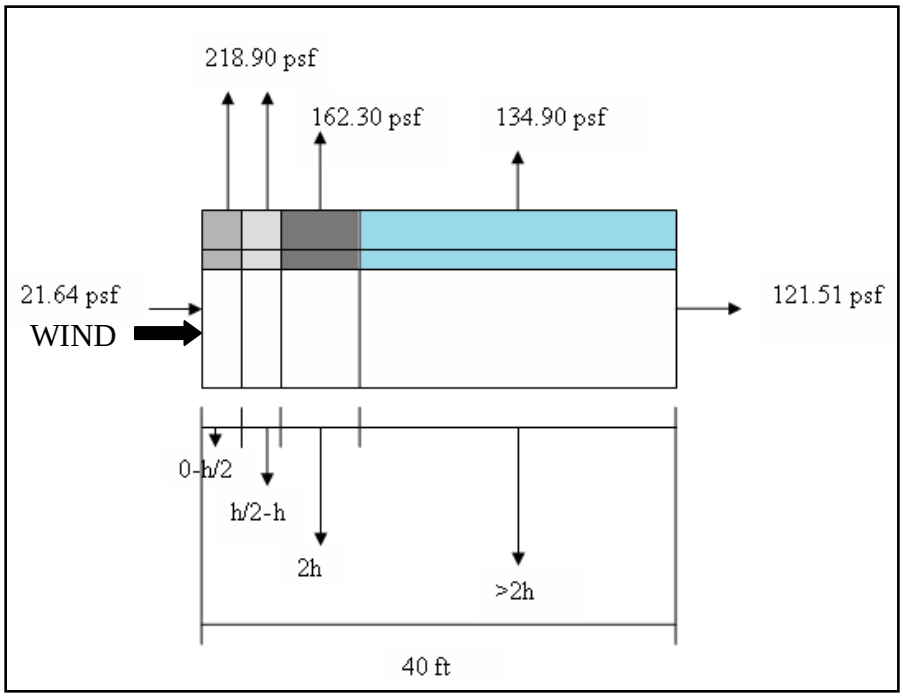

(c) Side View

Figure 4.4. Critical MWFRS Pressures for Wind Normal to Short Wall of Shelter and Positive Internal Pressure. (Mean Roof Height, h = 85 in, Shaded Areas Indicate Roof Sections, Arrows Indicate Pressures on Surface Areas, not Concentrated Loads.)

4.4.1.3—Determination of Which Wind Direction Results in Higher Wind Pressures

To determine which wind direction resulted in higher wind pressures, the wind pressures normal to the long wall of the shelter were compared to those pressures normal to short wall of the shelter. Hence, the wind pressures from Table 4.1 (or Figure 4.3) were compared to the wind pressures from Table 4.2 (or Figure 4.4), respectively. The comparison between Table 4.2 and Table 4.3 or Figure 4.3 and Figure 4.4 clearly demonstrated that the wind direction flowing normal to the long wall of the shelter gave higher positive wind pressures than the wind pressures from the other direction (wind normal to the short wall). This agreed with the expectation presented earlier in the *Loads on Shelter* discussion. Therefore, these critical wind pressures will be used for comparison with the critical wind pressures from the CFD design approach.

4.4.2—Loads on C&C

The focus of the research was to determine the design wind pressures for the MWFRS of the shelter. Loads on C&C for the shelter were not in the scope of this research. Therefore, the loads on C&C were not provided.

4.5—Computational Fluid Dynamic Design Approach

The question arises whether designing a shelter with high wind speed and complex geometry of the shelter in accordance to the ASCE 7-05 would be reliable to use for design, especially for the complex shape shelter as presented here. Therefore, computational fluid dynamic (CFD) analysis was necessary in the present study as a way to validate the wind pressures predicted earlier by the ASCE 7-05. The software that used

to solve for the CFD analysis of this research was HYBRID3D, which is a powerful tool that uses numerical method and algorithms to solve, analyze problems and refine designs that involve fluid flows.

Simulation of fluid flow over complex configurations has advanced considerably over the past decade, and numerous notable successes have been reported in the literature [24 - 29]. Simulation of many complex flow features such as the randomness of the flow and the turbulence behavior can be captured in the CFD analysis through turbulence modeling [29]. The turbulence modeling is done by defining the viscosity of the flow: laminar and turbulence viscosity. The laminar viscosity and turbulence viscosity both define a fluid property, where the laminar viscosity is a function of temperature, and the turbulence viscosity is a function of the flow. Sutherland's formula can be used to estimate the laminar viscosity, whereas, some model such as the Spallart-Allmaras one equation model can be used to estimate the turbulent viscosity [29]. The incorporation of these contributions can closely predict the wind flow behaviors, which are important to identify in building designs.

The governing equations used to solve for the finite volume method are based on the Navier-Stokes Equations, which are derived from the conservation of mass, momentum and energy applied to a *control volume* Ω that is bounded by a *control surface* $\partial\Omega$ [29]. According to Koomulli [29], the control surface is assumed moving with a *velocity c* with respect to a stationary inertial frame. The conservation of mass, momentum, and energy within the control volume are described by Equations 4.4, 4.5, and 4.6, respectively:

$$\frac{d}{d\,\vec{t}}\int_{\Omega}\vec{\rho}\,d\Omega+\oint_{\partial\Omega}\rho(\vec{u}-\vec{c})\cdot\vec{n}\,\vec{ds}=0 \tag{4.4}$$

$$\frac{d}{d\overset{\Delta}{t}}\int_{\Omega}\overset{\Delta}{\rho}\overset{\Delta}{u}\,d\Omega+\oint_{\rho\Omega}\overset{\Delta}{\rho}\overset{\Delta}{u}(\overset{\Delta}{u}-\overset{\Delta}{c})\cdot\overset{\Delta}{n}\overset{\Delta}{ds}=\int_{\Omega}\overset{\Delta}{\rho}\overset{\Delta}{f}\,d\Omega+\oint_{\rho\Omega}\overset{\Delta}{T}\cdot\overset{\Delta}{n}\overset{\Delta}{s} \tag{4.5}$$

$$\frac{d}{d\overset{\Delta}{t}}\int_{\Omega}\overset{\Delta}{\rho}\overset{\Delta}{e_t}\,d\Omega+\oint_{\rho\Omega}\overset{\Delta}{\rho}\overset{\Delta}{e_t}(\overset{\Delta}{u}-\overset{\Delta}{c})\cdot\overset{\Delta}{n}\overset{\Delta}{s}=\int_{\Omega}\overset{\Delta}{\rho}(\overset{\Delta}{u}\cdot\overset{\Delta}{f})d\Omega+\oint_{\rho\Omega}\overset{\Delta}{u}\cdot\overset{\Delta}{\tau}\overset{\Delta}{s}-\oint_{\rho\Omega}\overset{\Delta}{q}\cdot\overset{\Delta}{n}\overset{\Delta}{s} \tag{4.6}$$

where

Δ = *dimensional quantities*

$\overset{\Delta}{t}$ = *time*

$\overset{\Delta}{\rho}$ = *density*

$\overset{\Delta}{u}$ = *local velocity with u, v and w as the components in the x, y, and z coordinate directions*

$\overset{\Delta}{n}$ = *outward unit normal to the control surface*

ds = cell face area for 3-dimensions and the edge length in 2-dimensions

$\overset{\Delta}{f}$ = *body force per unit volume*

$\overset{\Delta}{\rho}\overset{\Delta}{e_t}$ = *total energy per unit volume, which is the sum of internal and kinetic energies*

$\overset{\Delta}{T}$ = *stress tensor, which is defined as:*

$$\overset{\Delta}{T}=-\overset{\Delta}{p}I+\overset{\Delta}{\lambda}div(\overset{\Delta}{u})I+2\overset{\Delta}{u}\overset{\Delta}{D} \tag{4.7}$$

$$\overset{\Delta}{D}=\frac{1}{2}\left(grad(\overset{\Delta}{u})+(grad(\overset{\Delta}{u}))^{T}\right) \tag{4.8}$$

$$\overset{\Delta}{\tau}=\overset{\Delta}{T}\cdot\overset{\Delta}{n} \tag{4.9}$$

where

$\overset{\Delta}{p}$ = = *pressure*

I = unit tensor of total energy per unit volume

$\overset{\Delta}{u}$ *= laminar coefficient of viscosity*

$\overset{\Delta}{\lambda}$ *= turbulence coefficient of viscosity*

To simplify the above relations, the Stokes relation is generally used in the simulation of the fluid flow. It can be described as follows:

$$3\overset{\Delta}{\lambda} + 2\overset{\Delta}{u} = 0 \tag{4.10}$$

The Stokes relation is related to temperature through Sutherland's formula [29] as follows:

$$\overset{\Delta}{u} = c_1 \frac{\overset{\Delta}{T}^{3/2}}{\overset{\Delta}{T} + c_2} \tag{4.11}$$

where

c_1, c_2 = *constants for a given gas*

For air at moderate temperatures, c_1 and c_2 can be taken as 1.458 x 10^{-6} kg/(m-s $K^{1/2}$) and 110.4 K, respectively.

The system of fluid dynamic equations are closed by using the equation of state for a perfect gas, i.e.,

$$\overset{\Delta}{p} = \overset{\Delta}{\rho}\overset{\Delta}{R}\overset{\Delta}{T} \tag{4.12}$$

where

$\overset{\Delta}{R}$ *= gas constant (for air at standard conditions,* $\overset{\Delta}{R} = 287.04\ m^2/s^2K$)

CFD Modeling

Wind pressure calculations for the studied shelter with dimensions of 40 ft x 12 ½ ft x 7 ½ ft (12.20 m x 3.81 m x 2.29 m) were also carried out by the CFD analysis. The first step of the processing was to model the physical geometry of the shelter and the wind flow domain around the shelter. The 40 feet shelter was modeled as a 3-D structure as illustrated in Figure 4.5. It was created as a solid structure placing on a six-inch concrete platform. The length and width of the concrete were taken as 528 in. (13.41 m) and 198 in. (5.03 m), respectively. It can be seen that each panel from the model was split into three separate sections in order to capture the variation of wind pressures acting on the shelter. As discussed earlier, wind pressure is a function of height and velocity, and a variation of heights and velocities produces a variation of pressures. For this reason, each panel of the shelter was split into three different parts to account for such issues.

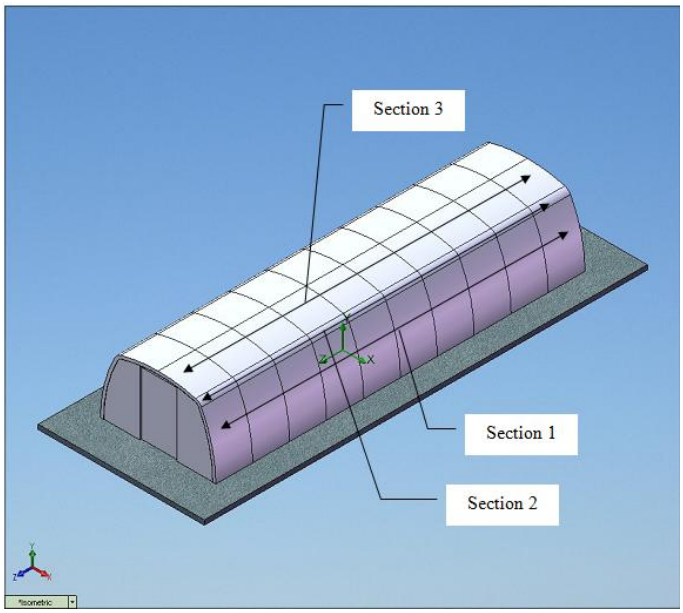

Figure 4.5. The Shelter was modeled as a 3-D Structure in a CAD Software Package. (Each Panel of the Shelter Was Divided into 3 Different Sections.)

After the 3D model was created from a CAD software package, the next step was to import the model to the CFD software called HYBRID3D for modeling and meshing the extent of the finite flow domain in which the flow was to be simulated. HYBRID3D analysis was used to perform million of calculations required to simulate the interaction between liquids (air) and shelter surfaces defined by boundary conditions. The most fundamental consideration in the CFD is how a continuous fluid in a discretized fashion is treated. A finer mesh, with more elements, will generally produce more accurate results at the expense of longer processing time. Hence, the model was discretized into small cells to form a volume mesh or grid to achieve accurate results from the CFD analysis (Figure 4.6). It was created with the tetrahedral mesh using the Mix-Element Grid Generator in 3-Dimensions (MEGG3D). It can be seen from this figure that the finer mesh was around the surfaces of the shelter to provide enough elements to resolve the flow field in the regions of interest. As the mesh was further away from the shelter, it became coarser due to a larger surface area of the flow domain and that there was no flow features of interest in this area.

The MEGG3D was used because this type of grid offered easy simulation in the refinement or de-refinement of elements since the data structure had to be changed only locally [28], [29]. In addition, this helped in adaptation of the grid to the flow features by adding more points where the gradients of the flow properties were significant [27 - 32] and removing points from the regions where there are no flow features of interest.

Other consideration included the portions of the boundary of the flow domain were coincided with the surfaces of the body geometry. Other surfaces were free boundaries over which the flow entered or leaved. The geometry and flow domain were

modeled in such a manner as to provide input for the grid generation. Thus, the modeling took into account of the structure and topography of the grid generation. Figure 4.7 shows the hybrid grids used for flow simulation, which represents the wind flow field around the shelter.

The physical domains for representing the wind flow field of the shelter were taken as ten times the length of the shelter from the upstream of the leading edge, downstream of the trailing edge, and above the shelter. The wind flow field was modeled with the physical domain just described in order to see the effect of wind turbulence on the structure. However, if the physical domains were a lot smaller than the physical domain just described, then the results of the wind turbulence on the structure would not be as accurate. As seen from Figure 4.7, the hybrid grids are a combination of different sizes of the polygon, which are necessary to use for storing the grid information [29].

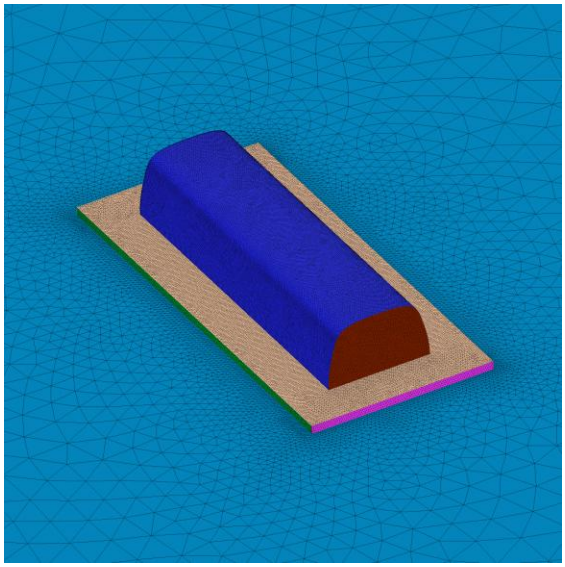

Figure 4.6. Hybrid Grid on and around the Shelter using Mix-Element Generator in 3-Dimensions (MEG3D).

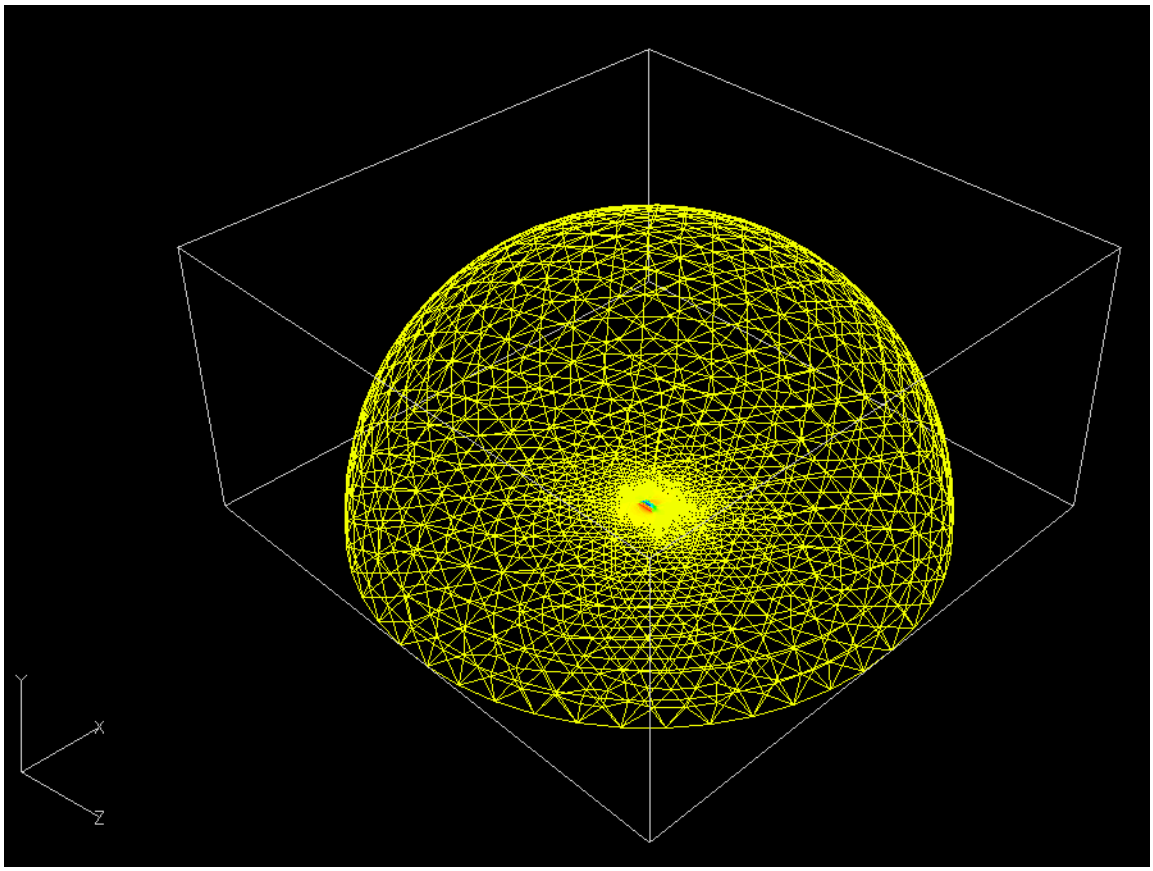

Figure 4.7. Simulation of the Shelter with Wind Flow Field (where Flow Enters and Leaves) was represented by the Grid Used.

After the finite flow domain was specified, physical conditions were required on the boundaries of the flow domain. This involved specifying the fluid behaviors and properties around the boundaries of the shelter. The fluid behaviors were defined as the velocity of air traveling at 300 mph (134.11 m/s); and the flow type was defined as laminar, and turbulence flow. The angle of attack for the analysis was taken as 0 degree. The standard thermodynamic parameters for ambient pressure and temperatures were also defined as initial conditions of the flow domain. The static pressure was taken as 14.6959473 lb/in^2. The reference temperature was taken as 68.09°F.

The wind velocity of 300 mph (134.11 m/s) was input into the CFD along with the standard ambient pressure and temperature. In order to determine which wind direction creates the most impact with the greatest vulnerability on the shelter, two wind directions were specified similar to the ASCE 7-05 [6]. The first case modeled the wind blowing perpendicular to the long wall of the shelter. The second case modeled the wind blowing perpendicular to the short wall of the shelter. The internal pressures may act inward or outward and they were combined with external pressures on the shelter roofs and walls. Total horizontal shear was not affected by internal pressure.

After the flow and boundary conditions of the shelter were specified, the simulation was performed. As the simulation was preceded, the solution was monitored to determine if a "converged" solution has been obtained. After the solution was converged, post-processing was the last step that allowed the simulation to get the results. This involved extracting the desired flow properties (drag coefficient, density, momentum, etc,) from the computed flow field.

4.5.1—First Case: Wind Velocity Applied Normal to Long Wall of Shelter

This section provides the post-processing results from the CFD analysis, where the wind was considered flowing normal to the long wall of the shelter. Section 4.5.1.1 provides the effect of wind results as the wind moved around the shelter. Section 4.5.1.2 provides the *drag coefficient*, C_p, results. Section 4.5.1.3 provides the wind-induced pressure results.

4.5.1.1—Considering the Effect of Wind Moving Through the Shelter for Wind Normal to Long Wall of Shelter

After the simulation was completed, different results can be observed from the post-processing. One of the results that can be observed from the post-processing was the impact of the 300 mph wind velocity as it hit the structure (Figure 4.8). This figure shows the effects of wind moving through the structure as the velocity of air varied around the surface of the structure. It can be seen that, initially, the wind approached the shelter with the speed of 300 mph (134.11 m/s). The instance it hit the side surfaces of the shelter, the velocity decreased to zero, but it gained back up as it reached the inclined surface (roof pitch) of the shelter. As the wind traveled across the rooftop and toward the leeward wall, the wind speed rapidly decreased.

As the wind reached the roof pitch on the leeward side, the wind speed rapidly increased, but when it reached the roof pitch on the leeward side, the wind speed rapidly decreased. This sudden change in the wind speed was due to a sudden change in the shape of the geometry when the wind experienced an uneven slope from the point of contact. Consequently, the roof shape played a significant role in the roof performance, both structurally and with respect to the magnitude of the wind loads. As the wind speeds varied with height and experienced a sudden change in the shape of the geometry, the magnitude of the wind loads rapidly increased or decreased. From this figure, one can see that wind speeds, even in the extreme wind events, rapidly increase and decrease. It is safe to say that a variation of wind velocity produces a variation of pressure on the surface of the structure.

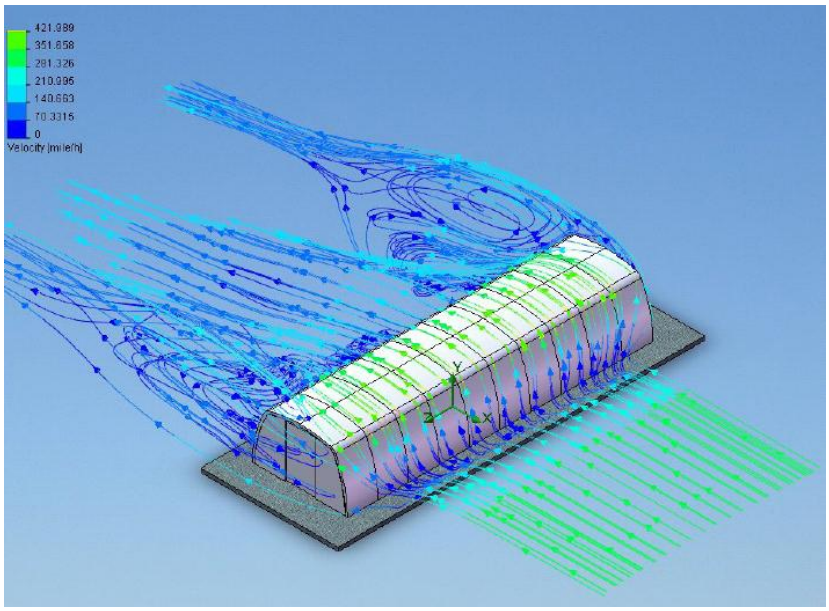

(a) Isometric View

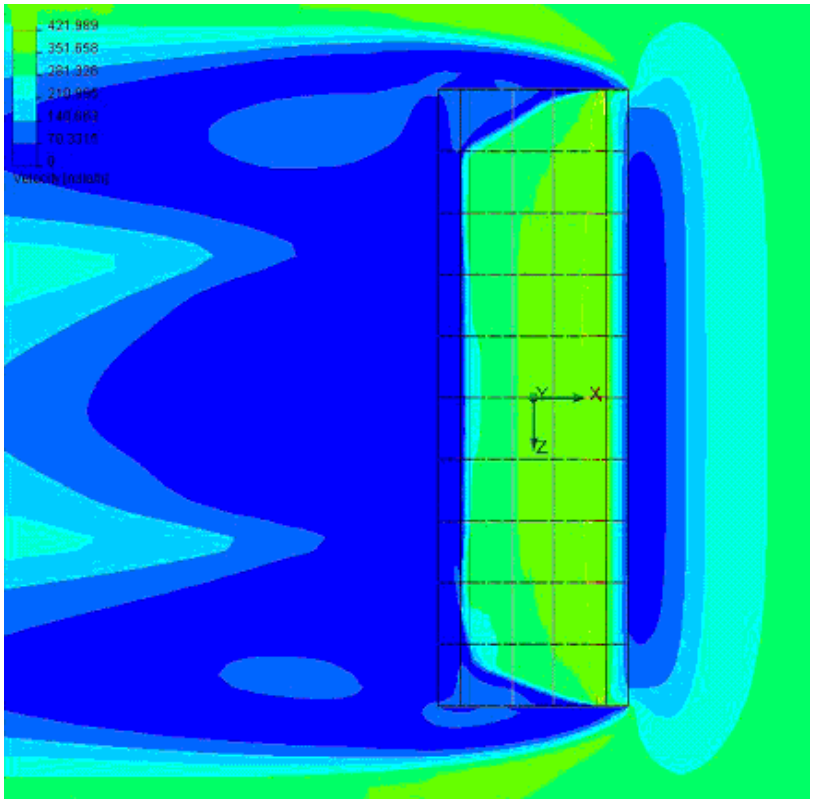

(b) Top View

Figure 4.8. Plot of Wind Velocities for Wind Normal to the Long Wall of the Shelter.

4.5.1.2—Drag Coefficient, C_p, Obtained From CFD Analysis for Wind Normal to Long Wall of Shelter

Another desired flow property that can be obtained from post-processing was the *drag coefficient*, C_D or C_P as defined in the CFD analysis. Drag coefficient is important in determining the drag force or pressure exerted on the shelter. In fluid dynamics, the drag equation is a practical formula used to calculate the drag force experienced by an object due to movement through a fully- enclosing fluid (like air or water). The force on an object due to a fluid is represented by the following equation [33]:

$$F_d = \frac{1}{2}\rho \upsilon^2 C_D A \tag{4-13}$$

where

F_D = *drag force (Si:N)*

ρ = *density of the fluid (SI: kg.m^3)*

ν = *velocity of the body relative to the medium (Si: m/s)*

C_D *(or* C_P*) = drag coefficient. (Si: dimensionless)*

A = *cross-sectional area perpendicular to the flow (Si: m^2)*

In order to determine the aerodynamic drag force on the shelter from Equation 4.13, C_p must be determined first. Figure 4.9 shows the wind flow and distribution of C_P values on different surfaces of the shelter. The minus sign in C_p values from Figure 4.9 indicates that the wind direction was acting outward, creating suction on the surfaces of the shelter. The plus sign in C_P values indicates that the wind direction was acting toward the surfaces of the shelter, creating compression on the surfaces of the shelter. It can be seen from Figure 4.9 that the C_p value was very high in compression (1.075, indicated in

the letter F), when the wind hit the windward side of the concrete foundation and shelter surfaces. As the wind reached the roof pitch, C_P values switched from compression to suction. The highest C_P value obtained from the suction event was when the shape of shelter changed with the increasing in height of the shelter. This agreed with Figure 4.8. The wind velocity increased greatly as it reached the roof pitch.

In the same manner, the change in roof pitch created a large change in the C_P value. The change in roof pitch on the windward side had a C_p value of -3.145, which is indicated in the letter A, whereas, across the rooftop, the C_P value was -1.457, which is indicated in the letter C. On the windward side, the roof pitch had a C_P value of -2.301 (indicated in the letter B), where, again, changes in the shape of the geometry made C_P value to pick back up. The leeward wall had a C_P value of -0.613, as indicated in the letter D. The sidewalls had C_P values of -1.457 as indicated in the letter C. The C_P values could be summarized and presented in Figure 4.10 and Table 4.3.

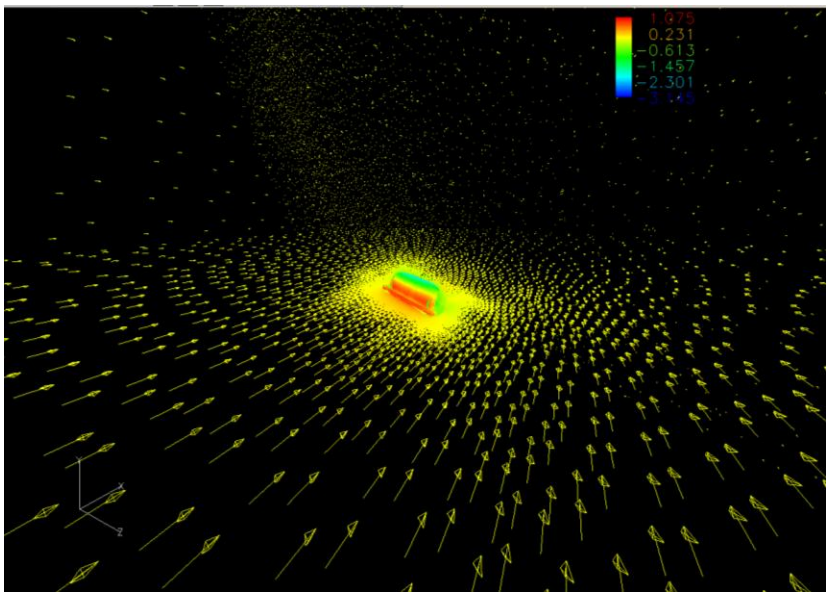

(a) Flow Field and Drag Coefficient, C_P, Values on the Surfacces of the Shelter

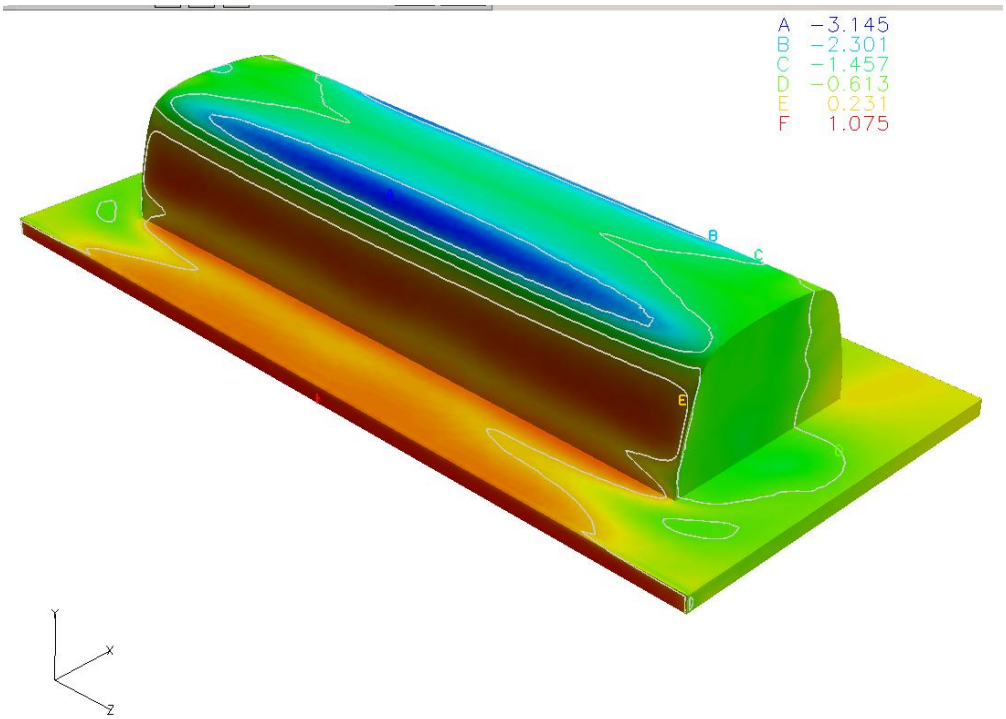

(b) Winward, Sidewalls and Roof C_P Values (Isometric View)

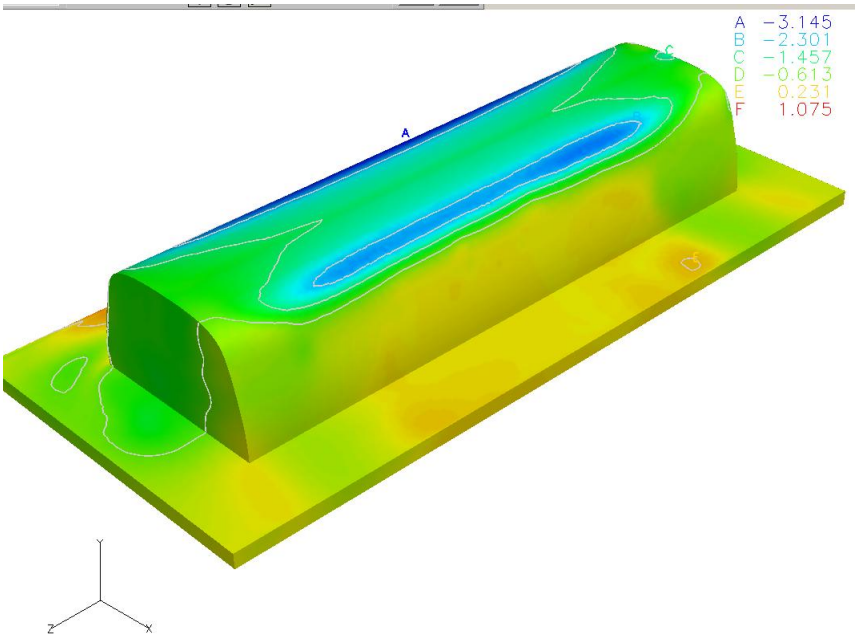

(c) Leeward, Sidewalls, and Roof C_P Values (Isometric View)

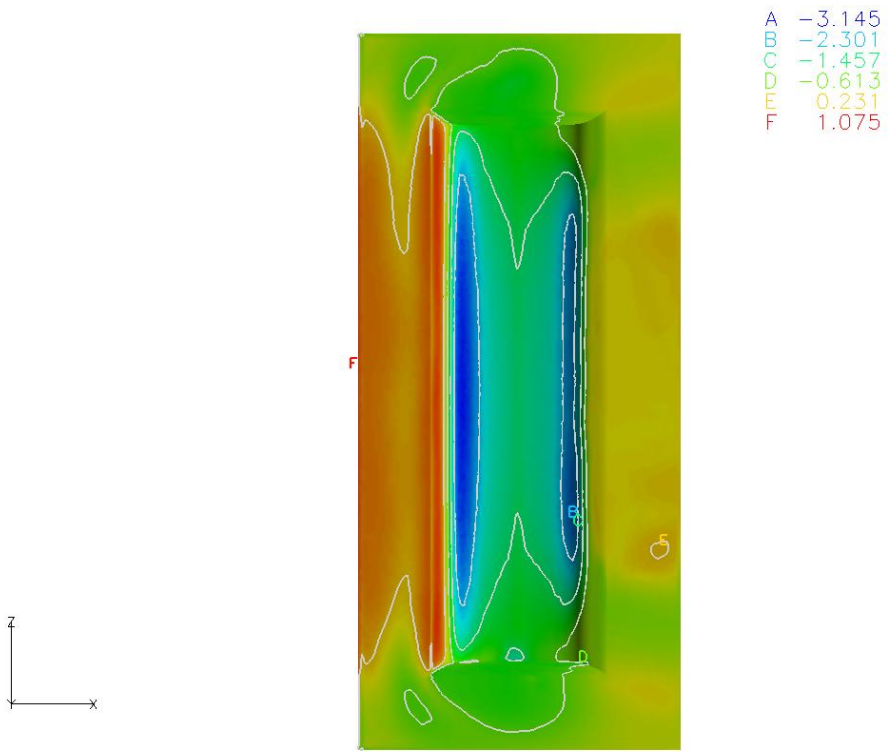

(d) Windward. Leeward, and Roof C_P Values (Top View)

Figure 4.9. The Variation of Wind Speeds Resulted in Variation of Drag Coefficients, C_P.

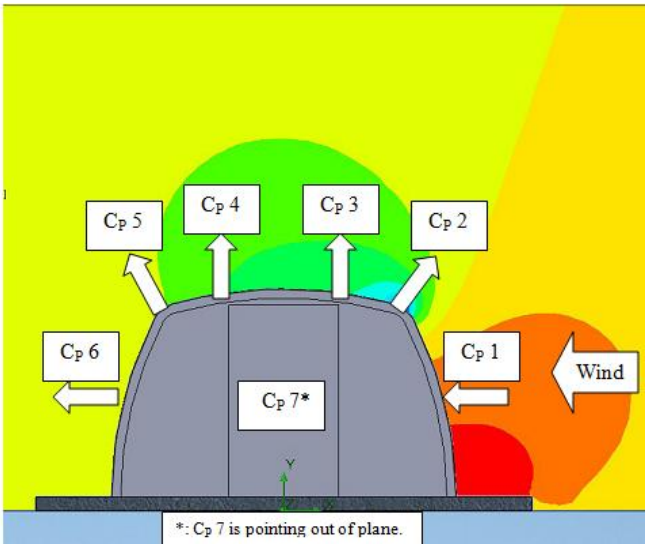

Figure 4.10. Illustration of C_p Directions on the Shelter Surfaces When the Wind Acted Normal to Long Wall of Shelter.

Table 4.3. Summary of C_P Values on the Shelter Surfaces

Place Number	Area for Each Section per Panel		C_P Value
C_P 1= Windward Wall	3,658 in^2	2.36 m^2	1.075
C_P 2 = Roof Pitch	465 in^2	0.3 m^2	-3.145
C_P 3 = Roof Top	2,216.5 in^2	1.43 m^2	-1.457
C_P 4 = Roof Top	2,216.5 in^2	1.43 m^2	-1.457
C_P 5 = Roof Pitch	465 in^2	0.3 m^2	-2.301
C_P 6 = Leeward Wall	368 in^2	2.36 m^2	0.231
C_P 7 = Sidewalls	11,870 in^2	7.66 m^2	-1.457

4.5.1.3—Wind-Induced Pressures on Shelter for Wind Normal to Long Wall of Shelter

After the C_p values on the surfaces of the shelter were determined, they were in plugged into Equation 4.13 to obtain the drag force. The following parameters were input into the equation to determine the drag force on the shelter. The density of air, ρ_{air}, was taken as 1.22 kg/m^3 (0.076 lb/ft^3). The wind velocity was taken as 300 mph (134.11 m/s). The cross-sectional area was taken as the area from each surface of the shelter that was perpendicular to the flow. The drag force acting on the shelter is shown in Table 4.4.

Table 4.4. Shelter Drag Force

Place No. (Ref. to Figure 4.10)	C_P Values	Area per Panel (m^2)	Density, ρ (kg/m^3)	Velocity (m/s)	Drag Force	
					(N)	(lb)
C_P 1	1.075	2.36	1.22	134.112	27,834.64	6,257.50
C_P 2	-3.145	0.3	1.22	134.112	-10,351.59	2,327.13
C_P 3	1.457	1.43	1.22	134.112	-22,859.18	5,138.95
C_P 4	-1.457	1.43	1.22	134.112	-22,859.18	5,138.95
C_P 5	-2.301	0.3	1.22	134.112	-7,573.61	1,702.62
C_P 6	-0.613	2.36	1.22	134.112	-5,983.75	1,345.20
C_P 7	-1.457	7.66	1.22	134.112	-122,448.49	27,527.52
			Total Load (Absolute Value)		219,910.44	49,437.87

Besides obtaining the drag force on the shelter, the wind-induced pressure on the shelter can also be achieved from the drag force equation. The wind pressure on each surface of the shelter was obtained from the following equation:

$$P = \frac{F_D}{A} = \frac{\frac{1}{2} C_D A \rho v^2}{A} \tag{4.14}$$

where

P = derived wind pressure from drag force equation (N/m^2 or lbf/in^2)

F_D = drag force from equation 4.13 (N or lbf)

A = cross-sectional area perpendicular to the flow (m^2 or in^2)

From Equation 4.14, it can be seen that the cross-sectional areas for the top and bottom terms canceled out, which then simplified Equation 4.14 into the following equation:

$$P = \frac{1}{2} C_D \rho v^2 \tag{4.15}$$

From this equation, the wind pressures were obtained. Table 4.5 summarizes the wind pressure on each section of the shelter obtained from the aerodynamic calculation. The NF abbreviation in Table 4.5 represents the normal force perpendicular to the surface of the shelter, and the arrows in Figure 4.11 indicate the directions of the wind pressures, which helps to clarify how the pressures were acting on the shelter. Table 4.5 and Figure 4.11 can be read concurrently to see the effects of wind pressures on the shelter.

Table 4.5. Distribution of Wind Pressures on Each Section of the Shelter for Wind Normal to Long Wall of Shelter

Place Number (Ref. to Figure 4.11)	Pressure on Each Section of Panel	
	(N/m^2)	(lb/in^2)
NF 1 = Windward Wall	11,794.34	0.983
NF 2 = Roof	-34,505.30	-2.875
NF 3 = Roof	-15,985.44	-1.332
NF 4 = Roof	-15,985.44	-1.332
NF 5 = Roof	-25,245.37	-2.104
NF 6 = Leeward Wall	-6,725.52	-0.560
NF 7 = Sidewalls	-15,985.44	-1.330

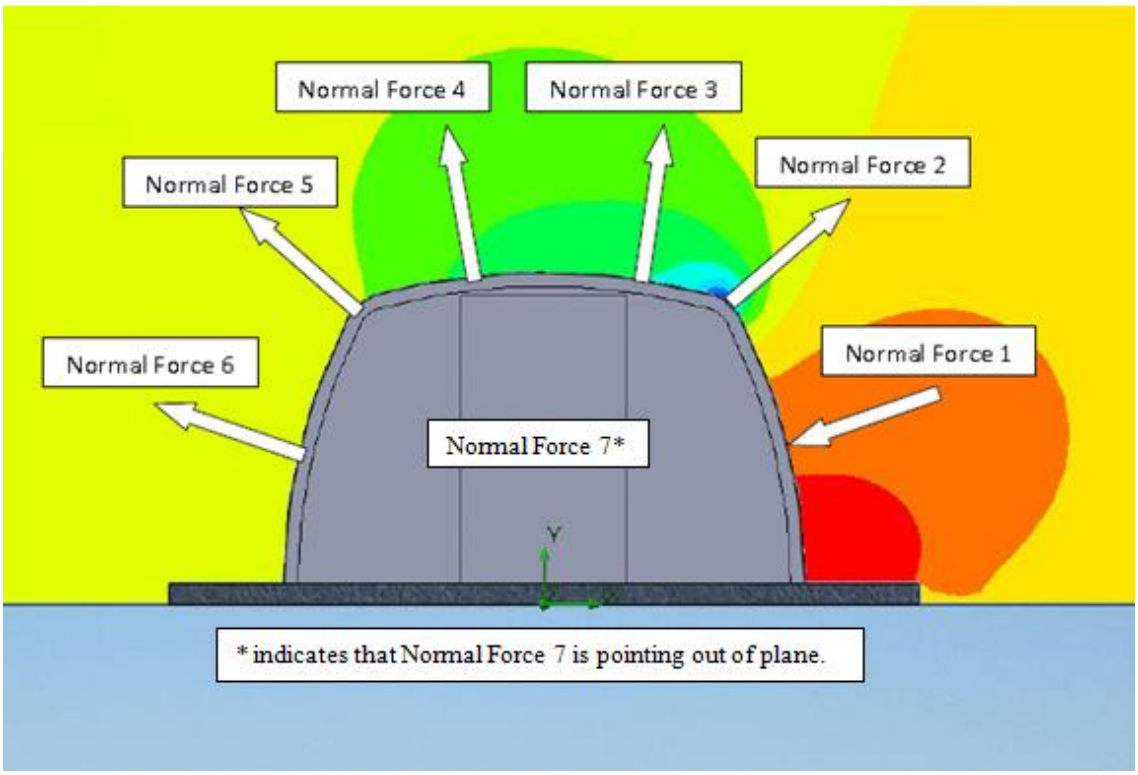

Figure 4.11. Illustration of Wind Pressures Applied to Each Section of the Shelter for Wind Normal to Long Wall Shelter (Elevation View).

4.5.2—Second Case: Wind Velocity Applied Normal to Short Wall of Shelter

This section provides the post-processing results from the CFD analysis, where the wind was assumed flowing normal to the short wall of the shelter. The attack angle of the wind flow was taken as zero degree. Section 4.5.2.1 provides the effect of wind results as the wind moved around the shelter. Section 4.5.2.2 provides the *drag coefficient, C_p,* results. Section 4.5.2.3 provides the wind-induced pressure results.

4.5.2.1—Considering the Effect of Wind Moving Through the Shelter for Wind Normal to Short Wall of Shelter

In similar manner as the first case, post-processing of the wind simulation was able to capture the effect of wind velocity as the wind moved around the shelter. Figure 4.12 shows the flow path and variation of wind velocity on the shelter. From this figure, it can be seen that the wind speed rapidly increased and decreased as the wind experienced changes in the roof shape and height.

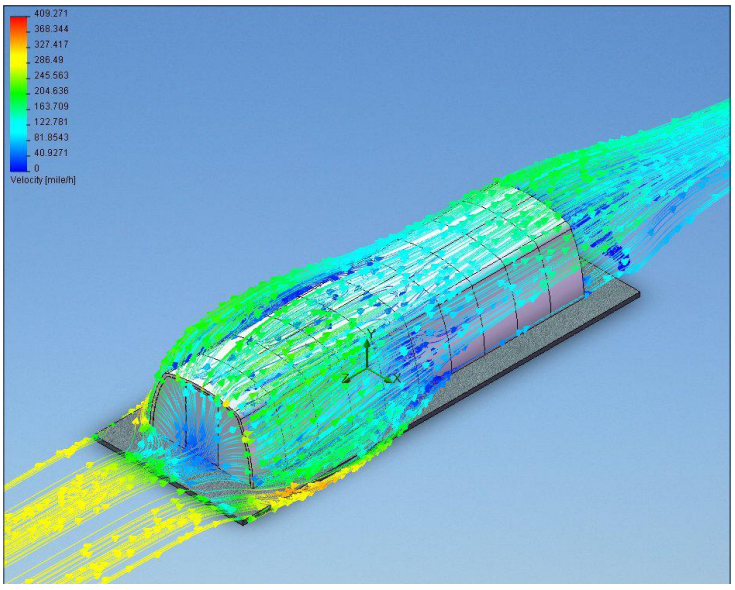

(a) Isometric View

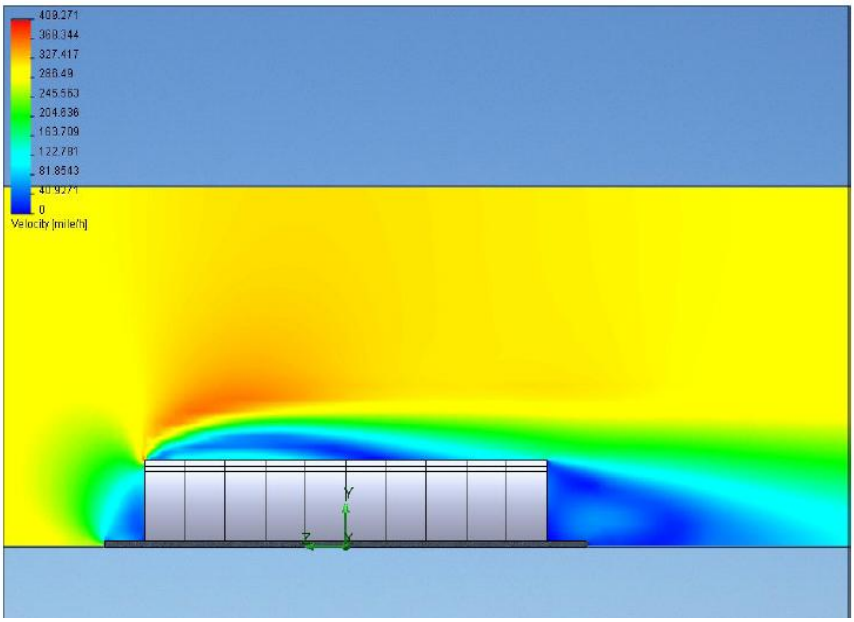

(b) Right View

Figure 4.12. Plot of Wind Velocities for Wind Normal to Short Wall of Shelter (Front Side of Shelter).

4.5.2.2—Drag Coefficient, C_p, Obtained From CFD Analysis for Wind Normal to Short Wall of Shelter

Figure 4.13 shows the flow direction of the wind and its distribution of C_p values on the surfaces of the shelter. Table 4.6 summarizes C_p values and Figure 4.14 illustrates the directions of the wind flow. Table 4.6 and Figure 4.14 can be read concurrently to fully understand which direction associates with which C_p.

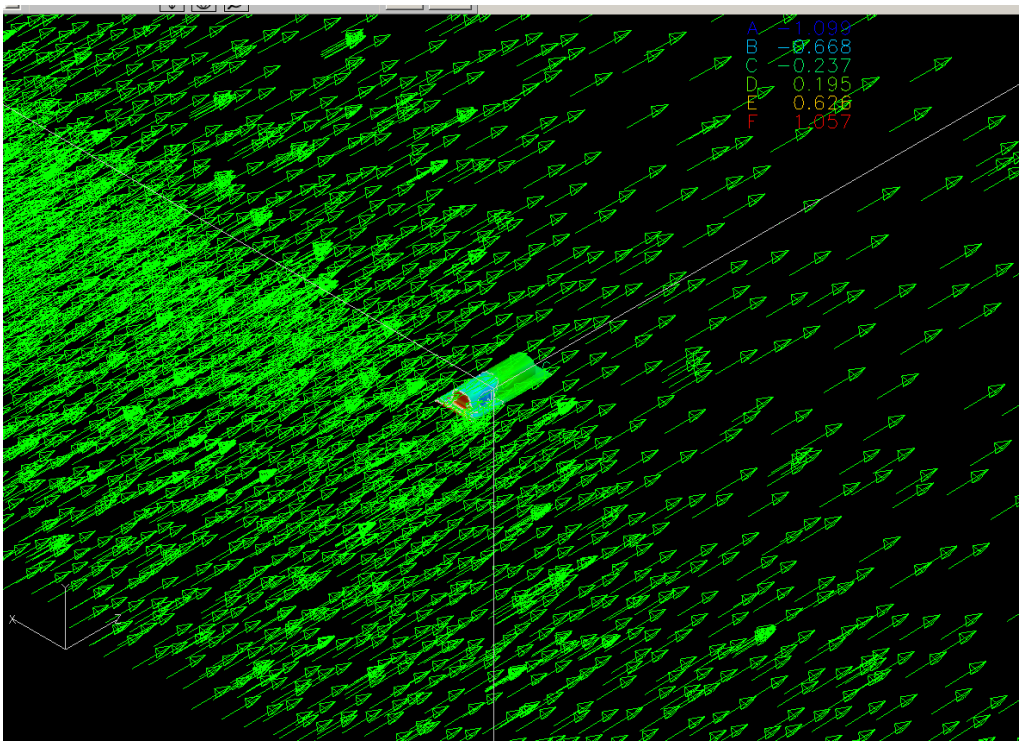

(a) Wind Flow and C_p Distribution on the Shelter

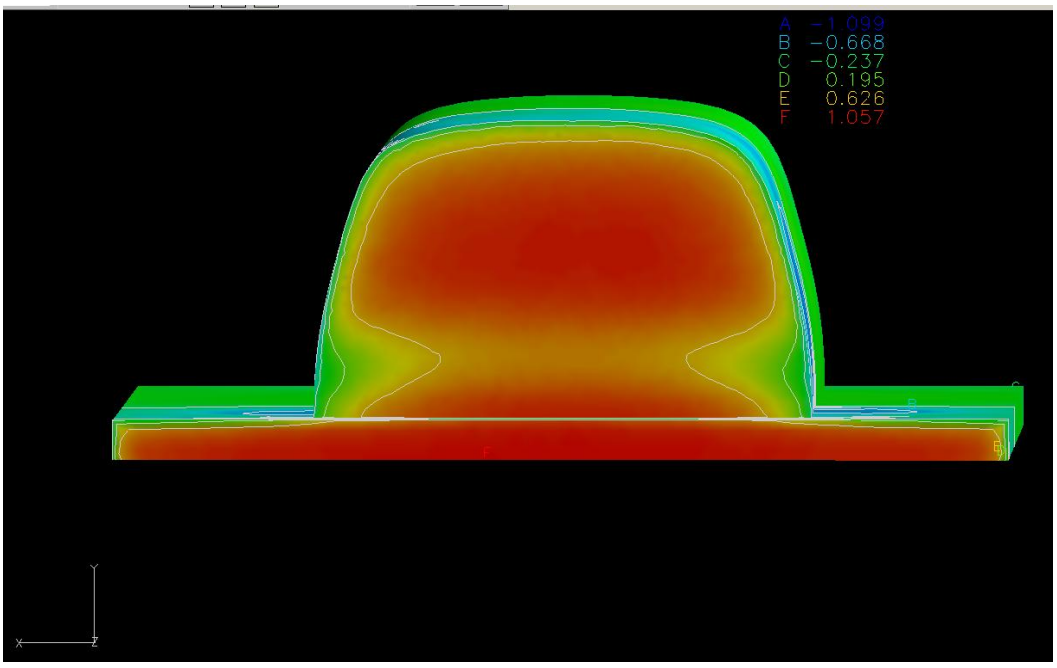

(b) C_p Values (Front View)

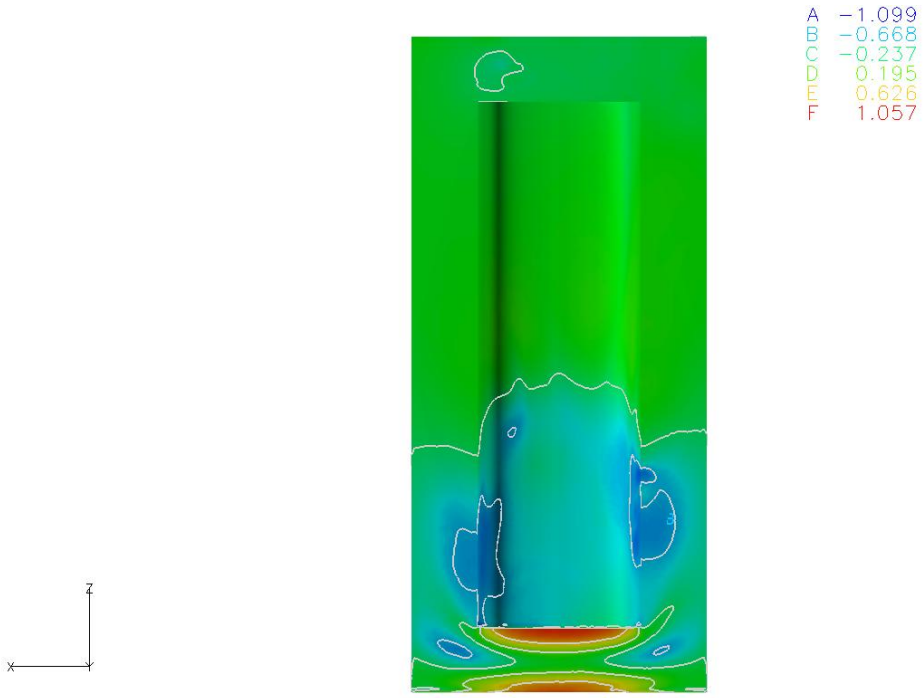

(c) C_p Values (Top View)

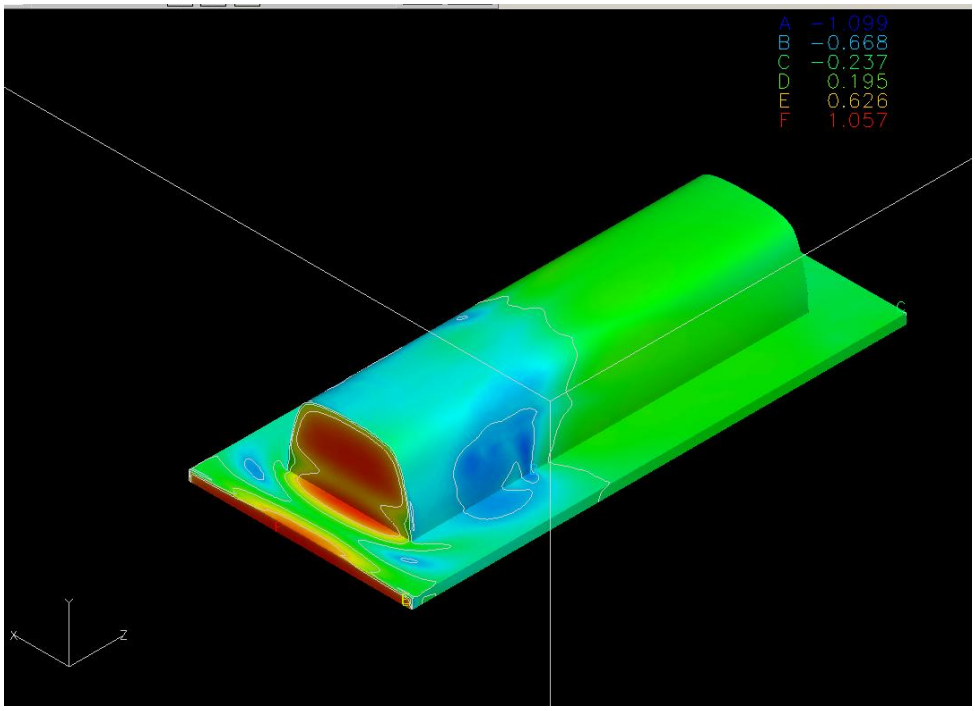

(d) C_p Values (Isometric View)

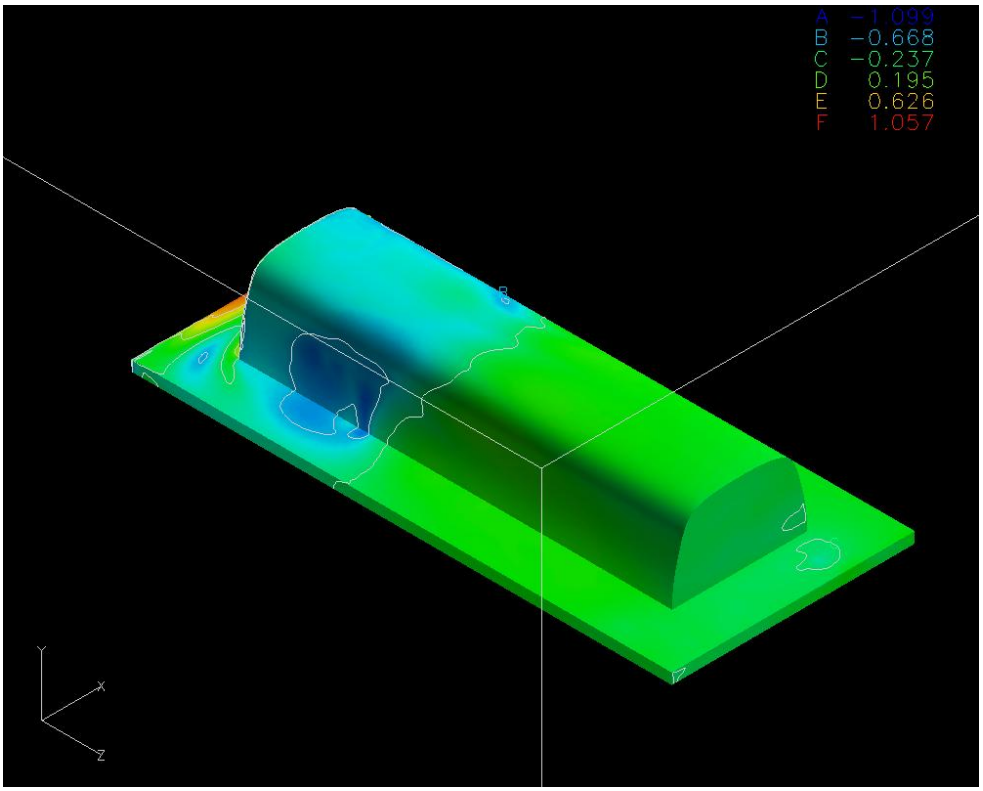

(e) C_p Values (Isometric View)

Figure 4.13. Wind Flow and Distribution of C_p Values on the Shelter for Wind Normal to the Short Wall of Shelter.

Table 4.6. Distribution of C_p Values on the Shelter for Wind Normal to Short Wall of Shelter

Place No. (Reference to Figure 4.14)	C_p Value	Average C_p Value
Front Panel C_p	1.057	-
Roof C_p 1 to C_p 5*	-0.668	Average C_p = -0.45
Roof C_p 6 to C_p 10*	-0.237	
Sidewall C_p 1 to C_p 5	-1.099	Average C_p = -0.668
Sidewall C_p 6 to C_p 10	-0.237	
Back Panel C_p	-0.237	-

* indicates C_p values were for the top horizontal surface, and inclined surfaces.

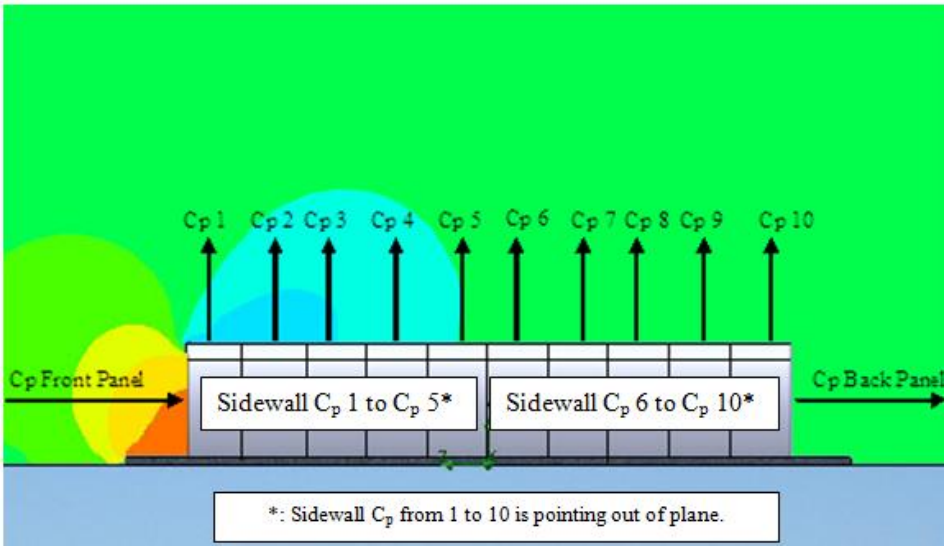

Figure 4.14. Illustration of the C_p Directions when the Wind Acted Normal to the Short Wall of Shelter.

4.5.2.3—Wind-Induced Pressures on Shelter for Wind Normal to Short Wall of Shelter

After C_p values are determined, the wind pressures on the shelter were found from Equation 4.15. The pressure distribution on each surface of the shelter can be seen from Table 4.7. Figure 4.15 illustrates the surfaces of the shelter that correspond to the surfaces listed in Table 4.7. Table 4.7 and Figure 4.15 can be read concurrently to see how the wind distributed through out the shelter.

Table 4.7. Distribution of Wind Pressure on the Shelter for Wind Normal to Short Wall of Shelter

Place No. (Reference to Figure 4.15)	C_p Value	Pressure	
		(N/m^2)	(lb/in^2)
Front Panel NF	1.057	6,663.09	0.9664
Roof NF 1 to NF 5	-0.668	4,210.63	-0.6107
Roof NF 6 to NF 10	-0.237	1,494.09	-0.2167
Sidewall NF 1 to NF 5	-1.099	6,927.85	-1.0048
Sidewall NF 6 to NF 10	-0.237	1,494.09	-0.2167
Back Panel NF	-0.237	2,494.09	-0.2167

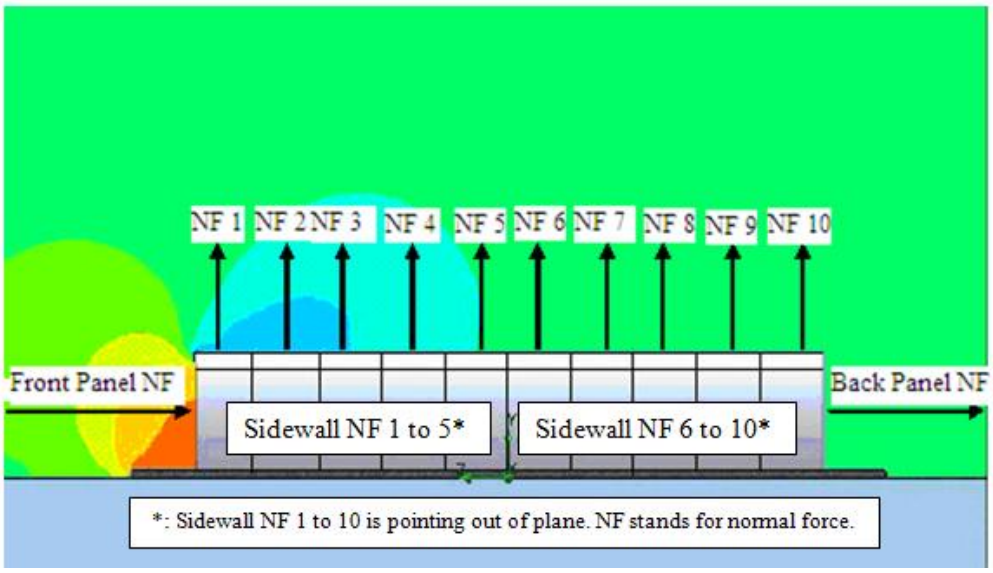

Figure 4.15. Illustration of Wind Pressure Directions Applied to Each Section of the Shelter for Wind Normal to Short Wall of Shelter (Right View).

4.5.3—Determination of Which Wind Direction from the CFD Design Approach Results in Higher Wind Pressures

Sections 4.4 discussed the design wind pressures for the shelter using the ASCE 7-05 design approach; whereas Section 4.5 discussed the design wind pressures for the shelter using the CFD design approach. Both of these approaches considered the two wind directionalities for the shelter: (1) wind acted normal to the long wall of the shelter (Case 1), and (2) wind acted normal to the short wall of the shelter (Case 2). These two cases of wind directions were considered in order to determine which direction would create the maximum forces for instability.

The wind pressures from Table 4.5 represent the wind pressures resulted from Case 1, whereas the wind pressures from Table 4.7 represent the wind pressures resulted from Case 2. The pressures from Table 4.5 and Table 4.7 were put together and reproduced as shown in Table 4.8 for comparison.

It can be seen from Table 4.8 that the wind pressures from Case 1 produced higher positive wind pressures than the wind pressures from Case 2. This also agreed with the ASCE 7-05 design approach. Therefore, the critical wind pressures from Case 1 were chosen for the wind design directionality. In addition, the wind pressures from Case 1 will be input into the FEA for the stress analysis on the shelter.

Table 4.8. Comparison of Wind Pressures between Case 1 and Case 2 Wind Directions

Wind Direction	Place Number	Pressure on Each Section of Panel	
		(N/m^2)	(lb/in^2)
Case 1: Wind Normal to Long Wall of Shelter	NF 1 = Windward Wall	11,794.34	0.983
	NF 2 = Roof	-34,505.30	-2.875
	NF 3 = Roof	-15,985.44	-1.332
	NF 4 = Roof	-15,985.44	-1.332
	NF 5 = Roof	-25,245.37	-2.104
	NF 6 = Leeward Wall	-6,725.52	-0.560
	NF 7 = Sidewalls	-15,985.44	-1.330
Case 2: Wind Normal to Short Wall of Shelter	Front Panel NF	6,663.09	0.9664
	Roof NF 1 to NF 5	4,210.63	-0.6107
	Roof NF 6 to NF 10	1,494.09	-0.2167
	Sidewall NF 1 to NF 5	6,927.85	-1.0048
	Sidewall NF 6 to NF 10	1,494.09	-0.2167
	Back Panel NF	2,494.09	-0.2167

4.6—Determination of Wind Pressure Design Approach

The purpose of comparing the ASCE 7-05 design approach to the CFD design approach was to evaluate the accuracy of the ASCE 7-05 approach. The wind pressures from Case 1 of the two design approaches are reproduced for comparison as shown in Table 4.9. As seen from Table 4.9, the percent difference between the total wind pressures of the two approaches was about 10%. The percent difference between the two

approaches for each individual section such as NF 3, NF 4 and NF 7 were less than 11%. However, the percent difference for the sections NF 1, NF2, NF 5 and NF 6 ranged from 30 to 83%.

Table 4.9. Comparison of Wind Pressures between the ASCE 7-05 and CFD Design Approaches for Wind Acted Normal to the Long Wall of Shelter

Place Number (Ref. Figure 4.11)	Pressure from ASCE Approach (psi)	Pressure from CFD Approach (psi)	% Difference
NF 1 = Windward Wall	1.42	0.983	30.77
NF 2 = Roof Pitch	-1.573	-2.875	82.77
NF 3 = Roof Top	-1.491	-1.332	10.66
NF 4 = Roof Top	-1.491	-1.332	10.66
NF 5 = Roof Pitch	-1.153	-2.104	82.48
NF 6 = Leeward Wall	-1.13	-0.560	50.44
NF 7 = Sidewalls	-1.32	-1.33	0.76
Total (Absolute Value)	9.578	10.516	9.79

The reason for the large difference was that the ASCE 7-05 wind pressure equation was developed based on the assumption that K_z and K_h (Exposure Coefficients) were different due to variation in height (Figure 4.16). Meaning, the velocity pressures were based on K_z and K_h, where z was the height of the windward wall, and h was the height measured from the base of the structure to the mean roof height. The variable h may be considered as a special value of z. q_z was defined as the velocity pressure for windward walls evaluated at height z above the ground. q_h was defined as the velocity pressure for leeward walls, sidewalls, and roofs, evaluated at height h. Note that in the equation for q_z and q_h, the only difference was in the variables K_z and K_h.

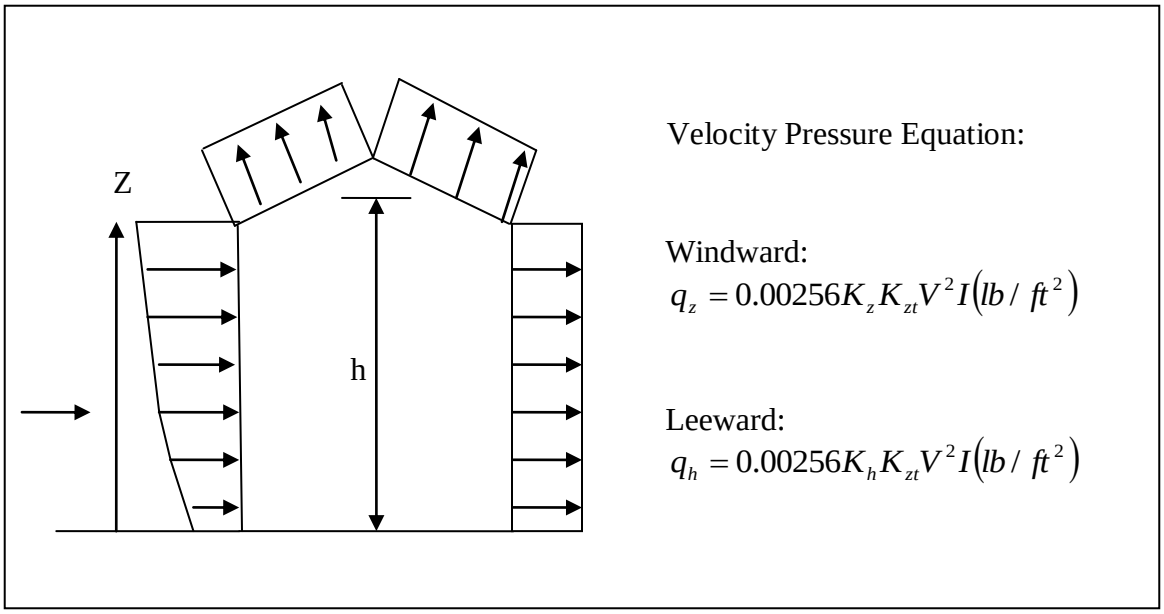

Figure 4.16. Velocity Pressure Equation is depended upon the Exposure Coefficients (K_z and K_h).

From the velocity pressure equation, it was expected that as the height increases, the velocity pressure and exposure coefficients also increase. The code does not however account for the height difference in *z* and *h* for structures that are less than 15 ft tall. According to Table 6.3 of the ASCE 7-05 code [6], the exposure coefficients (K_z and K_h) with height above ground level (z) from 0-15 ft are 0.85. This means that q_z was equal to q_h, and that the velocity pressures for windward wall, leeward wall, and roof are equal.

This was where the ASCE 7-05 approach differed from the CFD approach in this research. Because the velocity pressures for the shelter on the leeward side and roof did not depend on *h*, the wind pressures on these surfaces from the ASCE 7-05 approach were smaller than the CFD approach. The CFD approach produced higher wind pressures than the ASCE 7-05 approach because it was able to better simulate how the wind laminar and turbulence would act on the shelter at these heights. Since the CFD approach

was accounted for the size, geometry, and aerodynamics of the shelter, it better predicted how the wind would act on the shelter. Hence, the wind pressures on the shelter from the CFD approach were believed to be more accurate. Therefore, the wind pressures from the CFD approach were used and multiplied with a factored wind load to get the final wind loads to be input into the ANSYS models. The factored wind load is described in the following section of this thesis.

4.7—Load Combinations Using Strength Design

Load combinations are necessary in building designs in order to determine the worst possible combinations of the loads that might occur at one time. The load combinations of shelters may be based on the Allowable Stress Design (ASD) or Load Resistance Factor Design (LRFD). It does not matter which method the designer decides to use. For this research, the LRFD method was used.

The load combinations for the ASD method specified in the FEMA 361 [1] and ASCE 7-05 [6] are as follows:

$$\textit{Load Combination 1: } 1.0D + 1.0W_x + 0.5L$$

$$\textit{Load Combination 2: } 0.6D + 1.0W_x$$

where

D = dead load

L = live load

W_x = extreme wind load based on wind speed selected from the wind speed map

The load combinations for the LRFD method specified in the FEMA 361 [1] and ASCE 7-05 [6] are as follows:

$$\textit{Load Combination 1: } 1.2D + 1.0W_x + 0.5L$$

$$\textit{Load Combination 2: } 0.9D + 1.0W_x + 0.5L$$

$$\textit{Load Combination 3: } 0.9D + 1.2W_x$$

where

D = dead load

L = live load

W_x = extreme wind load based on wind speed selected from the wind speed map

Since the LRFD load combination was used for this research, it is important to understand how the load factors are used in the load combination. The dead load factor of 1.2 as presented in the LRFD first load combination is used if the dead load adds to the wind loads of the structure [1], [6]. Contrary, the dead load factor of 0.9 in the second and third load combinations is used if the dead load counteracts with the wind loads. The extreme wind load factor of 1.0 is used if the dead load and live load counteract with the extreme wind load. A factored load of $1.2W_x$ is used if the dead load and the extreme wind load are the only two loads acting on shelter. Depended upon the application of the shelter, the designer should determine which load combination is best to use for considering the maximum effects of all the loads assumed to act on the structure.

The third load combination of the LRFD method was used for this research. The reason being was that Alabama is in Category 5 zone of the wind speed map, where there is rarely any seismic activity, therefore, seismic loads for the shelter in Alabama was not

investigated. In addition, the shelter had only one level; hence, the effect of live load was not considered. The only loads left to consider in the load combination were the dead load and the extreme wind load on the shelter; therefore, the third load combination was used and the extreme wind load was the only load acting on the shelter, therefore a factored load 1.2 was used. The CFD design wind pressures from Table 4.9 were multiplied with a factored wind load of 1.2 to get the final wind loads, which yielded the results shown in Table 4.10. These wind loads were then input into the ANSYS models for the stress analysis of the shelter.

Table 4.10. The Final Wind Load Pressures were obtained by multiplying the CFD Wind Pressures with the Wind Load Factor of 1.2 used in the LRFD Method

Place Number (Ref. to Figure 4.11)	Wind Pressure from CFD W_x (lb/in^2)	Wind Pressure from Load Combination, $1.2W_x$ (lb/in^2)
NF 1 = Windward Wall	0.983	1.1796
NF 2 = Roof Pitch	-2.875	-3.4500
NF 3 = Roof Top	-1.332	-1.5984
NF 4 = Roof Top	-1.332	-1.5984
NF 5 = Roof Pitch	-2.104	-2.5248
NF 6 = Leeward Wall	-0.560	-0.6720
NF 7 = Sidewalls	-1.33	-1.5960

CHAPTER 5

EXPERIMENTAL TESTING & DESIGN VERIFICATION

Before the FEA was judged as an appropriate representation of the actual situation under loading, the experimental testing of the FRP panels from the two models must be carried out to study the composite's structural behaviors under loading. The results from the flexural testing were then compared to the FEA results. The purpose of comparison was (1) to validate the FEA model, (2) to see whether the FEA results could be judged as appropriate representation of the panels under loading.

It is important to know that for the full-scale FRP panels, the supports will be different and more complicated than the ones shown here in this chapter. Since wind tunnel testing is expensive and not within the scope of this research, it was decided that the best way to validate the FEA model was to carry out the flexural testing on the FRP beams to study their flexural behaviors under loading. This was the simplest way to understand how the FEA works and help to approach bigger models such as the models presented in the next two chapters.

5.1—Flexural Testing of Sandwich Composite Model

5.1.1 —Test Set Up and Instrumentation

The experimental testing was used as a blueprint, where the FEA model can be compared to for accuracy and performance issues. For this research, the flexural testing

was carried out by a three-point bending test on the beam made up of Glass/PP and EPS materials in accordance to the ASTM C-393. The thicknesses of the facesheets and the core used for the testing were 3.048 mm (0.12 in.) and 139.7 mm, (5.5 in.), respectively. The testing beam span was 558 mm (22 in.). The test set up is shown in Figure 5.1. The Tinium-Olsen, Universal Testing Machine with the capacity of 266,893 N (60,000 lbs) was used as the load for the flexural testing. The beam was loaded with a loading rate of 0.08 N/sec until the maximum deflection was reached. The ultimate load of the beam was tested by loading to the rupture point, where the complete failure was occurred. A linear variable displacement transducer (LVDT) was used to measure the deflection at the mid-span of the beam. Strain gauges were attached to the beam on the tensile side at the center of the beam to record the longitudinal strains.

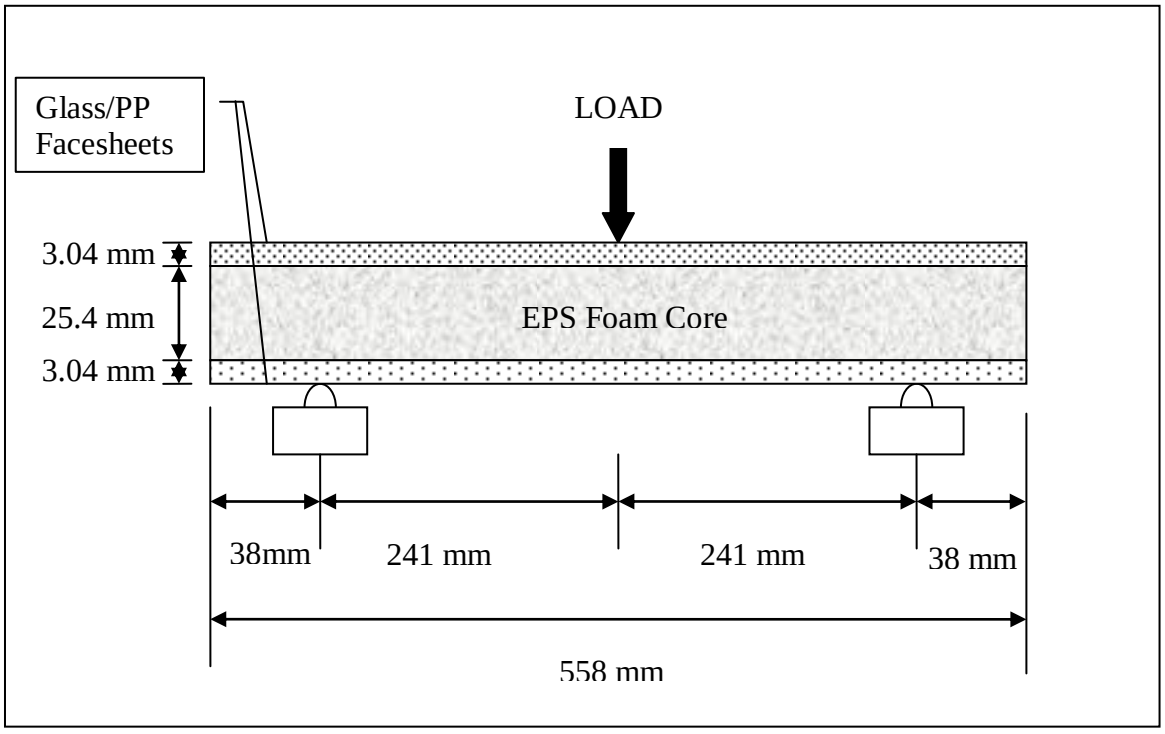

Figure 5.1. Test Setup of Three-Point Bending Test.

5.1.2—Test Results

A plot of the load versus deflection of the beam is shown in Figure 5.2. As seen in Figure 5.2, the load was approximately linear up to 250 N (56.2 lb) with the deflection of 21 mm (0.827 in.). The beam reached the rupture load at 300 N (67.45 lb) with the maximum deflection of 38.1mm (1.5 in.). As the load increased from this point, the deflection began to increase at a greater rate as seen in Figure 5.3. This was due to the stress in the beam was in the plastic range. Shear cracks were seen in the foam core approximately at 250 N (56.2 lb). The cracks were seen near the supports and their failure modes were 45º from the horizontal. There was no sign of slip bond failure between the facesheets and the core. In addition, it was observed that there was no fiber breakage in the facesheets.

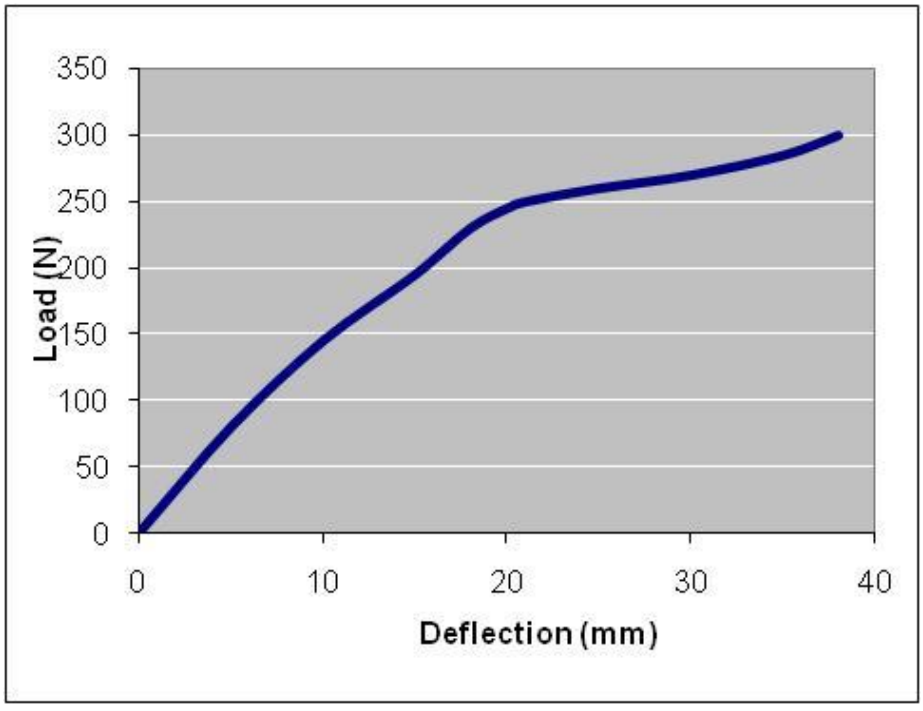

Figure 5.2. Load vs. Deflection Plot for the Beam made up of the Glass/PP Facesheets and the EPS Foam Core. (Note: The number of specimen tested was 3).

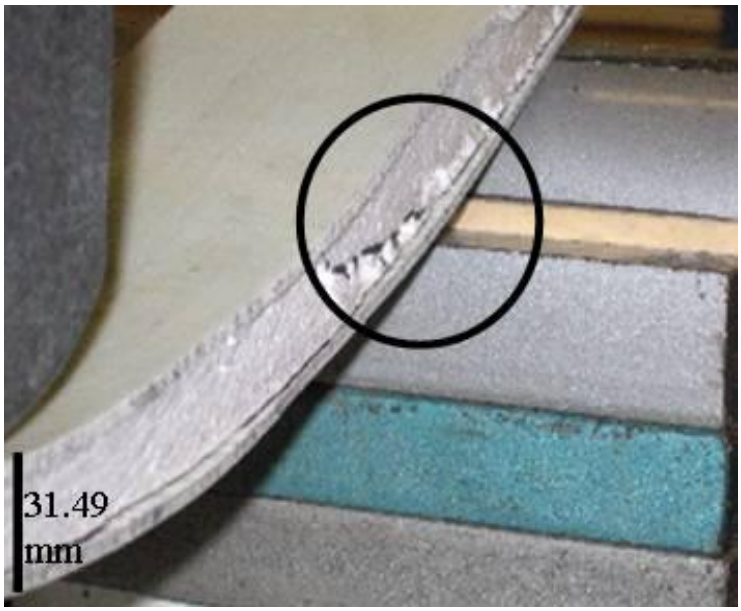

Figure 5.3. Shear Cracks developed in the Foam Core at 45 º from the Horizontal Once the Load Exceeded 250 N (56.2 lbf).

5.2—Component Verification

A small-scale model representing the E-Glass/PP and EPS sandwich composite beam was modeled and defined with the same properties and boundary conditions from the experimental testing. The model simulated the experimental three-point bending test. A linear static analysis was performed and compared. The geometric and material linear characteristics were carried up to the elastic limit under the applied load. The load vs. deflection plot was extracted from the solution.

5.2.1—Geometry

A three dimensional model for the beam was prepared, which simulated the same flexural, three point bending test of the Glass/PP and EPS beam that is seen in Figure 5.1.

The full geometric model was selected with a comparatively coarser mesh, but without affecting any significant convergence issues.

The geometric model incorporated a distinction between the Glass/PP facesheets and inner EPS foam core. The adhesions between the Glass/PP facesheets to the EPS foam core were assumed a perfect bond. There were no substantial bond failures between these interfaces during the experimental testing. Therefore, slip bond criteria was not defined in the model, and that a perfect bond between the interfaces was simulated by sharing the same nodes assigned to each material at their divisions. In this case, contact elements were not needed.

5.2.2—Element Types

It is important to determine the type of element used for descritization. Both the shell and solid element types can be used for the analysis. However, the choice depends on the level of post-processing desired. The shell element requires less number of nodes as compared to the solid elements because the shell element simplifies the model dramatically by reducing the three-dimensional element analysis into two-dimensional element analysis [5]. The solid three-dimensional element is generally used when the deformation of the thickness of element is desired.

For this model, the three-dimensional element type was used. The top and bottom facesheets were modeled using Solid191 element [5], representing the skin of the composite. The inner EPS foam core was modeled using Solid95 element [5]. Solid191 element [5] is defined by 20 nodes, layer thicknesses, layer-material-direction angles, and orthotropic material properties. It is a layered version of the 20-node structural Solid95

element [5]. Both elements have three degrees of freedom at each node, namely, translations in the nodal x, y, and z direction. Figure 5.4 shows the geometries of the Solid191 and Solid95.

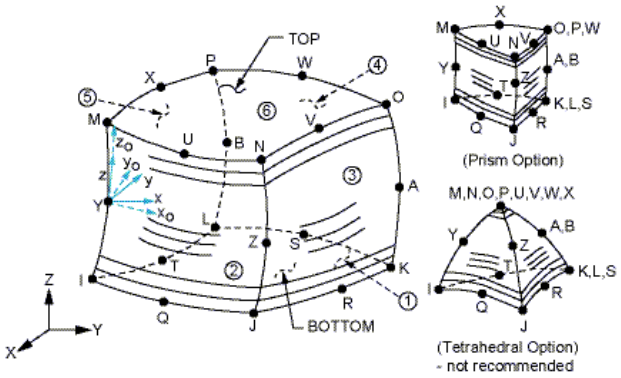

(a) Solid191 Geometry (for Facesheets)

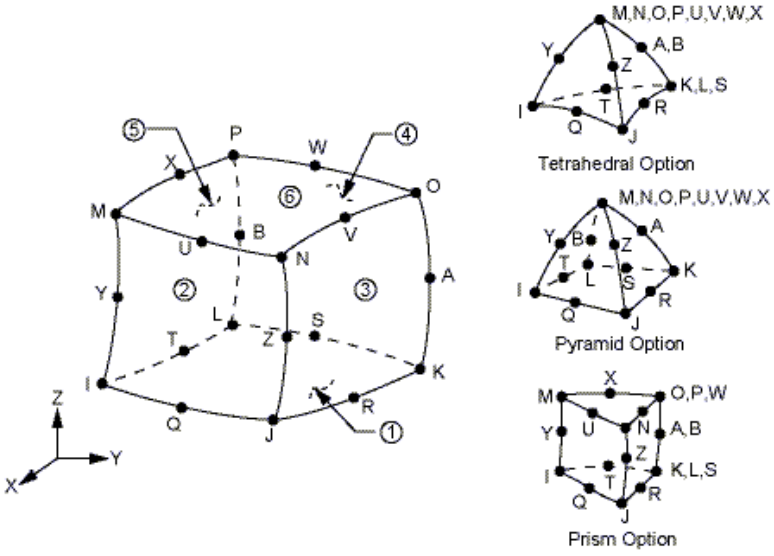

(b) Solid95 Geometry (for Core)

Figure 5.4. Solid191 and Solid95 Geometries [5].

5.2.3—Material Properties

An important step in modeling FRP composite materials is the input of material properties. The materials could either be isotropic or orthotropic materials. Isotropic materials, such as steel, have infinite number of planes of symmetry, where their properties are independent of their orientation [34]. Only two constants are required for input in the model to represent elastic properties. The constants include the Young's Modulus, *E*, and the Poisson's Ratio, υ. On the other hand, orthotropic materials, such as FRP composites, have three planes of symmetry (Figure 5.5) that coincide with the coordinate planes [34]. Nine constants are required for the orthotropic materials. They include three constants for the Young's Modulus (*E*) in the x, y, and, z directions, three constants for the Poisson's Ratios (γ) in the xy, yz, and xz planes, and last three constants for the Shear Modulus (*G*) in the xy, yz, and xz planes.

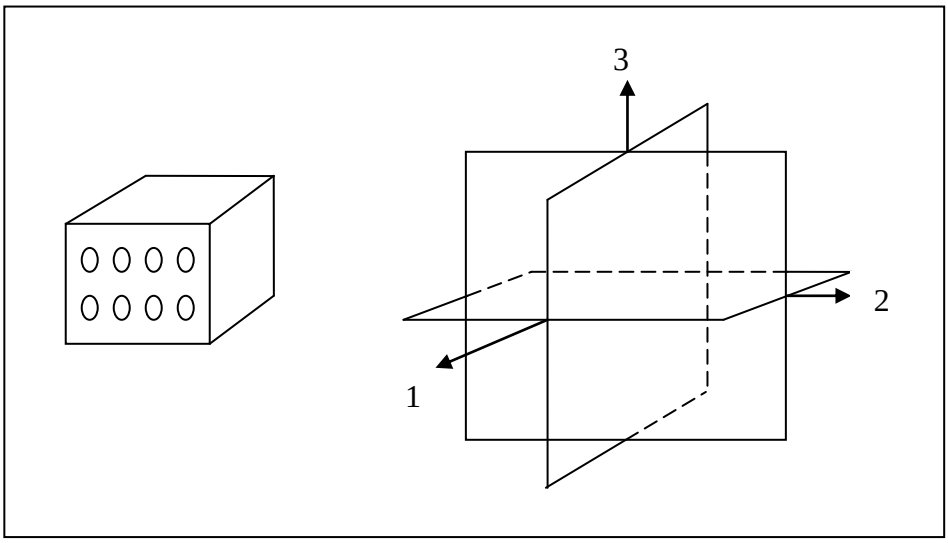

Figure 5.5. Orthotropic Material.

The material properties listed in Table 5.1 were directed along the local axis of the element, where the directions of the fibers were oriented parallel to the local x- and y-axes. The local directions of the fibers were also parallel to the global X (0º) and Y axes (90º).

Since the glass fibers reinforced composite are consisted of 70% bidirectional fibers [31], they are considered orthotropic materials. Each layer (top or bottom) of the Glass/PP facesheet was represented by two layer stacking sequence of the glass fibers with 0º/90º laminated fiber configurations. The EPS foam was input into the finite element model as linear isotropic material, meaning it was defined as completely homogeneous in all directions. No thickness constants are required for the EPS input since the solid element was used for the analysis.

Table 5.1. Properties of Glass/PP Facesheets and EPS Foam Core of Sandwich Composite Model

Material		Top/Bottom Layer for Glass/PP Facesheet	EPS Foam Core
Material Model Designation		Orthotropic	Isotropic
Young's Modulus (psi)	E_x	2,200,000	200
	E_y	2,200,000	200
	E_z	149,000	200
Poisson's Ratio	υ_{xy}	0.11	0.3
	υ_{yz}	0.22	0.3
	υ_{xz}	0.22	0.3
Shear Modulus (psi)	G_{xy}	261,000	300
	G_{yz}	109,000	300
	G_{xz}	109,000	300
Tensile Strength (psi)	-	46,000	-
Shear Strength (psi)	-	-	20

5.2.4—Meshing

The beam was meshed using the Solid191 and Solid95 elements for the Glass/PP facesheets and EPS foam core, respectively. The element-meshed sizes were divided evenly among the lines between the length, width, and thickness of the beam so that the convergence issue would not be affected. Care was taken to make sure the nodes between the interfaces share the same nodes so that a perfect bond and complete stress transfer could be simulated. The volume sweep command was used by meshing horizontally from one end to the next end of each volume. Figure 5.6 shows the meshing of the beam model.

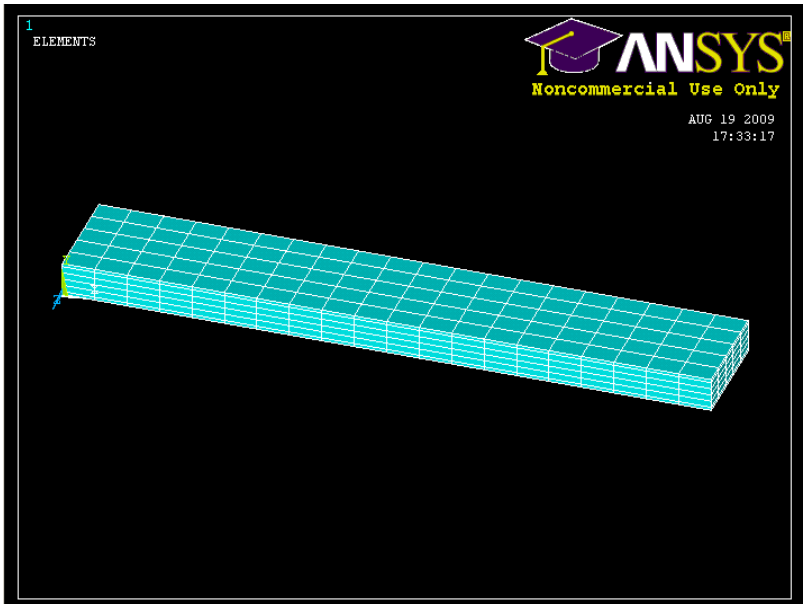

Figure 5.6. Meshing of the Glass/PP and EPS Beam.

5.2.5—Loading and Boundary Conditions

To simulate the boundary conditions shown in Figure 5.1, the nodes at the locations of the supports must be restrained. Restraining the nodes with all degrees of

freedom means that the nodes are restrained in the translations of the x, y, and z directions and rotations about the x, y, and z-axes, representing a fixed support condition. Therefore, rotations about the x, y, and z-axes were not restrained to reflect the experimental test environment. Whereas, the nodes at the two end supports were restrained in the translations in the y directions.

To simulate the loading applied on the top surface of the beam, the load was simulated as point loads. Since the width of the beam was divided into five segments that contained six nodes, the load was divided into sixths. From the results of the experiment, the elastic load was 250 N (56.2 lb). Therefore, the elastic load applied on each node was 42 N (9.37 lb) and the total load was equal to six times the point load applied at each node. Figure 5.7 shows the FEA loading and boundary conditions of the beam.

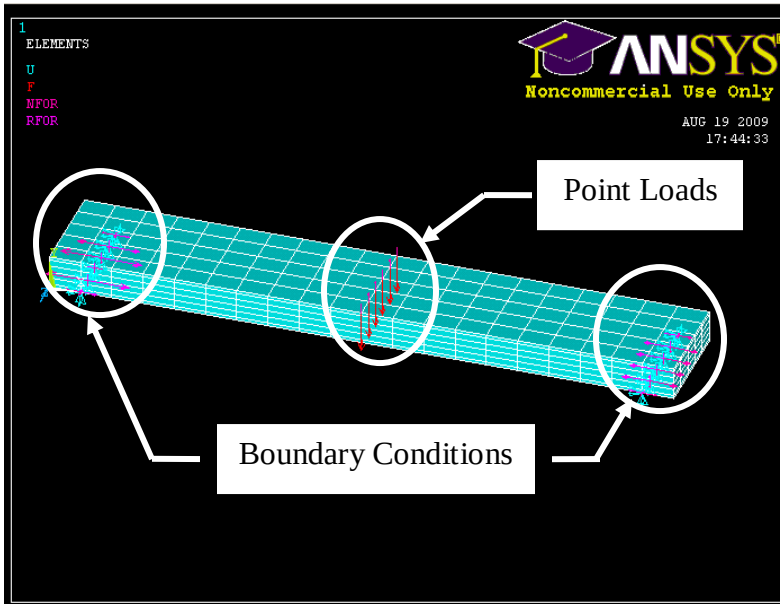

Figure 5.7. Loading and Boundary Conditions of the Beam.

5.2.6—Solution and Discussion of FEA Results

A nonlinear static analysis was performed with the FEA. As seen from Figure 5.8a, the maximum deflection of the beam made up of the Glass/PP and EPS materials with the load of 56.202 lb (250 N) was 0.657 in. (16.68 mm). It can be seen from this figure that the FEA result showed that the maximum deflection occurred at the center of the beam and predicted the same behavior as the experimental testing. Figure 5.8b shows the maximum deflection in the x-direction occurred near the supports of the beam, which is also seen from the experimental shear cracks developed from within the core. This was due to the transfer of the stresses from the two facesheets to the EPS foam core, which was responsible for taking up almost all the shear stresses.

The deflection obtained from the experimental testing under the same loading was 0.827 in. (21 mm). The percent difference between the FEA results and the experimental results in terms of the load versus deflection was 21%. The reasons for the difference were the uniformity in the material and the boundary conditions input into the FEA. Material input into the FEA was assumed uniform and that there were no defects in the materials and the geometric properties, whereas, the actual specimens often have small variations and defects in their geometric dimensions and materials. The boundary conditions were also responsible for the difference because at the time of loading during the experiment, there were slippage in the two end supports and 5 in. (0.127 m) permanent deformation, which were also not accounted in the FEA modeling. Hence, the FEA model was stiffer than the physical specimen was. However, the load versus displacement plot from the FEA and the experimental testing showed similar trend as shown in Figure 5.9. The FEA contour plot was considered accurate in predicting the

beam flexural behavior under loading. The FEA results were within a reasonable limit as compared to the experimental results. From this analysis, it was concluded that the FEA results could be used as a representation of the experimental testing under loading. In addition, similar analysis could be carried out on the full-scaled FRP panels without conducting the experimental testing on them.

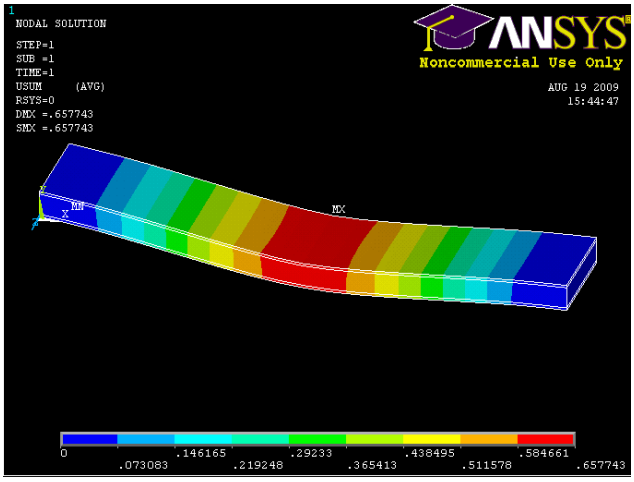

(a). Maximum Deflection Occurred at the Center of the Beam

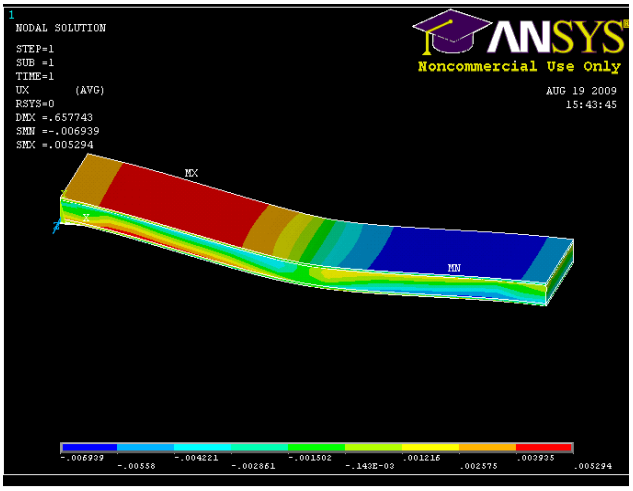

(b) Maximum Deflection in the X-Direction Occurred at the Supports of the Beam

Figure 5.8. Nodal Deflection Contours.

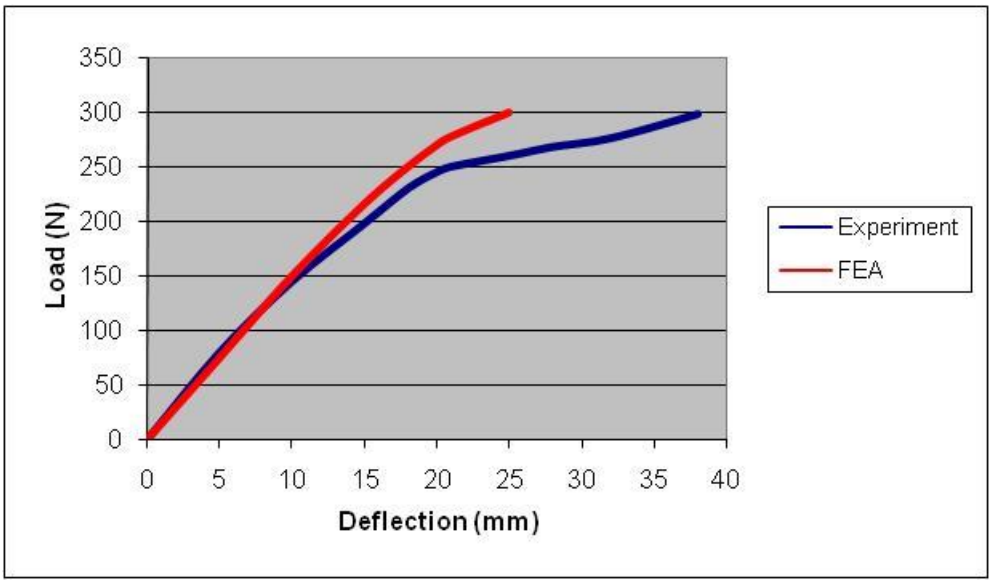

Figure 5.9. Load versus Deflection Plot for the FEA and the Experimental Results. (Note: The number of specimen tested was 3).

5.3—Flexural Testing and FEA of Wire-Meshed Model

The objective of the research was to study two different FRP materials as described previously in Chapter 3. The reason was to have alternative materials if one of the two materials (sandwich composite model) did not work to carry the external loads then the other material could be used as the backup material (wire-meshed model). Since the FEA results of the sandwich composite model were similar with the experimental results under the flexural testing, the FEA wire-meshed model was assumed to behave as wire-meshed beam under flexural testing. Therefore, no experimental testing or FEA were conducted on the wire-meshed model.

CHAPTER 6

DESIGN & FINITE ELEMENT MODELING OF PANELS

6.1—Overview of Design in FEM

Chapter 5 shows the results obtained from the FEA, which was validated by comparing its results to the experimental results. The FEA results were very similar to the experimental results under the flexural loading. The FEA has provided insight into predicting the structural behavior of the specimen and it can be used as a valuable source in predicting the specimen behavior under other loading such as high wind pressure loading. Since the small-scaled beam model has proven to be useful in predicting the structural behavior, the shelter model can be simulated at the full-scale level, where the wind pressure loading can be applied to each panel of the shelter.

This chapter provides the design and analysis of the panels of the sandwich composite model and the wire-meshed model under the wind pressure loading, which was are presented in Chapter 4. The design of the panels for each model was done through the FEA, where the stress results obtained from the model would be compared to the strength of the fibers through failure criteria. This comparison determined whether the panel had failed under the applied load. If fail under the applied load, then the design would be changed by adding more layers of the FRP laminates or increasing the material properties to give higher properties and strength.

For the preliminary design, the Glass/PP and EPS model was kept with the same thickness of 5.74 in. (14.58 cm) as the Glass/PP and EPS beam presented in Chapter 5. For the wire-meshed model, the preliminary design of the composite had a thickness of 0.69 in. (1.75 cm). More layers would be added if necessary. A linear static analysis was conducted on the panels of both models.

6.2—Design & FEM of Composite Panels

6.2.1— Modeling Geometry of Shelter

The geometry of the shelter with dimensions 7 ½ ft x 12 ½ ft x 40 ft (12.20 m x 3.81 m x 2.29 m) was constructed from the bottom to top approach, where it was made from constructing the key points, to lines, to areas, and then to volumes. Initially, the geometry for different materials of the shelter was created as shell models, where the shell elements were represented by the mid-surface of the real shells that were located halfway through the thickness. The thickness of each layer of the composite was input as the real constant without actually modeling the real geometry with the thickness. According to Barbero [34], creating a structure using shell elements is certainly an advantage for modeling thin composite plates because a change of a fiber volume fraction or constituents, for example, the thickness of the plates, can easily be changed by assigning the real constants to represent the real physical thickness of the plates. On the other hand, a change in a fiber volume fraction or constituents cannot be represented by real constants when the solid elements are used because the real physical thickness of the geometry has to be physically created. However, there is a disadvantage associated with using the shell elements. The results of the shell elements are usually less accurate than

the results of the solid elements, simply because there are fewer nodes in the shell elements than there are in the solid elements for capturing the close proximity of the real situation. Therefore, it was decided that the models would be created as solid models.

The final geometries of the sandwich composite model and the wire-meshed model were formed as solid models, but only halves of the models were utilized. Due to a large numbers of the solid elements used to solve the layer stacking sequence (LSS), loading, and constraint equations in the full composite models, the computational time and memory requirements were so large that they had affected the convergence issues. Therefore, it was decided that only halves of the models would be used instead of the full models in order to overcome the convergence issues. Figure 6.1 shows only half of the shelter was being created.

For the design and analysis of the panels, different components within the bolted connections such as the bolts, connection geometry, and endplates were not included in the geometry. However, in ANSYS 11.0 [5], which has the "glue" option that allows objects to be glued to each other and treats as welded parts. In this case, each panel was glued to the neighboring panel of the shelter and the panel-to-panel connections were treated as welded connections, which were responsible for holding the shelter together under the wind pressure loading.

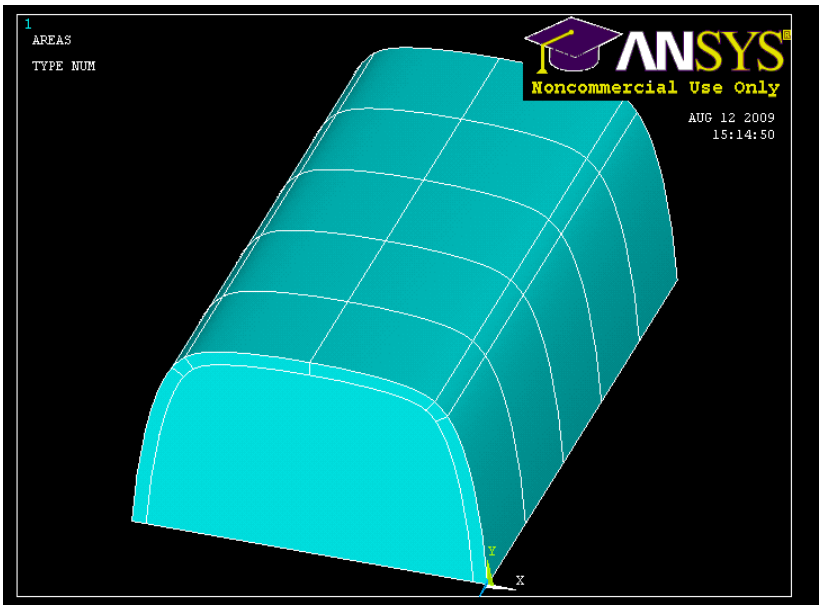

Figure 6.1. The Geometry of the Shelter Modeled as a Half Shelter.

6.2.2—Element Types

Important to modeling FRP materials is the choice of element used because it determines the element formulation used [5], [34]. Each layer of the composites (sandwich composite model and wire-meshed model) was modeled using Solid191 element [5]. Again, as explained earlier in Chapter 5, it is a layered, linear solid element, which has 20 nodes, 6 degrees of freedom (DOF) at each node: 3 DOFs in the translations of the x, y, and z-directions, and 3 DOFs of rotations about the x, y, and z-axis. It is a layered element, which takes into consideration of the ply sequence in a laminated composite, where each fiber layer, direction of the fibers, layer thickness and material properties of each layer are input into the solid elements to represent the physical and mechanical properties of the FRP laminates [5].

6.2.3—Material Properties

To assign the material properties for each model (Glass/PP and EPS sandwich composite and wire-meshed composite), the elements in each model must be coupled with their materials. By choosing the Solid191 element [5], the FRP materials were input into the models by assigning the isotropic properties and orthotropic properties to the composites.

An important consideration in defining the orthotropic properties of the facesheets or laminates was the material coordinate system with respect to the global coordinate system of the entire model. The material properties described in Chapter 3 were input into the ANSYS models and directed along the local coordinate system for which they were assigned. For the purpose of clarity, the local coordinate system was distinguished from the global coordinate system by assigning xx = 1, yy = 2, and zz = 3 to represent the local x, y, and z coordinates, respectively. The global coordinate system was represented by capital letters X, Y and Z to distinguish from the local coordinate system xx, yy, and zz. Figure 6.2 shows the illustration of the local coordinate system with respect to the global coordinate system used in ANSYS.

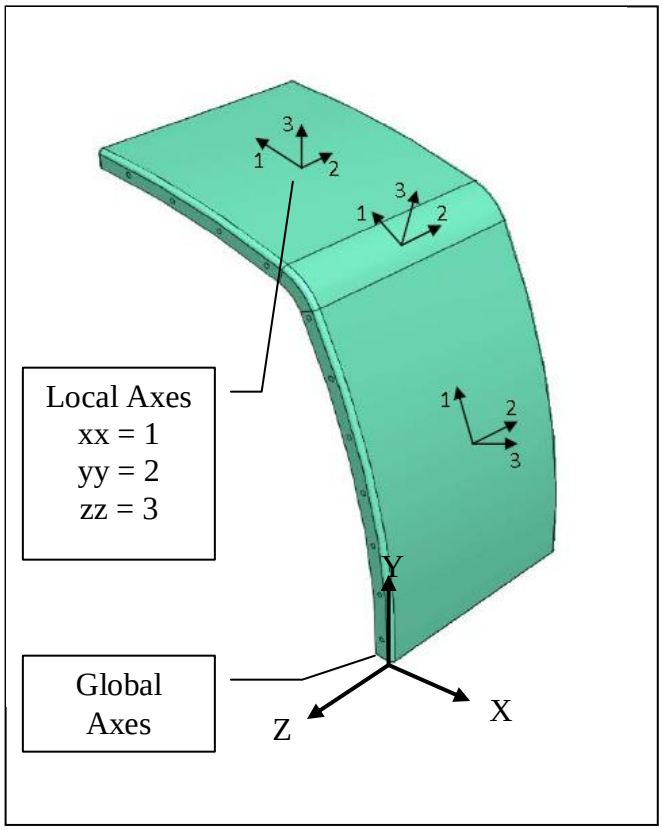

Figure 6.2. Illustration of Local Coordinate System with respect to Global Coordinate System.

6.2.3.1—Model 1: SIPs made up of Glass/PP Facesheets and EPS Foam Core

For the Glass/PP and EPS composite model, the isotropic properties were assigned to the EPS foam core, and the orthotropic materials were assigned to the top and bottom layers of the Glass/PP facesheets. Two constants were required for input to represent the materials of the EPS foam core. The two constants were the elastic modulus and the Poisson's ratio (Table 5.1). On the other hand, nine constants were required for the orthotropic materials of the Glass/PP facesheets. The nine constants were the elastic modulus, the Poisson's ratios, and the shear modulus. These constants were obtained from Table 5.1.

Since the Glass/PP was bidirectional fibers, the major directions of the fibers were directed along the xx (0º) and yy (90º) local directions. Each bidirectional layer was modeled as two individual layers, where one layer had the 0º fiber direction and the other layer had the 90º fiber direction. The total thickness of each Glass/PP layer was divided in half to account for the two different fiber directions, as shown in Figure 6.3.

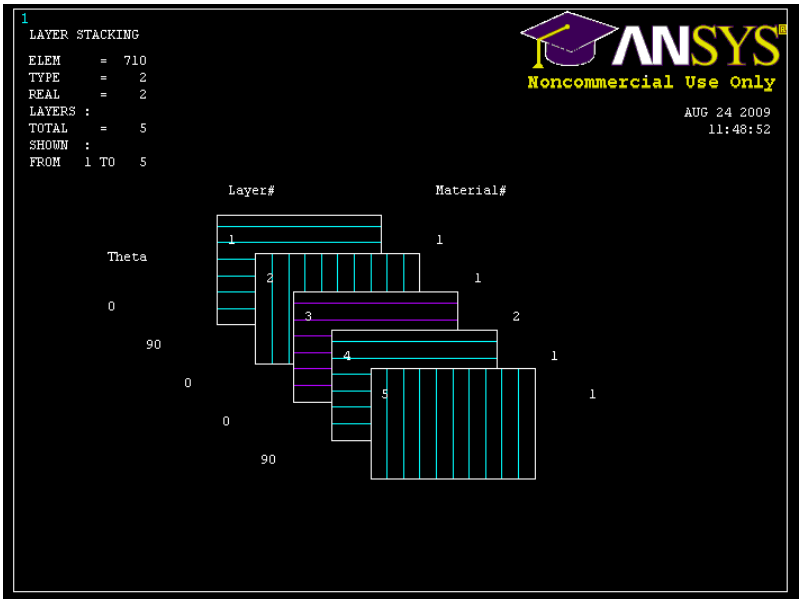

Figure 6.3. Layer Fiber Directions and Material Resignations were represented by Layer Stacking Sequence (LSS). The Glass/PP Facesheets and EPS were assigned with Materials 1 and 2, respectively.

6.2.3.2—Model 2: SIPs made up of Glass/Polyester and Glass Wire-Meshed/Polyester Facesheets

For the wire-meshed model, orthotropic materials were assigned to each layer of the FRP laminate within the wire-meshed composite. Nine constants were also required for this model. The nine constants were obtained from Table 3.3. The number of layers in the composite was incorporated into the model by using LSS of the Solid191 element,

where the fiber orientations, layer number and thickness of each layer were defined as material constants. Figure 6.4 shows the LSS for the wire-meshed laminates.

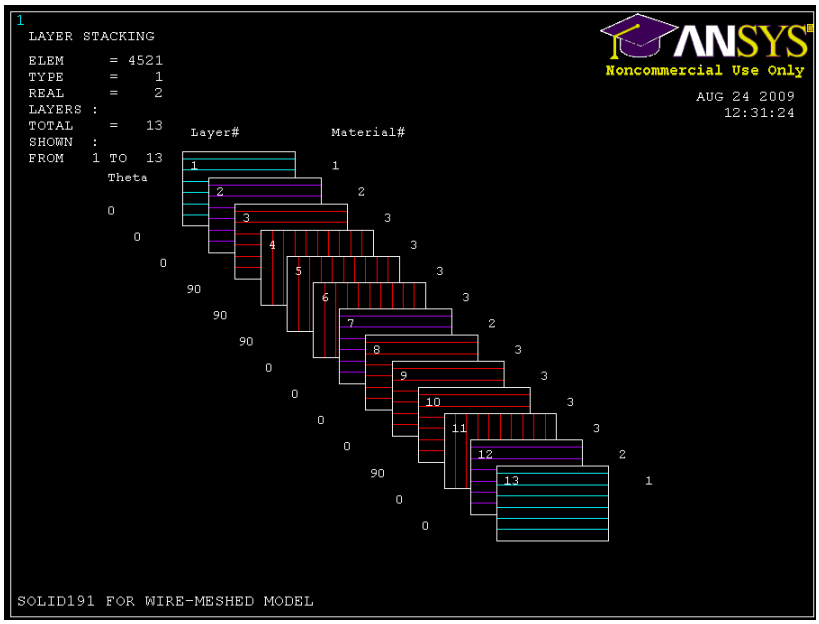

Figure 6.4. Illustration of LSS, where Materials 1, 2, and 3 indicated the Gel Coat Laminates, Backup Laminates, and Wire-Meshed Laminates, respectively.

6.2.4—Meshing of Models

The geometries of both models were meshed with quadrilateral shape with smart element sizing. Smart element sizing is a meshing option that provides a range of settings (from coarser to fine mesh) for models [5]. The advantage of using Smart Sizing is that it gives the mesher a better chance of creating reasonably shaped elements during the meshing generation without affecting the aspect ratio (ratio between the shortest surface dimension *a* and the thickness *t*) of the elements. The Smart Sizing algorithm first computes estimated element edge lengths for all lines in the areas or volumes being meshed by setting an even number of line divisions around each area or volume [5]. The

edge lengths on these lines are then refined for curvature and proximity of features in the geometry. This technique of meshing gives accurate stress distribution and reasonably analysis time. Figure 6.5 shows the mesh distribution of the Glass/PP and EPS sandwich composite model using Smart Sizing technique. Figure 6.6 shows the mesh distribution of wire-meshed model using Smart Sizing technique.

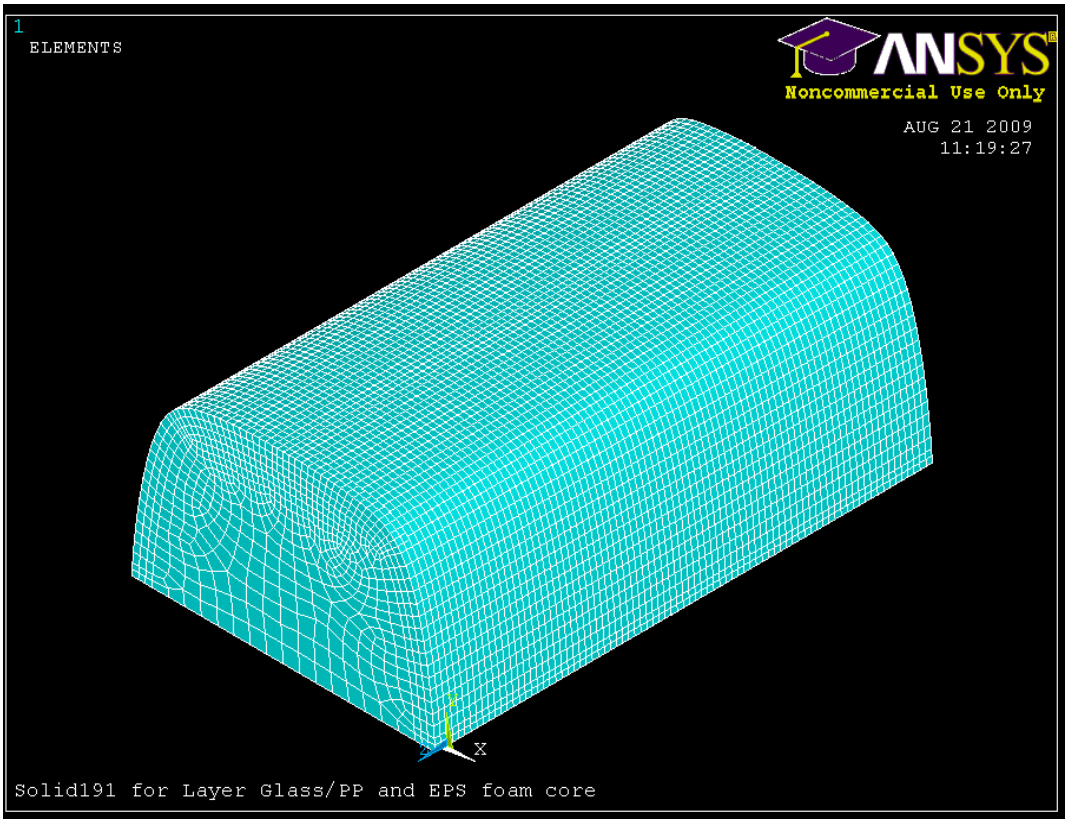

(a) Mesh of Glass/PP and EPS Half Model (Front Isometric View)

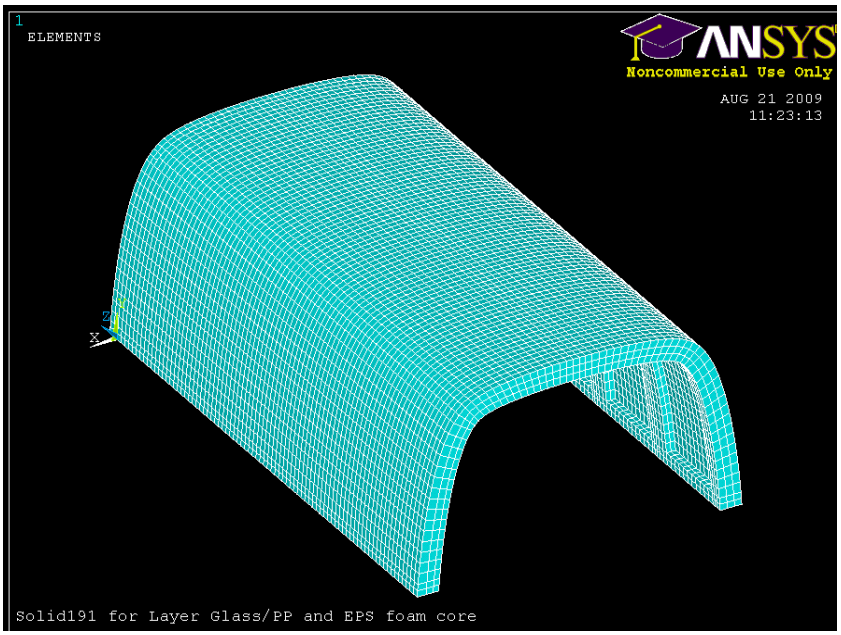

(b) Mesh of Glass/PP and EPS Half Model (Back Isometric View)

Figure 6.5. Mesh Distribution of the Glass/PP and EPS Sandwich Composite Model with Thickness of 5.74 in. (14.58 cm).

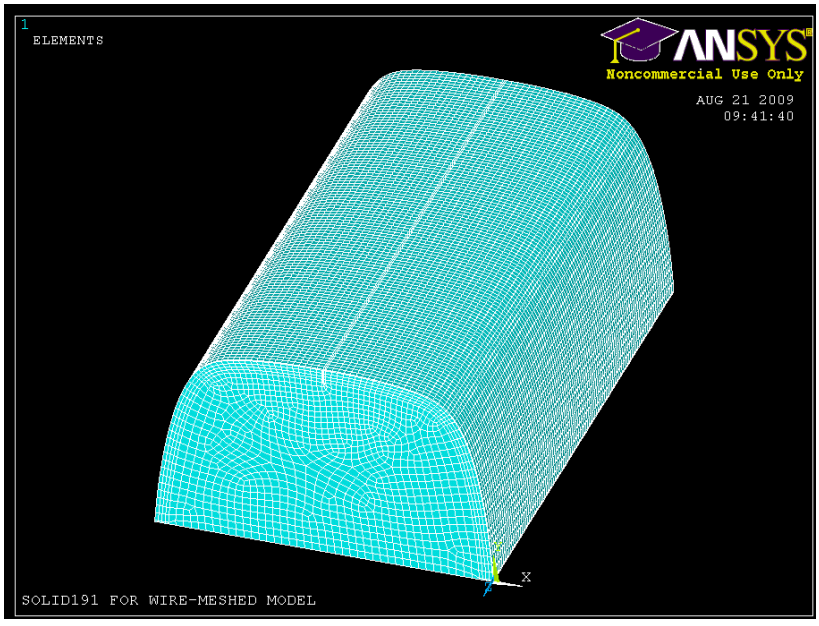

(a) Mesh of Wire-Meshed Half Model (Front Isometric View)

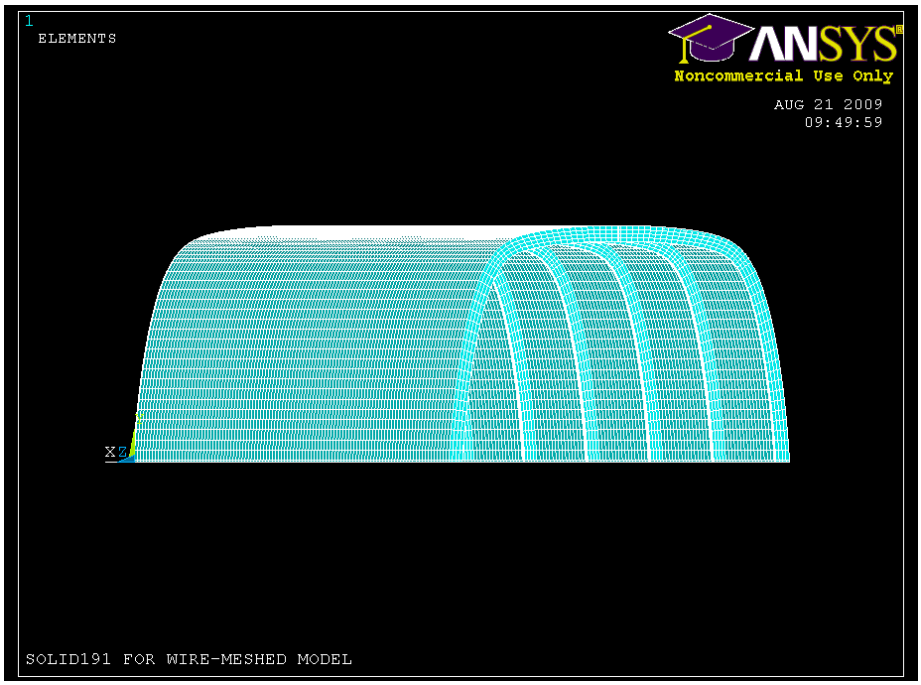

(b) Mesh of Wire-Meshed Half Model (Back Isometric View)

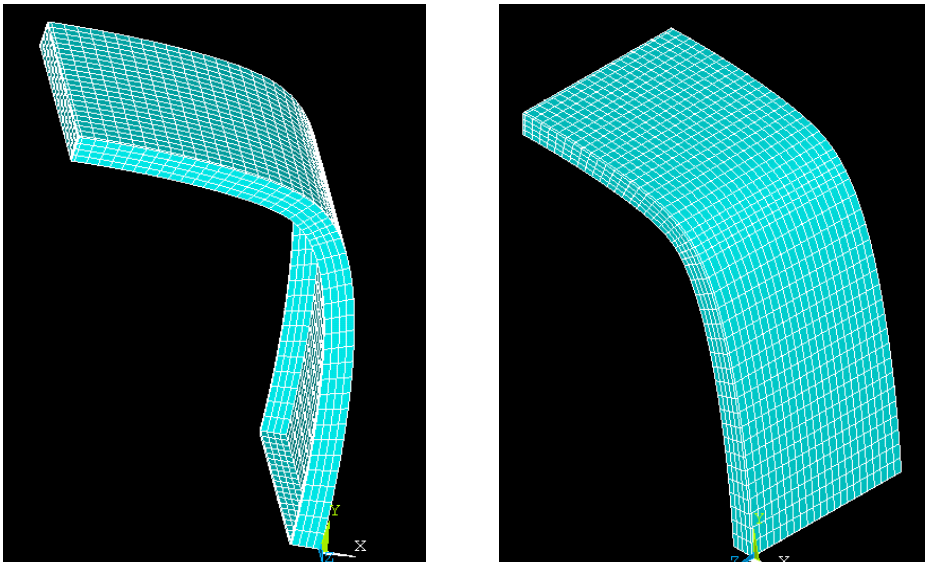

(c) Mesh of a Wire-Meshed Panel with Panel Thickness of 0.69 in.(1.75 cm)

Figure 6.6. Mesh Distribution of the Wired-Meshed Model.

6.2.5—Loading & Boundary Conditions

The variables that varied between the two models were the material properties; therefore, the loading and boundary conditions were kept constant for the two models for the FEA. Since only half of the shelter was modeled, a symmetry boundary condition was applied on the FRP flanges along the symmetry plane. A symmetry boundary condition means that out-of-plane translations and in-plane rotations were set to zero [5]. The use of symmetry is listed in Figure 6.7. Figure 6.8a shows the application of the symmetry conditions on the symmetry plane of the shelter.

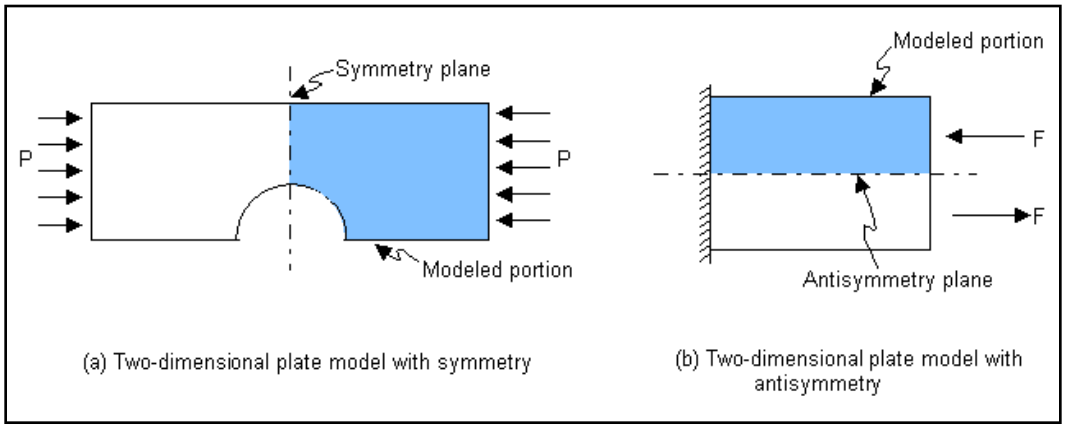

Figure 6.7. Example of Symmetry Conditions [5].

Rotations about the x, y, and z coordinates and displacements in the x, y, and z directions were restrained at the bottom of all FRP flanges where they encountered the concrete slab. Restraining the displacements in the x, y, and z directions and rotations about the x, y, and z coordinates were necessary in order to represent the rigid connections at these locations.

The wind pressure loading from Table 4.10 was applied on the surface areas of the shelter as uniform static pressures. The plus and minus pressures from Table 4.10 indicate the directions of the wind pressures that are applied on the shelter. The ANSYS sign convention is opposite to the sign convention used in this thesis. Hence, it is important to apply the magnitudes and directions of wind pressures in ANSYS models correctly in order to imitate the real behaviors of the wind on the structure. The ANSYS sign convention is as follows: compression pressure over a surface area is introduced using a negative number and tension pressure over a surface area is introduced using a positive number [5].

To account for the $0.9D + 1.2W_x$ load combination, where D is the dead weight of the structure and W_x is the extreme wind pressure, as described in Chapter 4, the FEA models also took into account of the load combination happening all at once. The wind load factor of 1.2 was already encountered in the calculations as shown in Table 4.10. Therefore, the wind load factor of 1.2 was not considered again in the ANSYS models, when the wind pressures from Table 4.10 were already adjusted for the load factor. The wind pressures were applied onto the models as the way they were presented in Table 4.10. They were applied as uniform static pressures over the surface areas.

On the other hand, since there was no dead load encountered in the calculations, the dead load was factored in the models to achieve the dead load effect. To consider the dead load effect of the models, two inputs were required: the gravity and the mass of the materials of the models. To consider the effect of gravity pulling down on a structure, ANSYS 11.0 [5] uses consistent gravity acceleration as 32.2 ft/s^2 for U.S units and 9.8 m/s^2 for metric units. Even if the units used for the models were in in/s^2, the gravity

acceleration was still 32.2 ft/s^2 (9.81 m/s^2) pointing in the positive Y-direction to be consistent with the universal gravity. In another word, a positive acceleration in the y direction stimulates the gravity in the negative Y direction. As seen from Figure 6.8b, a red arrow pointing in the positive Y direction indicates that the acceleration had been defined in the Y direction.

The gravity acceleration of 32.2 ft/s^2 (9.81 m/s^2) with the dead load factor of 0.9 and the mass of the materials of each model were applied onto each model as the dead weight of the shelter. The masses of the Glass/PP, EPS and wire-meshed laminates were defined by inputting the densities of the materials into the models. The densities of the Glass/PP and EPS materials were taken from Table 3.2, where the density of the wire-meshed model was obtained from Table 3.3. The two models had the same loading and boundary conditions. Figure 6.8 shows the representation of symmetry, boundary and loadings on the shelter for both models.

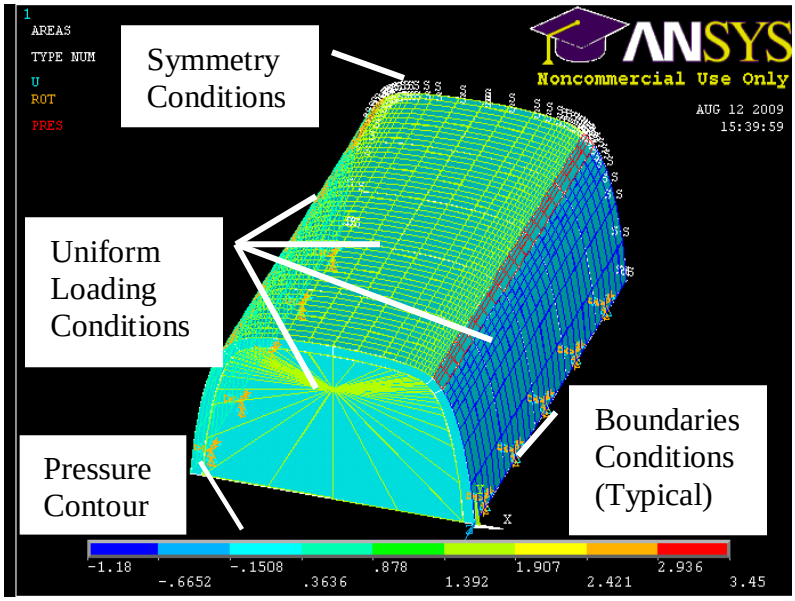

(a) Loading and Boundary Conditions of Sandwich Composite Model and Wire-Meshed Model

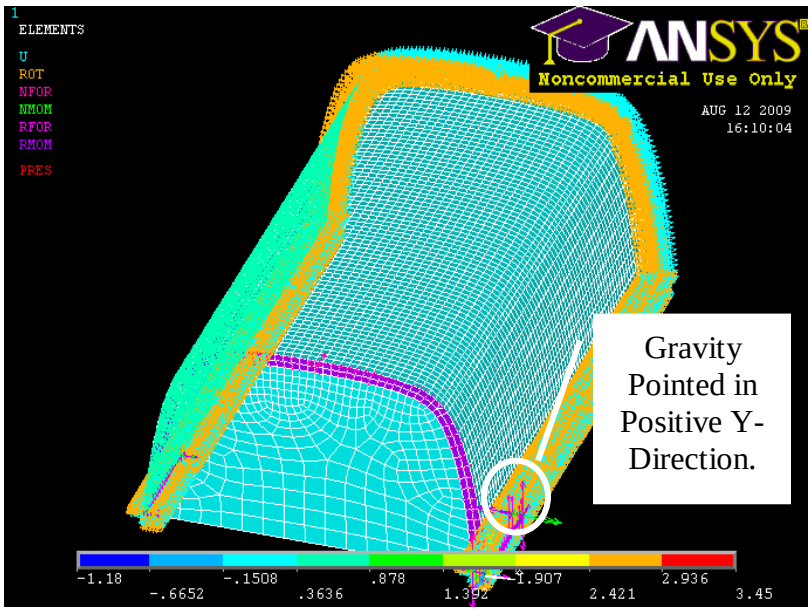

(b) Application of Gravity

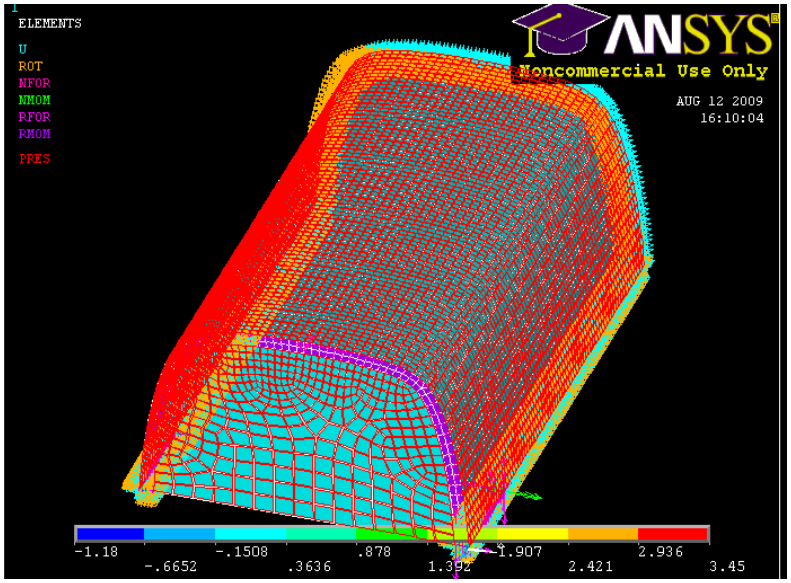

(c). Loading Transferred to FE

Figure 6.8. Symmetry, Boundary and Loadings on the Shelter.

6.2.6—Solutions and Discussions of Results

This section provides the results obtained from the linear static simulations. The results for the two FRP models are divided into two separate sections for discussions. Section 6.2.5.1 shows the results and discussions of the results of the FRP model made up of E-Glass/PP and EPS materials. Section 6.2.5.2 shows the results and discussions of the results of the model made up of E-Glass/Polyester wire-meshed materials.

6.2.6.1—Results and Discussion of Results of E-Glass/PP and EPS Model

The maximum deflection obtained from the linear static analysis was 4.669 in. (11.9 cm). The overall maximum deflections in the X, Y, and Z directions were 2.881 in. (7.32 cm), 0.596 in. (1.51 cm), and 0.209 in. (0.531 cm), respectively. Figure 6.9 shows the deflections obtained for the E-Glass/PP and EPS sandwich composite model.

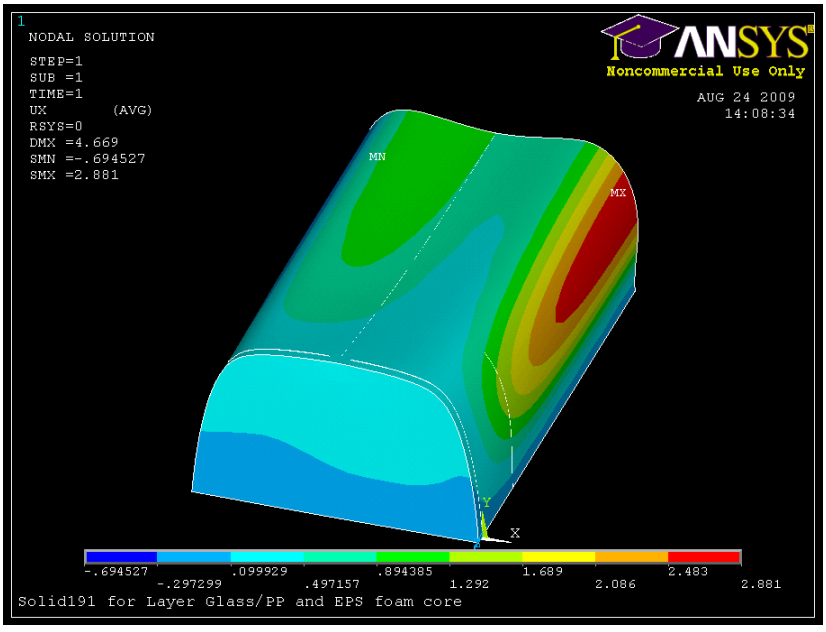

(a) Maximum Deflection in the Global X-Direction was 2.881 in. (7.32 cm)

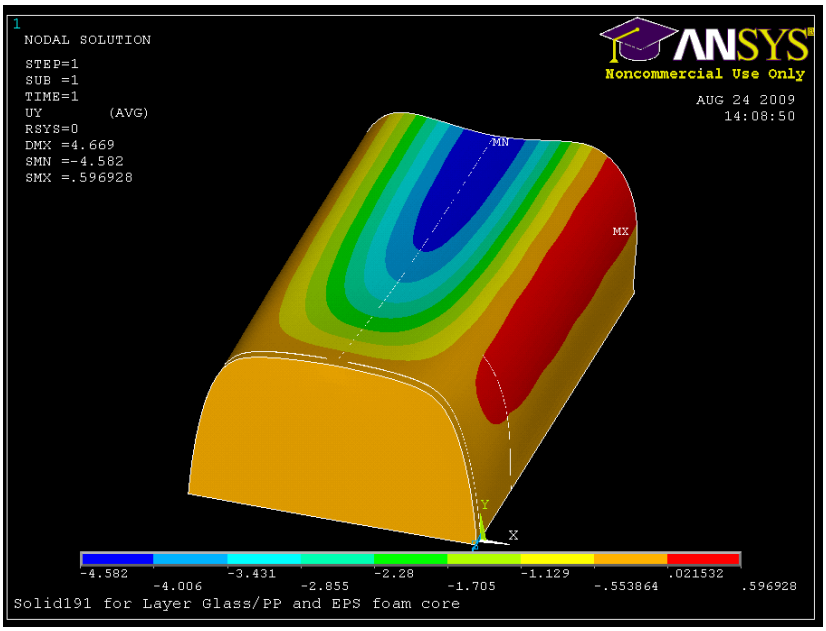

(a) Maximum Deflection in the Global Y-Direction was 0.596 in. (1.51 cm)

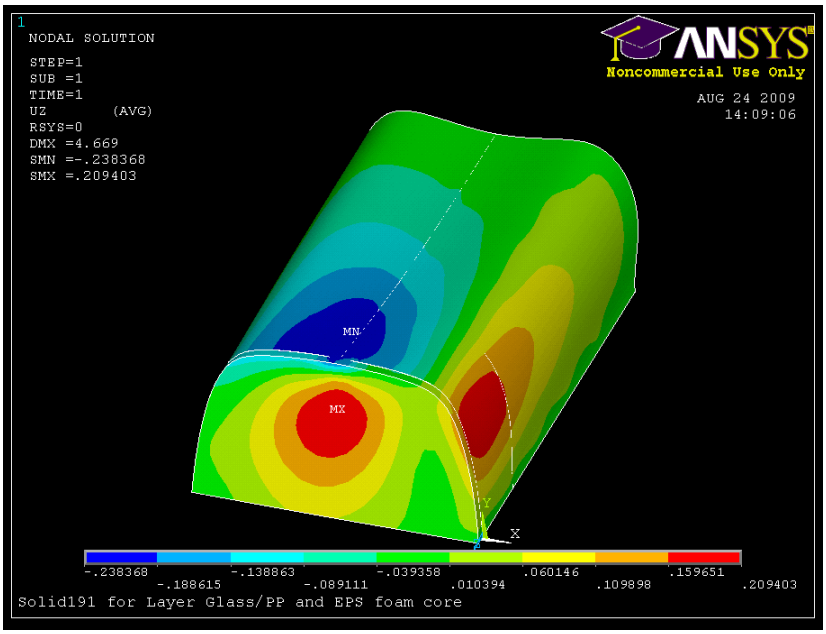

(c) Maximum Deflection in the Global Z-Direction was 0.209 in. (0.531 cm)

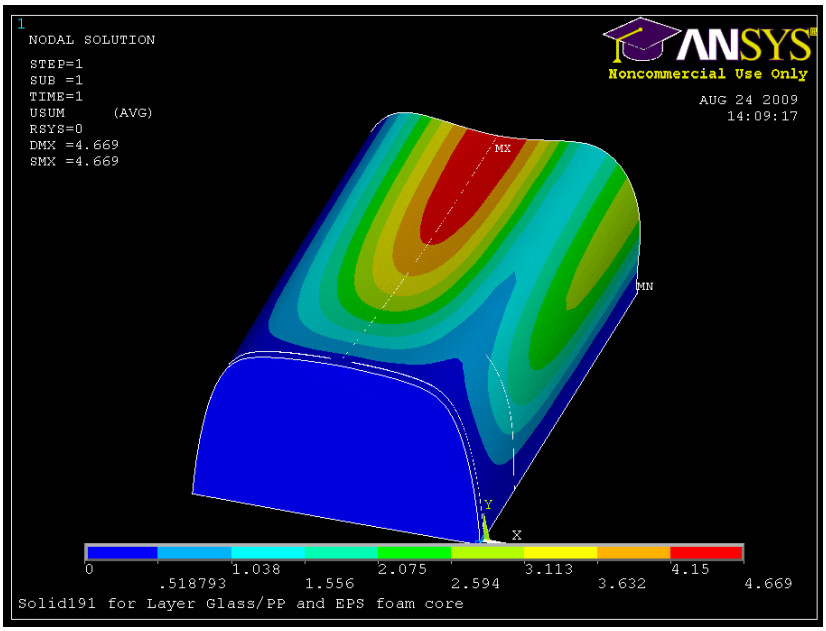

(d) Maximum Displacement Vector Sum was 4.669 in. (11.86 cm)

Figure 6.9. Maximum Deflections of Glass/PP and EPS Sandwich Composite Model.

The maximum stresses in each layer of the sandwich composite model obtained from the FEA analysis are presented in Table 6.1. The maximum principal stress that the Glass/PP facesheets could take was 10,375 psi (71,533,106.8 N/m^2). The Principal Stress 1 was higher than the Principal Stresses 2 and 3, because it was responsible for taking up the main stress directed along the thickness direction. As seen from Table 6.1, the maximum Principal Stress 1 was higher than any other principal stresses in all the layers. Layer 4 had the highest Principal Stress 1 and the YZ shear stress. Figure 6.10 shows the maximum stresses that Layer 4 could take in the local x, y, and z directions were 7,730 psi (53,296,473.8 N/m^2), 7,922 psi (54,620,267.2 N/m^2), and 5,551 psi (38,272,797.7 N/m^2), respectively.

Table 6.1. Maximum Local Stresses of Glass/PP and EPS Model Produced at Wind Pressure Loading

Layer Number	Maximum Stress (psi)					
	Principal 1	Principal 2	Principal 3	XY Shear	YZ Shear	XZ Shear
1	8970	2438	704.90	4479	5205	2955
2	9079	2559	809.75	4480	5274	2932
3	8.095	2.57	2.53	2.611	2.46	2.13
4	10375	2180	1011	4522	5322	2174
5	10082	2214	1043	4523	5228	2154

1 psi = 6,894.8 N/m^2

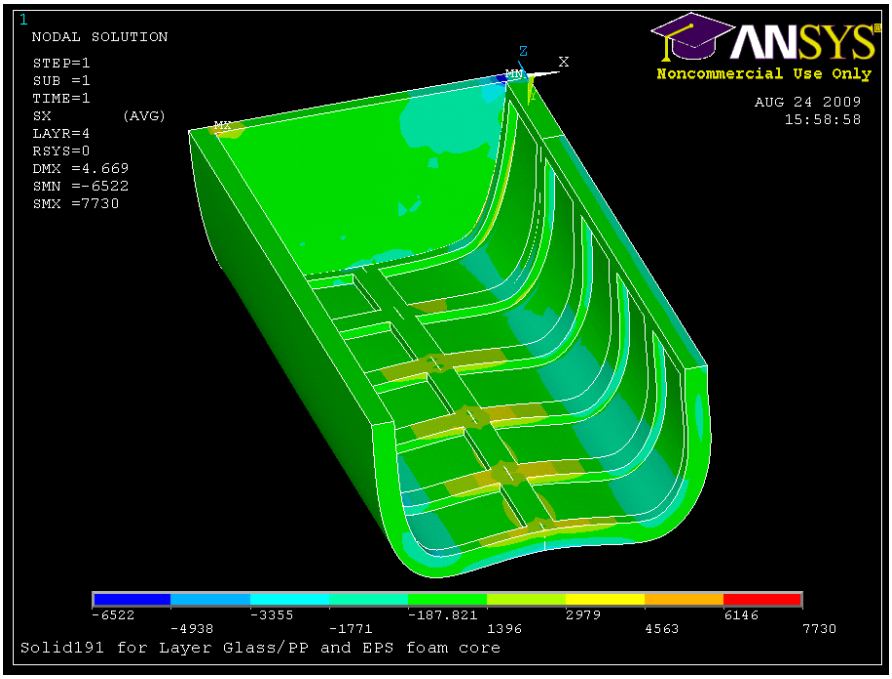

(a) The Maximum Stress in the Local x-Direction of Layer 4 was 7,730 psi (53,296,473.8 N/m^2), which was at the Bottom of the FRP flanges, where the Flanges and Concrete Slab Met

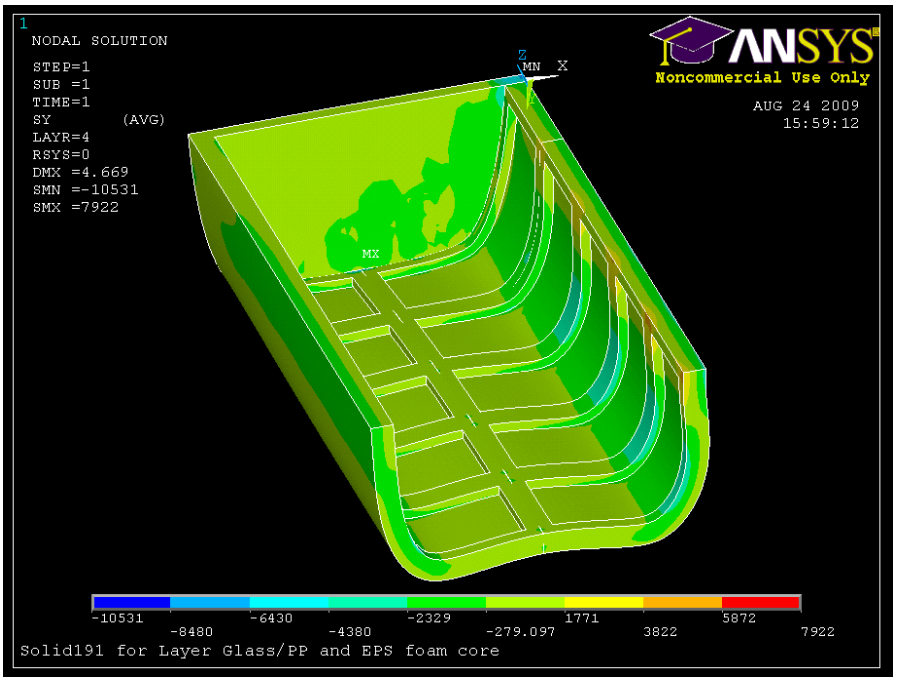

(b) The Maximum Stress in the Local y-Direction of Layer 4 was 7,922 psi (54,620,267.2 N/m^2), which was at the Bottom of the FRP flanges, where the Flanges and Concrete Slab Met

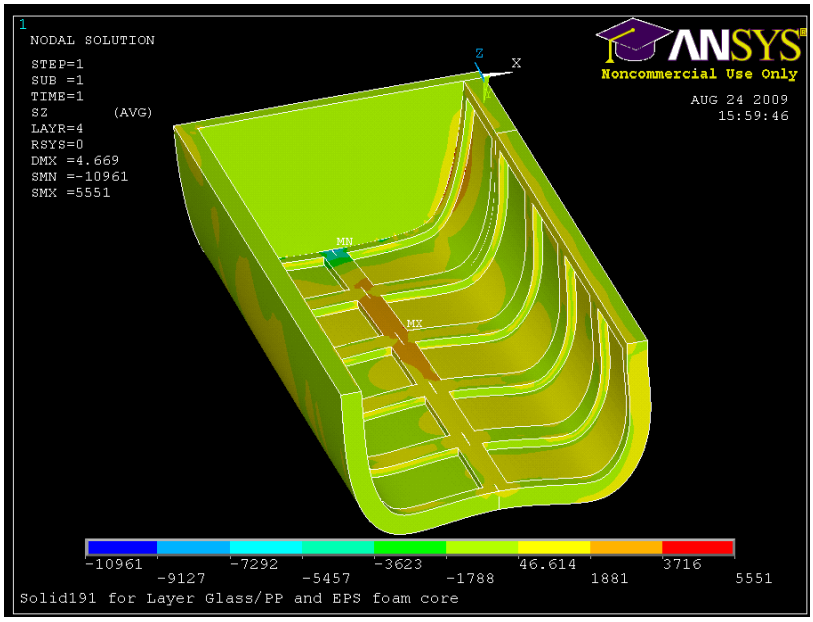

(c) The Maximum Stress in the Local z-Direction of Layer 4 was 5,551 psi (38,272,797.7 N/m^2) which was between the Top FRP Flanges where the Connections were to be Bolted Together

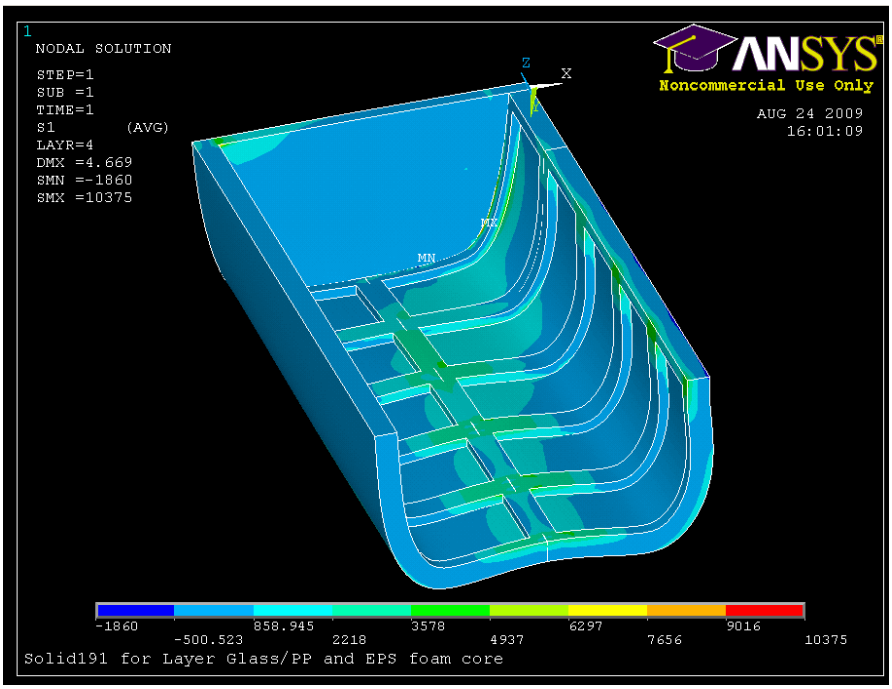

(d) The Maximum Principal Stress 1 of Layer 4 was 10,375 psi (71,533,106.8 N/m^2) which was the Highest Stress Relative to Other layers

Figure 6.10. Maximum Stresses in Layer 4, which was the Glass/PP Layer of Sandwich Composite Model.

Because the Glass/PP laminates were the main reinforcements for the analysis, the failure analysis was carried out on those laminates. Failure criteria can be described by Barbero [34] as follows: "Failure criteria are curved fits of experimental data that attempt to predict failure under multiaxial stress based on experimental data obtained under uniaxial stress." The general failure criteria [34] defined in many FEA packages are presented using the notation of failure index as:

$$I_F = \frac{stress}{strength} \tag{6.1}$$

Failure criteria are predicted when $I_F \geq 1$ and the strength ratio is the inverse of the failure index as:

$$R = \frac{1}{I_F} = \frac{strength}{stress} \tag{6.2}$$

where $R \leq 1$ means that failure has occurred.

In this thesis, the Tsai-Wu failure criterion was conducted to predict the first occurrence of failure in one of the laminates, not tracking damage propagation up to laminate failure. The Tsai-Wu criteria states that failure occurs when

$$I_F = \frac{1}{R} = \left[-\frac{B}{2A} + \sqrt{\left(\frac{B}{2A}\right)^2 + \frac{1}{A}} \right]^{-1} \tag{6.3}$$

where

$$A = \frac{\sigma_1^{\,2}}{F_{1t}F_{1c}} + \frac{\sigma_2^{\,2}}{F_{2t}F_{2c}} + \frac{\sigma_3^{\,2}}{F_{3t}F_{3c}} + \frac{\sigma_4^{\,2}}{F_4^{\,2}} + \frac{\sigma_5^{\,2}}{F_5^{\,2}} + \frac{\sigma_6^{\,2}}{F_6^{\,2}} + c_4 \frac{\sigma_2\sigma_3}{\sqrt{F_{2t}F_{2c}F_{3t}F_{3c}}} + c_5 \frac{\sigma_1\sigma_3}{\sqrt{F_{1t}F_{1c}F_{3t}F_{3c}}} + c_6 \frac{\sigma_1\sigma_2}{\sqrt{F_{1t}F_{1c}F_{2t}F_{2c}}} \tag{6.4}$$

and

$$B = \left(F_{1t}^{\,-1} - F_{1c}^{\,-1}\right)\sigma_1 + \left(F_{2t}^{\,-1} - F_{2c}^{\,-1}\right)\sigma_2 + \left(F_{3t}^{\,-1} - F_{3c}^{\,-1}\right)\sigma_3 \tag{6.5}$$

where

c_i, $i = 4..6$ = *Tsai-Wu coupling coefficients, by default are taken as -1*

$\sigma_{1,2,3}$ = *principal stress tensors*

$\sigma_{4,5,6}$ = *shear stress tensors*

F_{1t} = *longitudinal tensile strength*

F_{2t} = *transverse tensile strength*

F_{3t} = *transverse-thickness tensile strength*

F_{1c} = *longitudinal compressive strength*

F_{2c} = *transverse compressive strength*

F_{3c} = *transverse-thickness compressive strength*

I_F = *failure index*

The Tsai-Wu failure criterion occurs when $I_F \geq 1$, meaning the ratio of the stress divided by the strength is greater than 1.0. The longitudinal and transverse tensile strength and the longitudinal and transverse compressive strength obtained from Table 3.2 were input into ANSYS failure criteria to determine the failure index. The tensile strength and the flexural strength of the Glass/PP fibers were 46,000 psi (317,158,834.9 N/m^2) and 60,000 psi (413,685,436.8), respectively. Table 6.2 shows the failure index from the failure analysis of the Glass/PP facesheets. It can be seen that all the failure indexes were less than 1.0, which means that the glass/PP facesheets were strong enough to withstand the extreme wind pressures from the analysis in addition to the dead load effect. This also means that design of the Glass/PP and EPS panels had passed. The final panel thickness would be 5.74 in. (14.58 cm) and the laminate configurations were kept the same as presented in the analysis.

Table 6.2. Failure Index of the Glass/PP Facesheets

Layer Number	I_F	If $I_F \geq 1$, then Fail, otherwise Pass
1, 0º	0.366	Pass
2, 90º	0.355	Pass
4, 0º	0.334	Pass
5, 90º	0.330	Pass

6.2.6.2—Results and Discussions of Results of E-Glass/Polyester Wire-Meshed Model

The linear static analysis was conducted on the wire-meshed panels using the mesh and the boundary and loading conditions described earlier of this chapter. The maximum deflections in the x, y, and z-directions with respect to the global X, Y, and Z-axes were 0.582 in., 0.0993 in., and 0.251 in. in tension, respectively. The maximum global deflection was 0.879 in. as presented in Figure 6.11.

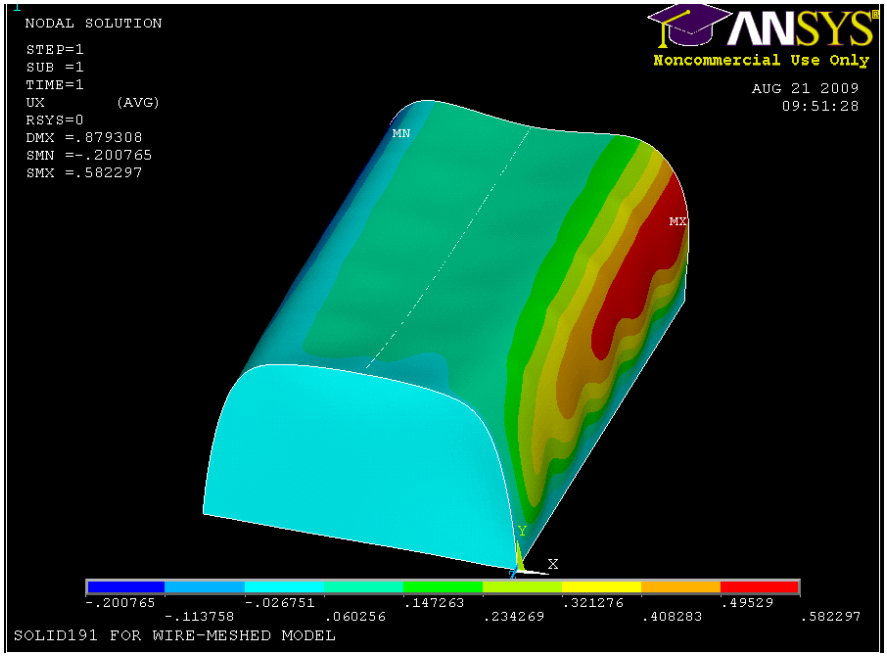

(a) Maximum Deflection in the Global X-Direction was 0.582 in. (1.47 cm)

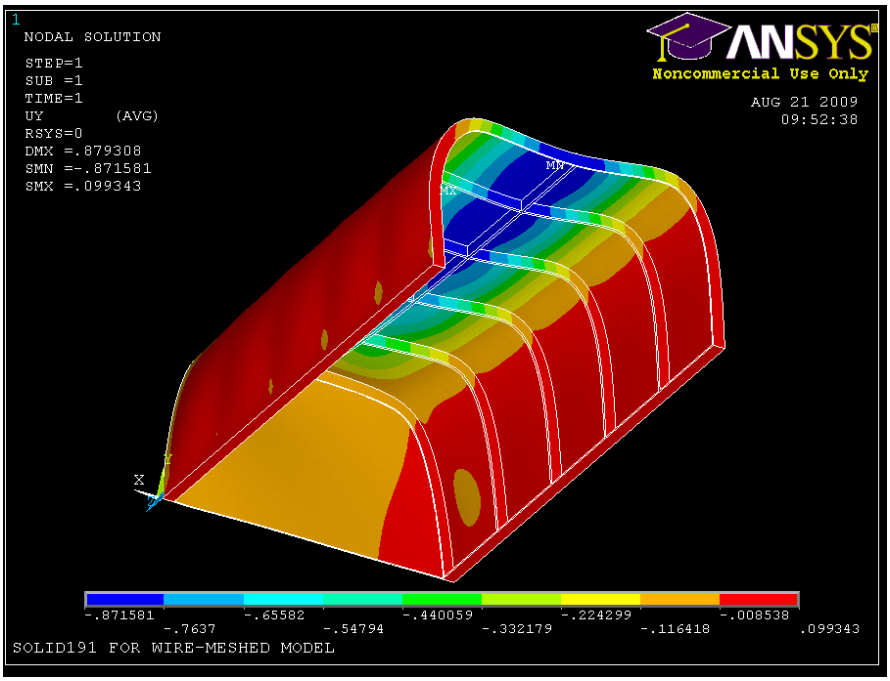

(b) Maximum Deflection in the Global Y-Direction was 0.0993 in. (.252 cm)

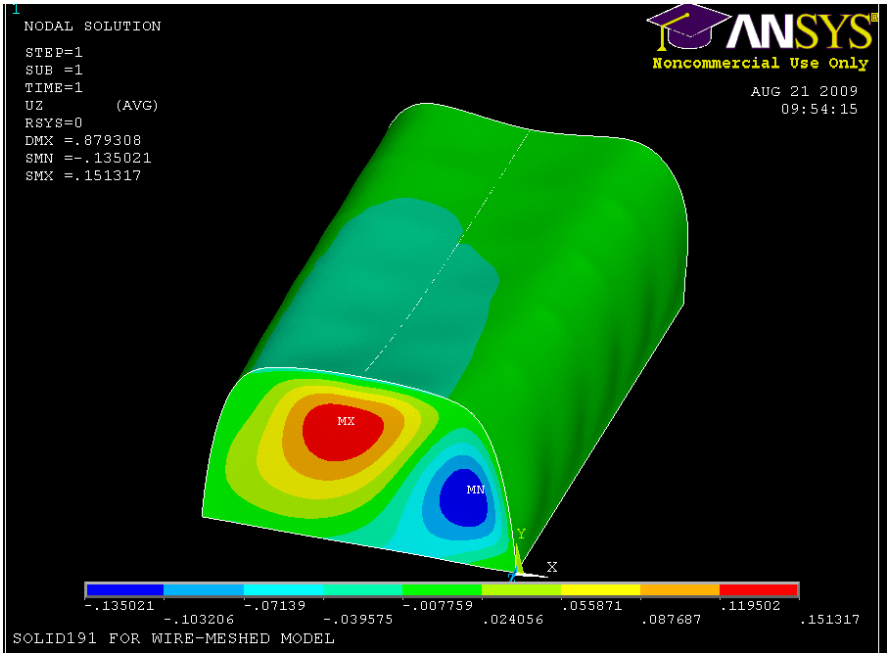

(c) Maximum Deflection in the Global Z-Direction was 0.151 in. (0.384 cm)

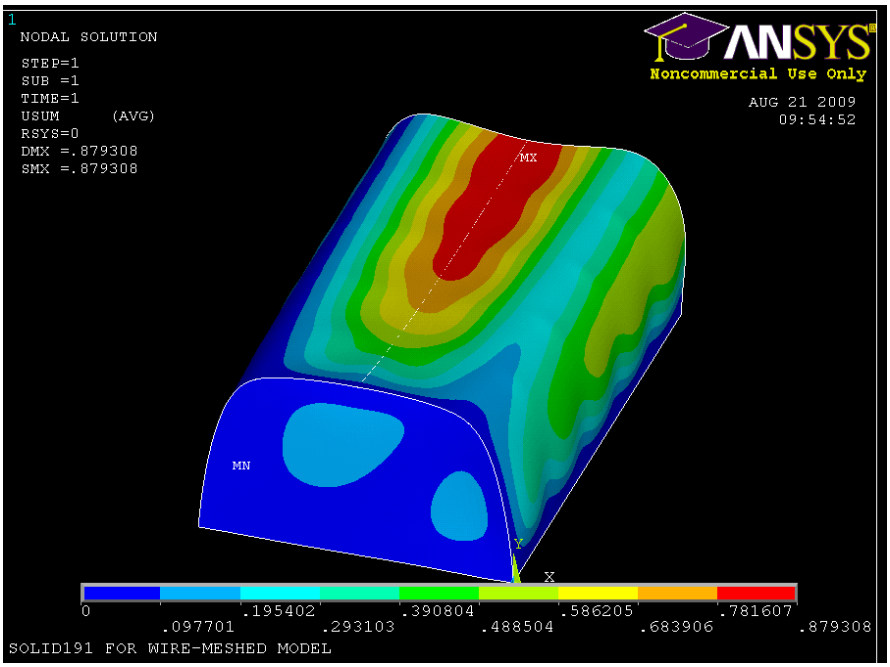

(d) Maximum Deflection in All Global Directions Combined was 0.879 in. (2.23 cm)

Figure 6.11. Deflections of the Wire-Meshed Model.

Table 6.3 lists the results of the local maximum stresses of Layer 2 to Layer 12 of the wire-meshed model. Layer 1 and Layer 13 were not considered in the analysis and not presented in Table 6.3, because the properties of the gel coats were insignificant to the in plane loading. Layers 2, 7, and 12 were the backup laminates and the rest of the layers (3, 4, 5, 6, 8, 9, 10, and 11) were the wire-meshed laminates. Since the wire-meshed laminates were the main reinforcements for the model, only the stresses of the wire-meshed layers are presented here in this section for discussion.

The Principal Stress 1 was responsible for taking up the main stress in the thickness direction. Therefore, the Principal Stress 1 had the highest stress relative to other stresses. As seen from Table 6.3, Layer 4, which was one of the wire-meshed layers, had the highest principal stress than any other layers. The maximum stress that it

could take was 22,853 psi (157,565,888.1 N/m^2), which was also less than the strength of the wire-meshed fibers, which was 164,211 psi (1,132,194,987.7 N/m^2) obtained from Table 3.3. Figure 6.12 shows all stresses in Layer 4.

Table 6.3. Maximum Local Stresses in Layers 2 to 12 Produced at Wind Pressure Loading

Layer Number	Maximum Stress (psi)					
	Principal 1	Principal 2	Principal 3	XY Shear	YZ Shear	XZ Shear
2	6016	1969	1674	727	2960	1286
3	8936	1649	470	1077	3119	2857
4	22853	1369	599	707	4674	1877
5	20104	1414	642	702	4978	1867
6	17413	1593	684	702	5303	1971
7	7948	2278	1993	518	3150	1641
8	9165	2087	550	890	4088	2916
9	9717	2118	481	1039	4350	3178
10	10288	2141	722	1189	4626	3448
11	13689	2428	1656	963	6937	2740
12	10521	3339	2428	865	4285	2496

1 psi = 6,894.76 N/m^2

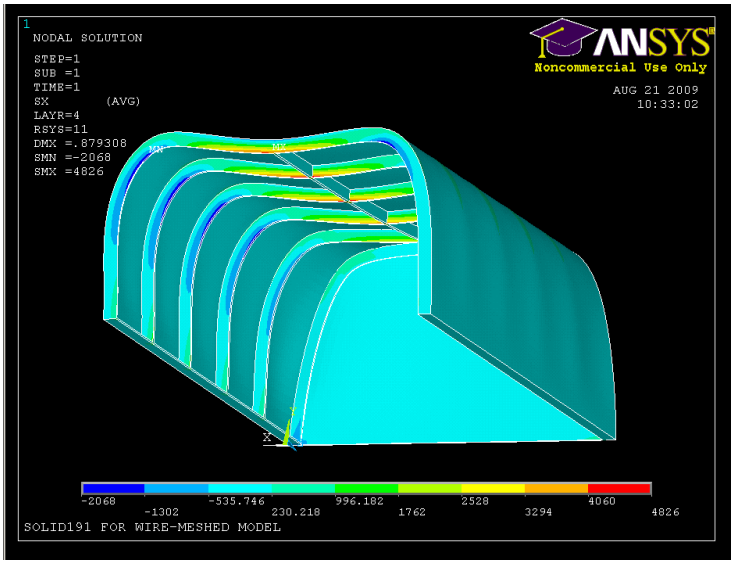

(a) Layer 4's Maximum Stress in Local X-Direction was 4,826 psi (33,274,098.6 N/m^2)

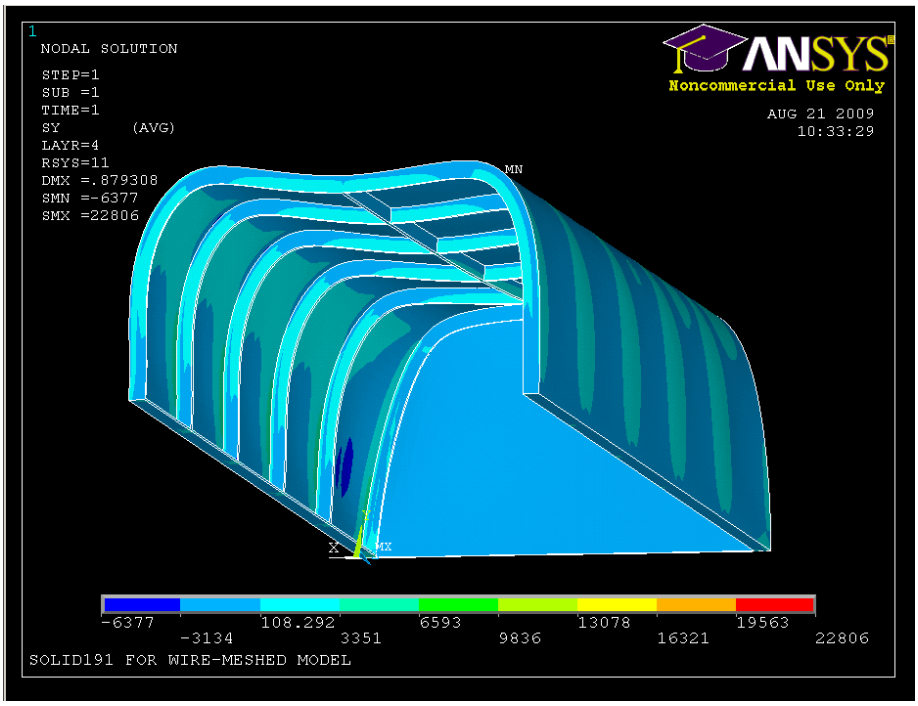

(b) Layer 4's Maximum Stress in Local Y-Direction was 22,806 psi (157,241,834.5 N/m^2)

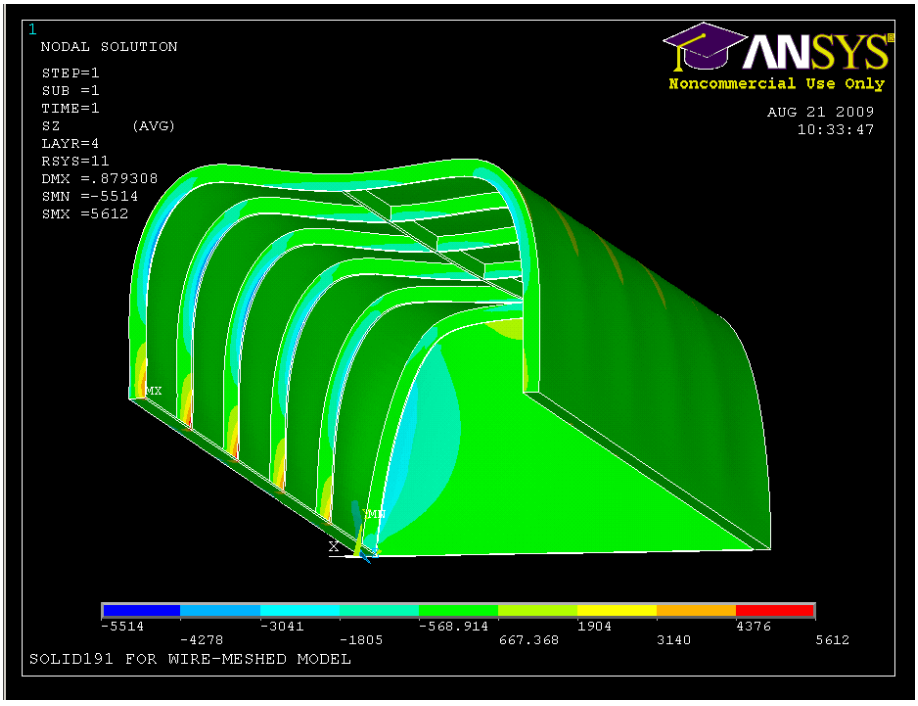

(c) Layer 4's Maximum Stress in Local Z-Direction was 5,612 psi (38,693,377.9 N/m^2))

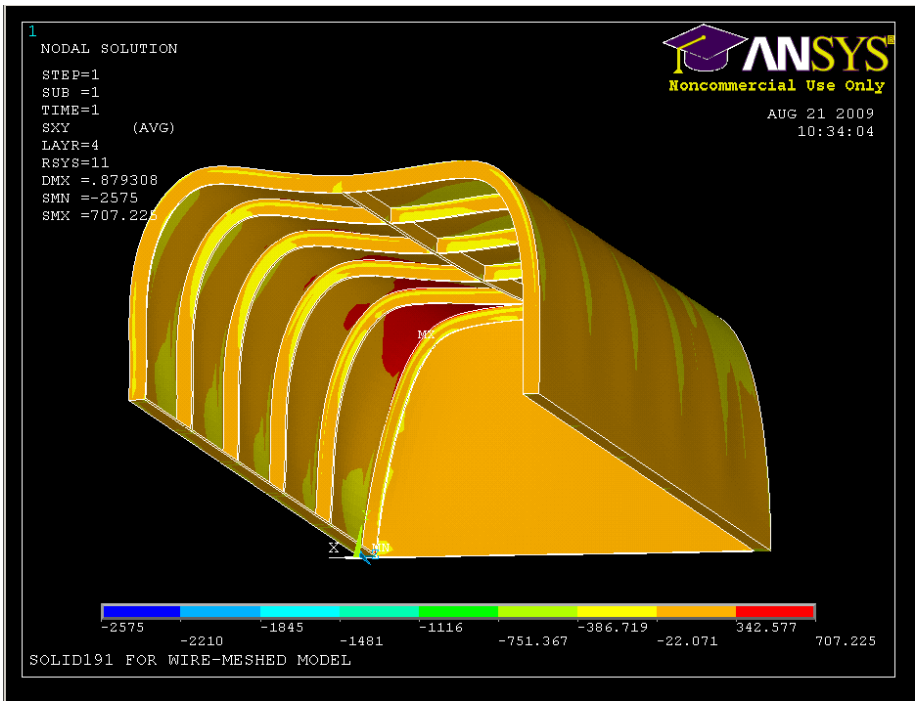

(d) Layer 4's Maximum Shear Stress in XY Plane was 707 psi (4,874,593.4 N/m^2)

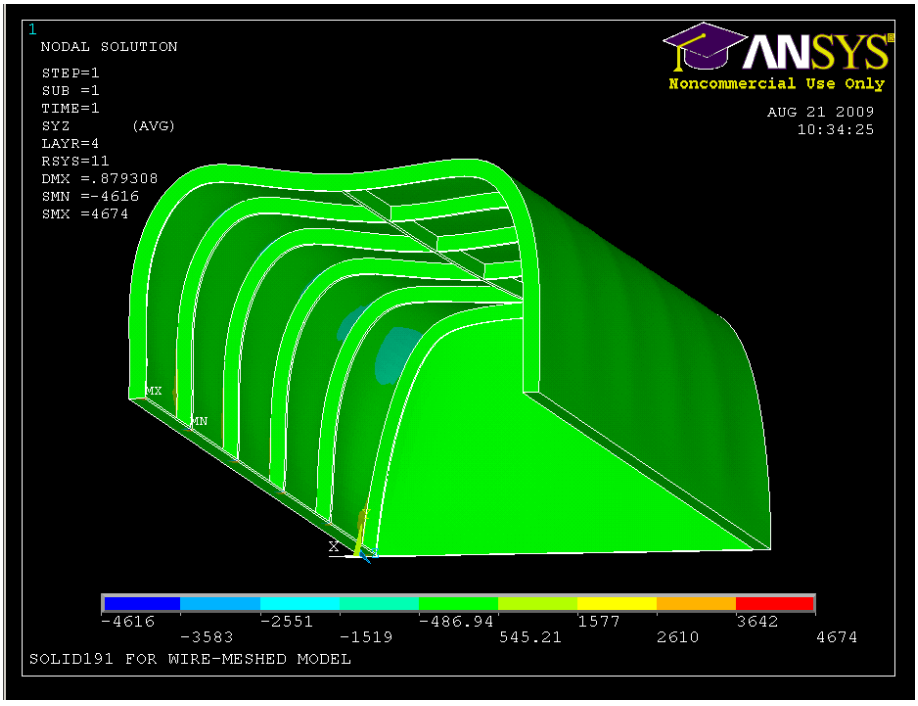

(e) Layer 4's Maximum Shear Stress in YZ Plane was 4,674 psi (32,226,095.5 N/m^2)

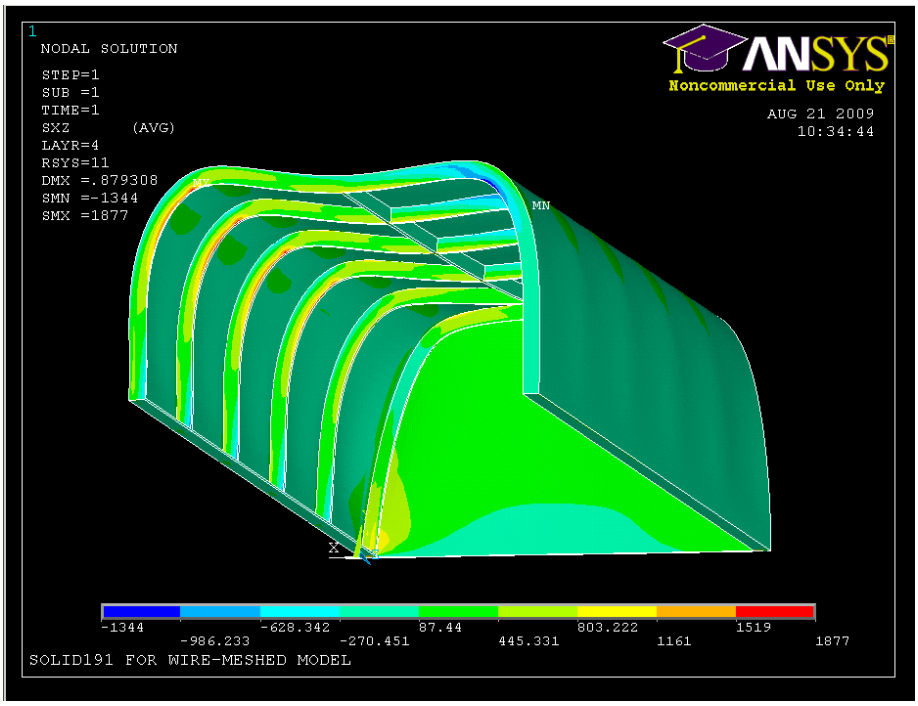

(f) Layer 4's Maximum Shear Stress in XZ Plane was 1,877 psi (12,941,459.4 N/m^2)

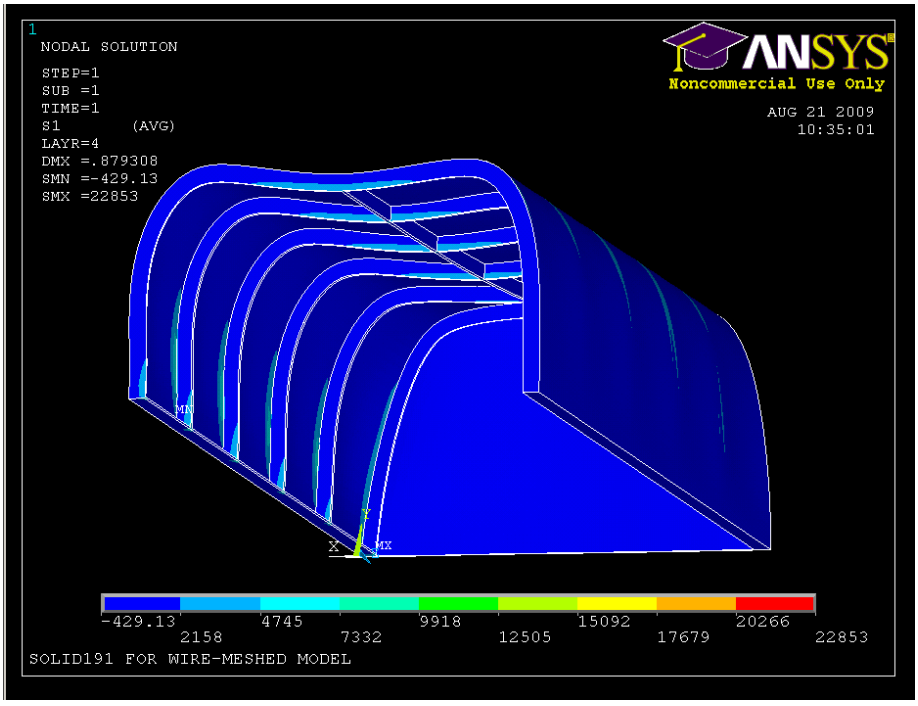

(g) Layer 4's Maximum Principal Stress was 22,853 psi (157,565,888.1 N/m^2)

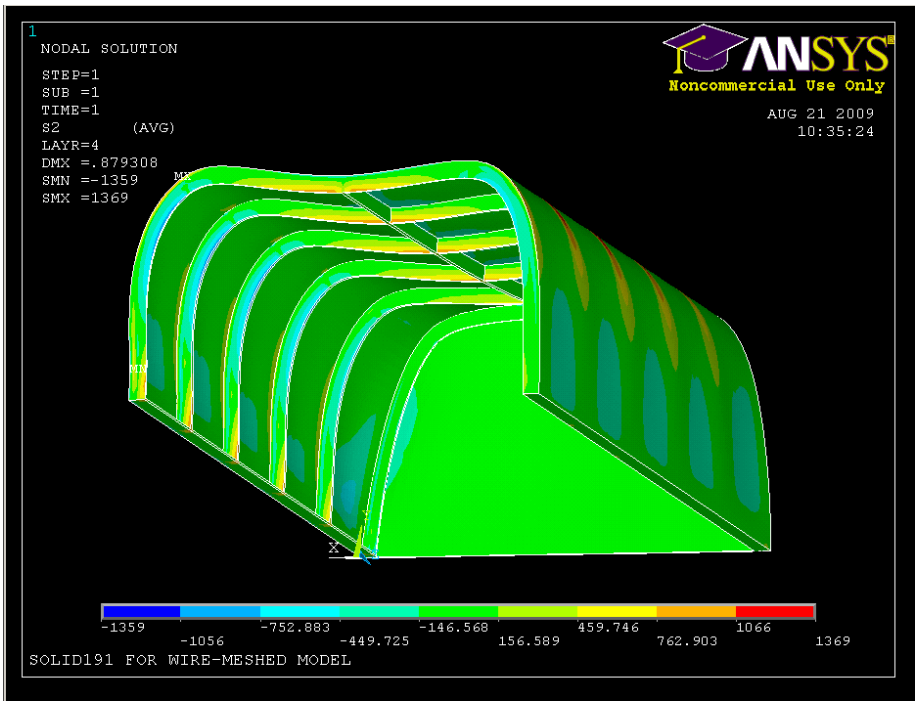

(f) Layer 4's Maximum Principal Stress was 1,369 psi (9,438,922.7 N/m^2)

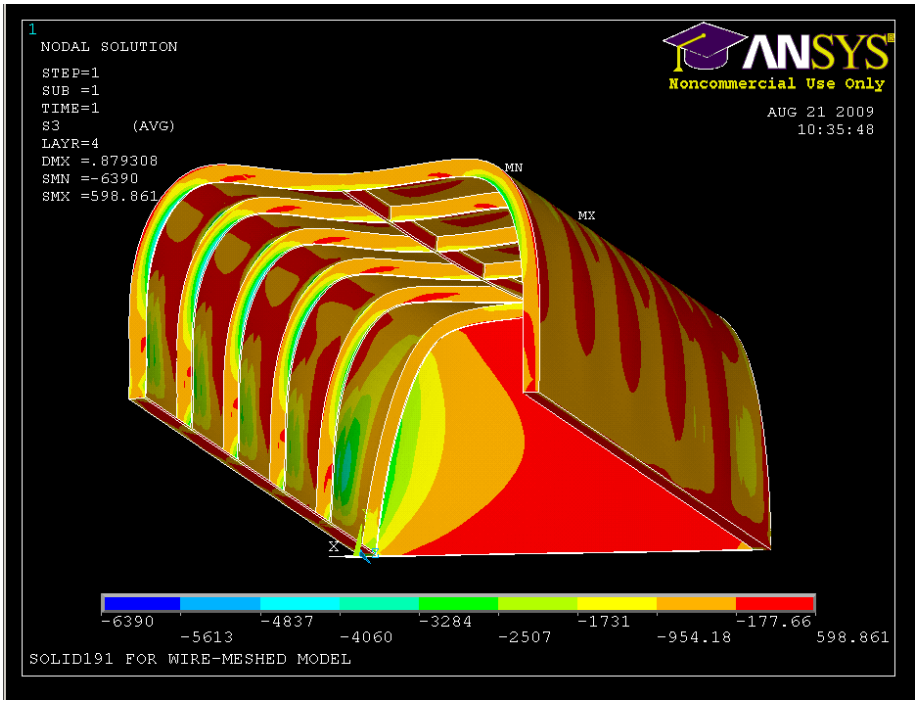

(g) Layer 4's Maximum Principal Stress in XZ Plane was 599 psi (4,129,959.6 N/m^2)

Figure 6.12. Stresses in Layer 4 of Wire-meshed Model.

It can be seen from Table 6.3 that the stresses in the wire-laminates were higher than the backup laminates. Because the wire-meshed laminates were the main reinforcements for the analysis, the Tsai-Wu failure analysis was carried out on the wire-meshed laminates.

The Tsai-Wu failure criterion occurs when $I_F \geq 1$, meaning the ratio of the stress divided by the strength is greater than 1.0. The longitudinal and transverse tensile strength and the longitudinal and transverse compressive strength obtained from Table 3.3 was 164,211 psi (1,132,194,987.7 N/m^2), which were input into the ANSYS failure criteria to determine the failure index. Table 6.4 shows the wire-meshed laminate failure index from the failure analysis. It can be seen that all the failure indexes of all the wire-meshed layers were less than 1.0, which means that the wire-meshed model was strong enough to withstand the extreme wind pressures from the analysis in addition to the dead load effect. This also means that design of the wire-meshed panel with the panel thickness of 0.69 in. (1.75 cm) was safe. The final panel thickness would be 0.69 in. (1.75 cm) and the laminate configurations were kept as presented in the analysis.

Table 6.4. Failure Index for Wire-Meshed Laminate Layers

Layer #	I_F	If $I_F \geq 1$, then, Fail, otherwise Pass
3, 0º	0.105	Pass
4, 90º	0.143	Pass
5, 90º	0.127	Pass
6, 90º	0.112	Pass
8, 0º	0.106	Pass
9, 0º	0.107	Pass
10, 0º	0.109	Pass
11, 90º	0.090	Pass

CHAPTER 7

CONNECTION DESIGN BY FINITE ELEMENT ANALYSIS

7.1—Introduction

This chapter focuses on the design and analysis of the bolted joint connections of the shelter. Since the bolted joint connections are the most critical components of the shelter, careful considerations in modeling the connections of the shelter were taken to maintain an acceptable level of the structural integrity and efficiency. The main purpose of a connection is to transfer loads across different members of a structural system. Two types of loads that can be transferred across a connection are tensile load and shear load. The bolted joint connections have to be strong enough to resist the applied tensile and shear loads, otherwise the connections will fail.

Bolted joints are made up of the bolt assembly and the connecting elements. The bolt assembly includes the head, stud and nut. The connecting elements include the top and bottom flanges with or without gusset plates. Figure 7.1 shows the members in the bolted joints. The bolted joint connections are designed to hold the parts together to prevent structural failure. Three failure modes exist in the bolted joints are bearing, shear out, and net tension (normal), or combinations of the three failure modes. Bearing failure occurs when there is an excessive bearing pressure inducing on the connecting flanges from the bolts. When the bearing pressure exceeds the compressive yield strength of the connecting flanges, the connecting flanges will be torn out or possessed plastic

deformation. Shear failure occurs when the applied shear load is higher than the bolt shear strength, which causes the bolt to fail in shear. Tension failure occurs when sufficient load causes the bolted connections to separate. When the bolted connections fail in shear or tension due to high loads, the bolted connections ultimately affect the structural integrity of the whole structure. The bolted joint connections must be designed with sufficient strength to maintain an acceptable level of structural integrity and efficiency of the structure. The bolts must generate sufficient clamp force or preload to prevent bolt failure or joint movement caused by axial and/or shear loads. When the preload applied to the bolt is greater than the yield strength of the bolt, the bolt will fail due to direct tensile failure. Therefore, the applied force should not be greater than the bolt's yield strength.

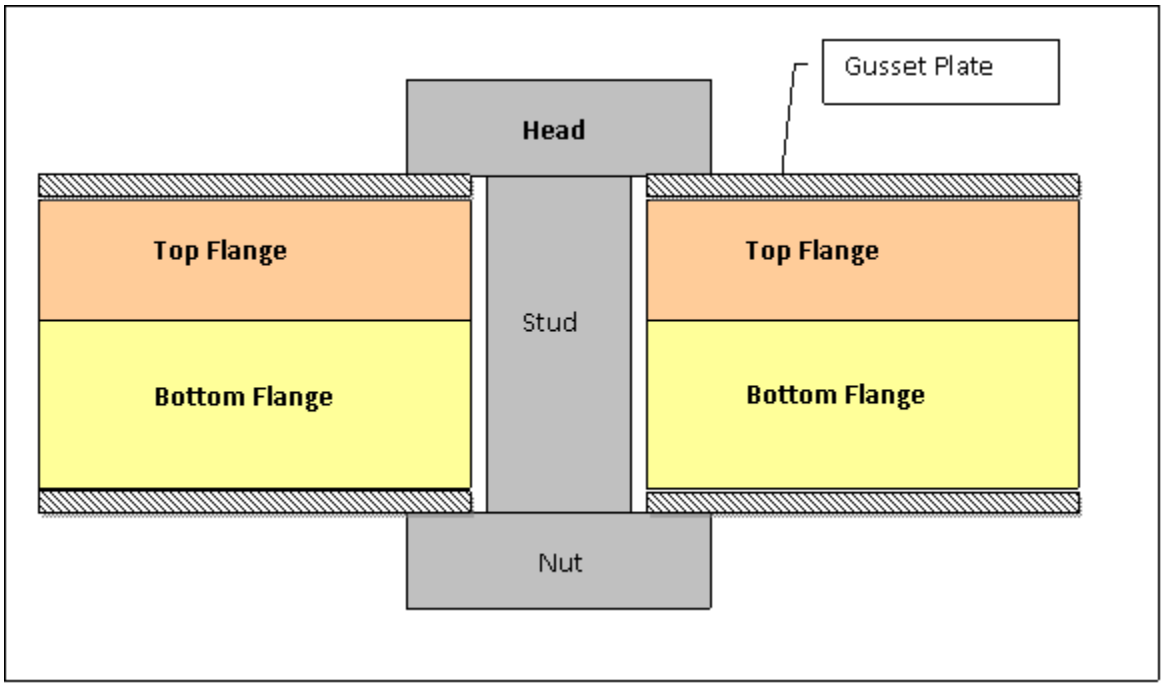

Figure 7.1. Example Members in Bolted Joints.

The analysis of the bolted joint connections for the sandwich composite model and the wire-meshed model was carried out through FEA. A three dimensional finite element model was developed for the bolted joint connections. The analysis will carefully determine whether (1) the bolts fail under tension and/or shear stresses, (2) the connecting flanges fail under bearing stresses or applied loadings.

7.2—Development of Models

Initially, the bolted joint connection models were represented using the solid elements. However, it was found that the simulation of the multi-bolted joint connections using the solid elements was computational expensive. The combination of the solid elements used to represent the connecting flanges along with the contact interactions (Figure 7.2) between the bolt head/nut to flange interaction and between flanges themselves had increased the model size and the analysis time significantly, which contributed to difficulty with convergence issues. To overcome the limitations in computational capabilities and the convergence issues, simplifications of the majority of the models to simulate the behavior of the multi-bolted system were necessary. The final models were created by simplifying the number of elements used in the bolts in order to obtain reasonable analysis time, but without affecting the accuracy of the solution.

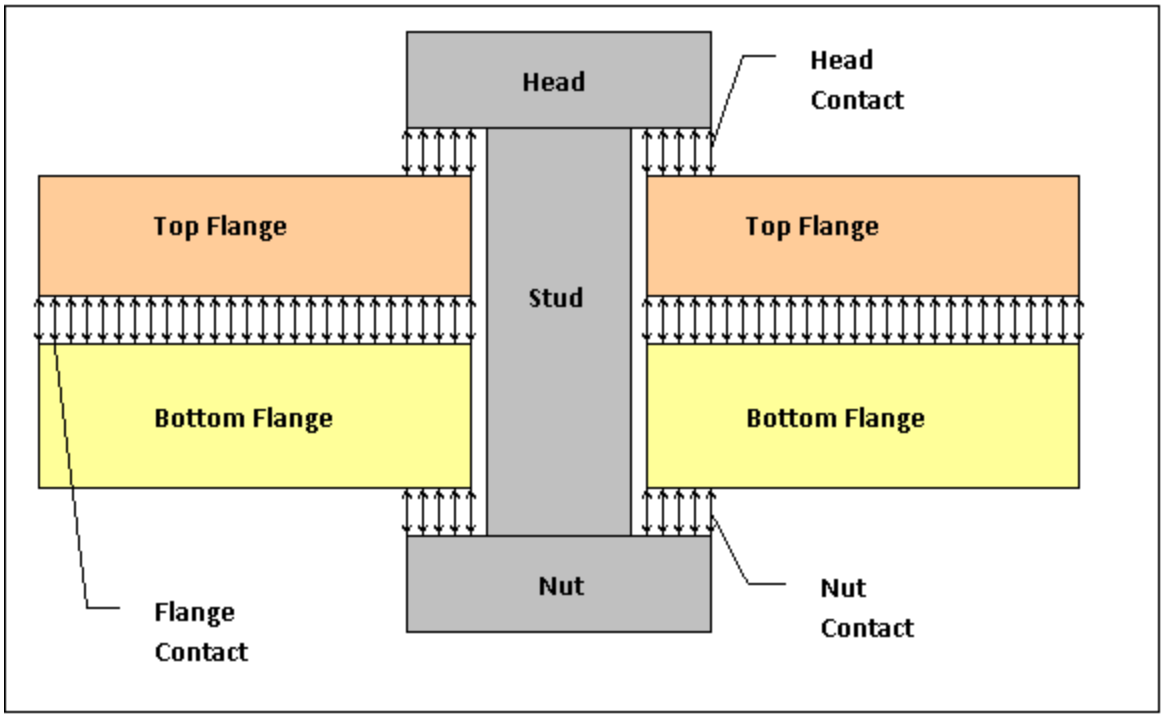

Figure 7.2. Contact Surfaces (Without Gusset Plates).

The method for modeling the bolts is based on Ginal [35]. The bolted joint simulation was carried out for the multi-bolted system on the four panels of the shelter. These middle panels were chosen to simulate the worst possible effect of the connections as shown in Figure 7.3. It is important to clarify that it was impossible to cover every possible design situation and model the whole geometry of the shelter. As results, the design of the shelter was based upon the one that caused the largest stresses on the shelter, which occurred at the center of the shelter. In addition, the simulation showed that the analysis of the three dimensional models was more efficient when the shell elements and line elements were used for the connecting flanges and the bolts, respectively. Both models (sandwich composite model and wire-meshed model) would be best represented using the shell elements and the line elements for the FRP flanges and

the bolts, respectively. For simplicity, the two models were modeled with the same geometry and loading conditions, but with different material properties for the FRP flanges.

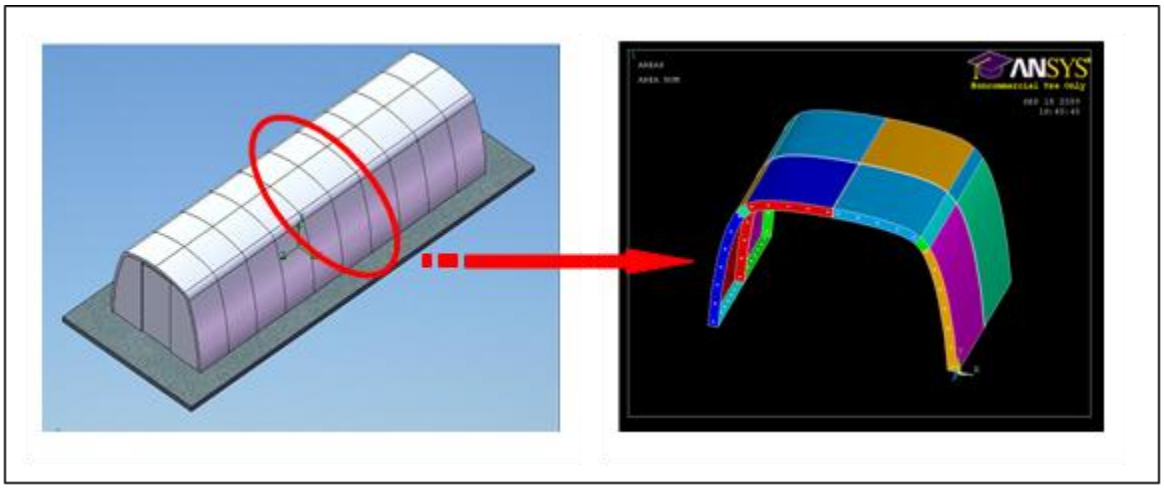

Figure 7.3. Simplified Model Geometry for Connection Design.

7.2.1—Development of Sandwich Composite Model and Wire-Meshed Composite Model

The bolts were modeled using line elements, Beam4, which is a uni-axial element with tension, compression, torsion and bending capabilities [5]. The element has six DOFs at each node: translations in the nodal x, y, and z directions and rotations about the nodal x, y, and z-axes [5]. The bolt heads and nuts were modeled using the coupling nodes, which were done with constraint equations [5]. A list of nodes was defined along with the nodal x, y, and z directions in which the nodes were to be coupled. Various nodes with degrees of freedom were coupled into a set to allow the results calculated for one member of the set to be the same for all members of the set. Each coupling set was constrained in the nodal x, y and z translations and rotations.

The connecting flanges were represented using Shell91, which is a 3D shell element with layered stacking sequence capabilities [5]. The advantage of using Shell91 element was that the thickness of the plates for the sandwich composite model and the wire-meshed model could easily be changed by assigning the real constants to the models without physically modeling the models with the thicknesses. In another word, the geometry of the shelter was only created once, but the material properties and the thickness of each model could be entered into the geometry of the model as real constants, which could be changed as many times for analysis. The same was true for using line elements, because, for example, different diameters of the bolts could be entered as real constants for analysis and the "restart" option would start the analysis all over again with the assigned constants.

For the preliminary design, the bolt type chosen for both models was A325 high-strength bolt in a bearing type connection with the threads excluded from the shear plane [36]. Each side flange had twelve bolts and each top and bottom flange had eight bolts. The spacing between the bolts for the side flanges was twelve in. from center-to-center of bolts. The spacing between the bolts for each top and bottom flange was six in. from center-to-center of bolts. The edge distance from the closest/furthest bolts to the outside fiber of the flange was 3 in. (7.62 cm). The bolt stud diameter was 3/8 in. (0.9525 cm.) The head and nut diameter of the bolts were 1 in. (2.54 cm) with standard-size holes. The flange thickness for the sandwich composite model and the wire-meshed model was 5.74 in. (14.58 cm) and 0.69 in. (1.75 cm), respectively. Figure 7.4 shows the general layouts of the connecting panels and bolts for the sandwich composite model and the wire-meshed model. Figure 7.5 shows the final arrangement of mesh descretization for both

models. Figure 7.6 shows the assembly of coupling nodes around the bolts, where each node of the bolts was fully restrained in the nodal x, y and z translations and rotations.

The symmetry boundary conditions were applied to the front and back flanges of the panels, as illustrated in Figure 7.7a. Information on how symmetry boundary conditions works can be referenced to Chapter 6 for more detail. The wind pressures from Chapter 4 were applied to the body flanges of the shelter for the connection design as shown in Figure 7.7a. This was done exactly the same way as described in Chapter 6. The nodes at the bottom of the bolt line elements were constrained in all directions in order to simulate the rigid body conditions of the anchor bolts, which are illustrated in Figure 7.7b.

The FRP material properties for the two models could be obtained from Chapter 6. The bolt geometric and material properties input for analysis are presented in Table 7.1. The bolts were defined as elastic isotropic material with a Modulus of Elasticity of 29,000,000 psi (199.9 GPa) and a Poisson's Ratio of 0.3. The linear static analysis was carried out on the models.

Table 7.1. Geometric and Material Properties of Bolts for Both Models

Property	Equation	Value
Cross Sectional Area, A	$A = \frac{\pi d^2}{4}$	0.1104 in^2 (0.712 cm^2)
Area Moment of Inertia, I_{zz}	$I_{zz} = \frac{\pi d^4}{6}$	9.704 E -4 in^4
Area Moment of Inertia, I_{yy}	$I_{yy} = \frac{\pi d^4}{6}$	9.704 E -4 in^4
Thickness Along Z-Axis, *TKZ*	-	0.375 in.
Thickness Along Y-Axis, *TKY*	-	0.69 in.
Orientation About X-Axis	-	0
Initial Strain	-	0
Torsional Moment of Inertia, I_{xx}	$I_{xx} = \frac{\pi d^4}{32}$	1.941 E -3 in^4
Modulus of Elasticity, *E*	-	29 E 6 psi
Poisson's Ration, *PRXY*	-	0.30
Density	-	0.284 lb/in^3
Ultimate Shear Strength	-	60 ksi
Ultimate Tension Strength	-	90 ksi
Diameter of Bolt = d	-	0.375 in.

1 in = 2.54 cm; 1 in^2 = 6.45 cm^2; 1 in^4 = 41.6 cm^4; 1 ksi = 6,894,757.28 N/m^2

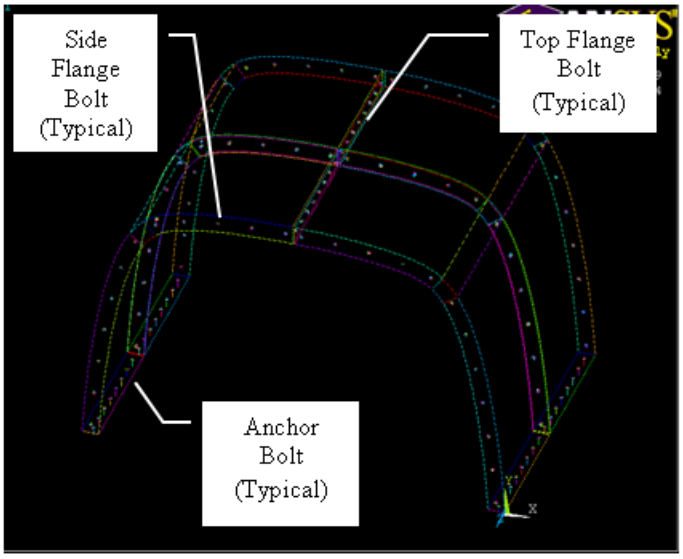

(a) 3 Different Locations for Bolts (Isometric View)

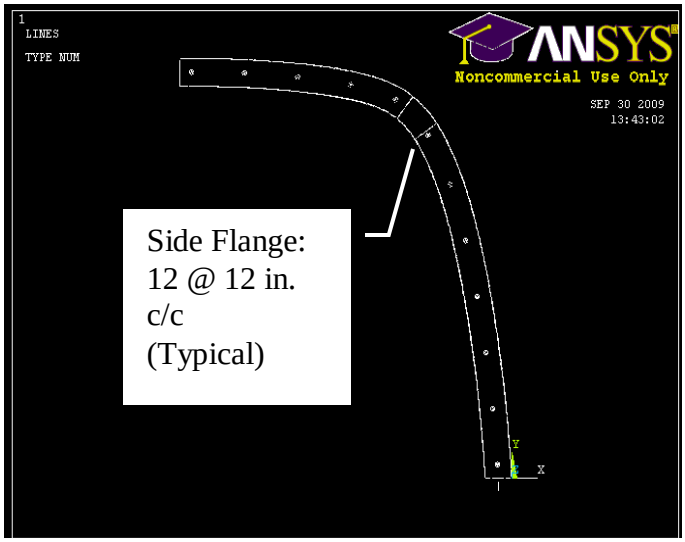

(b) Bolt Spacing of Side Flange for Both Models (Front View)

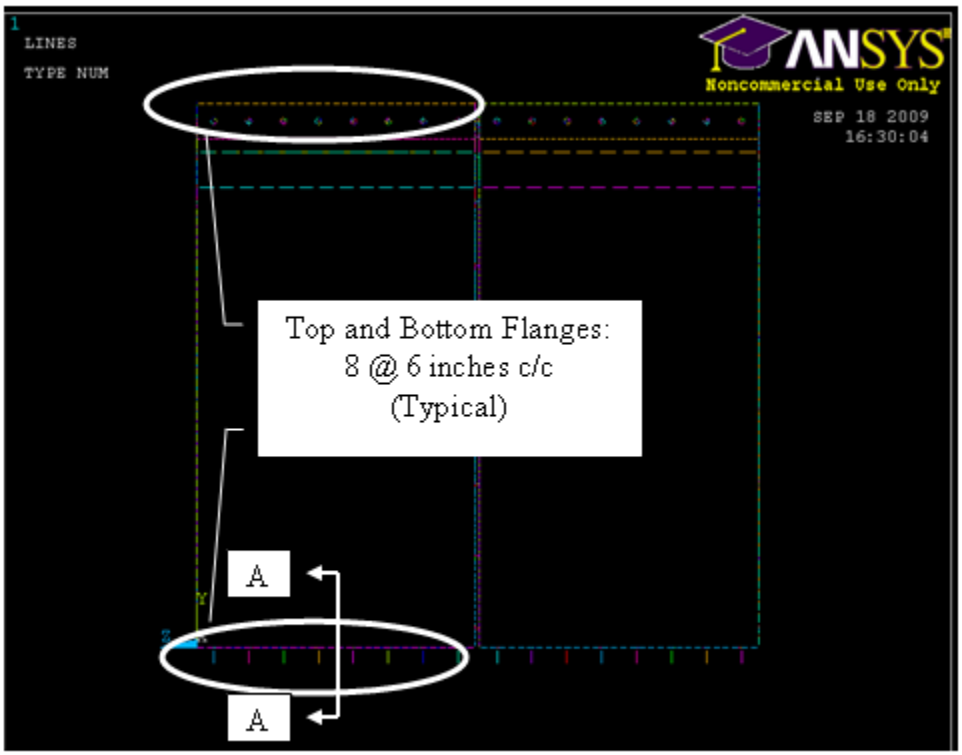

(c) Bolt Spacing of Top and Bottom Flanges for Both Models (Side View)

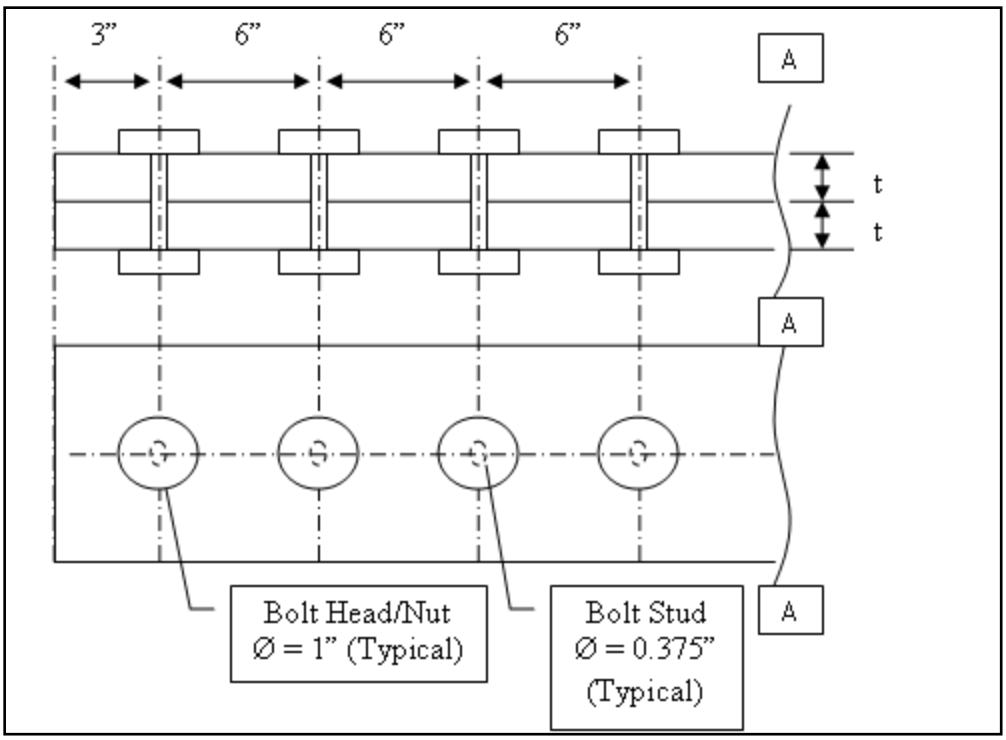

(d) Bolt Spacing of Top and Bottom Flanges for Both Models for Section A-A

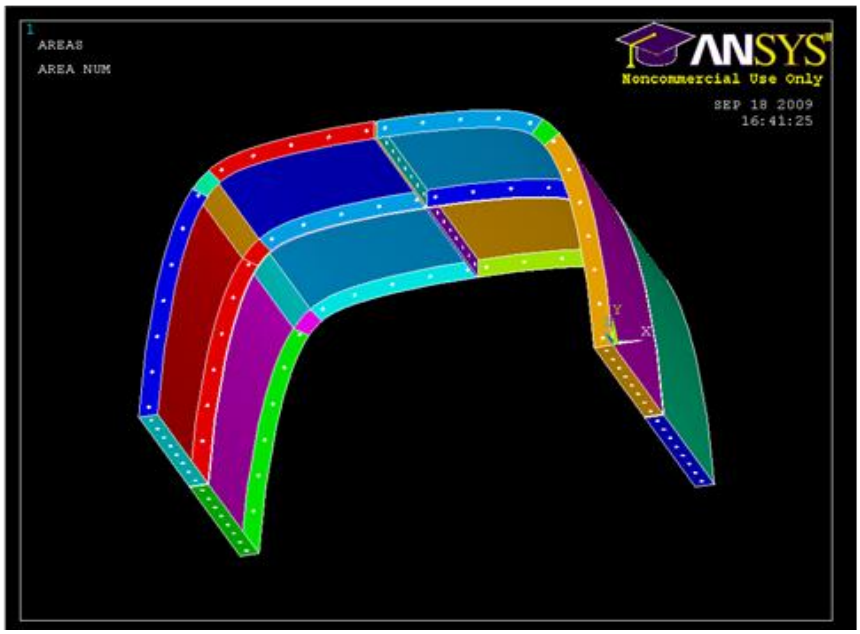

(e) Overall Layout for Both Models

Figure 7.4. General Layout of FRP Flanges and Bolts for Both Models.

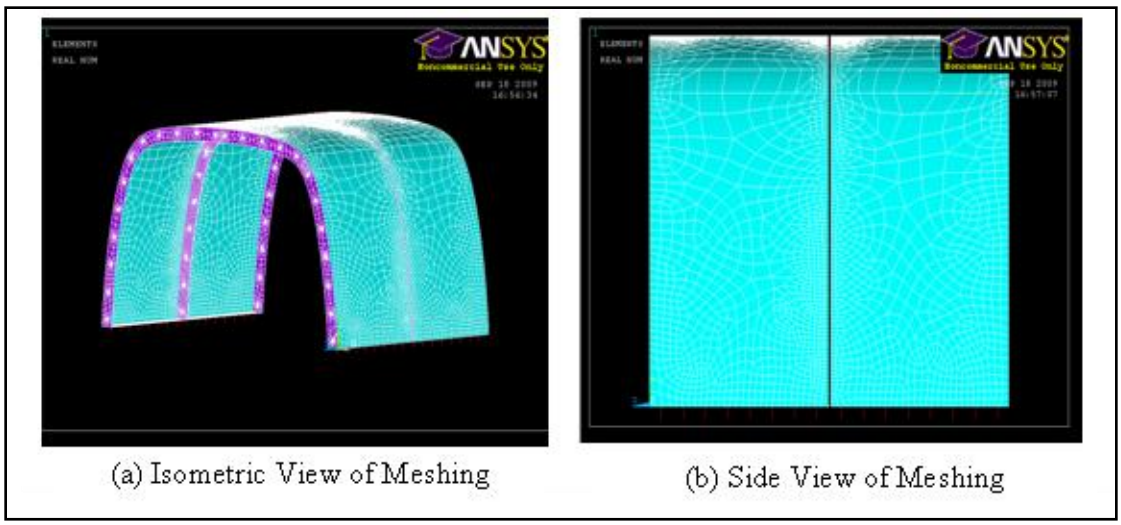

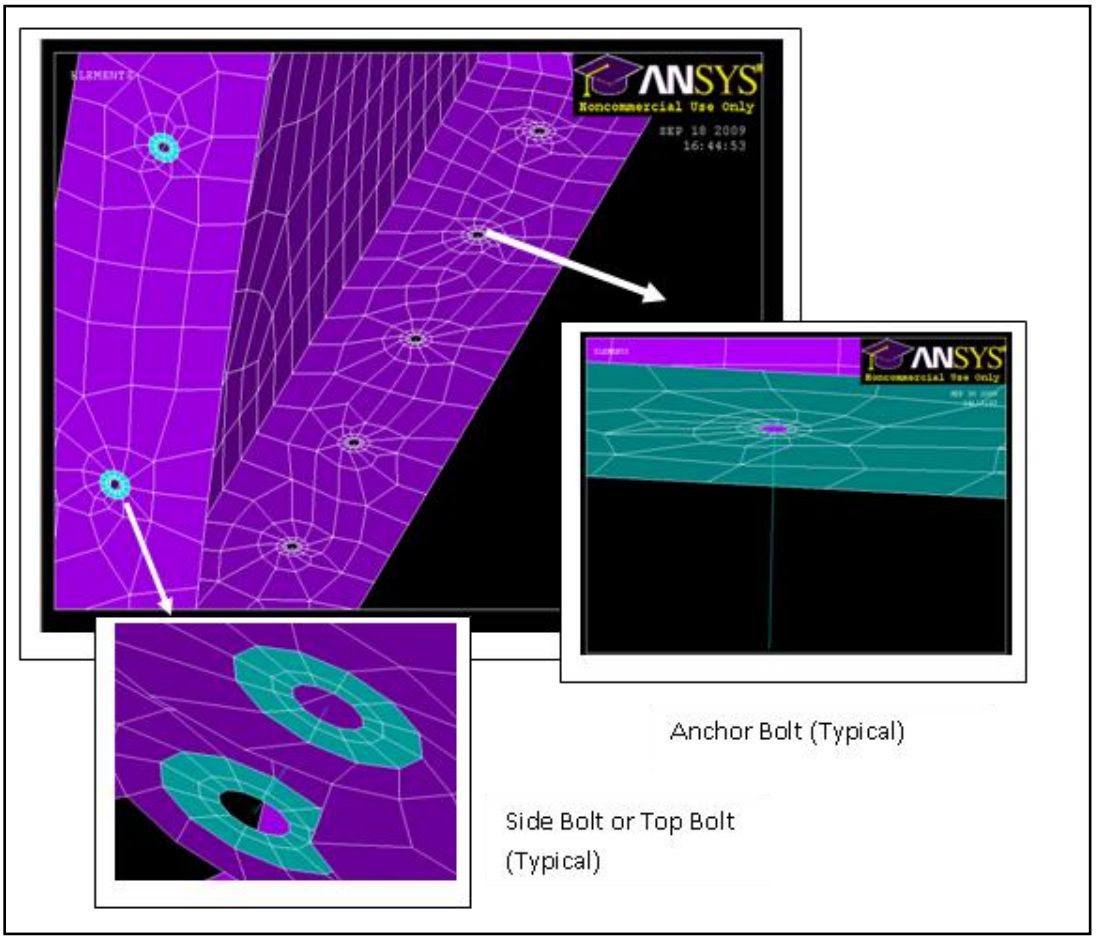

(c) Zoom View at Bolts

Figure 7.5. Mesh Descretization for Both Models.

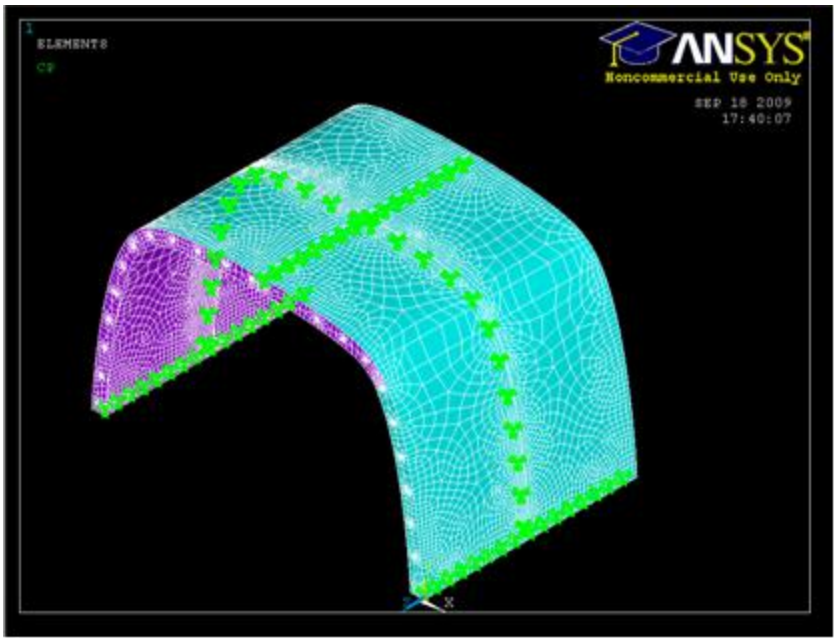

(a) Overall Coupled Sets and Bolt Assembly

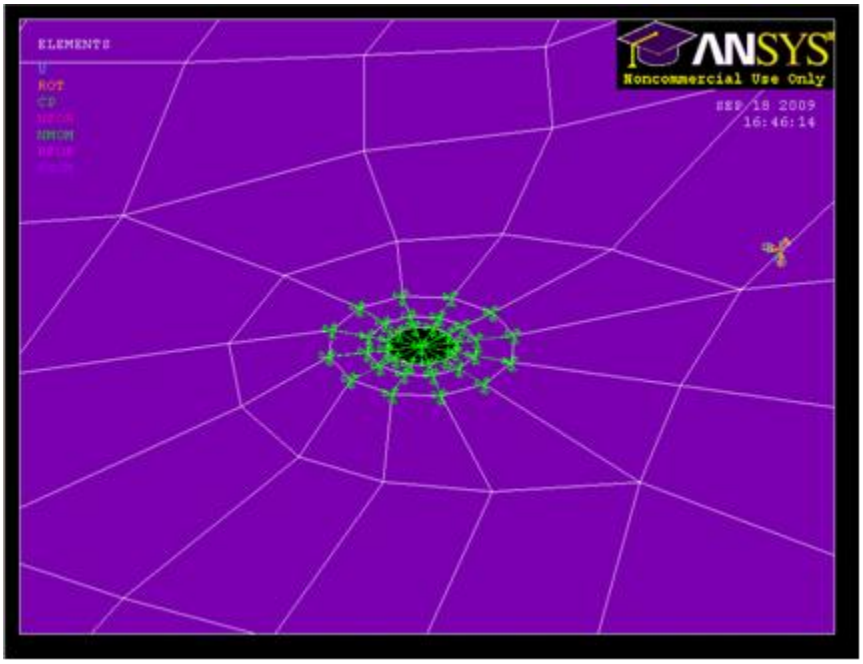

(b) A Typical Coupled Set for a Bolt

Figure 7.6. Bolt-Coupled Constraints for Both Models.

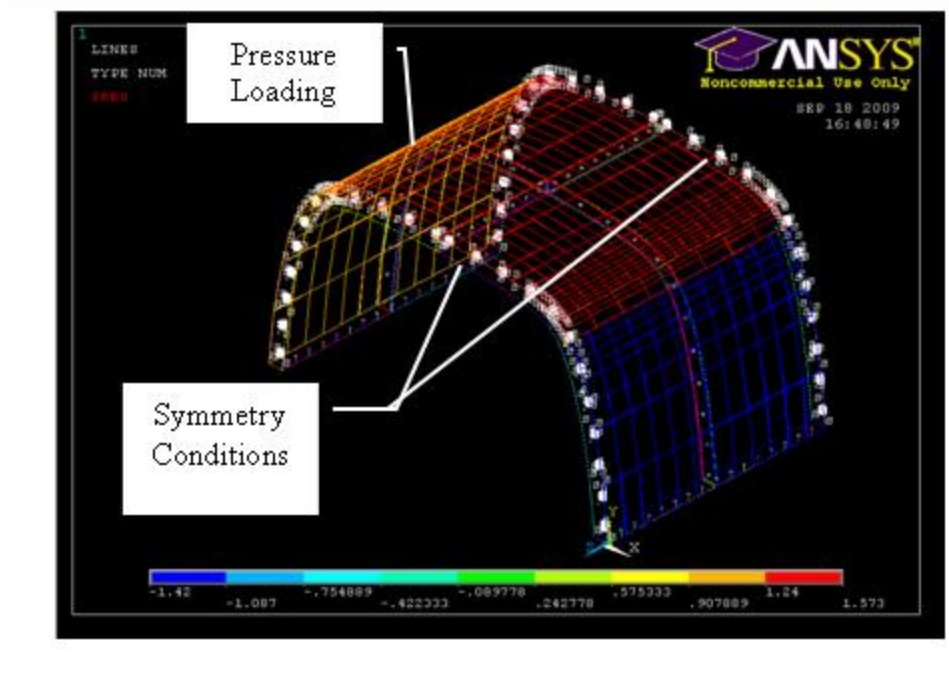

(a) Symmetry Conditions and Pressure Loading for Both Models

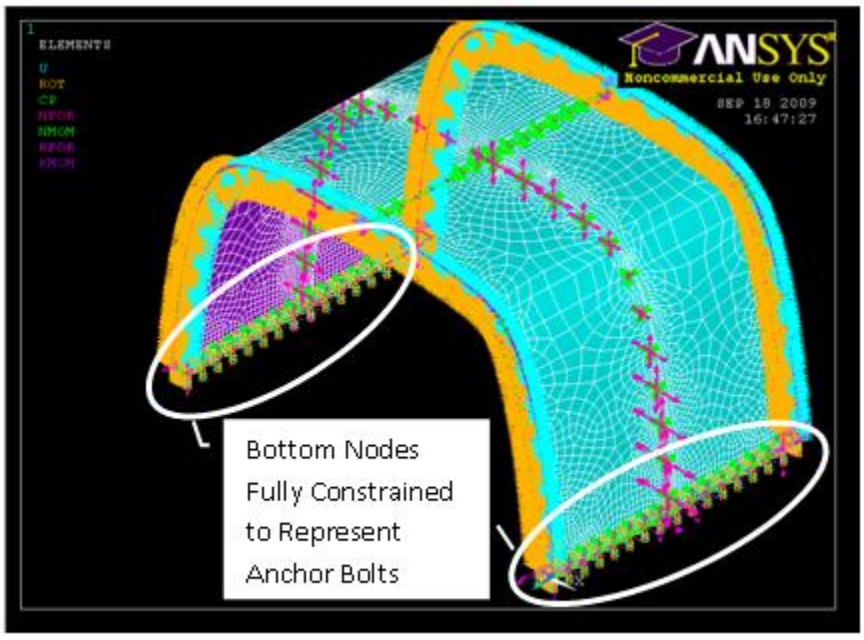

(b) Overall Loadings and Constrained Conditions for Both Models

Figure 7.7. Loading and Boundary Conditions Applied on Both Models.

7.3—FEA Results

After all the loadings and boundary conditions were applied on the sandwich composite model and the wire-meshed model, linear static analysis was carried out on these models to determine the bolt stresses of the models. Section 7.3.1 presents the FEA results of the sandwich composite model. Section 7.3.2 presents the FEA results of the wire-meshed model.

In order to determine how much force were transferred between the anchor bolts, side bolts and top bolts, three separate bolt locations were considered for analysis. The force results will be shown with respect to the global coordinate system. It is important to note that the forces were calculated per unit length in the element coordinate system, but they will be presented in terms of the combined sum for all layers in the global coordinate system [5]. Since the bolts were oriented in different directions, the following bullets are shown to help clarify the directions of the forces for the anchor bolts, side bolts and top bolts for both models

The forces in the anchor bolts with respect to the global directions can be interpreted as follows:

- FX = Shear Force
- FY = Normal Force
- FZ = Transverse Shear Force Normal to FX

The forces in the side flange bolts with respect to the global axes can be interpreted as follows:

- FX = Shear Force
- FY = Transverse Shear Force Normal to FX
- FZ = Normal Force

The forces in the top flange bolts with respect to the global coordinate system can be interpreted as follows:

- FX = Normal Force
- FY = Shear Force
- FZ = Transverse Shear Force Normal to FY

In addition, the maximum shear forces along the XY, YZ, and XZ shear planes of both models will be shown for analysis in order to determine the strength of materials around the bolt holes. The element stress directions are corresponded to the global coordinate directions.

7.3.1—First Model: FEA Results of Sandwich Composite Model

7.3.1.1—Deflection

The maximum deflection from the vector summation of the global X, Y and Z directions obtained from the linear static analysis of the sandwich composite model was 7.41 in., which occurred at the top centerline of the shelter (Figure 7.8). The overall deflections with respect to the global X, Y and Z directions were -6.961 in. (17.7 cm), 3.381 in. (8.59 cm), and 0.0683 in. (0.173 cm), respectively (Figure 7.8).

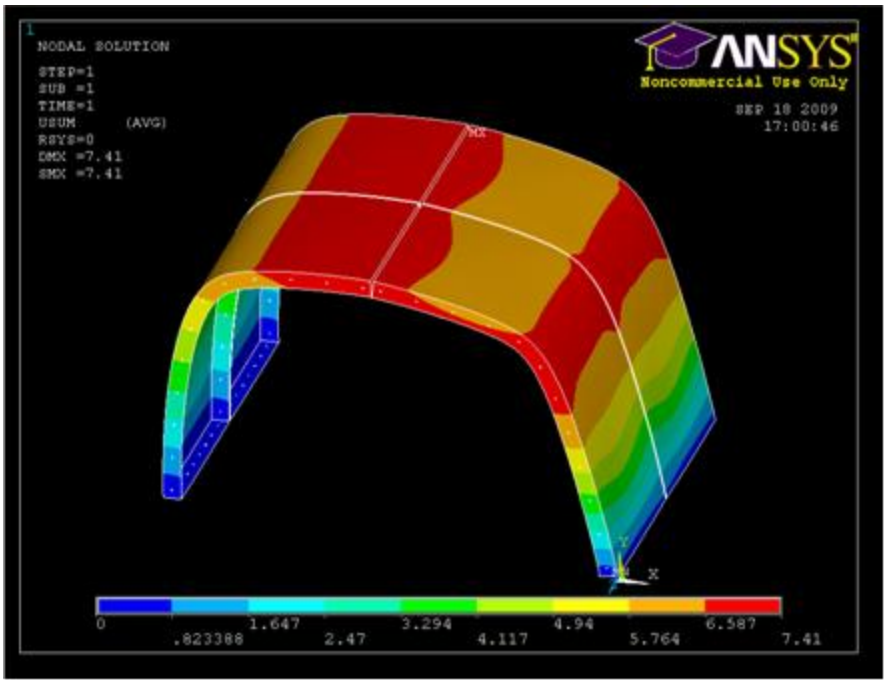

(a) Maximum Deflection Obtained from Vector Summation of X, Y, and Z Directions of Sandwich Composite Model

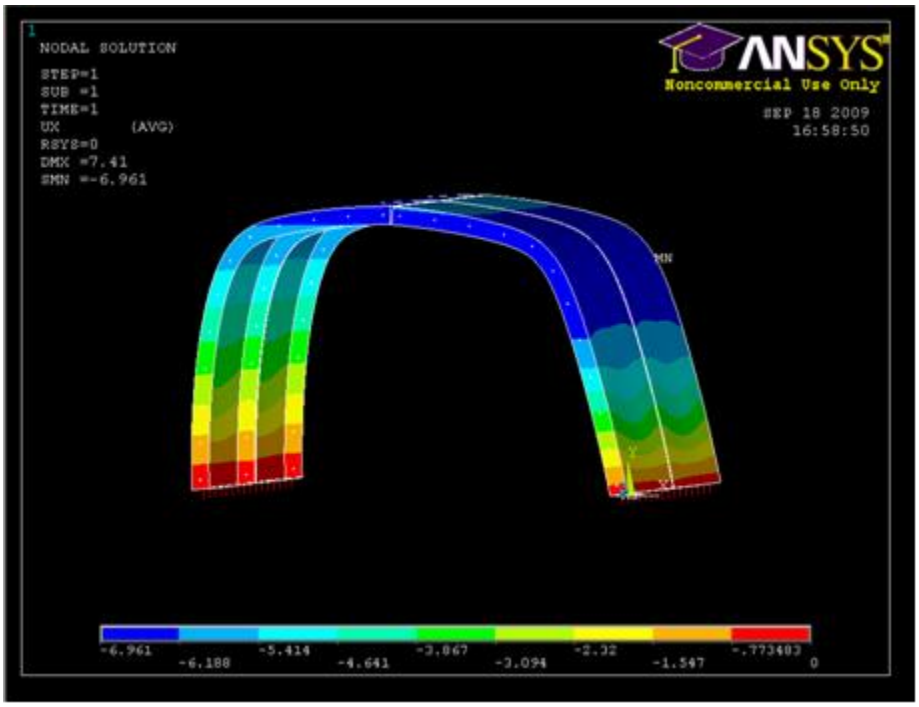

(b) Maximum Deflection in Global X-Direction of Sandwich Composite Model

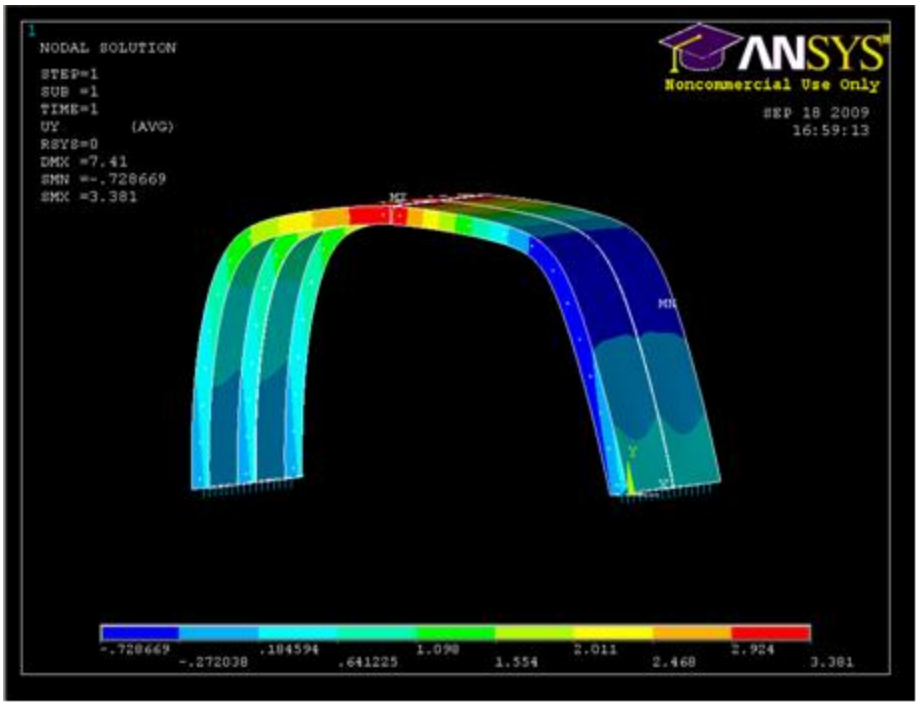

(c) Maximum Deflection in Global Y-Direction of Sandwich Composite Model

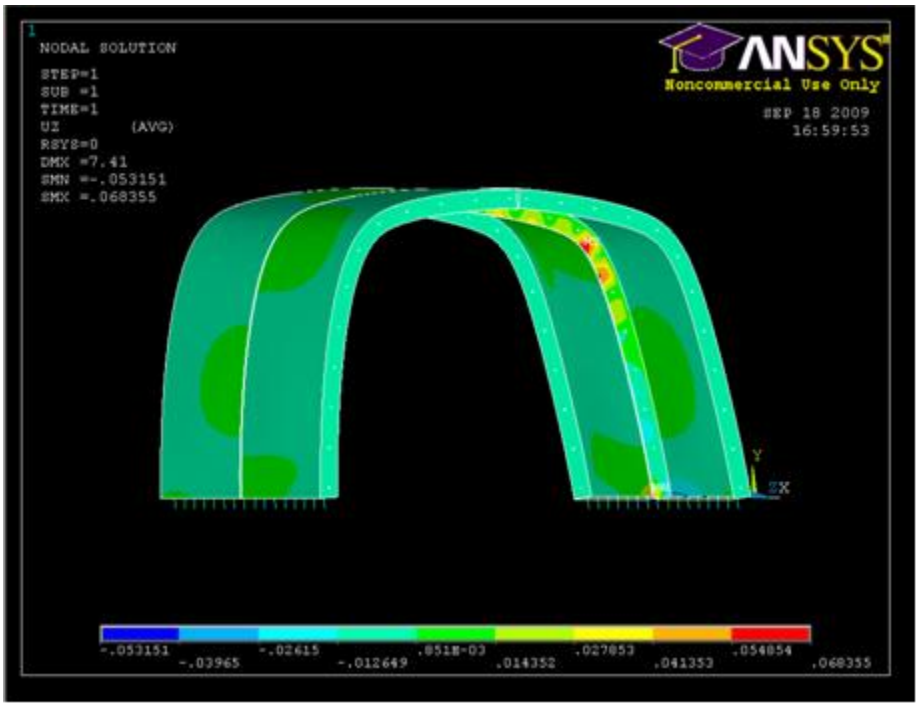

(d) Maximum Deflection in Global Z-Direction of Sandwich Composite Model

Figure 7.8. Displacements of Sandwich Composite Model.

7.3.1.2—Forces of Anchor Bolts of Sandwich Composite Model

Since connections are the most critical part for protecting the structure from coming apart, the aim of the connection design was to be conservative with the design results. The connection design will be designed for the bolts that created the most shear and tensile forces on the shelter in order to determine the maximum stresses from those forces. The approach was to design for the maximum shear and tension forces for the entire bolt connections.

The reaction forces obtained from the FEA for the sandwich composite model under the combination loadings as shown in Chapter 4 are presented in Table 7.2. There were 32 bolts with two nodes per line element representing each bolt. The forces at the anchor bolts are shown with respect to the global coordinate axes in terms of the nodal forces. FX and FZ forces are shear components of the anchor bolts, while FY forces are the normal components of the anchor bolts. The resultant shear forces are determined from FX and FZ forces. Figure 7.9 shows the locations of maximum shear and normal forces of the anchor bolts.

It can be seen from Table 7.2 that the bolt with Node 102457 (Element 32215) gave the highest resultant shear force than any other nodes. The resultant shear forces obtained from these nodes were 1,499 lbs (6,667.9 N). The highest tensile forces occurred at Node 102473 (Element 32223) with tensile values of 6,329.1 lbs (28,153 N). Table 7.2 and Figure 7.9 can be read concurrently to determine where the maximum shear and normal forces occurred at the anchor bolts.

Table 7.2. Anchor Bolt Reaction Forces of Sandwich Composite Model

Node	$F_X = V_1$ (lbs)	$F_Y = T$ (lbs)	$F_Z = V_2$ (lbs)	F_R (lbs)	Node	$F_X = V_1$ (lbs)	$F_Y = T$ (lbs)	$F_Z = V_2$ (lbs)	F_R (lbs)
102411	124.0	5082.7	238.6	268.9	102442	1112.0	5430.0	456.1	1201.9
102413	290.6	496.3	-12.6	290.9	102443	-1112	-5430	-456.1	1201.9
102415	270.7	678.8	-10.0	270.9	102444	603.7	844.9	-24.07	604.2
102417	278.4	709.0	-14.5	278.7	102445	-603.7	-850.3	24.07	604.2
102419	321.1	735.3	-19.9	321.7	102446	459.7	914.0	-13.73	459.9
102421	404.6	770.9	-25.6	405.4	102447	-459.7	-919.0	13.73	459.9
102423	536.4	585.2	-19.2	536.8	102448	388.7	856.7	-12.64	388.9
102425	559.7	3987.1	-241.2	609.4	102449	-388.7	-862.1	12.64	388.9
102427	568.2	4125.6	253.8	622.3	102450	432.3	830.8	-7.033	432.4
102429	546.5	569.4	19.1	546.9	102451	-432.3	-836.2	7.033	432.4
102431	406.8	774.4	26.1	407.6	102452	622.8	832.6	2.395	622.8
102433	322.7	735.8	19.9	323.3	102453	-622.8	-837.9	-2.395	622.8
102435	280.0	709.5	14.2	280.4	102454	965.5	579.1	32.58	966.0
102437	272.1	681.8	10.2	272.3	102455	-965.5	-584.5	-32.58	966.0
102439	292.1	494.2	12.3	292.3	102456	1848.0	4535.0	-468.2	1906.4
102441	118.7	5057.1	-236.6	264.7	102457	-1848	-4540	468.2	1906.4
102443	928.8	6319.0	293.5	974.1	102458	1844.0	4501.0	463.6	1901.4
102445	618.9	610.5	-9.5	618.9	102459	-1844	-4506	-463.6	1901.4
102447	559.8	689.8	-1.5	559.8	102460	964.3	579.9	-32.81	964.9
102449	544.7	614.0	1.5	544.7	102461	-964.3	-585.3	32.81	964.9
102451	598.3	580.4	6.2	598.4	102462	621.9	832.5	-1.854	621.9
102453	734.5	588.1	12.2	734.6	102463	-621.9	-837.8	1.854	621.9
102455	945.8	300.2	30.0	946.3	102464	432.9	829.8	6.165	432.9
102457	1471.7	5177.6	-284.5	1499.0	102465	-432.9	-835.2	-6.165	432.9
102459	1468.7	5139.8	281.5	1495.4	102466	389.1	855.8	10.78	389.2
102461	944.8	302.0	-30.3	945.3	102467	-389.1	-861.2	-10.78	389.2
102463	733.7	587.3	-11.9	733.8	102468	460.9	916.7	12.28	461.1
102465	598.3	579.5	-6.7	598.3	102469	-460.9	-922.0	-12.28	461.1
102467	545.0	614.6	-2.6	545.0	102470	607.2	838.9	23.87	607.7
102469	560.7	692.3	0.7	560.7	102471	-607.2	-844.2	-23.87	607.7
102471	620.7	605.9	9.4	620.8	102472	1110.0	5441.0	-457.3	1200.5
102473	927.2	6329.1	-294.3	972.8	102473	-1110	5447.0	457.3	1200.5

V_1 = Shear Force; V_2 = Shear Force; T = Normal Force; F_R = Resultant Shear Force, $F_R = \sqrt{V_1^2 + V_2^2}$

Maximum Resultant Shear Force =

Maximum Normal Force =

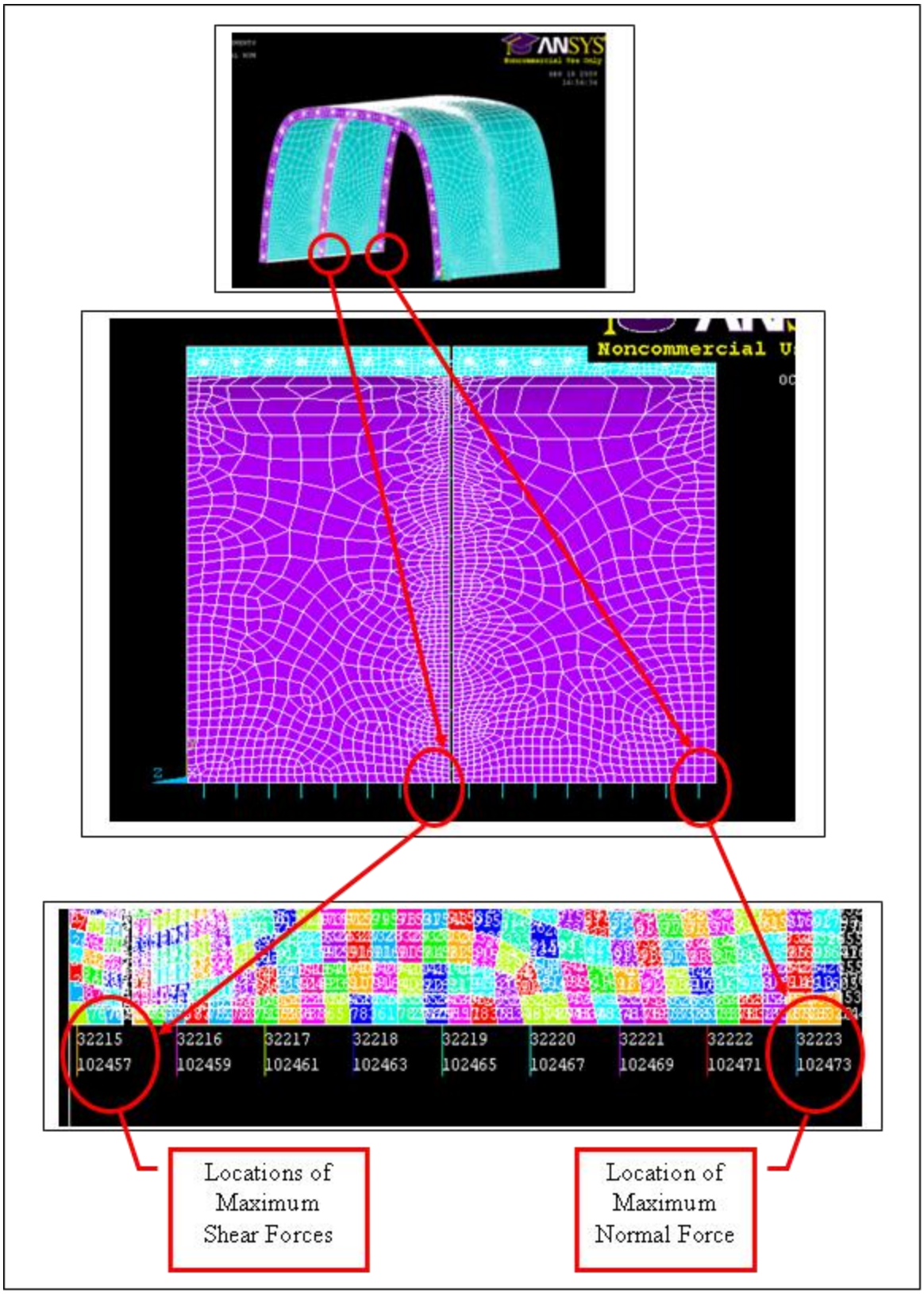

Figure 7.9. Node & Element Numbers of Anchor Bolts of Sandwich Composite Model.

7.3.1.3—Forces of Side Bolts of Sandwich Composite Model

The side bolt forces for the sandwich composite model are shown in Figure 7.10. Table 7.3 shows the resultant shear forces calculated from the FX and FY forces of the side bolts. The nodal FX and FY forces were the shear components of the side bolts, while FZ forces were the normal forces of the side bolts. The maximum resultant shear forces occurred at Nodes 102476 and 102477 for the same bolt with shear values of 47 lbs (209.1 N) and the maximum normal forces occurred at Nodes 102502 and 102503 for the same bolt with normal force values of 1,471 lbs (6,543.3 N). Figure 7.10 shows the locations of the maximum shear and normal forces of the side bolts. Table 7.3 and Figure 7.10 can be read concurrently to know the exact locations that created the most shear and normal forces on the side bolts.

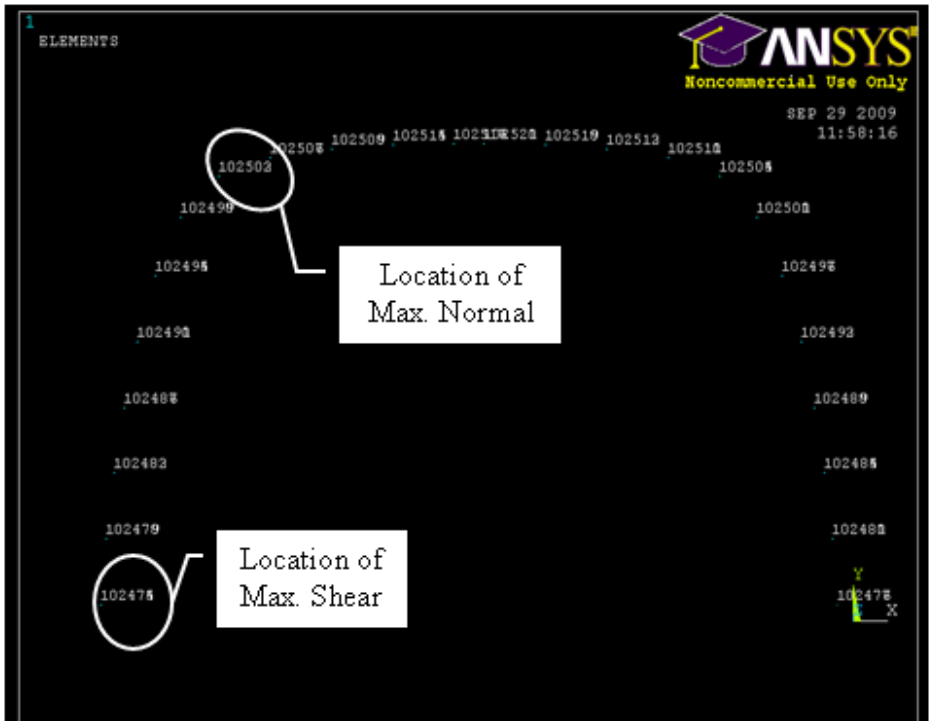

Figure 7.10. Locations of Maximum Shear and Normal Forces of Side Bolts of Sandwich Composite Model.

Table 7.3. Side Bolt Resultant Forces of Sandwich Composite Model

Node	FX = V_1 (lbs)	FY = V_2 (lbs)	FZ = T (lbs)	F_R (lbs)	Node	FX = V_1 (lbs)	FY = V_2 (lbs)	FZ = T (lbs)	F_R (lbs)
102474	-4.0	-24.8	1136.0	25.2	102498	-5.9	0.0	1318.0	5.9
102475	4.0	23.6	-1136.0	23.9	102499	5.9	-1.2	-1318.0	6.1
102476	19.4	42.3	827.2	46.6	102500	4.1	7.2	-416.2	8.3
102477	-19.4	-43.6	-827.2	47.7	102501	-4.1	-8.4	416.2	9.4
102478	0.3	3.8	-370.5	3.8	102502	-1.5	1.8	1471.0	2.4
102479	-0.3	-5.0	370.5	5.0	102503	1.5	-3.1	-1471	3.4
102480	-4.4	7.1	-2.9	8.3	102504	-2.5	1.9	-415.4	3.2
102481	4.4	-8.3	2.9	9.4	102505	2.5	-3.2	415.4	4.1
102482	-0.2	-0.1	-150.4	0.2	102506	0.5	-3.5	648.7	3.5
102483	0.2	-1.2	150.4	1.2	102507	-0.5	2.2	-648.7	2.3
102484	-1.5	4.3	278.0	4.5	102508	-3.8	1.1	360.5	3.9
102485	1.5	-5.5	-278.0	5.7	102509	3.8	-2.4	-360.5	4.4
102486	1.2	3.4	145.7	3.6	102510	-4.3	1.7	-155.0	4.6
102487	-1.2	-4.7	-145.7	4.8	102511	4.3	-2.9	155.0	5.2
102488	-0.9	-3.6	256.9	3.7	102512	-1.4	-0.8	-22.5	1.6
102489	0.9	2.3	-256.9	2.5	102513	1.4	-0.4	22.5	1.5
102490	4.0	2.5	476.4	4.7	102514	3.0	3.6	245.1	4.6
102491	-4.0	-3.8	-476.4	5.5	102515	-3.0	-4.8	-245.1	5.7
102492	3.6	-5.1	84.1	6.2	102516	8.9	-2.3	18.7	9.2
102493	-3.6	3.8	-84.1	5.3	102517	-8.9	1.1	-18.7	9.0
102494	-1.5	-4.3	832.8	4.6	102518	-3.0	0.0	23.8	3.0
102495	1.5	3.1	-832.8	3.4	102519	3.0	-1.2	-23.8	3.2
102496	3.2	1.2	-147.9	3.4	102520	-2.0	-2.7	115.8	3.4
102497	-3.2	-2.4	147.9	4.0	102521	2.0	1.4	-115.8	2.5

V_1 = Shear Force; V_2 = Shear Force; T = Normal Force; F_R = Resultant Shear Force, $F_R = \sqrt{V_1^2 + V_2^2}$
Maximum Resultant Shear Force =
Maximum Normal Force =

7.3.1.4—Forces of Top Bolts of Sandwich Composite Model

The nodal FX, FY, and FZ forces of the top bolts are shown in Table 7.4. The FX forces were the normal forces, whereas the FY and FZ forces were the shear force components of the top bolts. The resultant shear forces were calculated from FY and FZ shear force components. It was observed that Nodes 102536 and 102537 had the highest

resultant shear forces. The resultant shear forces that these nodes could take were 1,047 lbs (4,657.3 N) and 1,049 lbs (4,666.2 N), respectively, which occurred at the same bolt location as illustrated in Figure 7.11. The maximum normal forces occurred at Nodes 102533 and 102534 at the same bolt location with same normal force values of 691.9 lbs (3,078 N).

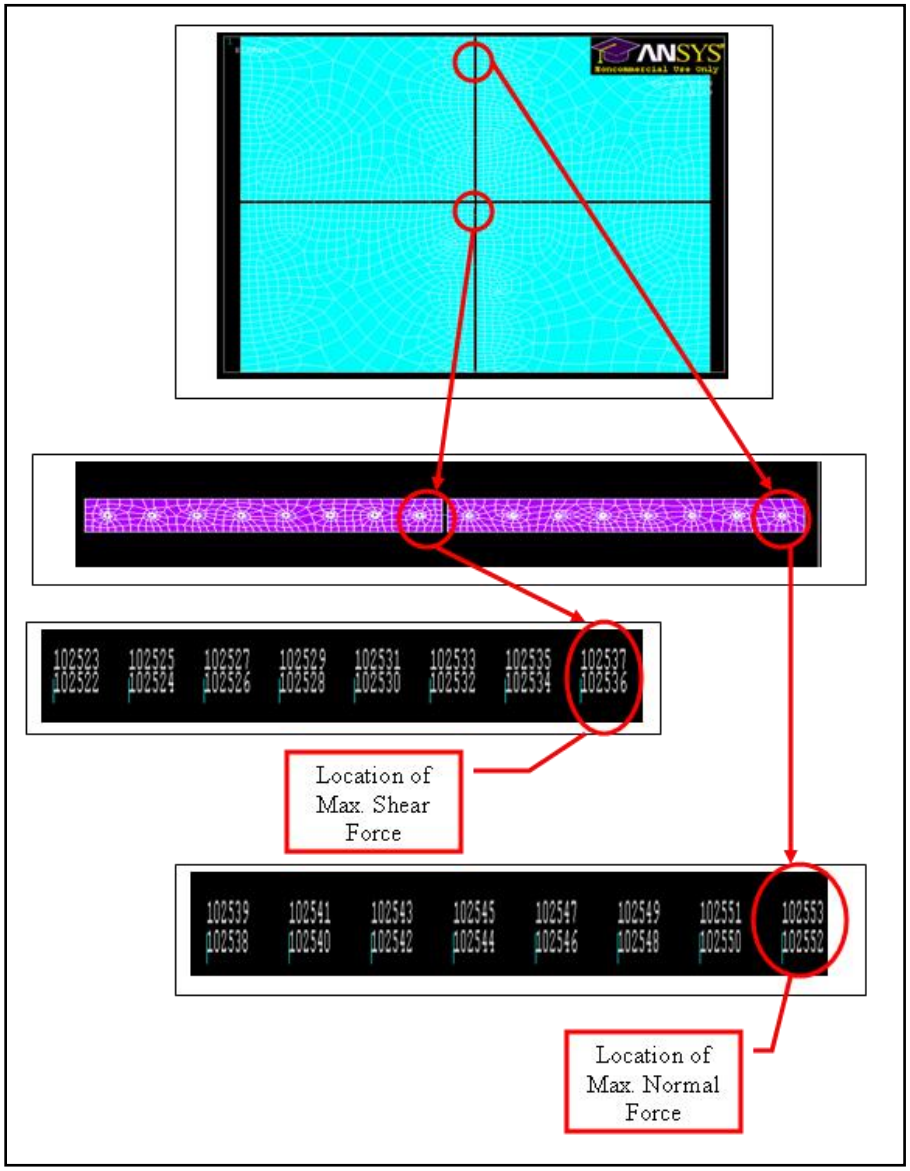

Figure 7.11. Locations of Maximum Shear and Normal Forces of Top Bolts of Sandwich Composite Model.

Table 7.4. Resultant Forces of Top Bolts of Sandwich Composite Model

Node	FX = T (lbs)	FY = V_1 (lbs)	FZ = V_2 (lbs)	F_R (lbs)
102522	-690.4	629.4	33.1	630.3
102523	690.4	630.6	-33.1	631.5
102524	418.2	140.6	121.5	185.8
102525	-418.2	-141.9	-121.5	186.8
102526	398.9	22.4	95.6	98.2
102527	-398.9	-23.6	-95.6	98.5
102528	406.5	-8.2	59.5	60.0
102529	-406.5	7.0	-59.5	59.9
102530	404.6	-31.5	20.4	37.5
102531	-404.6	30.2	-20.4	36.5
102532	385.9	-43.2	-36.2	56.3
102533	-385.9	42.0	36.2	55.4
102534	415.5	69.5	-98.7	120.7
102535	-415.5	-70.8	98.7	121.4
102536	-334.0	1047.0	-0.8	1047.0
102537	334.0	-1049.0	0.8	1049.0
102538	-339.7	1046.0	1.8	1046.0
102539	339.7	-1047.0	-1.8	1047.0
102540	415.7	69.0	99.2	120.8
102541	-415.7	-70.2	-99.2	121.5
102542	387.2	-43.9	35.5	56.5
102543	-387.2	-42.7	-35.5	55.5
102544	403.8	-29.2	-22.9	37.1
102545	-403.8	27.9	22.9	36.1
102546	408.2	-10.0	-60.0	60.8
102547	-408.2	8.8	60.0	60.6
102548	397.9	23.4	-98.7	101.4
102549	-397.9	-24.6	98.7	101.7
102550	418.5	139.2	-121.9	185.0
102551	418.5	-140.4	121.9	185.9
102552	-691.9	628.4	-33.3	629.3
102553	691.9	-629.7	33.3	630.6

V_1 = Shear Force; V_2 = Shear Force; T = Normal Force; F_R = Resultant Shear Force, $F_R = \sqrt{V_1^2 + V_2^2}$

Maximum Resultant Shear Force =

Maximum Normal Force =

7.3.1.5—Summary of Bolt Forces of Sandwich Composite Model

The maximum forces within the anchor bolts, side bolts and top bolts determined from the FEA are listed in Table 7.5. These forces will be used to determine the stresses within the bolts, which will be discussed later of this chapter.

Table 7.5. Summary of Bolt Forces of Sandwich Composite Model

	Anchor Bolts		Side Bolts		Top Bolts	
Maximum	Shear	Tension	Shear	Tension	Shear	Tension
Units	lbs	lbs	lbs	lbs	lbs	lbs
Value	1,499.0	6,329.1	47.7	1,471.0	1,049.0	691.0

1 lb = 4.45 N

7.3.1.6—Stresses of Flanges of Sandwich Composite Model

In addition to obtaining the forces in the bolts, the stresses in the flanges were also obtained from the solution in order to determine the bolt-bearing stress on the connecting flanges. The effects of the bolt bearing had on the FRP flanges of the sandwich composite model are analyzed in terms of the three independent normal (tensile) stresses and shear stresses. The element stress is formed to clarify the directions of the stress (Figure 7.12).

As seen from the element stress, the element has three independent normal (tensile) and shear stresses associated with the global element. It is important to note that only the one that created the most normal (tensile) stress and shear stress will be used for design. In this case, the maximum tensile stress that the sandwich composite panel could have under the wind pressure loading was 39,700 psi (274 MPa) (Figure 7.13). The maximum shear stress that the sandwich composite panel could take was 31,236 psi (215 MPa) (Figure 7.14).

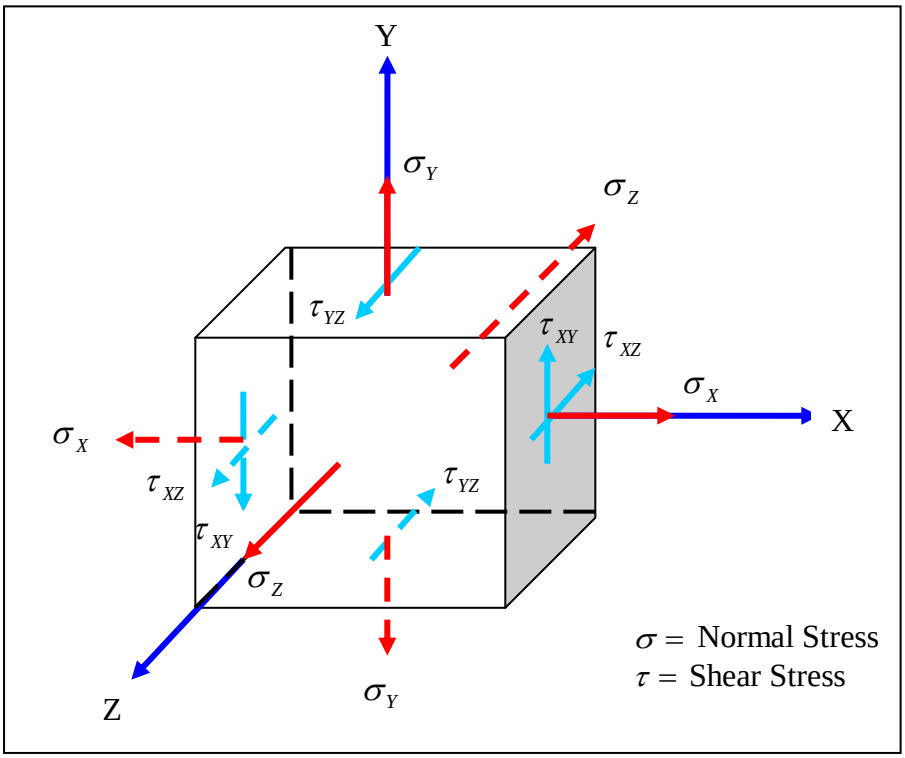

Figure 7.12. Illustration of Element Stress Parallel to Right Hand Rule.

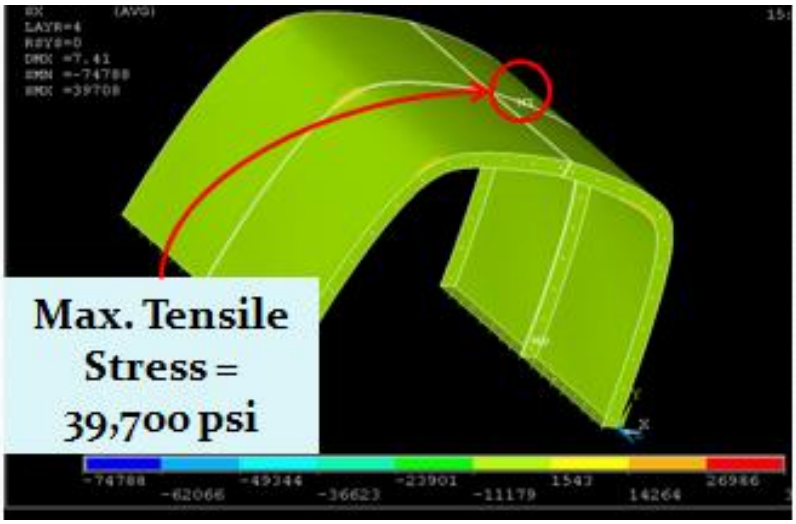

Figure 7.13. Maximum Tensile Stress of Sandwich Composite Panel.

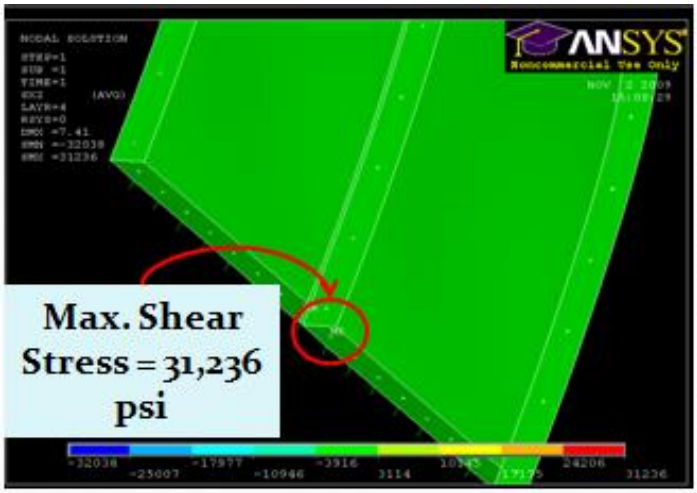

Figure 7.14. Maximum Shear Stress of Sandwich Composite Panel.

7.3.2—Second Model: FEA Results of Wire-Meshed Model

7.3.2.1—Deflection

The FEA results revealed the summation of displacement vectors of 2.905 in. (7.38 cm). The maximum deflections in the global X, Y and Z-directions were 2.679 in. (6.80 cm), 1.218 in. (3.09 cm), and 0.040 in. (0.102 cm), respectively. Figure 7.21 presents the deflections in each direction with respect to the global coordinate system.

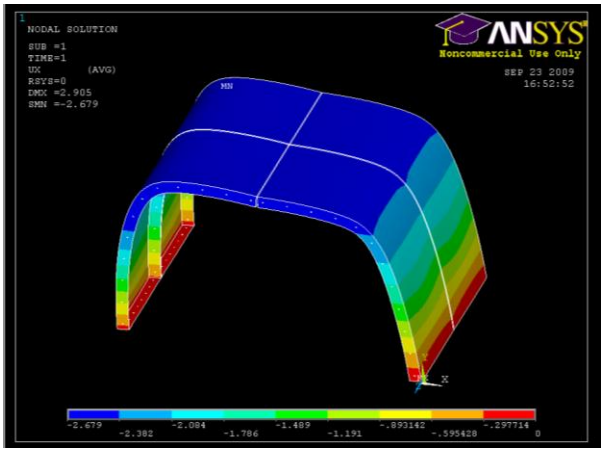

(a) Maximum Deflection in Global X-Direction of Wire-Meshed Model

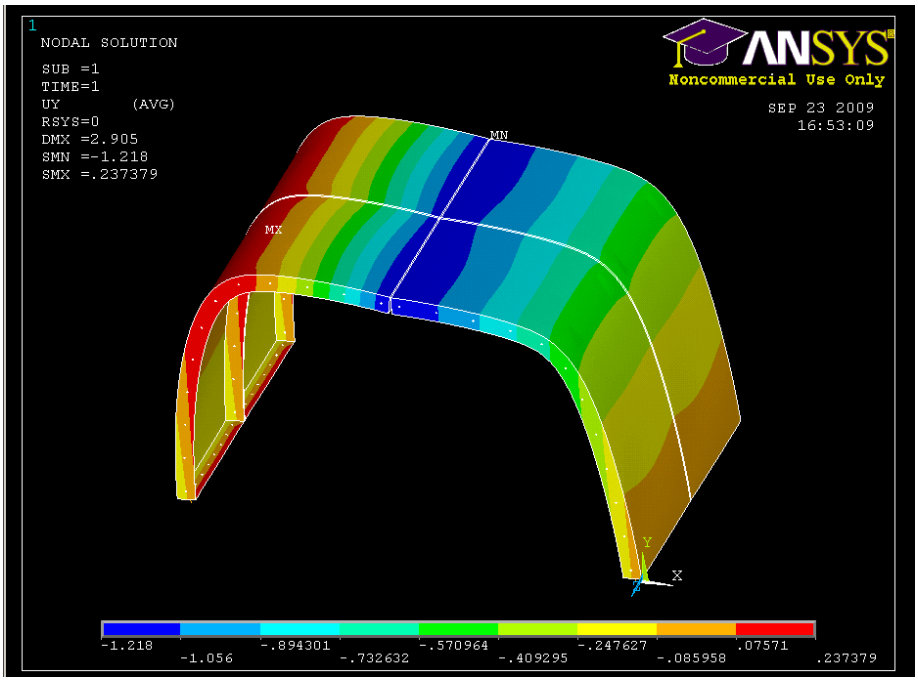

(b) Maximum Deflection in Global Y-Direction of Wire-Meshed Model

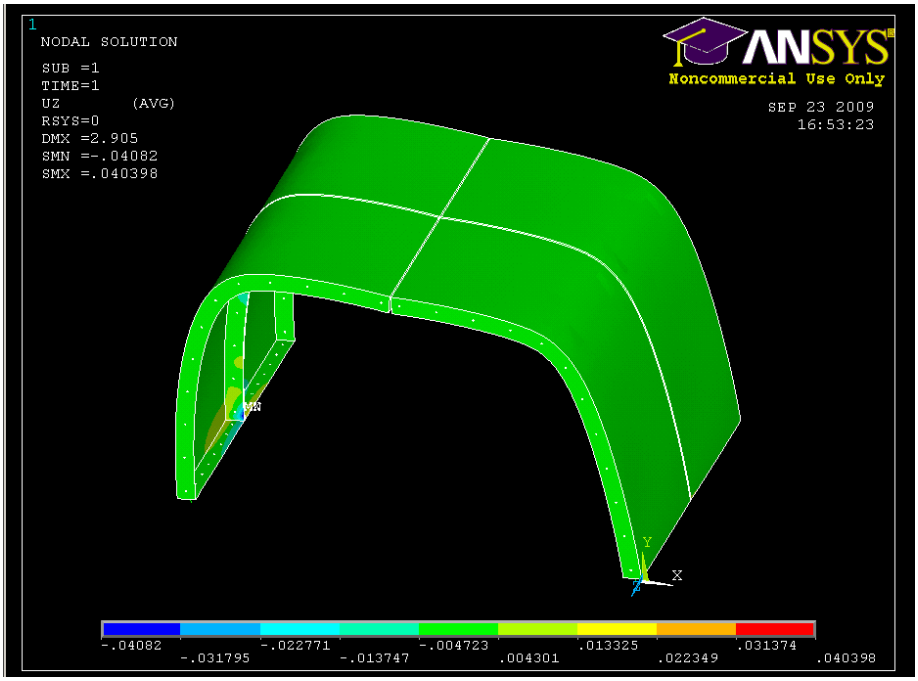

(c) Maximum Deflection in Global Z-Direction of Wire-Meshed Model

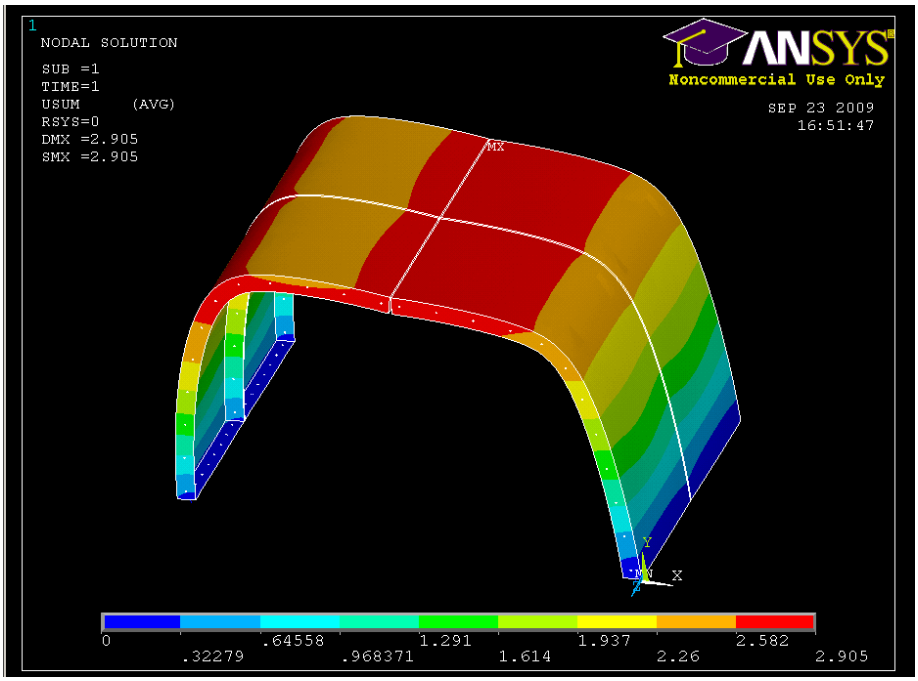

(d) Total Deflection of Wire-Meshed Model

Figure 7.15. Maximum Deflections with Respect to Global Coordinate System of Wire-Meshed Model.

7.3.2.2—Forces of Anchor Bolts of Wire-Meshed Model

The reaction forces of the anchor bolts of the wire-meshed model are presented in Table 7.6. The forces are shown with respect to the global coordinate axes. The forces at the anchor bolts are FX and FZ forces are shear components of the anchor bolts, while FY forces are the normal components of the anchor bolts. The resultant shear forces are determined from FX and FZ forces.

It can be seen from Table 7.6 that Node 102457 gave the highest resultant shear forces than any other nodes with a shear value of 1,499 lbs (6,668 N). The maximum tensile force occurred at Node 102473 with a tensile value of 6,329.1 lbs (28,153 N). The maximum reaction forces at these node locations can be seen in Figure 7.16. Table 7.6

and Figure 7.16 can be read concurrently to determine where the maximum shear and tension occurred at the anchor bolts. As expected, the reaction forces of the sandwich composite model are equaled to the reaction forces of the wire-meshed model.

7.3.2.3—Forces of Side Bolts of Wire-Meshed Model

Table 7.7 presents the FX, FY and FZ forces at each node of the side bolts. FX and FY forces were the shear components of the side bolts, while FZ forces were the normal forces of the side bolts. The resultant shear forces were calculated from FX and FY forces of the side bolts. It can be seen from Table 7.7 that the maximum resultant shear forces occurred at Nodes 102476 and 102477 with shear values of 47 lbs (209 N) and the maximum tensile forces occurred at Nodes 102502 and 102503 with tensile values of 1,471 lbs (6,543 N). Figure 7.17 shows the locations of the maximum shear and normal forces of the side bolts. Table 7.7 and Figure 7.17 can be read concurrently to know the exact locations that caused the most shear and tension on the side bolts.

Table 7.6. Resultant Forces of Anchor Bolts of Wire-Meshed Model

Node	$F_X = V_1$ (lbs)	$F_Y = T$ (lbs)	$F_Z = V_2$ (lbs)	F_R (lbs)	Node	$F_X = V_1$ (lbs)	$F_Y = T$ (lbs)	$F_Z = V_2$ (lbs)	F_R (lbs)
102411	124.0	5082.7	238.6	268.9	102442	1112.0	5430.0	456.1	1201.9
102413	290.6	496.3	-12.6	290.9	102443	-1112	-5430.0	-456.1	1201.9
102415	270.7	678.8	-10.0	270.9	102444	603.7	844.9	-24.07	604.2
102417	278.4	709.0	-14.5	278.7	102445	-603.7	-850.3	24.07	604.2
102419	321.1	735.3	-19.9	321.7	102446	459.7	914.0	-13.73	459.9
102421	404.6	770.9	-25.6	405.4	102447	-459.7	-919.0	13.73	459.9
102423	536.4	585.2	-19.2	536.8	102448	388.7	856.7	-12.64	388.9
102425	559.7	3987.1	-241.2	609.4	102449	-388.7	-862.1	12.64	388.9
102427	568.2	4125.6	253.8	622.3	102450	432.3	830.8	-7.033	432.4
102429	546.5	569.4	19.1	546.9	102451	-432.3	-836.2	7.033	432.4
102431	406.8	774.4	26.1	407.6	102452	622.8	832.6	2.395	622.8
102433	322.7	735.8	19.9	323.3	102453	-622.8	-837.9	-2.395	622.8
102435	280.0	709.5	14.2	280.4	102454	965.5	579.1	32.58	966.0
102437	272.1	681.8	10.2	272.3	102455	-965.5	-584.5	-32.58	966.0
102439	292.1	494.2	12.3	292.3	102456	1848.0	4535.0	-468.2	1906.4
102441	118.7	5057.1	-236.6	264.7	102457	-1848	-4540.0	468.2	1906.4
102443	928.8	6319.0	293.5	974.1	102458	1844.0	4501.0	463.6	1901.4
102445	618.9	610.5	-9.5	618.9	102459	-1844	-4506.0	-463.6	1901.4
102447	559.8	689.8	-1.5	559.8	102460	964.3	579.9	-32.81	964.9
102449	544.7	614.0	1.5	544.7	102461	-964.3	-585.3	32.81	964.9
102451	598.3	580.4	6.2	598.4	102462	621.9	832.5	-1.854	621.9
102453	734.5	588.1	12.2	734.6	102463	-621.9	-837.8	1.854	621.9
102455	945.8	300.2	30.0	946.3	102464	432.9	829.8	6.165	432.9
102457	1471.7	5177.6	-284.5	1499.0	102465	-432.9	-835.2	-6.165	432.9
102459	1468.7	5139.8	281.5	1495.4	102466	389.1	855.8	10.78	389.2
102461	944.8	302.0	-30.3	945.3	102467	-389.1	-861.2	-10.78	389.2
102463	733.7	587.3	-11.9	733.8	102468	460.9	916.7	12.28	461.1
102465	598.3	579.5	-6.7	598.3	102469	-460.9	-922.0	-12.28	461.1
102467	545.0	614.6	-2.6	545.0	102470	607.2	838.9	23.87	607.7
102469	560.7	692.3	0.7	560.7	102471	-607.2	-844.2	-23.87	607.7
102471	620.7	605.9	9.4	620.8	102472	1110.0	5441.0	-457.3	1200.5
102473	927.2	6329.1	-294.3	972.8	102473	-111	5447.0	457.3	1200.5

V_1 = Shear Force; V_2 = Shear Force; T = Normal Force; F_R = Resultant Shear Force, $F_R = \sqrt{V_1^2 + V_2^2}$

Maximum Resultant Shear Force =

Maximum Normal Force =

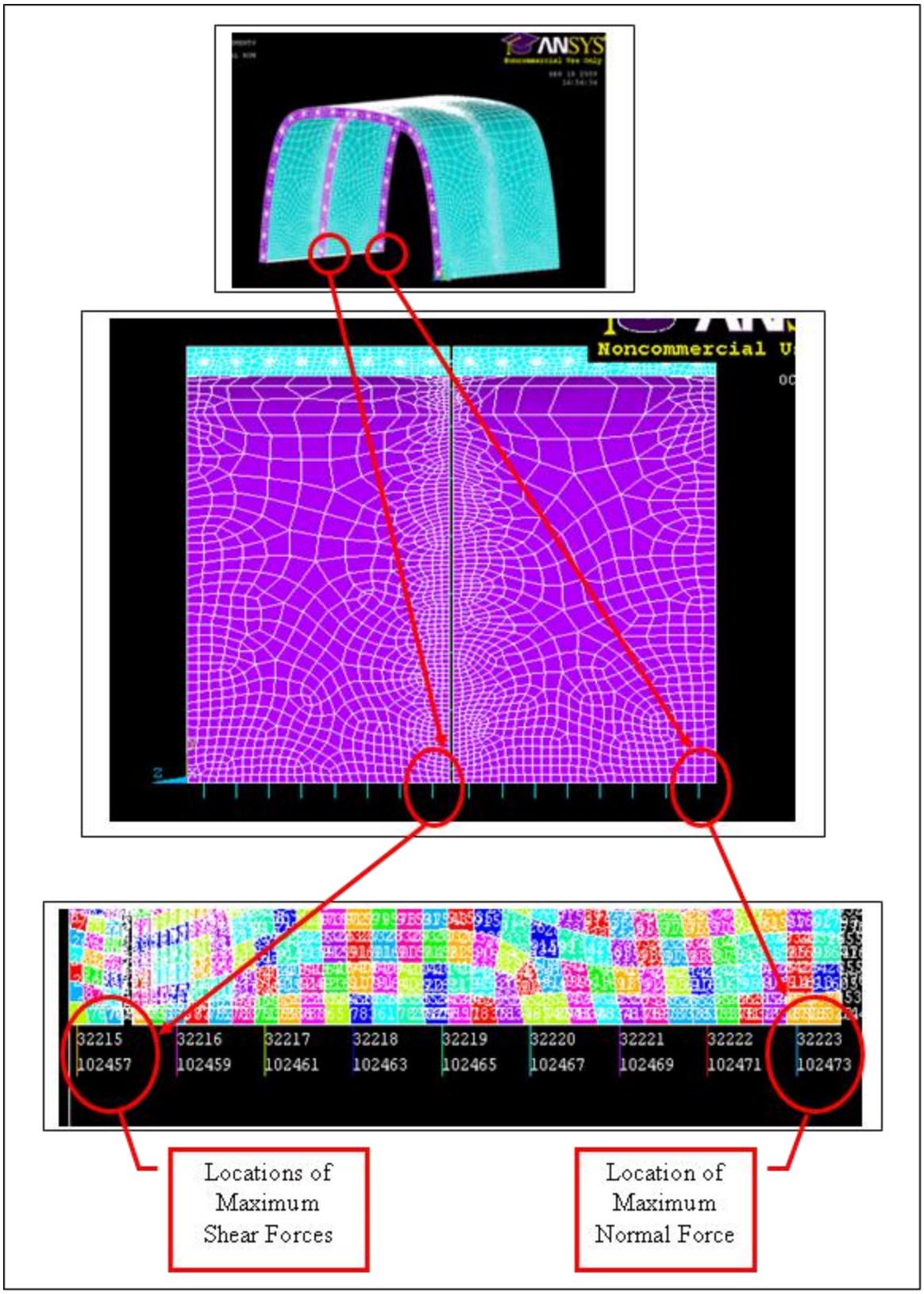

Figure 7.16. Node and Element Numbers of Anchor Bolts of Wire-Meshed Model.

Table 7.7. Forces of Side Bolts of Wire-Meshed Model

Node	FX = V_1 (lbs)	FY = V_2 (lbs)	FZ =T (lbs)	F_R (lbs)	Node	FX = V_1 (lbs)	FY = V_2 (lbs)	FZ =T (lbs)	F_R (lbs)
102474	-4.0	-24.8	1136.0	25.2	102498	-5.9	0.0	1318.0	5.9
102475	4.0	23.6	-1136.0	23.9	102499	5.9	-1.2	-1318.0	6.1
102476	19.4	42.3	827.2	46.6	102500	4.1	7.2	-416.2	8.3
102477	-19.4	-43.6	-827.2	47.7	102501	-4.1	-8.4	416.2	9.4
102478	0.3	3.8	-370.5	3.8	102502	-1.5	1.8	1471.0	2.4
102479	-0.3	-5.0	370.5	5.0	102503	1.5	-3.1	-1471.0	3.4
102480	-4.4	7.1	-2.9	8.3	102504	-2.5	1.9	-415.4	3.2
102481	4.4	-8.3	2.9	9.4	102505	2.5	-3.2	415.4	4.1
102482	-0.2	-0.1	-150.4	0.2	102506	0.5	-3.5	648.7	3.5
102483	0.2	-1.2	150.4	1.2	102507	-0.5	2.2	-648.7	2.3
102484	-1.5	4.3	278.0	4.5	102508	-3.8	1.1	360.5	3.9
102485	1.5	-5.5	-278.0	5.7	102509	3.8	-2.4	-360.5	4.4
102486	1.2	3.4	145.7	3.6	102510	-4.3	1.7	-155.0	4.6
102487	-1.2	-4.7	-145.7	4.8	102511	4.3	-2.9	155.0	5.2
102488	-0.9	-3.6	256.9	3.7	102512	-1.4	-0.8	-22.5	1.6
102489	0.9	2.3	-256.9	2.5	102513	1.4	-0.4	22.5	1.5
102490	4.0	2.5	476.4	4.7	102514	3.0	3.6	245.1	4.6
102491	-4.0	-3.8	-476.4	5.5	102515	-3.0	-4.8	-245.1	5.7
102492	3.6	-5.1	84.1	6.2	102516	8.9	-2.3	18.7	9.2
102493	-3.6	3.8	-84.1	5.3	102517	-8.9	1.1	-18.7	9.0
102494	-1.5	-4.3	832.8	4.6	102518	-3.0	0.0	23.8	3.0
102495	1.5	3.1	-832.8	3.4	102519	3.0	-1.2	-23.8	3.2
102496	3.2	1.2	-147.9	3.4	102520	-2.0	-2.7	115.8	3.4
102497	-3.2	-2.4	147.9	4.0	102521	2.0	1.4	-115.8	2.5

V_1 = Shear Force; V_2 = Shear Force; T = Normal Force; F_R = Resultant Shear Force, $F_R = \sqrt{V_1^2 + V_2^2}$

Maximum Resultant Shear Force =

Maximum Normal Force =

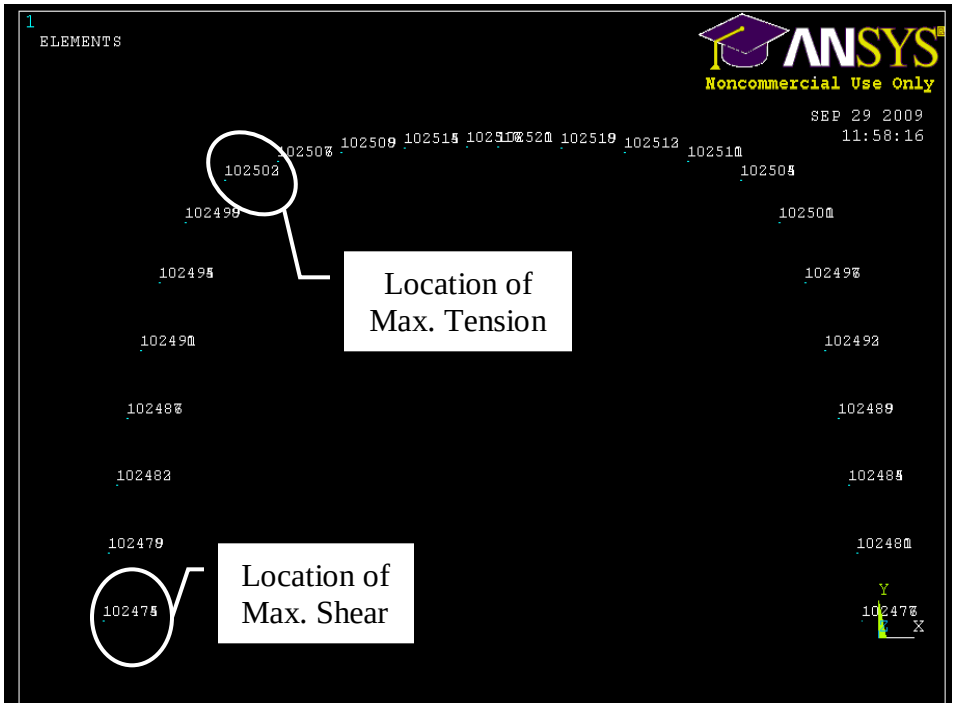

Figure 7.17. Locations of Maximum Shear and Normal Forces of Side Bolts of Wire-Meshed Model.

7.3.2.4—Forces of Top Bolts of Wire-Meshed Model

The FX, FY, and FZ forces at each node of the top bolts in Table 7.8 are shown with respect to the global coordinate system. FX was the normal force, whereas FY and FZ were the shear force components of the top bolts. The resultant shear forces were calculated from FY and FZ shear force components. It was observed that Nodes 102536 and 102537 had the highest resultant shear forces than any other nodes. The shear forces that these nodes could take were 1,052 lbs (4,680 N), which occurred at the same bolt location as illustrated in Figure 7.18. The maximum normal forces occurred at Nodes 102552 and 102553 with same tensile values of 520.2 lbs (2,314 N) (Figure 7.18).

Table 7.8. Resultant Forces of Top Bolts of Wire-Meshed Model

Node	FX = T (lbs)	FY = V_1 (lbs)	FZ = V_2 (lbs)	F_R (lbs)
102522	-518.4	622	30.47	622.2
102523	518.4	-622	-30.47	622.9
102524	357.5	154	111.1	190.2
102525	-357.5	-155	-111.1	190.8
102526	344.4	26	92.21	95.9
102527	-344.4	-27	-92.21	96.1
102528	353.0	-10	59.54	60.4
102529	-353.0	10	-59.54	60.3
102530	351.8	-35	21.88	40.9
102531	-351.8	34	-21.88	40.3
102532	335.3	-40	-30.83	50.8
102533	-335.3	40	30.83	50.3
102534	357.3	97	-84.65	129.0
102535	-357.3	-98	84.65	129.5
102536	-206.6	1052	-0.616	1052.0
102537	206.6	-1052	0.616	1052.0
102538	-211.5	1050	1.166	1050.0
102539	211.5	-1050	-1.166	1050.0
102540	357.8	97	85.11	128.9
102541	-357.8	-98	-85.11	129.5
102542	336.4	-41	30.47	50.8
102543	-336.4	40	-30.47	50.3
102544	351.4	-33	-24.33	40.8
102545	-351.4	32	24.33	40.2
102546	354.3	-12	-60.06	61.2
102547	-354.3	11	60.06	61.1
102548	343.6	27	-94.64	98.5
102549	-343.6	-28	94.64	98.7
102550	357.8	153	-111.7	189.7
102551	-357.8	-154	111.7	190.2
102552	-520.2	620	-30.99	621.1
102553	520.2	-621	30.99	621.8

V_1 = Shear Force; V_2 = Shear Force; T = Normal Force; F_R = Resultant Shear Force, $F_R = \sqrt{V_1^2 + V_2^2}$

Maximum Resultant Shear Force =

Maximum Normal Force =

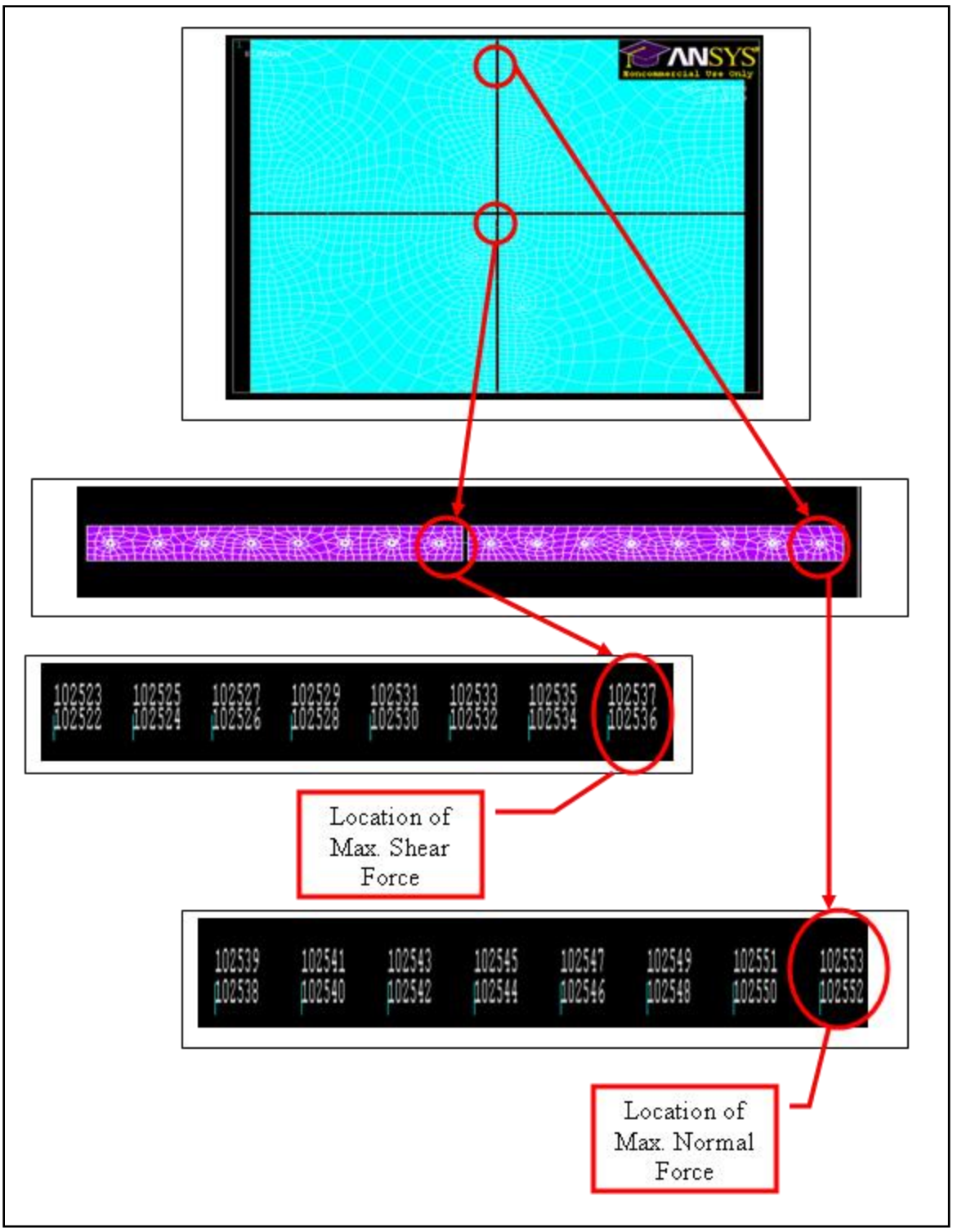

Figure 7.18. Locations of Maximum Shear and Normal Forces of Top Bolts of Wire-Meshed Model.

7.3.2.5—Summary of Bolt Forces of Wire Meshed Model

The maximum forces within the anchor bolts, side bolts and top bolts determined from the FEA are listed in Table 7.9. These forces will be used to determine the stresses within the bolts, which will be discussed later of this chapter.

Table 7.9. Summary of Bolt Forces of Wire-Meshed Model

	Anchor Bolts		Side Bolts		Top Bolts	
Maximum	Shear	Tension	Shear	Tension	Shear	Tension
Units	lbs	lbs	lbs	lbs	lbs	lbs
Value	1,499.0	6,329.1	47.0	1,471.0	1,052.0	520.2

1 lb = 4.45 N

7.3.2.6—Stresses of Connecting Materials of Wire-Meshed Model

Figure 7.19 and Figure 7.20 show the maximum tensile stress and shear stress obtained from the flanges of the wire-meshed model, respectively. The maximum tensile stress that the wire-meshed flange could have was 132,800 psi (916 MPa). The maximum shear stress that the wire-meshed flange could take was 73,804 psi (509 MPa).

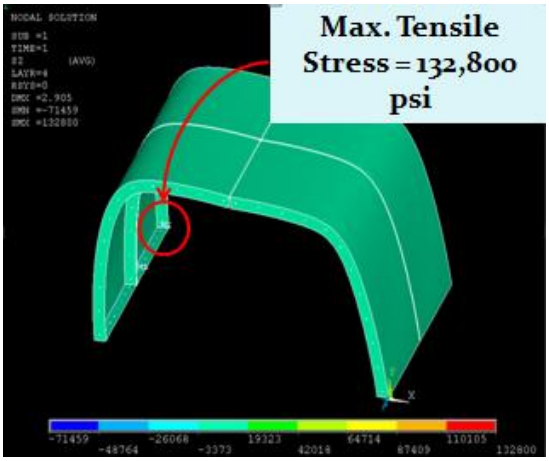

Figure 7.19. Maximum Tensile Stress of Wire-Meshed Model.

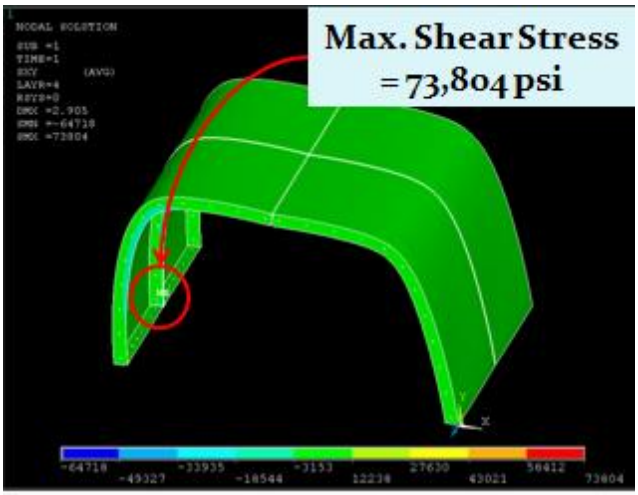

Figure 7.20. Maximum Shear Stress of Wire-Meshed Model.

7.4—Discussion of FEA Results

Section 7.4.1 discusses the FEA results of the sandwich composite model. Section 7.4.2 discusses the FEA results of the wire-meshed model. The discussions of these models include the determination of the shear and normal stresses of the anchor bolts, side bolts and top bolts. The bolt stresses will be compared to the nominal strength of the bolts in order to determine if the chosen bolt size had sufficient strength to resist the applied loadings. In addition, the discussions will include the comparison of the strength of the FRP materials versus the stress in the FRP materials. This comparison will determine if the FRP materials had enough strength to resist bolt-bearing forces.

7.4.1—Discussion of FEA Results of Sandwich Composite Model

Section 7.4.1.1 discusses the bolt forces and determination of the bolt stresses. Section 7.4.1.2 discusses the stresses developed in the FRP materials and determines if the FRP materials had enough strength to resist the bolt bearing stresses.

7.4.1.1—Bolt Stresses of Sandwich Composite Model

The primary objective of the bolt analysis was to determine if the bolts had enough strength to resist the applied loadings. This was done by comparing the bolt stresses to the bolt strength capacities per LRFD Specification. The LRFD Specification was used to reduce the probability of joint failure. Since joint failure is a particular safety concern, this comparison will ultimately increase safety and reduce the risks of joint failure. The aim of the connection design was to choose an appropriate bolt size and bolt type to have a positive overall impact on the performance of the joint. The comparison will determine if the chosen bolt size and type were appropriate, if they were not, then the bolts must be upgraded to bigger sizes, higher bolt strength or smaller bolt spacing. Most importantly, the chosen bolt size or type, and so on, must have their design strength equals or exceeds the required strength determined by the structural analysis for the combined factored loads acting on the shelter [36].

The shearing stress and tensile (normal) stress of the bolts can be determined from the following equations of the LRFD Specification, respectively [36]

$$f_v = \frac{V_u}{N_b A_b} \tag{7.1}$$

$$f_t = \frac{T_u}{N_b A_b} \tag{7.2}$$

where

f_v = *shearing stress of bolt*

f_t = *tensile stress of bolt (refers to as normal stress of bolt in this thesis)*

V_u = *factored shear load determined from structural analysis*

T_u = *factored tensile load determined from structural analysis*

N_b = *number of bolt*

A_b = *cross-sectional area of bolt* $(= \frac{\pi d^2}{4})$

The shearing stress, f_v, of a bolt must be compared to the shear strength of a bolt. The nominal shear strength of a bolt can be obtained from any structural analysis books or from a manual of steel construction, LRFD specification. For a typical A325 bolt, when threads are excluded from the shear planes, the tensile strength of the bolt is 90 ksi (620 MPa); and the shear strength of the bolt in bearing-type connections is 60 ksi (414 MPa) [36]. The design tensile and shear strengths are generally multiplied with a resistance factor, ϕ, of 0.75 [36]. As results, the design tensile strength and shear strength become 67.5 ksi (465,396,116 N/m^2) and 45 ksi (310,264,077 N/m^2), respectively. Furthermore, the design tensile stress for a bolt subjected to combined tension and shear equals ϕF_t, which is calculated from the following equation [36]:

$$\phi F_t = \phi[(117 - 2.0 f_v) \leq 90][ksi] \tag{7.3}$$

It is also important to note that this equation only holds true for A325 bolts when threads are excluded from the shear plane.

The bolt shear stress, tensile stress, and limiting tensile stress subjected to both tension and shear forces of the sandwich composite model were determined from Equations [7.1 - 7.3], respectively. Figure 7.21 presents the determination of the bolt stresses obtained from these equations for the anchor bolts, side bolts, and top bolts; and the obtained bolt stresses were compared to the nominal strengths of the bolts. As seen from Figure 7.21, the bolt stresses were less than the nominal strengths of the A325 bolts. The bolt connection designs satisfied the requirements of the LRFD Specification under

the applied loadings. Hence, the final bolt diameters of the anchor bolts, side bolts, and top bolts will be kept as 0.375 in. (0.953 cm) as described in the FEA. The bolt spacing will be remained as described in the FEA.

Anchor Bolts:

V_u = 1499 lbs
T_u = 6329.1 lbs
A_b = 0.1104 in^2
Shear Stress, $f_v = V_u/A_b$ = 1499/0.1104 = 13.6 ksi < 45 ksi **OK**
Tensile Stress, $f_t = T_u/A_b$ = 6329.1/0.1104 = 57.3 ksi

Limiting Tensile Stress Subjected to Both Tension and Shear Forces:

$$\phi F_t = \phi\left[\left(117 - 2.0 f_v\right) \le 90\right][ksi]$$

$$\phi F_t = 0.75\left[117 - 2*13.6\right] \le \phi 90$$

$$\phi F_t = 67.35ksi > 57.3 \text{ ksi}$$ **OK**

Side Bolts:

V_u = 47.7 lbs
T_u = 1471 lbs
A_b = 0.1104 in^2
Shear Stress, $f_v = V_u/A_b$ = 47.7/0.1104 = 0.435 ksi < 45 ksi **OK**
Tensile Stress, $f_t = T_u/A_b$ = 1471/0.1104 = 13.3 ksi

Limiting Tensile Stress Subjected to Both Tension and Shear Forces:

$$\phi F_t = \phi\left[\left(117 - 2.0 f_v\right) \le 90\right][ksi]$$

$$\phi F_t = 0.75\left[117 - 2*0.435\right] \le \phi 90$$

$$\phi F_t = 67.5ksi > 13.3 \text{ ksi}$$ **OK**

Top Bolts:

V_u = 1049 lbs
T_u = 691 lbs
A_b = 0.1104 in^2
Shear Stress, $f_v = V_u/A_b$ = 1049/0.1104 = 9.5 ksi < 45 ksi **OK**
Tensile Stress, $f_t = T_u/A_b$ = 691/0.1104 =6.3 ksi

Limiting Tensile Stress Subjected to Both Tension and Shear Forces:

$$\phi F_t = \phi\left[\left(117 - 2.0 f_v\right) \le 90\right][ksi]$$

$$\phi F_t = 0.75\left[117 - 2*9.5\right] \le \phi 90$$

$$\phi F_t = 67.5ksi > 6.3 \text{ ksi}$$ **OK**

Connections are satisfactory!

Figure 7.21. Determination of Bolt Shear and Tensile Stresses in Sandwich Composite Model.

7.4.1.2—Stresses of FRP Flanges of Sandwich Composite Model

As seen from Figure 7.13, the maximum tensile stress of the sandwich composite flanges was 39,700 psi (274 MPa). The maximum shear stress in the FRP flanges was 31,236 psi (215 MPa) (Figure 7.14). The failure criteria dicussed in Chapter 6 was also carried out for the sandwich composite flanges here. The failure index was carried out on the flanges based on the maximum stresses in the sandwich composite flanges, to determine whether the FRP flanges failed under the applied loading. The failure index of the sandwich composite flanges was 0.86, which was less than a ratio of 1.0. This means that the FRP flanges had sufficient strength to resist the applied tensile load. This also means that they had passed the minimum wind load criteria of the ASCE 7-05. Hence, the strength of the FRP flanges was sufficient to resist the applied 300 mph wind forces.

7.4.2—Discussion of FEA Results of Wire-Meshed Model

Section 7.4.2.1 discusses the bolt forces and determination of the bolt stresses. Section 7.4.2.2 discusses the stresses developed in the FRP materials and determines if the FRP materials had enough strength to resist the bolt bearing stresses.

7.4.2.1—Bolt Stresses of Wire-Meshed Model

The same analysis form Section 7.4.1.1 was used to determine the bolt stresses of the wire-meshed model. The bolt shear stress, tensile stress, and limiting tensile stress subjected to both tension and shear forces of the sandwich composite model were determined from Equations [7.1 - 7.3], respectively. Figure 7.22 presents the determination of the bolt stresses obtained from these equations for the anchor bolts, side

bolts, and top bolts; and the obtained bolt stresses were compared to the nominal strengths of the bolts. As seen from Figure 7.22, the bolt stresses were less than the nominal strengths of the A325 bolts. The bolt connection designs satisfied the requirements of the LRFD Specification under the applied loadings. Hence, the final bolt diameters of the anchor bolts, side bolts, and top bolts will be kept as 0.375 in. (0.953 cm) as described in the FEA. The bolt spacing will be remained as described in the FEA.

Anchor Bolts:

V_u = 1499 lbs
T_u = 6329.1 lbs
A_b = 0.1104 in^2
Shear Stress, $f_v = V_u/A_b$ = 1499/0.1104 = 13.6 ksi < 45 ksi **OK**
Tensile Stress, $ft = T_u/A_b$ = 6329.1/0.1104 = 57.3 ksi

Limiting Tensile Stress Subjected to Both Tension and Shear Forces:

$$\phi F_t = \phi\left[\left(117 - 2.0 f_v\right) \le 90\right][ksi]$$

$$\phi F_t = 0.75\left[117 - 2*13.6\right] \le \phi 90$$

$\phi F_t = 67.35ksi$ > 57.3 ksi **OK**

Side Bolts:

V_u = 47.0 lbs
T_u = 1471 lbs
A_b = 0.1104 in^2
Shear Stress, $f_v = V_u/A_b$ = 47.7/0.1104 = 0.425 ksi < 45 ksi **OK**
Tensile Stress, $ft = T_u/A_b$ = 1471/0.1104 = 13.3 ksi

Limiting Tensile Stress Subjected to Both Tension and Shear Forces:

$$\phi F_t = \phi\left[\left(117 - 2.0 f_v\right) \le 90\right][ksi]$$

$$\phi F_t = 0.75\left[117 - 2*0.425\right] \le \phi 90$$

$\phi F_t = 67.5ksi$ > 13.3 ksi **OK**

Top Bolts:

V_u = 1052 lbs
T_u = 520.2 lbs
A_b = 0.1104 in^2
Shear Stress, $f_v = V_u/A_b$ = 1052/0.1104 = 9.5 ksi < 45 ksi **OK**
Tensile Stress, $ft = T_u/A_b$ = 520/0.1104 = 4.7ksi

Limiting Tensile Stress Subjected to Both Tension and Shear Forces:

$$\phi F_t = \phi\left[\left(117 - 2.0 f_v\right) \le 90\right][ksi]$$

$$\phi F_t = 0.75\left[117 - 2*9.5\right] \le \phi 90$$

$\phi F_t = 67.5ksi$ > 4.7 ksi **OK**

Connections are satisfactory!

Figure 7.22. Determination of Bolt Shear and Tensile Stresses in Wire-Meshed Model.

7.4.2.2—Stresses of FRP Flanges of Wire-Meshed Model

As seen from Figure 7.19 and Figure 7.20, the maximum tensile stress and shear stress of the wire-meshed flanges were 132,800 psi (916 MPa) and 73,804 psi (509 MPa), respectively. The failure index obtained from the maximum stresses was 0.81, which was also less than 1.0. This indicates that the FRP stress was less than the FRP strength and that the FRP flanges had sufficient strength to resist the applied load. Hence, the strength of the FRP flanges was sufficient to resist the applied 300 mph wind forces.

CHAPTER 8

SUMMARY, CONCLUSIONS AND FUTURE RESEARCH

Tornadoes and hurricanes often produce extreme wind speeds that put structures and people at great risks. The purpose of this research was to design an innovative community storm shelter that can protect people during the extreme wind events. The research proposed using innovative, Glass-FRP storm shelter to resist 300 mph wind induced forces.

The design wind pressures from the 300 mph induced wind forces were calculated by the ASCE 7-05 design philosophy and the CFD analysis. The final wind pressures from the ASCE 7-05 methodology was compared to the final wind pressures of the CFD methodology.

Finite element analysis and design were carried out on both of the proposed FRP panels and connections to investigate the effect of important parameters on stresses of the panels under the applied wind pressure loading. The following conculusions were drawn from the analysis and design:

- The ASCE 7-05 underestimated design wind pressures especially at roof corners (pitch) and for this particular shape of the shelter.
- The connection design was satisfactory for transferring loads between members
- The proposed FRP materials were feasible for carrying extreme wind loads.

- The proposed FRP materials were feasible for preventing penetration by missiles.
- The shelter was considered safe to protect its occupants.

The future work in this project involves the structural testing of the wire-meshed panels at the performance level. In addition, wind tunnel tesing will be carried out for both the sandwich composite model and wire-meshed model, where factory manufactured SIPs are connected to each other through bolted joint connections and subjected to 300 mph wind forces.

LIST OF REFERENCES

1 FEMA 361. Design and Construction Guidance for Community Shelters. Second Edition. August 2008.

2 FEMA 543. Risk Management Series, Design Guide for Improving Critical Facility Safety from Flooding and High Winds. January 2007.

3 FEMA 320. Taking Shelter from the Storm: Build a Safe Room Inside Your Home, First Edition. September 1998.

4 Tang, Benjamin. *Fiber Reinforced Polymer Composites Applications in USA*. U.S Department of Transportation Federal Highway Administration. Korea and USA. Road Workshop Proceedings. January 28-29, 1997.

5 Ansys Inc., Ansys 11.0 Documentation.

6 American Society of Civil Engineering, ASCE 7-05.

7 Liu, Henry. Wind Engineering, A Handbook for Structural Engineers. Prentice Hall, Englewood Cliffs, New Jersey 1991.

8 Uddin, Nasim and Vaidya, Uday. "Ballistic Testing of Polymer Composites to Manufacture Emergency Safe House Shelters", Technical Notes Journal of Composites for Construction ASCE, pp 370-375, July-August 2005.

9 http://www.shelterplus.com/tornado.html. Web Visisted: September 9, 2009.

10 PermaTherm, Insulation Innovation. www.permatherm.net/eps.html. Web Visited: 7/27/2009.

11 Jones, R. Mechanics of Composite Materials, 2nd Ed. Scripta Book Co., Washington, 1975.

12 Villabobos, Adolfo. Design, Analysis and Evaluation of A Long Fiber Thermoplastic Composite Tailcone for Army Application. University of Alabama at Birmingham, Thesis, 2005.

13 Nasim Uddin, Uday Vaidya, and Amol Vaidya. "Innovative Multifunctional Structural Panels for Cost-Effective Panelized Construction." National Science

Foundation, Civil, Mechanical and Manufacturing Innovation (CMMI) Engineering Research, Grant # 0533306.

14 Ning, Haibin. "The Application of Thermoplastic Composites in Mass Transit.". University of Alabama at Birmingham. Ph.D, 2006.

15 *RL Hudson. Thermoset vs. Thermoplastic Materials, 2009. http://www.rlhudson.com. Web Visited: 9/8/2008.*

16 Marguerre, K. The Optimum Buckling of a Flexible Supported Plate Composed of Two Sheet Joined by A Light Weight Filler When Under Longitudinal Compression. Deutsche Viertaljahrsschrist fur Lieralurwissenschaft und Giests Giests Geschichte, D.V.L. October 1994.

17 Company Literature. Lowes.

18 Company Literature. Crane Composites Inc., 23525 W. Eames Channahon, IL 60410, U.S.A.

19 Company Literature. Universal Packaging Inc., 2216 Greenspring Drive Lutherville, MD 21093, U.S.A.

20 Company Literature. 3M. http://www.tapecase.com/p.136.36/3m-3794-3m-scotch-weld-hot-melt-adhesive-high-tack-psa.aspx. Web Visited: 9/8/2008.

21 Company Literature. Collano, Inc., 111 Smith Hines Road, Greenville, SC 29607.

22 Web Article: http://www.greenbuildingtalk.com/Forum/tabid/53/forumid/5/postid/12103/view/topic/Default.aspx. Web Visited: 9/8/2008.

23 Greenville Products Group, Inc., Greenville, Alabama.

24 Lohner, R. "Adaptive Remeshing for Transient Problems with Moving Bodies," AIAA 88-3737.1988.

25 Marcum, D.L, and Weatherill, N.P., "Aerospace Applications of Solution Adaptive Finite Element Analysis," Computer Aided Geometric Design, vol 12, pp 709-731, 1995.

26 Marvriplis, D.J., and Jameson, A., "Multigrid Solution of the Navier Stokes Equation on Triangular Meshes," AIAA Journal vol 28, No 8, August 1990.

27 Mavriplis, D.J., and Venkatakrishnan, V., "Agglomeration Multigrid for the Three Dimensional Euler Equations," AIAA 94-0069.1994.

28 Koumullil, Roy Paulose. Flow Simulation System for Generalized Static and Dynamic Grids." Ph.D Dissertation, Mississippi State University, May 1997.

29 Ito, Y., Fujita, T. and Nakahashi, K., "Interactive Generation of Unstructured Surface Grid on CAD Data," *Computational Fluid Dynamics Journal*, Vol. 9, No. 1, April 2000, pp. 417-422.

30 Marcum, D.L., and Weatherill, N.P., "Aerospace Applications of Solution Adaptive Finite Element Analysis," Computer Aided Geometric Design, vol 12, pp 709-731, 1995.

31 Baum, J. D., Luo, H., and Lohner, R., "A New ALE Adaptive Unstructred Methodology for the Simulation of Moving Bodies," AIAA 94-0414. 32nd Aerospace Sciences Meeting and Exhibit, Reno, NV, January 1-013, 1994.

32 Marcum, D.L., and Weatherill, N. P., "Unstructured Grid Generation Using Iterative Point Insertion and Local Reconnection," AIAA 94-1926. 12th AIAA Applied Aerodynamics Conference. Colorado Springs, CO. Juune 20-22, 1994.

33 National Aeronautics and Space Administration, The Drag Equation. Glen Research Center. http:///www.grc.nasa.gov.WWW/k-12/airplane/short.html. Web Visited: 10/1/2008.

34 Barbero, Ever J. Finite Element Analysis of Composite Materials. Department of Mechanical and Aerospace Engineering. West Virginia University. CRC Press, Taylor and Francis Group, New York, 2008.

35 Ginal, Scott. "Fatigue Performance of Full-Span Sign Support Structures Considering Truck-Induced Gust And Natural Wind Pressures." Master Thesis, Marquette University, Milwaukee, Wisconsin, 2003.

36 Load and Resistance Factor Design, AISC Manual, Third Edition, American Institute Steel Construction, Inc., 2001

APPENDIX

ASCE DESIGN WIND PRESSURE

Given:

Length =	480 inches
Width =	150 inches
Height =	90 inches
Mean Roof Height:	85 inches

Determine: Design Wind Press Acting on the Roof and Sides of the Building for MWFRS Using ASCE 7-05 Specifications.

Solutions:

Design Procdure:

Velocity Pressure at Elevation z:

Basic Wind Speed, V	=	300	mph
Velocity Pressure Exposure Coefficient, K_z	=	0.85	
Topographic Factor, K_{zt}	=	1.0	
Wind Driectionality Factor, K_d	=	0.9	
Importance Factor, I	=	1.0	

Velocity Pressure at Elevation z:

$$q_z = 0.00256 K_z K_{zt} K_d V^2 I \left(\frac{lb}{ft^2} \right)$$

q_z = 166.46 lb/ft^2

Design Wind Pressures for MWFRS:

$$p = qGC_p - q_i \left(GC_{pi} \right) \left(\frac{lb}{ft^2} \right)$$

where

Gust Factor, G =	=	0.85
External Pressure Coefficient, C_p	=	Unknown
Internal Pressure Coefficient (for Partially Enclosed Building, GC_{pi} *)*	=	± 0.55

To determine C_p, External Pressure Coefficient, Reference to ASCE 7-05, Figure 6-6

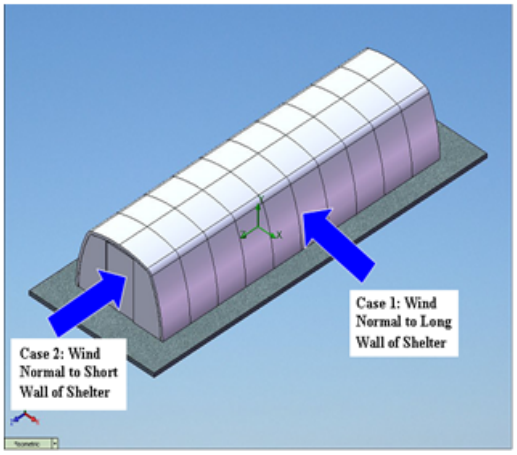

Case 1: Determine Wind Pressures for Wind Perpendicular to Ridge

Parameters for Determining C_p:

Height above Ground, z			
Mean Roof Height, h	=	7.08	inches
Horizontal Dimension of Building, B, in feet, Measured Normal to Wind Direction	=	40	ft
Horizontal Dimension of Building, L, in feet, Measured Parallel to Wind Direction	=	12.5	ft
Roof Angle, $\theta \leq 10^\circ$			

Note: Interpolation is permitted for values of L/B, h/L and angle other than shown. Interpolation shall only carried out between values of the same sign. When no value of the same sign is given, assume 0.0 for interpolation purposes.

Wall External Pressure Coefficients, C_p			
Wall Surface	**L/B**	**C_p**	**Use With**
Windward Wall	All Values	0.8	$q_z = q_i$
Leeward Wall	12.5/40	-0.5	$q_z = q_i$
Sidewall	All Values	-0.7	$q_z = q_i$

Roof External Pressure Coefficients, C_p			
Roof Surface	**h/L**	**C_p**	**Use With**
Windward Roof	7.08/12.5	-0.956	$q_z = q_i$
Leeward Roof	7.08/12.5	-0.528	$q_z = q_i$
0 to h/2	7.08/12.5	-0.956	$q_z = q_i$
h/2 to h	7.08/12.5	-0.872	$q_z = q_i$
h to 2h	7.08/12.5	-0.528	$q_z = q_i$

Wind Pressure for MWFRS Normal to Ridge					
Surface	**z (ft)**	**q_z (psf)**	**C_p**	**Design Pressure (psf)**	
				$(+GC_{pi})$	**$(-GC_{pi})$**
Windward Wall	0-7.5	166.46	0.8	21.6	204.78
Leeward Wall	All	166.46	-0.5	-162.09	20.78
Sidewall	All	166.46	-0.7	-190.35	-7.48
Roof (Horizontal Distance from Windward Edge)	0 to h/2	166.46	-0.956	-226.53	-43.66
	h/2 to 2h	166.46	-0.872	-214.66	-31.79
	h to 2h	166.46	-0.528	-166.05	16.82

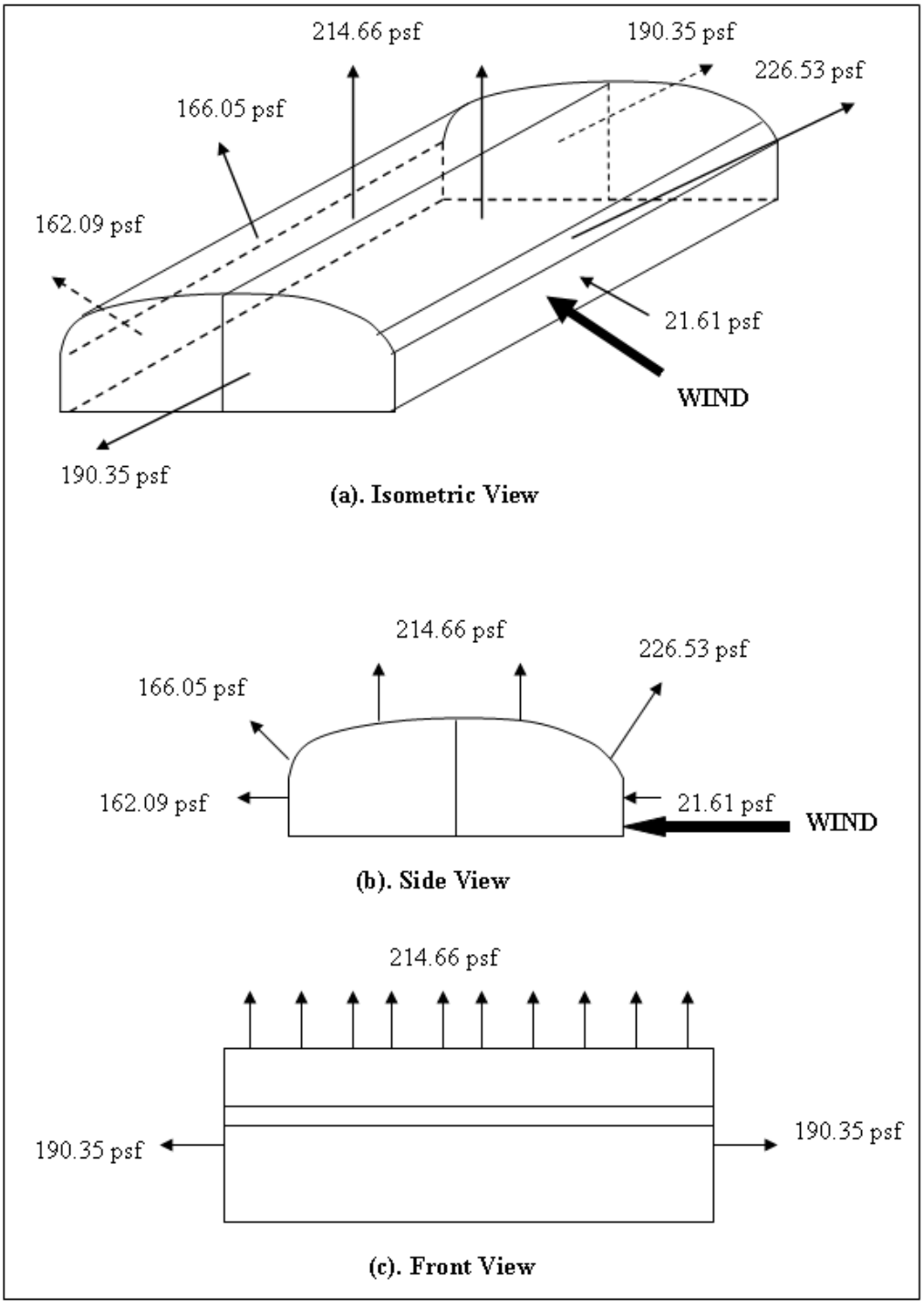

Schematic of Wind Pressure Distribution for MWFRS for Wind Normal to Ridge

Case 2: Determine Wind Pressures for Wind Parallel to Ridge

Parameters for Determining C_p:

Height above Ground, z			
Mean Roof Height, h	=	7.08	inches
Horizontal Dimension of Building, B, in feet, Measured Normal to Wind Direction	=	12.5	ft
Horizontal Dimension of Building, L, in feet, Measured Parallel to Wind Direction	=	40	ft
Roof Angle, $\theta \leq 10^\circ$			

Wall External Pressure Coefficients, C_p			
Wall Surface	**L/B**	**C_p**	**Use With**
Windward Wall	All Values	0.8	$q_z = q_i$
Leeward Wall	40/12.5	-0.24	$q_z = q_i$
Sidewall	All Values	-0.7	$q_z = q_i$

Roof External Pressure Coefficients, C_p			
Roof Surface	**L/B**	**C_p**	**Use With**
Windward Wall	All	0.8	$q_z = q_i$
Leeward Wall	40/12.5	-0.24	$q_z = q_i$
Sidewalls	All	-0.7	$q_z = q_i$
0 to h/2	7.08/12.5	-0.9	$q_z = q_i$
h/2 to h	7.08/12.5	-0.9	$q_z = q_i$
h to 2h	7.08/12.5	-0.5	$q_z = q_i$
> 2h	7.08/12.5	-0.3	$q_z = q_i$

Wind Pressure for MWFRS Parallel to Ridge					
Surface	**z (ft)**	**q_z (psf)**	**C_p**	**Design Pressure (psf)**	
				($+GC_{pi}$)	**($-GC_{pi}$)**
Windward Wall	0 - 7.5	166.46	0.8	21.64	204.75
Leeward Wall	All	166.46	-0.24	-125.51	57.6
Sidewall	All	166.46	-0.7	-190.6	-7.49
Roof (Horizontal Distance from Windward Edge)	0 to h/2	166.46	-0.9	-218.9	35.79
	h/2 to h	166.46	-0.9	-218.9	-35.79
	h to 2h	166.46	-0.5	-162.3	20.81
	> 2h	166.46	-0.3	-134	49.11

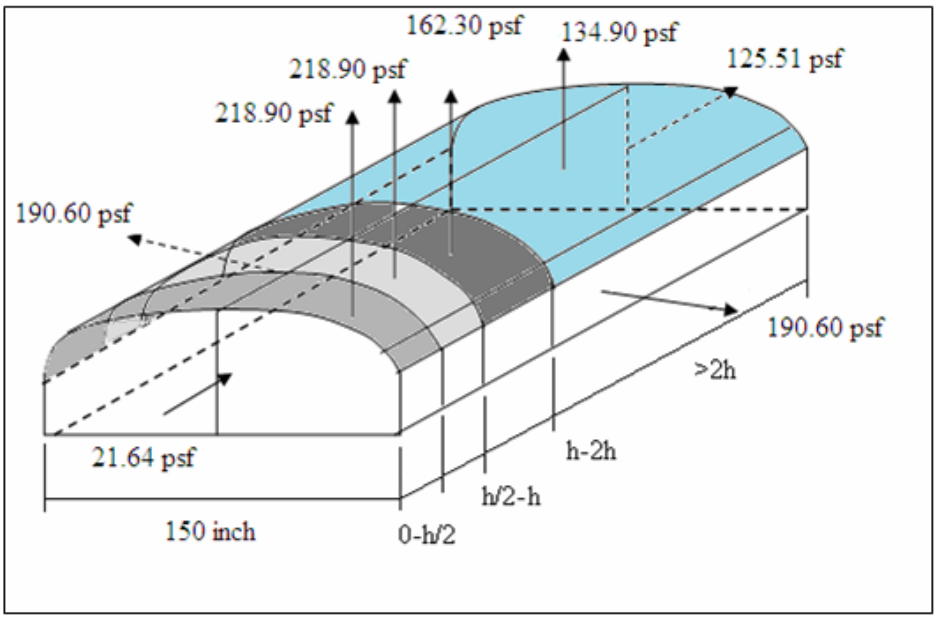
162.30 psf
134.90 psf
125.51 psf
218.90 psf
218.90 psf
190.60 psf
190.60 psf
>2h
21.64 psf
h-2h
h/2-h
150 inch
0-h/2

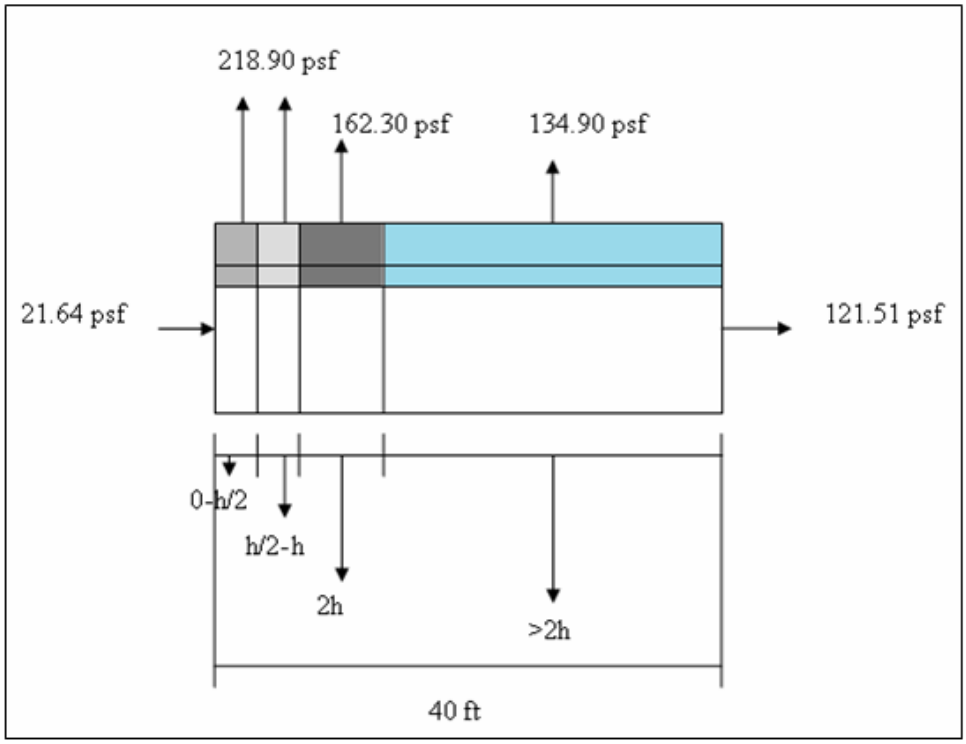
218.90 psf
162.30 psf
134.90 psf
21.64 psf
121.51 psf
0-h/2
h/2-h
2h
>2h
40 ft